Stochastic Finite Element Model Updating and its Application in Aeroelasticity

Thesis submitted in accordance with the requirements of
the University of Liverpool
for the degree of Doctor in Philosophy

by
Hamed Haddad Khodaparast

September 2010

To my son, Ali

Abstract

Knowledge in the field of modelling and predicting the dynamic responses of structures is constantly developing. Modelling of uncertainty is considered as one of the tools that increases confidence by providing extra information. This information may then be useful in planning physical tests. However, the complexity of structures together with uncertainty-based methods leads inevitably to increased computation; therefore deterministic approaches are preferred by industry and a safety factor is incorporated to account for uncertainties. However, the selection of a proper safety factor relies on engineering insight. Hence, there has been much interest in developing efficient uncertainty-based methods with a good degree of accuracy.

This thesis focuses on the uncertainty propagation methods; namely Monte Carlo Simulation, first-order and second-order perturbation, asymptotic integral, interval analysis, fuzzy-logic analysis and meta-models. The feasibility of using these methods (in terms of computational time) to propagate structural model variability to linear and Computational Fluid Dynamic (CFD) based aeroelastic stability is investigated. In this work only the uncertainty associated with the structural model is addressed, but the approaches developed can be also used for other types of non-structural uncertainties.

Whichever propagation method is used, an issue of very practical significance is the initial estimation of the parameter uncertainty to be propagated particularly when the uncertain parameters cannot be measured, such as damping and stiffness terms in mechanical joints or material-property variability. What can be measured is the variability in dynamic behaviour as represented by natural frequencies, mode shapes, or frequency response functions. The inverse problem then becomes one of inferring the parameter uncertainty from statistical mea-

sured data. These approaches are referred to as stochastic model updating or uncertainty identification.

Two new versions of a perturbation approach to the stochastic model updating problem with test-structure variability are developed. A method based on minimising an objective function is also proposed for the purpose of stochastic model updating. Distributions of predicted modal responses (natural frequencies and mode shapes) are converged upon measured distributions, resulting in estimations of the first two statistical moments of the randomised updating parameters. The methods are demonstrated in numerical simulations and in experiments carried out on a collection of rectangular plates with variable thickness and also variable masses on a flat plate.

Stochastic model updating methods make use of probabilistic models for updating same as the perturbation methods developed in this work. This usually requires large volumes of data with consequent high costs. In this work the problem of interval model updating in the presence of uncertain measured data is defined and solutions are made available for two cases. In the first case, the parameter vertex solution is used but is found to be valid only for particular parameterisation of the finite element model and particular output data. In the second case, a general solution is considered, based on the use of a meta-model which acts as a surrogate for the full finite-element/mathematical model. The interval model updating approach is based on the Kriging predictor and an iterative procedure is developed. The method is validated numerically using a three degree of freedom mass-spring system with both well-separated and close modes. Finally the method is applied to a frame structure with uncertain internal beams locations. The procedure of interval model updating, incorporating the Kriging model, is used to identify the locations of the beams at each configuration and to update the bounds of beams positions based on measured data. The method successfully identifies the locations of the beams using six measured frequencies. The updated bounds are found to be in good agreement with the known real bounds on the position of the beams as well.

Acknowledgements

I would like to express my deepest gratitude to my supervisor, Professor John E Mottershead, for his continuous encouragement, guidance and support which were essential to the completion of this work. It is my sincere hope that we can continue working together beyond the boundaries of this appointment.

Also, I would like to thank my second supervisor Professor Kenneth J Badcock for his valuable instructions and for providing me the opportunity to work with his research group in the CFD laboratory.

My thankfulness also goes to Professor Hamid Ahmadian, my initial supervisor in IUST, who has provided educational guidance and incentive through course work and through valuable advice regarding my research.

A special thank you goes to Dr Simon James who has always been ready to help when I was doing experiments in the Dynamics and Control Lab and whose knowledge and advice is greatly valued.

I also thank the guidance from Professor Huajiang Ouyang in Dynamics and Control group at the University of Liverpool. I would also like to thank my colleagues and friends, Dr Marco Prandina, Dr Simao Marques, Dr Gareth Vio, Dr Nurulakmar Abu Husain, Dr Mehdi Ghoreyshi, Dr Maryam Ghandchi Tehrani, Dr Dan Stancioiu, Dr Weizhuo Wang and Mr Mohammad Yazdi Harmin in the Dynamics and Control Group and CFD Lab at the University of Liverpool for their friendship and support.

Finally, I would like to thank my wife, Maryam Shalforoshan, who encourages me and supports me emotionally while I was doing this work. I am also so grateful to my father, Hosseinali Haddad Khodaparast, and my mother, Sorayya Naemi Azghadi for their constant support, help and care during my life.

This work is funded by the European Union for the Marie Curie Excellence Team ECERTA under contract number MEXT-CT-2006 042383.

Contents

List of Figures

List of Tables

List of Symbols and Abbreviations

X	General random parameter
$\Delta\mathbf{x}$	General random vector/matrix
$P(\bullet)$	Probability of event $\bullet$
$F_{\bullet}(\bullet)$	Cumulative distribution function of $\bullet$
$E(\bullet)$	Expected value of $\bullet$
$\mathbf{V}_{\bullet}$	Covariance matrix of $\bullet$
$\mathrm{Cov}(\bullet, \circ)$	Covariance of $\bullet$ and $\circ$
$\mathrm{Var}(\bullet)$	Variance of $\bullet$
$\mathbf{I}$	Identity matrix
$\mathbf{G}$	Hessian matrix
$C(\bullet, \circ)$	Correlation function
$\mathbf{S}$	Sensitivity matrix
$\mathbf{T}$	Transformation matrix
$\mathbf{M}_{\phi}$	Modal mass matrix
$\mathbf{C}_{\phi}$	Modal damping matrix
$\mathbf{K}_{\phi}$	Modal stiffness matrix
$\mathbf{B}_{\phi}$	Modal aerodynamic damping matrix
$\mathbf{Q}_{\phi}$	modal aerodynamic stiffness matrix
$\mathbf{W}$	Weighting matrix
$\mathbf{A}_{ff}$	Weighting matrix
$\mathbf{R}_f$	Fluid residual
$\mathbf{R}_s$	Structural residual
$\mathbf{A}_{ff}$	Fluid Jacobian matrix
$\mathbf{A}_{fs}$ ($\mathbf{A}_{sf}$)	Fluid-structure (Structure Fluid) Jacobian matrix
$\mathbf{A}_{ss}$	Structural Jacobian matrix
E	Elastic modulus

V	Velocity
I	Moment of inertia
A	Area
L	Length
$L_\bullet(\bullet)$	Log-likelihood function of $\bullet$
$\mathbf{R}$	Correlation matrix
$\breve{I}$	Indicator function
$N_\bullet$	$\bullet$-dimensional multivariate normal (Gaussian) distribution
$\breve{M}$	Moment generator
$\mathbf{x}$	Vector of inputs (in general)
x_i	i^{th} input (in general)
$\mathbf{y}$	Vector of outputs (in general or aeroelastic response)
y_i	i^{th} output (in general or aeroelastic response)
n_r	Number of responses
p	Number of parameters
n_s	Number of samples
n_s	Number of normal modes
m	Mass parameter
k	Stiffness parameter
r_g	Regularisation parameter
b_f	Bifurcation parameter
$\mathbf{p}$	Complex eigenvector
$\mathbf{z}_m$	Measured output data
$\mathbf{z}$	Analytical/numerical output data
$f_\bullet(\bullet)$	Probability Density Function of $\bullet$
s_k	Skewness
k_u	Kurtosis
$\mathbf{g}$	Gradient vector
e, exp	Exponential function
$\mathbf{w}_f$	Fluid unknowns
$\mathbf{w}_s$	Structural unknowns
kr	Kernel function
β	Regression coefficient

$\mu^{'(r)}$	The r^{th} raw moment of a random parameter
$\mu^{(r)}$	The r^{th} central moment of a random parameter
$\kappa^{(r)}$	The r^{th} central moment of a random parameter
σ	Standard deviation
λ	Eigenvalue
ρ	Mass density
ρ	Correlation coefficient
θ	Structural parameters
ω	Frequency
γ	Damping or eigenvalue real part
$\eta(\bullet)$	Fuzzy membership function of $\bullet$
ϵ	Errors or residual
$\upsilon(\bullet)$	random field
ϕ	Mode shape (eigenvector)
$\Delta\theta$	Random structural parameters
χ	Eigenfunction
ξ	A set of uncorrelated random parameter
ζ, ν	Correlation parameters
$\Re$	One-dimensional real domain
$\Re^{\bullet}$	$\bullet$-dimensional real domain
$\Re^{\bullet\times\circ}$	$\bullet \times \circ$-dimensional Real domain
$\sum$	Summation
$\prod$	Multiplication
$\int$	Integral
$\|\bullet\|$	Euclidian norm of $\bullet$
$\|\bullet\|_F$	Frobenius norm of $\bullet$
$\|\bullet\|$	Determinant of matrix $\bullet$ or absolute value of scalar $\bullet$
$\underline{\bullet}$	Lower bound of $\bullet$
$\overline{\bullet}$	Upper bound of $\bullet$
$\widehat{\bullet}$	Mean value of $\bullet$
$\frac{\partial \bullet}{\partial \circ}$	First partial derivative of $\bullet$ to $\circ$
$\frac{\partial^2 \bullet}{\partial \circ \partial *}$	Second partial derivative of $\bullet$ to $\circ$ and $*$
$\widetilde{\bullet}$	Uncertain parameter represented with interval/fuzzy set

PDF	Probability Density Function
CDF	Cumulative Distribution Function
RSM	Response Surface Method
MSE	Mean Square Estimator
CCD	Composite Central Design
MCS	Monte Carlo Simulation
MCMCS	Markov Chain Monte-Carlo Simulation
LHS	Latin Hypercube Sampling
MAC	Modal Assurance Criterion
COMAC	Coordinate Modal Assurance Criterion
CFD	Computation Fluid Dynamic
GVT	Ground Vibration Test
COV	Coefficient of Variation
FRF	Frequency Response Function
Mach	Mach number
UB	Upper Bound
LB	Lower Bound
FD	Feasible Direction
LCO	Limit Cycle Oscillation

Chapter 1

Introduction

1.1 Introduction

A general introduction of the research and motivation for the work is given in this chapter. Several areas including finite element methods (Section 1.2), model updating techniques (Section 1.3), structural variability propagation and identification methods (Section 1.4) are covered in this chapter. The scopes of this thesis and its relative topics are presented in Section 1.5. Finally, Section 1.6 explains the organisation of the thesis.

1.2 Finite Element Method (FEM)

The construction and analysis of large and sophisticated numerical models in modern computers has nowadays become an essential subject of structural design in engineering. Finite element method [1] is generally the most reliable and widespread technique for numerical modelling in engineering design. In the finite element method, complicated structures are divided into discrete areas or volumes known as 'elements' with simple and standard geometrical shapes (e.g. beams or shells). The dynamic behaviour of these simple structures is known. The original structure can then be rebuilt from such elements to understand its overal dynamic behaviour. Finite element modelling and analysis provides predictions of the dynamic behaviour of structures under different types of loadings. This can help design engineers to detect any deficiency in the structure from the early stages of the design process and consequently reduce the costs of design (e.g. by reducing the number of prototypes). However, the finite element methods

are approximate and there are different sources of errors in this approximation. Three sources of errors have been typically identified in finite element methods: model-structure errors, model-parameter errors and model-order errors.

Uncertainty in the governing equation or mathematical model of elements is a type of model-structure error. For example, it is not still fully understood how a mechanical joint behaves in a dynamic environment. This is a serious impediment to accurate modelling. The review paper by Ibrahim and Pettit [2] and references therein show the considerable attention that has already been paid to the subject of mechanical joint modelling.

Parameterisation of inaccurate parts in the finite element model and assignment of model parameter values are crucial to the construction of finite element models. The model output data such as natural frequencies and mode shapes are often sensitive to small changes in these parameters. Therefore inaccurate values of the model parameter can give misleading results. The application of informed engineering judgement is particularly important for model parameterisation. Experiments together with finite element model updating tools [3, 4] can also be used to improve the accuracy of model parameter values.

In order to obtain the element mass and stiffness matrices of the finite element model, an assumed displacement solution may be used for the element based on nodal variables. The mass and stiffness coefficients are then determined by the minimisation of either an energy functional or the residues of the equation of motion. However, the solution of the assembled system inevitably includes errors due to discretisation of the continuous system in the finite element model. This is referred to as the third source of error. The effect of model-order errors may be reduced by using different approaches for formulation of the element mass and stiffness matrices such as the inverse method proposed by Ahmadian et al. [5].

Among the methods that attempt to reduce the errors in finite element predictions. the finite element model updating techniques are considered in this thesis and described in the following section.

1.3 Finite element model updating methods

Finite element model updating, at its most ambitious, is about improving and correcting invalid assumptions by processing experimental results [3,4]. A vibration test provides data on the vibratory response, which is then used to update key parameters in the structural model to better match the measurements. The finite element model updating [3,4] is well established, both in the development of methods and in application to industrial-scale structures. These methods can be broadly classified into three categories, namely the direct methods, the iterative methods using modal data and the iterative methods using FRF data. In direct method, a 'representational' model including the updated global mass and stiffness matrices are obtained that is capable of reproducing the measured data exactly. The major disadvantage of these methods is the lack of insight into the modelling errors and confidence about the connectivity of the nodes. In the iterative methods using modal or FRF data, an iterative process based on sensitivity analysis is required in order to minimise an objective function which consists of the difference between predicted modal or FRF data and their measured counterparts. Issues of convergence and ill-conditioning of the matrices [6] are associated with these iterative methods.

It is evident that better accuracy of measured data often leads to a better estimation by the updating method. However, in practical exercises of model updating, the measured data are often imprecise, incomplete and variable. On the other hand, experimental variability exists due to different sources. It may arises from measurement noise, the use of sensors that affect the measurement or signal processing that might introduce bias. Such variability is reducible by increased information. The model updating techniques concerned with this type of variability are referred to as deterministic model updating. In these methods only one value is obtained for the updating parameters and the estimates of distributions/ranges of updating parameters are indicators of the level of confidence in the identified parameters. On the other hand, the experimental variability may be be inherent to the test structure-variability such as manufacturing and material variability in structures which is not reducible and needs to be considered as

part of the model. This introduces the subject of stochastic finite element model updating or uncertainty identification which is the main focus of this thesis. The stochastic finite element model updating/uncertainty identification is described in the next section.

1.4 Structural variability propagation and identification methods

The test structure-variability arises from existing variability in structural parameters such as thickness, material properties or joint parameters (stiffness and damping). Some of these parameters (e.g. thickness) are measurable and their range/distribution of variation can be directly determined by performing a series of measurements.

Different uncertain models may be considered to represent the uncertainty in the structural parameters. They may generally be categorized in two groups: probabilistic models and non-probabilistic (possibilistic) models. In probability theory, the uncertain parameters are defined as random variables in a sample space. The sample space represents the region that includes all possible events and the probability of an event is defined as the ratio of the number of occurrences of that event over the total number of occurrences in the sample space. For a continuous random variable, the role of the frequency function is taken by a Probability Density Function (PDF) [7]. Uniform, exponential, Gama and normal distribution functions are examples of PDFs for a random variable. Selection of the parameter probability distribution needs a large number of measurements. Normal (Gaussian) or multivariate normal distributions are frequently chosen in the literature. The main reasons for choosing the normal distribution are due to their well-known statistical properties, their easily estimated parameters, and their wide availability in software packages [8]. However the validity of this assumption needs to be justified. Probabilistic models have been the most popular for numerical uncertainty modelling so far.

Once the probabilistic model is chosen for the uncertain parameters, the consequent uncertainty in the numerical model prediction can be quantified. This is

referred to as uncertainty propagation, explained in Chapter 2. These methods are also called probabilistic finite element procedures [9] in some specific applications. The Monte Carlo Simulation (MCS) method is the most popular implementation of probabilistic numerical analysis [10,11]. In the MCS a large number of samples of the uncertain parameters selected from an assumed probability distribution is used to evaluate the dynamic responses of the deterministic numerical model. Kernel density estimation [12], applied to the discrete responses, results in a continuous probability density function by constructing a weighted sum of the Gaussian PDFs centred on each sample. However the MCS is computationally expensive and may be impractical for realistic numerical models due to the size and complexity of the structure (e.g. aircraft structure). Therefore there has been much interest in using efficient probabilistic approaches. The mean-centred perturbation method has been frequently used for forward propagation in structural dynamics (for example [13–15]). The perturbation method is computationally efficient compared with the MCS. However, the perturbation method works well when the uncertainties are small and the parameter distribution is Gaussian. Using higher order perturbation may improve the accuracy of the estimation. Adhikari and Friswell [16] proposed a method based on asymptotic approximation of multidimensional integrals. 'Small randomness' and Gaussian PDF assumptions are not required by this method.

During the last decade, there has been increased interest in using the non-probabilistic model of uncertain parameters in finite element approaches. This is due to lack of knowledge of the probability density function of uncertain parameters. A number of mathematical models have been developed in order to represent the uncertainty in parameters using a non-probabilistic approach with limited available information. The interval model is considered the simplest form of non-probabilistic model. Uncertain parameters are defined by variation within the range of an interval consisting of a lower and upper bound. The subject of interval vectors and matrices was introduced by Moore [17]. The propagation of structural uncertainty through finite element analysis, when the uncertain parameters are defined within intervals, is called the interval finite element method [18]. The solution of interval finite element equations focuses on finding the minimal

and maximal deterministic analysis results considering all possible values of input parameters within the interval uncertainty representation. The parameter vertex solution [19] is the simplest and most efficient method for interval analysis, but its application is only valid for restricted classes of dynamic problems. In the parameter vertex solution, the vertices of the uncertain input data (modelled with intervals) map to the vertices of the output data. The application of global optimisation procedure for estimation of the upper and lower bounds of the output data may be the most reliable technique for interval finite element analysis.

The interval model for representing uncertainty was later used in the development of the theory of fuzzy sets. The fuzzy description of uncertain parameters was introduced by Zadeh [20] for representing uncertainty in non-probabilistic form. The uncertainty is defined through a membership function which consists of the level of membership to the fuzzy set for each element in the domain [21]. The membership function values range from zero to one. A membership function value of one denotes that the point definitely belongs to the fuzzy set while a value of zero for membership function shows that the point is definitely not a member of the fuzzy set. The fuzzy finite element method, introduced by Chen and Rao [22], has been used recently by Moens and Vandepitte [23] for the calculation of uncertain frequency response functions of damped structures. The solution of the fuzzy finite element method is often provided with a number of numerical solutions of the underlying interval finite element problem at different membership function levels. The application of uncertainty propagation methods in the problem of flutter analysis will be presented in Chapter 4.

The propagation of uncertain parameters in finite-element models has been carried out frequently but is of limited value when the uncertain parameters cannot be measured, typically damping and stiffness terms in mechanical joints or material-property variability. In this case the variability in dynamic behaviour, as represented by natural frequencies or mode shapes, can be measured. The identification of the parameter uncertainty from statistical measured data may be cast as an inverse problem. This type of problem is referred to as stochastic model updating or uncertainty identification. Few research papers have addressed this problem in the literature. Fonseca et al. [24] proposed an optimisation pro-

cedure for the purpose of stochastic model updating based on the maximising a likelihood function and applied it to a cantilever beam with a point mass at an uncertain location. Mares et al. [25] adapted the method of Collins et al. [26] within a gradient-regression formulation for the treatment of test-structure variability. Hua et al. [27] used perturbation theory in the problem of test-structure variability. The predicted output mean values and the matrix of predicted covariances were made to converge upon measured values and in so doing the first two statistical moments of the uncertain updating parameters were determined. A comparative study on the performance of existing stochastic finite element model updating methods is carried out in this thesis and the results are shown in Chapter 3. New perturbation methods and the interval model updating method have been developed in this thesis and are explained in Chapters 5 and 6.

1.5 Scope of the thesis

The scope of this thesis is to model, propagate and identify the irreducible structural uncertainty in numerically expensive analysis such as aeroelastic analysis. It aims to consider existing models for representing uncertain structural parameters and to propagate them through aeroelastic analysis. Various propagation methods are tested in terms of computational efficiency together with their level of accuracy in predictions. In the forward propagation methods, the ranges/statistical distribution of output data are obtained from ranges/statistical distribution of input data. However, in some cases the input data are not directly measurable. In these cases, the inverse problem may be implemented to obtain the information on uncertain structural parameters from the measured output data. This later objective of the thesis is referred to as uncertainty identification or stochastic model updating.

Firstly, the problem of linear and Computational Fluid Dynamics (CFD) based flutter analysis in the presence of structural uncertainty is addressed. Whereas the propagation of uncertain structural parameters in finite element models has been carried out by a number of different methods, there appears to be less published work on the influence of random structural parameters on

flutter speed. Having a finite element model with an estimate of the possible distribution or range of these parameters, methods can be used to propagate structural parameter distributions/ranges through to flutter speed distributions. Different methods have been investigated: Monte-Carlo simulation, first and second order perturbation analysis, Fuzzy methods and interval analysis. These forward propagation methods have been used for both linear aeroelastic stability and CFD-based aeroelasticity.

The propagation of structural uncertainty to aeroelastic analysis raises the question of how the ranges or statistical distribution of immeasurable parameters can be estimated. To address this issue, the problem of stochastic finite element model updating has been defined. The thesis continues with this subject. A new method, based upon the perturbation procedure, is developed in two versions. In the first version of the method, the correlation between the updated parameters and measured data is omitted. This results in a procedure that requires only the first-order matrix of sensitivities. The second procedure includes this correlation (after the first iteration) but is a more expensive computation requiring the second-order sensitivities. It is shown in numerical simulations that the first method produces results that are equally acceptable to those produced by the second method. Another method based on an objective function for the purpose of stochastic model updating is also proposed. The objective function consists of two parts: 1- the Euclidean norm of the difference between mean values of measured data and analytical output vectors, and 2- the Frobenius norm of the difference between the covariance matrices of measured data and analytical outputs. The two methods are verified numerically and experimentally using multiple sets of plates with randomised thicknesses and masses.

Although the probabilistic perturbation method is quite efficient, its range of application is limited to small uncertainties and normal distributions. This method also works well in the presence of large volumes of test data. The interval model updating method is proposed in this thesis to overcome these limitations of the perturbation method. The problem of interval model updating in the presence of uncertain measured data is defined and solutions are made available for two cases. It is shown that the problem can be solved by using the parameter

vertex solution [19] when (i) the overall mass and stiffness matrices are linear functions of the updating parameters, (ii) the overall mass and stiffness matrices can be decomposed into non-negative-definite substructural mass and stiffness matrices and (iii) the output data are the eigenvalues of the dynamic system. Two recursive updating equations are developed to update the bounds of an initial hypercube of updating parameters in this case. However, it is shown that the parameter vertex solution is not available generally when, for example, the output data include the eigenvectors of the structural dynamic system and the system matrices are non-linear functions of the updating parameters. The general case is solved by using a meta-model which acts as a surrogate for the full finite element model, so that the region of input data is mapped to the region of output data with parameters obtained by regression analysis. The method is demonstrated in numerical simulations and experimental example including a frame structure with uncertain internal beam locations.

1.6 Outline of the thesis

Chapter 2 gives the background theory for uncertainty analysis. The uncertainty models and their mathematical properties are explained in detail. The uncertainty propagation methods are also described and the advantages and disadvantageous of them are discussed.

Chapter 3 provides a literature review on statistical model updating method in the presence of uncertain measured data. The minimum variance methods, Bayesian updating and stochastic model updating methods based on the maximum likelihood and perturbation theory are explained and a comparative study is carried out in a numerical example.

Chapter 4 addresses the problem of linear flutter analysis in the presence of structural uncertainty. Different forward propagation methods, interval, fuzzy and perturbation are applied to linear aeroelastic analysis for a variety of wing models (Goland wing with store and without store and a generic fighter aircraft). This chapter also explains the work done on the feasibility of using these methods (in terms of computational time) to propagate structural model variability to

aeroelastic stability prediction, when using CFD. The method uses an eigenvalue based method which can be configured for the purpose of computing stability for many similar structural models.

Chapter 5 describes the mathematical formulation of two new versions of the perturbation method. A further method based on minimisation of an objective function is also explained in this chapter. The verification of methods by numerical examples and experimental study, including plates with random thicknesses and masses, are demonstrated.

Chapter 6 shows the mathematical formulation of the problem of interval model updating. The method is verified numerically and experimentally using a frame structure with uncertain locations of internal beams.

Chapter 7 gives the conclusions of the research and suggestions for future work.

Chapter 2

Background theory for uncertainty modelling and propagation

2.1 Introduction

Nowadays the design of structures is mainly based on predictions from numerical models. However, the quality of the numerical results depends on their representation of physical behaviour. Inherent uncertainties in structural parameters arising from manufacturing processes, lead to the need for creating statistical rather than deterministic models. This can increase confidence by providing further information.

There are generally two classes of uncertainty: epistemic and aleatoric (irreducible) uncertainty [28]. Epistemic uncertainty is mainly caused by the lack of knowledge, which is reducible by further information. Lack of confidence arising from either the choice of numerical method or the fidelity of modelling assumptions is a form of this type of uncertainty. On the other hand, aleatory uncertainty includes randomness in parameters; For example, variability in structural parameters arising from the accumulation of manufacturing tolerances or environmental erosion. This type of uncertainty is irreducible and is the main concern of this work.

Several methodologies have been developed to introduce the effects of irreducible uncertainty into the design procedure or engineering analysis. Two popular classes of methods have emerged: probabilistic and non-probabilistic methods [29]. This chapter deals with the necessary mathematical tools that are used in this thesis. First, probabilistic and non-probabilistic models for uncer-

tainty modelling are explained. Basic properties of probabilistic models such as the Gaussian distribution are described, followed by some explanation of non-probabilistic models such as interval and fuzzy models. Interval and fuzzy models are then considered and explained for non-probabilistic models. Finally, methods for propagation of input parameter uncertainties through deterministic analysis, known as uncertainty propagation, are explained. The purpose of uncertainty propagation methods is to quantify the consequent uncertainty in the outputs. The propagation methods discussed in this chapter include Monte Carlo Simulation (MCS), perturbation methods, asymptotic integral, interval, fuzzy and meta-models.

2.2 Uncertainty modelling

Uncertainty can be modelled using different mathematical tools, which may be categorised into two groups: probabilistic models and non-probabilistic models. The probability theory (or random parameters) and random fields are used for the former and described in Sections 2.2.1 and 2.2.2, while the interval model and fuzzy sets are considered as non-probabilistic models which are explained in Sections 2.2.3 and 2.2.4.

2.2.1 Probabilistic models: Random parameters

A mathematical way of quantifying uncertainty is by the use of probability theory. In the probability theory, a domain of possible values for the random parameter X is defined and the frequency of occurrences or likelihood of the random parameter being inside a certain domain is given by a Probability Density Function (PDF) $f_X(x)$. The PDF has following properties: $f_X(x) \geq 0$ and $\int_{-\infty}^{+\infty} f_X(x)\,dx = 1$. The PDF can be used to evaluate the probability of occurrence of a random parameter in a particular domain of interest, i.e. if X is a random parameter with PDF $f_X(x)$, the probability that X falls in the interval $\left[\ a \quad b\ \right]$, indicated by $P(a \leq X \leq b)$, is [7]

$$P(a \leq X \leq b) = \int_{a}^{b} f_X(x)\, dx \tag{2.1}$$

Based on Eq. (2.1), another common definition used in finding the probability properties of a continuous random parameter X, known as the Cumulative Distribution Function (CDF), can be defined [7] as,

$$F_X(x) = P(X \leq x) = \int_{-\infty}^{x} f_X(x)\, dx \tag{2.2}$$

The CDF shows the probability that random parameter X is smaller than a deterministic value x. It can be seen in Eq. (2.2) that the PDF is the derivative of the CDF with respect to x, i.e., $f_X(x) = dF_X(x)/dx$.

The expected value (or expectation, mathematical expectation, or mean value or average) of a function $u(X)$ of the random parameter X is the most common value that can be obtained by calculating the integral

$$E(u(X)) = \int_{-\infty}^{+\infty} u(x) f_X(x)\, dx \tag{2.3}$$

The raw moments $\mu'^{(r)}$ of the random parameter X can be obtained by taking $u(X) = X^r$ where $r = 1$ gives the first moment $\widehat{X} = E(X)$, while the second raw moment, $E(X^2)$, is the mean-square of X. The features of a probabilistic quantity are often defined by the central moments associated with the PDF. The first central moment $\mu^{(r)}$ is equal to the first raw moment $\mu'^{(r)}$ which is the mean $\widehat{X}$. The r^{th} central moment $\mu^{(r)}$ $(r \geq 2)$ is given by,

$$\mu^{(r)} = \int_{-\infty}^{+\infty} \left(x - \widehat{X}\right)^r f_X(x)\, dx, \qquad r = 2, 3, 4, \ldots \tag{2.4}$$

which is related to the r^{th} raw moments using the following recursive equation [30]

$$\mu^{(r)} = E\left(\left(X - \widehat{X}\right)^r\right) = \sum_{k=0}^{r} \frac{r!}{k!\,(r-k)!} (-1)^{r-k} \mu'^{(r)} \widehat{X}^{r-k} \tag{2.5}$$

The second order central moment, known as the variance of the distribution, is the most commonly used central moment, and is denoted by $\text{Var}(X) = \sigma_X^2$. σ_X is

referred to as the standard deviation and is a common measure for the scattering of the distribution about its mean. The degree of uncertainty of X is described as the ratio of the standard deviation to the mean $\sigma_X/\widehat{X}$. This ratio is called Coefficient of Variation (COV). Skewness (s_k) , a measure of the asymmetry of the probability distribution, and kurtosis (k_u), a measure of the flatness of the probability distribution, are respectively defined as [31]

$$s_k = \frac{E\left[\left(X-\widehat{X}\right)^3\right]}{\sigma_X^3} \tag{2.6}$$

$$k_u = \frac{E\left[\left(X-\widehat{X}\right)^4\right]}{\sigma_X^4} \tag{2.7}$$

The mathematical formulations for the PDF and CDF of some well-known distributions namely Gaussian (normal), Log-normal, Exponential, Gamma and Chi-square are given in Table 2.1 [7,31]. The distributions of random parameters are often defined by the parameters of the probability distribution function. As can be seen in Table 2.1, the normal and log-normal distribution is defined by two parameters $\widehat{X}$ and σ_X, the exponential distribution is described by only one parameter a, while the Gamma and Chi-square distributions are defined with two parameters, a and b.

The definition of one dimensional random variables can be extended to the multi-dimensional random variables. A random vector $\Delta\mathbf{x} \in \Re^p$ includes an array of p random variables $\{\Delta x_1, \Delta x_2, ..., \Delta x_p\}$ and is characterised by the joint CDF as[1]

$$F_{\Delta\mathbf{x}}(\mathbf{x}) \equiv F(x_1, ..., x_p) \equiv P\left[\{\Delta x_1 \leq x_1\} \cap ... \cap \{\Delta x_p \leq x_p\}\right] \tag{2.8}$$

and the joint PDF $f_{\Delta\mathbf{x}}(\mathbf{x}) : \Re^p \mapsto \Re$ as

$$f_{\Delta\mathbf{x}}(\mathbf{x}) = \frac{\partial^p F(x_1, x_2, ..., x_p)}{\partial x_1 ... \partial x_p} \tag{2.9}$$

The marginal PDF of Δx_i (a component of the random vector $\Delta\mathbf{x}$) can be calculated as

[1]The term $\Delta\mathbf{x}$ is chosen here in order to be consistent with the random structural parameter vector $\Delta\boldsymbol{\theta}$, introduced in Chapter 5.

Table 2.1: Some common probabilistic models for random parameter

Probability distribution	PDF	CDF	Mean	Variance
Gaussian (normal)	$\frac{1}{\sqrt{2\pi\sigma_X^2}}e^{-\frac{1}{2}\left(\frac{x-\widehat{X}}{\sigma_X}\right)^2}$	$\frac{1}{2}+\frac{1}{2}\text{erf}\left(\frac{x-\widehat{X}}{\sqrt{2\sigma_X^2}}\right)$	$\widehat{X}$	σ_X^2
Log-normal distribution	$\frac{1}{x\sqrt{2\pi\sigma_X^2}}e^{-\frac{1}{2}\left(\frac{\ln x-\widehat{X}}{\sigma_X}\right)^2}, \quad x\geq 0$	$\frac{1}{2}+\frac{1}{2}\text{erf}\left(\frac{\ln x-\widehat{X}}{\sqrt{2\sigma_X^2}}\right)$	$e^{\left(\widehat{X}+\sigma_X^2/2\right)}$	$\left(e^{\sigma_X^2}-1\right)e^{\left(2\widehat{X}+\sigma_X^2\right)}$
Exponential	$ae^{-ax}, \quad x\geq 0$	$1-ae^{-ax}$	$\frac{1}{a}$	$\frac{1}{a^2}$
Gamma	$\frac{a^b x^{b-1}}{(b-1)!}e^{-ax}, \quad x\geq 0$	$1-\left(\sum_{i=0}^{b}\frac{(ax)^i}{i!}\right)e^{-ax}$	$\frac{b}{a}$	$\frac{b}{a^2}$
Chi-square	$\frac{(x/2)^{b/2-1}e^{-x/2}}{2\Gamma(b/2)}, \quad x\geq 0$	$\frac{1}{\Gamma(b/2)}\gamma\left(b/2,x/2\right)$	b	$2b$

Γ is the upper incomplete gamma function and is defined as $\Gamma(s,x)=\int_x^\infty t^{s-1}e^{-t}dt$

γ is the lower incomplete gamma function and is defined as $\gamma(s,x)=\int_0^x t^{s-1}e^{-t}dt$

erf is the 'error function' in integrating the normal distribution and is defined as $\text{erf}(x)=\frac{2}{\sqrt{\pi}}\int_0^x e^{-t^2}dt$

$$f_{\Delta x_i}(x_i) = \int_{-\infty}^{+\infty} \cdots \int_{-\infty}^{+\infty} f_{\Delta \mathbf{x}}(\mathbf{x})\, dx_1 \ldots dx_{i-1} dx_{i+1} \ldots dx_p \tag{2.10}$$

Joint Gaussian (normal) density function is a commonly used example of the joint PDF and is given by:

$$f_{\Delta \mathbf{x}}(\mathbf{x}) = \frac{1}{(2\pi)^{p/2} |\mathbf{V}_\mathbf{x}|} \exp\left(-\frac{1}{2} (\mathbf{x} - \widehat{\mathbf{x}})^{\mathrm{T}} \mathbf{V}_\mathbf{x}^{-1} (\mathbf{x} - \widehat{\mathbf{x}})\right) \tag{2.11}$$

where $|\bullet|$ denotes the determinant of matrix $\bullet$, $\widehat{\mathbf{x}}$ and $\mathbf{V}_\mathbf{x} = \mathrm{Cov}(\Delta \mathbf{x}, \Delta \mathbf{x})$ are the mean vector and the covariance matrix respectively which are explained later in this section. The joint PDF is also expressed as $f_{\Delta \mathbf{x}}(\mathbf{x}) = \exp\{-L_{\Delta \mathbf{x}}(\mathbf{x})\}$ for mathematical convenience, where $-L_{\Delta \mathbf{x}}(\mathbf{x})$ is the log-likelihood function. For example, log-likelihood function of the joint Gaussian distribution function of a random vector $\Delta \mathbf{x}$ with mean vector $\widehat{\mathbf{x}}$ and covariance matrix $\mathbf{V}_\mathbf{x}$ (given by Eq. (2.11)) is expressed as [16, 31]

$$L_\mathbf{X}(\mathbf{x}) = \frac{p}{2} \ln 2\pi + \frac{1}{2} \ln |\mathbf{V}_\mathbf{x}| + \frac{1}{2} (\mathbf{x} - \widehat{\mathbf{x}})^{\mathrm{T}} \mathbf{V}_\mathbf{x}^{-1} (\mathbf{x} - \widehat{\mathbf{x}}) \tag{2.12}$$

The first and second joint central moments of a random vector $\Delta \mathbf{x}$ can be obtained from their joint PDF. The expectation value (mean value or first moment), $\widehat{\mathbf{x}}$, is similar to the univariate distribution. The covariance matrix, the second order joint central moment, is defined as

$$\mathbf{V}_\mathbf{x} = \begin{bmatrix} \mathrm{Var}(\Delta x_1) & \mathrm{Cov}(\Delta x_1, \Delta x_2) & \ldots & \mathrm{Cov}(\Delta x_1, \Delta x_p) \\ \mathrm{Cov}(\Delta x_2, \Delta x_1) & \mathrm{Var}(\Delta x_2) & \ldots & \mathrm{Cov}(\Delta x_2, \Delta x_p) \\ \vdots & \vdots & \vdots & \vdots \\ \mathrm{Cov}(\Delta x_p, \Delta x_1) & \mathrm{Cov}(\Delta x_p, \Delta x_2) & \ldots & \mathrm{Var}(\Delta x_p) \end{bmatrix} \tag{2.13}$$

where $\mathrm{Cov}(\Delta x_i, \Delta x_j) = E((\Delta x_i - \widehat{x}_i)(\Delta x_j - \widehat{x}_j))$. The covariance matrix between two different random vectors $\Delta \mathbf{x}_1 \in \Re^{p_1}$ and $\Delta \mathbf{x}_2 \in \Re^{p_2}$ is expressed as:

$$\mathrm{Cov}\left(\Delta\mathbf{x}_1, \Delta\mathbf{x}_2\right) =$$
$$\begin{bmatrix} \mathrm{Cov}\left(\Delta x_{1_1}, \Delta x_{2_1}\right) & \mathrm{Cov}\left(\Delta x_{1_1}, \Delta x_{2_2}\right) & \cdots & \mathrm{Cov}\left(\Delta x_{1_1}, \Delta x_{2_{p_2}}\right) \\ \mathrm{Cov}\left(\Delta x_{1_2}, \Delta x_{2_1}\right) & \mathrm{Cov}\left(\Delta x_{1_2}, \Delta x_{2_2}\right) & \cdots & \mathrm{Cov}\left(\Delta x_{1_2}, \Delta x_{2_{p_2}}\right) \\ \vdots & \vdots & \vdots & \vdots \\ \mathrm{Cov}\left(\Delta x_{1_{p_1}}, \Delta x_{2_1}\right) & \mathrm{Cov}\left(\Delta x_{1_{p_1}}, \Delta x_{2_2}\right) & \cdots & \mathrm{Cov}\left(\Delta x_{1_{p_1}}, \Delta x_{2_{p_2}}\right) \end{bmatrix} \tag{2.14}$$

The following equations can be readily written based on Eqs. (2.13) and (2.14),

$$\mathbf{V}_\mathbf{x} = E\left((\Delta\mathbf{x} - \widehat{\mathbf{x}})(\Delta\mathbf{x} - \widehat{\mathbf{x}})^{\mathrm{T}}\right) \tag{2.15}$$

$$\mathrm{Cov}\left(\Delta\mathbf{x}_1, \Delta\mathbf{x}_2\right) = E\left((\Delta\mathbf{x}_1 - \widehat{\mathbf{x}}_1)(\Delta\mathbf{x}_2 - \widehat{\mathbf{x}}_2)^{\mathrm{T}}\right) \tag{2.16}$$

and the the following properties for covariance matrix can be obtained from Eqs. (2.15) and (2.16),

$\mathbf{V}_\mathbf{x}$: is symmetric and positive semi-definite

$$\mathrm{Cov}\left(\Delta\mathbf{x}_1, \Delta\mathbf{x}_2\right) = \mathrm{Cov}\left(\Delta\mathbf{x}_2, \Delta\mathbf{x}_1\right)^{\mathrm{T}}$$

$$\mathrm{Cov}\left(\Delta\mathbf{x}_1 + \Delta\mathbf{x}_2, \Delta\mathbf{x}_3\right) = \mathrm{Cov}\left(\Delta\mathbf{x}_1, \Delta\mathbf{x}_3\right) + \mathrm{Cov}\left(\Delta\mathbf{x}_2, \Delta\mathbf{x}_3\right)$$

$$\mathrm{Cov}\left(\Delta\mathbf{x}_1 + \Delta\mathbf{x}_2, \Delta\mathbf{x}_1 + \Delta\mathbf{x}_2\right) = \mathrm{Cov}\left(\Delta\mathbf{x}_1, \Delta\mathbf{x}_1\right) + \mathrm{Cov}\left(\Delta\mathbf{x}_1, \Delta\mathbf{x}_2\right) + \mathrm{Cov}\left(\Delta\mathbf{x}_2, \Delta\mathbf{x}_1\right) + \mathrm{Cov}\left(\Delta\mathbf{x}_2, \Delta\mathbf{x}_2\right)$$

$$\mathrm{Cov}\left(\mathbf{B}\Delta\mathbf{x}_1, \mathbf{C}\Delta\mathbf{x}_2\right) = \mathbf{B}\mathrm{Cov}\left(\Delta\mathbf{x}_1, \Delta\mathbf{x}_2\right)\mathbf{C}^{\mathrm{T}}$$

The diagonal terms of the covariance matrix represent the variances of each component of random vector. The off-diagonal terms give a measure of the interdependence between the random vector elements. The off-diagonal terms of covariance matrix can be used to assess the degree of correlation between random variables. The coefficient of correlation between two random variables Δx_1 and Δx_2 is expressed as

$$\rho_{\Delta x_1, \Delta x_2} = \frac{\mathrm{Cov}\left(\Delta x_1, \Delta x_2\right)}{\sigma_X \sigma_Y} \tag{2.17}$$

Two random variables are said to be perfectly correlated if $\rho_{\Delta x_1, \Delta x_2} = \pm 1$ and uncorrelated if $\rho_{\Delta x_1, \Delta x_2} = 0$. Note that if two random variables are independent,

they are uncorrelated but the reverse is not always true. Also, note that if the random variables, belonged to a joint distribution, are statistically independent from each other then the joint probability distribution is

$$f_{\Delta \mathbf{x}}(\mathbf{x}) = f_{\Delta x_1}(x_1) f_{\Delta x_2}(x_2) ... f_{\Delta x_p}(x_p) \tag{2.18}$$

and the off-diagonal terms of the covariance matrix are zeros.

In practical cases, the random variables and vectors exist in the form of discrete variables rather than being continuous. The mean and covariance of random variables (and vectors) can then be calculated from the population of samples using standard equations as shown as follows. In the presence of n_s samples of a p-dimensional random vector $\Delta \mathbf{x}$ in the form of

$$\Delta \mathbf{x} = \begin{bmatrix} \Delta x_{11} & \Delta x_{21} & ... & \Delta x_{p1} \\ \Delta x_{12} & \Delta x_{22} & ... & \Delta x_{p2} \\ . & . & ... & . \\ . & . & ... & . \\ . & . & ... & . \\ \Delta x_{1n_s} & \Delta x_{2n_s} & ... & \Delta x_{pn_s} \end{bmatrix} \tag{2.19}$$

the mean value of each component Δx_i , $i = 1, 2, ..., p$, can be estimated as [7]

$$\widehat{x}_i = \frac{1}{n_s} \sum_{j=1}^{n_s} \Delta x_{ij} \tag{2.20}$$

and each term of covariance matrix can be calculated as

$$\mathrm{Cov}(\Delta x_i, \Delta x_j) = \frac{1}{n_s - 1} \sum_{k=1}^{n_s} (\Delta x_{ik} - \widehat{x}_i)(\Delta x_{jk} - \widehat{x}_j) \tag{2.21}$$

where $\mathrm{Cov}(\Delta x_i, \Delta x_i) = \mathrm{Var}(\Delta x_i)$.

The mathematical formulations that are given in this section include only those which have been used in this thesis. However, a complete account of statistics can be found in the reference books such as [7, 31].

2.2.2 Probabilistic models: Random fields

Many parameters in a physical structure such as thickness, Young's modulus, shear modulus, density and damping are spatially distributed. Random fields can be used to model the spatial variation of these parameters over the region in

which the variation takes place. Figure 2.1, reproduced from [32], shows how the bending stiffness of a beam can be represented as a random field along the length of the beam. The deviations are shown from the baseline value (deterministic value with uniform distribution).

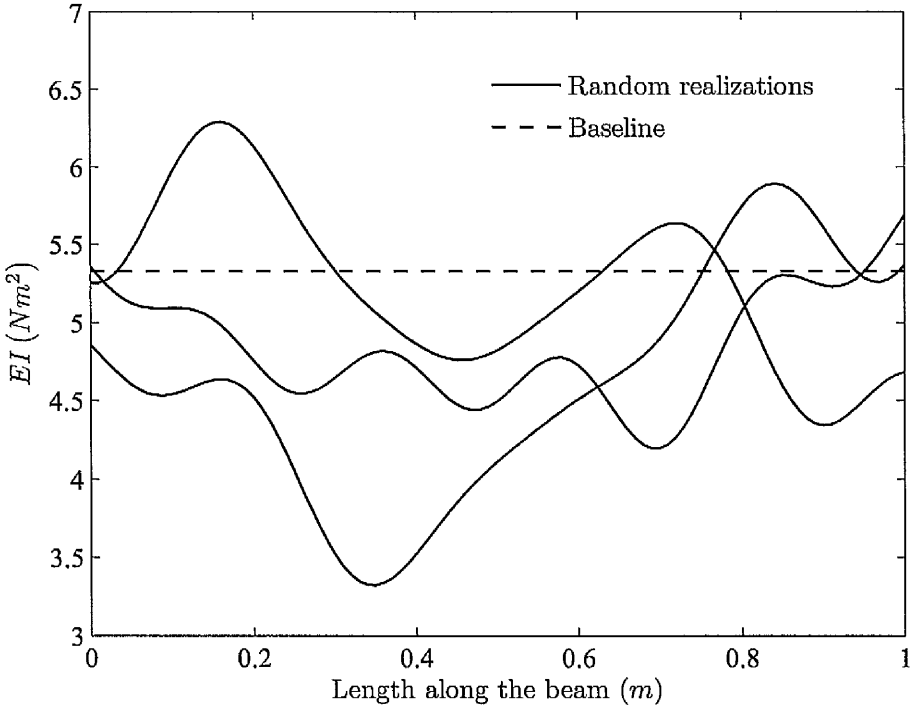

Figure 2.1: The representation of bending rigidity of the beam with mean value $\widetilde{EI} = 5.33Nm^2$ as a random field.

The random field $\upsilon\,(\mathbf{x})$ is the ensemble of random variables at infinite number of points with coordinates $\mathbf{x} = \{x_1, ..., x_{n_f}\}$ (where in theory $n_f \to \infty$) [31], which is impossible to obtain in reality. For example, consider the dynamic response at one point of a mechanical system due to random excitations. In practice, one may measure the time response for a limited period of time. However, the measurement can be repeated to obtain different realisation of the vibration response at each time step. Then, the following concepts may be defined to allow the analyst to make more efficient use of what little data are accessible [31].

- **Homogeneous random field** has a property that the joint PDF remains unchanged when the set $\{x_1, ..., x_{n_f}\}$ is translated in the space of the random variables. The term homogenous is commonly replaced by stationary for one-dimensional random processes, usually in time.

- **Isotropic random field** is a random field in which the joint PDF remains unchanged when the set $\{x_1, ..., x_{n_f}\}$ is rotated in the space of the random variables.

- **Ergodic random field** is a random field where all information about its statistical properties can be obtained from a single realisation of the random field.

In the example of the dynamic response of a mechanical structure due to random excitation, the vibration time response is said to be stationary if the statistical properties of the response (e.g. mean and covariance) remain unchanged when the time is shifted by τ, i.e,

$$E(u(t)) = E(u(t+\tau)) \quad \forall \tau \in \Re \tag{2.22}$$

$$E(u(t)\,u(t+\tau)) = E(u(0)\,u(\tau)) \quad \forall \tau \in \Re \tag{2.23}$$

Eq. (2.22) shows that the mean value remain unchanged. Eq. (2.23) implies that the covariance function depends only on τ which is the difference between two points in random field ($\tau = t_2 - t_1$ or generally $\tau = x_2 - x_1$).

It is not easy to deal with random fields directly in mathematical and numerical models. Therefore there is a need for discritisation of the random field in terms of random variables. Many techniques for the purpose of conversion of continuous random field into discrete random variables have been studied in the literature (e.g. [33]). A technique based on Karhunen-Loeve (KL) [34] expansion is found to be very useful in the application of stochastic finite element method. The KL expansion is defined in a Fourier-type series

$$\upsilon(\{x\}, \zeta) = \widehat{\upsilon}\{x\} + \sum_{i=1}^{\infty} \sqrt{\lambda_i}\chi_i(\{x\})\,\xi_i(\zeta) \tag{2.24}$$

where $\widehat{\upsilon}\{x\} = E[\upsilon(\{x\}, \zeta)]$ is the mean value of random field, $\xi_i(\zeta)$ is a set of uncorrelated random variables, ζ is the correlation parameter which is explained later in this section, the constants λ_i and functions $\chi_i(\{x\})$ are the eigenvalues and eigenfunctions of the correlation function $C(\{x_1\}, \{x_2\})$ as

$$\int_{\Omega} C\left(\{x_1\},\{x_2\}\right)\chi_i\left(\{x_1\}\right)dx_1 = \lambda_i\chi_i\left(\{x_2\}\right)\ \ \forall i = 1,2,... \tag{2.25}$$

The KL expansion decomposes the initial random field into a summation over an infinite number of uncorrelated random variables which are weighted with deterministic functions $\sqrt{\lambda_i}\chi_i\{x\}$. In practical cases, a truncated series of Eq. (2.24) is used. Since the eigenvalues λ_i in Eq. (2.25) are arranged in decreasing order, the truncated series contain lots of information about the random field. For example, to keep 90% information of series expansion, one may choose a number of terms, p, such that $\lambda_p/\lambda_1 = 0.1$ [32]. Many concepts for determining the correlation function have been proposed in the literature. As mentioned earlier, for a stationary random field, the correlation function between the random field values at two locations x_1 and x_2 is a function of the distance $\tau = |x_2 - x_1|$ between these points (where $|\bullet|$ denotes the absolute value of scalar $\bullet$). Reference [31] provides a comprehensive review of the random fields and corresponding correlation functions. The choice of correlation function and its parameters depends on the underlying behaviour of the random field and is often not readily evident. One may use the following correlation function [32]

$$C\left(\{x_1\},\{x_2\}\right) = e^{-\zeta|x_1-x_2|} \tag{2.26}$$

where $|\bullet|$ represents the absolute value of scalar $\bullet$ and ζ, the correlation parameter, is used for description of the random field. The correlation parameter usually only depends on the size of the domain under consideration. Very large values of the correlation parameter is used for representation of a delta-correlated random field. Small value of correlation parameter shows that the random field effectively becomes a random variable [32]. The solution of the eigenfunction problem in Eq. (2.25) with the above correlation function (Eq. (2.26)) in the domain of $-a \leq x \leq +a$ is given in [34].

The KL expansion is recently used for development of stochastic element mass and stiffness matrices for an undamped Euler-Bernoulli beam by Adhikari and Friswell [32]. The bending stiffness EI and mass per unit length of the beam ρA are treated as random field and represented by KL expansion as

$$EI(x,\zeta) = \widehat{EI}\left(1 + \check{\epsilon}_1 v_1\left(\{x\},\zeta\right)\right) \tag{2.27}$$

$$\rho A(x,\zeta) = \widehat{\rho A}\left(1 + \check{\epsilon}_2 v_2\left(\{x\},\zeta\right)\right) \tag{2.28}$$

where $\widehat{\bullet}$ represents the mean value, $0 < \check{\epsilon}_i \ll 1\,(i = 1,2)$ are deterministic constants and $v\left(\{x\},\zeta\right)$ is a random field given in Eq. (2.24) with zero mean. The uncorrelated random variables $\xi_i(\zeta)$ are assumed to have a Gaussian distribution with zero mean and unit standard deviation. Three realisations of bending stiffness treated as a random field, are shown in Figure 2.1. In this example it is assumed that $\zeta = 3/L$ and $\check{\epsilon}_1 = 0.1$ ($L = 1m$ is the length of the beam). The stochastic element stiffness and mass matrices can then be derived based on the KL expansion as [32]

$$K_e(\zeta) = \int_0^{l_e} \widehat{EI}\left(1 + \check{\epsilon}_1 v_1\left(\{x\},\zeta\right)\right) \mathbf{N}'' \mathbf{N}''^{\mathrm{T}} dx \tag{2.29}$$

$$M_e(\zeta) = \int_0^{l_e} \widehat{\rho A}\left(1 + \check{\epsilon}_2 v_2\left(\{x\},\zeta\right)\right) \mathbf{N}\mathbf{N}^{\mathrm{T}} dx \tag{2.30}$$

where $\mathbf{N}$ is the vector containing shape functions and $\bullet'' \equiv d^2(\bullet)/dx^2$. The final form of of these matrices are given in [32].

In this thesis, the random field is not directly used for uncertainty modelling and propagation method. However, the application of random field concept in the construction of a meta-model (Kriging) acting as a surrogate for the full finite-element or mathematical model is investigated in Section 2.3.6 and Chapter 6.

2.2.3 Non-probabilistic models: Interval model

The theory of interval models and analysis is quite old. Archimedes (287–212 BC) [35] calculated the bounds of irrational number π as $3\frac{10}{17} < \pi < 3\frac{1}{7}$ by approximating the circle with inscribed and circumscribed 96-side regular polygons. In the interval approach, the uncertain variables can vary within intervals between extreme values. Interval model is said to be non-probabilistic since no

assumption is made about the probability distribution of the uncertain variables. The uncertain variable $\widetilde{X}$, represented as an interval, is defined as

$$\widetilde{X} \in [\underline{x}, \overline{x}] = [x \in \Re \,|\, [\underline{x} \leq x \leq \overline{x}]] \tag{2.31}$$

The above interval is called 'close' since both upper bound and lower bound belong to the set. The midpoint m_x and radius r_x of an interval are expressed as

$$m_x = \frac{\underline{x} + \overline{x}}{2} \tag{2.32}$$

$$r_x = \frac{\overline{x} - \underline{x}}{2} \tag{2.33}$$

The definition of the interval scalar, given in Eq. (2.31), can be extended to the definition of interval vectors and matrices. The interval vector $\left\{\widetilde{X}_i\right\} \in \Re^p$ and the interval matrix $\left[\widetilde{X}_{ij}\right] \in \Re^{p \times q}$ consist of elements that belong to a number of disjoint interval scalars in $\Re$ which can be expressed as [21]

$$\left\{\widetilde{X}_i\right\} \in \left([\underline{x}_1, \overline{x}_1] \cup ... \cup [\underline{x}_p, \overline{x}_p]\right) \qquad i = 1, ..., p \tag{2.34}$$

$$\left[\widetilde{X}_{ij}\right] \in \left([\underline{x}_{11}, \overline{x}_{11}] \cup ... \cup [\underline{x}_{pq}, \overline{x}_{pq}]\right) \qquad i = 1, ..., p \qquad j = 1, ..., q \tag{2.35}$$

Eqs. (2.34) and (2.35) imply that the components of uncertain vectors/matrices are independent. Therefore, the interval vector represents a hypercube containing the set of all possible combinations of the vector elements. For example, the rectangular, shown in Figure 2.2, describes the space of the possible values of vector elements consisting of two uncertain components $\widetilde{X}_1 \in [\underline{x_1}, \overline{x_1}]$ and $\widetilde{X}_2 \in [\underline{x_2}, \overline{x_2}]$.

Another description of interval vectors $\left\{\widetilde{X}\right\}$ is based on hyperellipse representation as shown in Figure 2.2. The rectangular region, shown in the figure, or more generally the hypercube is replaced by an elliptical area (or hyperellipse). In this model, it is supposed that the points outside the ellipse but within the rectangle are unlikely to be reached. The mathematical description of a closed elliptical set is [21]

$$\left\{\widetilde{X}\right\}^{\mathrm{T}} \mathbf{L} \left\{\widetilde{X}\right\} \leq a \tag{2.36}$$

where $\mathbf{L}$ is a positive definite matrix and a is a positive constant.

In most engineering applications, the input parameters are statistically independent. Therefore, the description of these variables by a hypercube is generally more realistic than the elliptical modelling. The hypercube representation of interval variables is used in this thesis. However, more details about interval modelling can be found in Ref. [17].

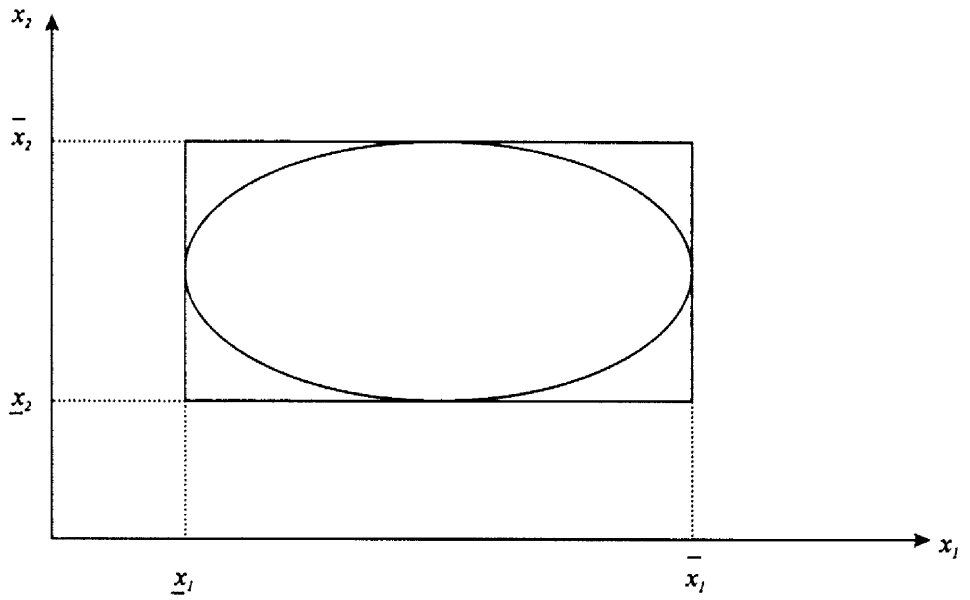

Figure 2.2: Interval representation of an uncertain 2-dimensional vector.

2.2.4 Non-probabilistic models: Fuzzy sets

The fuzzy logic concept for modelling uncertainty through indistinctive definition (instead of probability distribution) was first introduced by Zadeh [20] in 1965. The fuzzy set is considered as an extension of a conventional (crisp) set, which discriminates between elements that belong to the set and those which do not. In the fuzzy concept, a set of transitional states between the members and non-members are defined via a membership function $\eta(x)$ that indicates the degree to which each element in the domain belongs to the fuzzy set. The membership function of a fuzzy set $\eta(x)$ is defined as [21]

$$\widetilde{x} = \{(x, \eta(x)) \,|(x \in X)\ (\eta(x) \in [0,1])\} \tag{2.37}$$

where x is a member of domain X. As can be seen in Eq. (2.37), the membership function value varies between 0 and 1. A membership function value of one shows that x is definitely a member of the fuzzy set, while a membership function value of zero means that x definitely does not belong to the fuzzy set. For instance, the membership function of an uncertain Young's modulus may be considered as shown in Figure 2.3. According to the figure, the values of Young's modulus are definitely within the interval of [206 214] Gpa whereas it is not possible to have the Young's modulus of $E < 200$ Gpa or $E > 220$ Gpa. Moreover, the range of variation of Young's modulus in [203 217] Gpa is possible with the degree of possibility equal to 50%. This demonstrates that the fuzzy logic concept is based on possibility theory [36]. Although, from a strictly mathematical point of view the comparison of probabilistic distributions with fuzzy membership function is not allowed, it may still be useful from a practical engineering perspective. For example, the Gaussian probability function may be approximated by a triangle by equating the area under the normalised Gaussian distribution function with the area under triangular membership function as shown in Figure 2.4. This approximation is explained in [37]. As a result of this approximation the triangular fuzzy membership function can be defined as

$$\eta(x) = \max\left\{0, 1 - \frac{\left|x - \widehat{X}\right|}{\delta}\right\} \tag{2.38}$$

where $\delta = \sqrt{2\pi}\sigma_X$, $\widehat{X}$ and σ_X are the mean and standard deviation of the equivalent Gaussian distribution.

2.3 Uncertainty propagation

Consider an input-output system (e.g. an FE model) with uncertain input parameters, indicated by $\mathbf{x} = \{x_1, x_2, ..., x_p\}$[2]. Figure 2.5 shows a typical input-output system. Due to existing uncertainty in the input parameters, the output parameters, indicated by $\mathbf{y} = \{y_1, y_2, ..., y_p\}$ in the figure, are no longer deterministic and must be obtained from an uncertainty propagation method. Many different un-

[2]At this point what were previously referred to as random variable becomes random parameters, such as randomised parameters in a FE model.

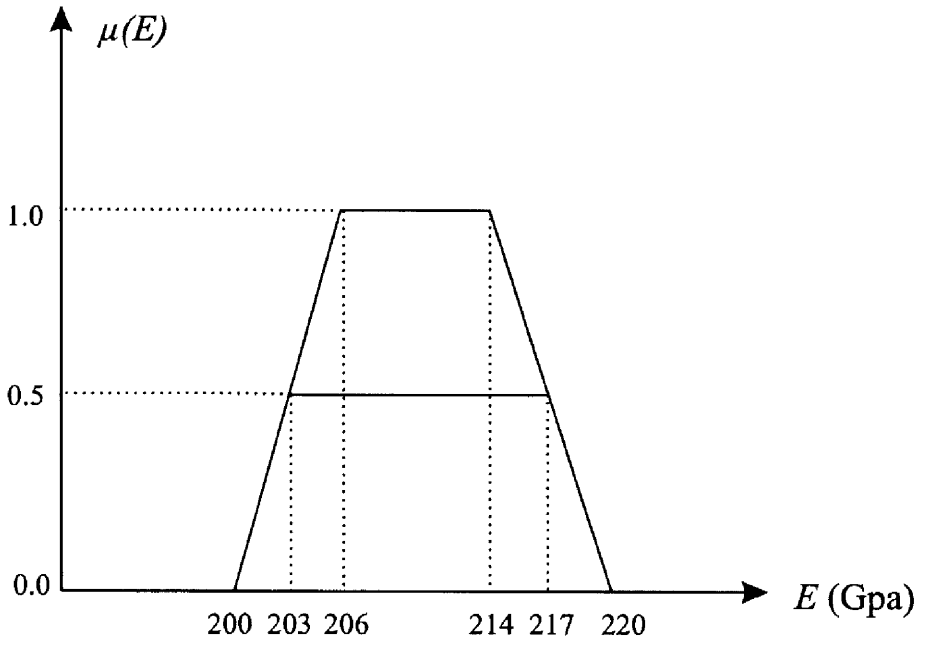

Figure 2.3: Membership function for Fuzzy representation of an uncertain variable (Young's modulus).

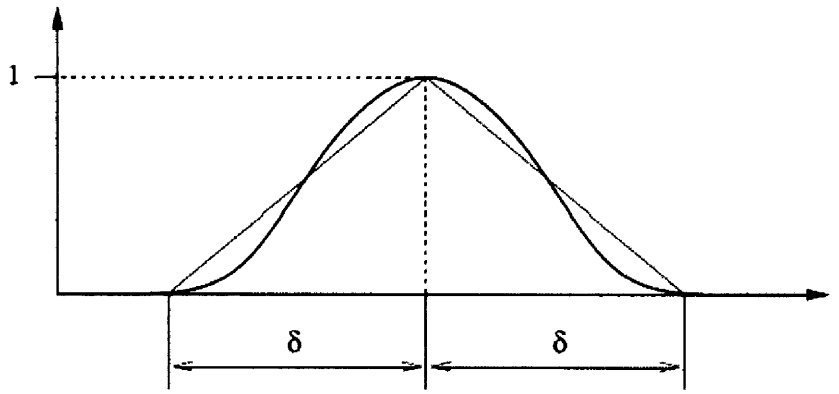

Figure 2.4: Linear approximation of a Gaussian distribution by triangular fuzzy number.

certainty propagation methods have been introduced in the literature e.g. those presented in [16] and [21]. Among existing methods, the Monte Carlo Simulation (MCS), the first and second order perturbation methods, the asymptotic integral method, the interval and the fuzzy logic are selected and explained in this work.

The Monte Carlo Simulation (MCS) is the most accurate and reliable propagation methods. The MCS is based on sampling method which performs sample evaluation of deterministic analysis. The MCS method is discussed in Section 2.3.1. The statistical properties of the responses may also be determined by the perturbation and asymptotic integral methods which incorporate low-order Taylor series. These methods are described in Sections 2.3.2 and 2.3.3 respectively. Interval analysis and fuzzy propagation methods are then explained in Sections 2.3.4 and 2.3.5. These methods are used when the uncertain input parameters are modelled using interval or fuzzy sets. Finally the meta-model is described in Section 2.3.6. The meta-model is not used as an uncertainty propagation method but it can be used together with the sampling and optimisation methods to reduce the computation time of uncertainty propagation method. The use of the Kriging predictor as a meta-model is explained in detail in this section.

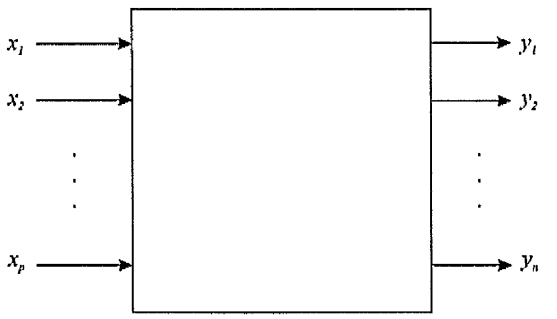

Figure 2.5: An input-output system.

2.3.1 The Monte Carlo Simulation

The MCS is a sample-based method and has been frequently used in the literature for the purpose of uncertainty propagation. In the Monte-Carlo process, a large number of samples (n_s) of uncertain parameter X is generated according to the assumed parameter PDF, while the respective response values, Y, are evaluated

from a deterministic analysis (for instance, FE analysis). The mean and covariance matrix of the output vector from the analytical/numerical model can then be directly evaluated from the scatter of responses and the system parameters that provide the input to the simulation. The flow chart shown in Figure 2.6 [38] illustrates how the analysis process is structured. The number of samples n_s in Figure 2.6 is often determined by displaying the evolution of statistics (e.g. mean and standard deviation) of output data. The convergence on the statistical properties of the data shows the requisite number of samples n_s for the analysis. An example of how the number of samples can be obtained from convergence plot is explained in this section.

The generation of samples in MCS can be carried out with different methods such as multivariate normal sampling [31], Latin Hypercube Sampling (LHS) [39] and Orthogonal Array Sampling [40]. The multivariate normal sampling and LHS have been used in this thesis and are now described.

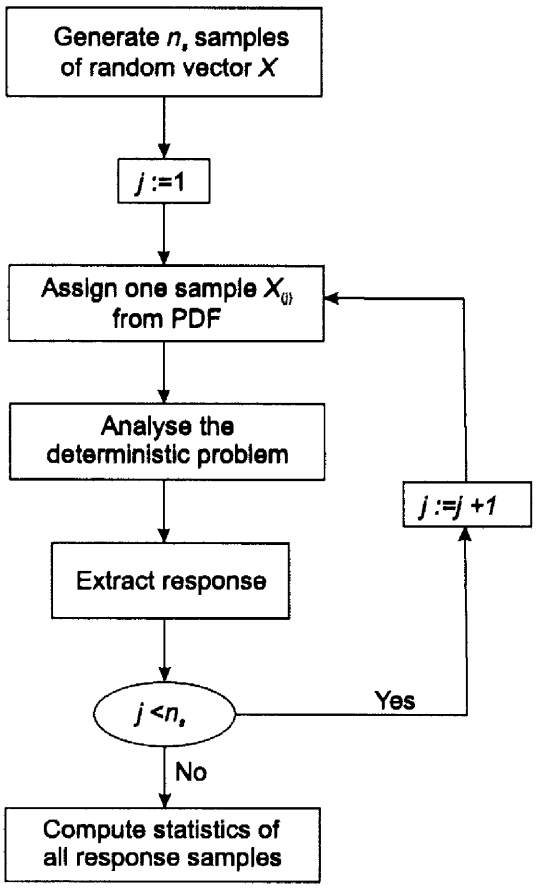

Figure 2.6: Flow of computation of MCS.

Multivariate normal sampling

This method can be used when the uncertain parameters belong to a multivariate normal distribution. If the uncertain parameters are uncorrelated, the covariance matrix is diagonal. The sampling in this case is straightforward as the samples from each component of the random vector can be taken independently to generate a number of sample vectors of the random vector. However, the procedure is slightly different when the uncertain parameters are correlated, where the off-diagonal terms of the covariance matrix are non-zero. As mentioned in Section 2.2.1, the covariance matrix is positive semi definite; therefore, it can be decomposed into the product of a lower triangular matrix $\mathbf{U}$ and its conjugate transpose using Cholesky decomposition [41] as

$$\mathbf{V_x} = \mathbf{U} \times \mathbf{U}^{\mathrm{T}} \tag{2.39}$$

Now, consider a random vector $\boldsymbol{\zeta}$ with uncorrelated random components which are normally distributed with zero mean and unit standard deviation. The sampling of random vector $\mathbf{X}$ with correlated random component can be obtained by sampling the random vector $\boldsymbol{\zeta}$ as

$$\Delta\mathbf{x} = \widehat{\mathbf{x}} + \mathbf{U}\boldsymbol{\zeta} \tag{2.40}$$

where $\widehat{\mathbf{x}}$ is the mean vector of $\Delta\mathbf{x}$.

To illustrate sampling procedure shown in Figure 2.6, consider a two dimensional multivariate normal random parameter $\Delta\mathbf{x} \in N_2\left(\widehat{\mathbf{x}}, \mathbf{V_x}\right)$; where N_2, represents a two-dimensional multivariate normal distribution with $\Delta\widehat{\mathbf{x}} = \left[\begin{array}{cc} 0 & 0 \end{array}\right]^{\mathrm{T}}$ and $\mathbf{V_x} = \mathrm{diag}\left(\left[\begin{array}{cc} 1 & 1 \end{array}\right]\right)$. In order to show the convergence on the statistical properties of a function of Δx_1 and Δx_2, the Rosenbrock's function is considered [42]. This function is expressed as

$$y = f\left(\Delta x_1, \Delta x_2\right) = 100\left(\Delta x_2 - \Delta x_1^2\right)^2 + \left(1 - \Delta x_1\right)^2 \tag{2.41}$$

The reason for choosing this function is due to the fact that it is an algebraic and nonlinear response function that exhibits some of the nonlinear trends often found in engineering analysis. The multivariate normal distribution sampling is used

to determine the statistical properties of the response y. Figure 2.7 shows the convergence diagram on mean and standard deviation of Rosenbrock function. As shown in the figure, after taking 9000 samples of uncertain parameters X_1 and X_2, the mean and standard deviation of the response converge to 409 and 1095, respectively. This shows that $n_s = 9000$ samples can give the asymptotic statistical properties of the output y.

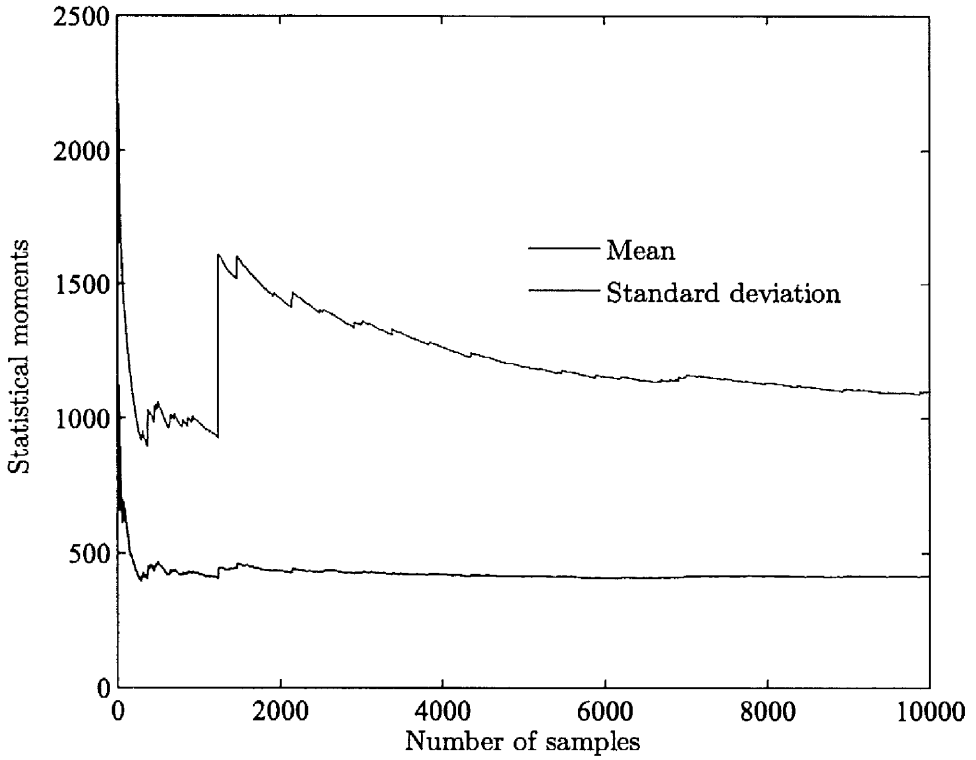

Figure 2.7: Convergence of the Monte Carlo method estimating the mean and standard deviation of Rosenbrock's function.

Latin hypercube sampling

The statistical uncertainty associated with MCS may be reduced by development of Latin Hypercube Sampling (LHS) technique [39]. This method, at its most ambitious, is about ensuring a good coverage of the random parameter space. The idea is to divide the parameter space in subspaces of equal probability. Samples are then taken from each subspace ensuring that every parameter is covered equally. For the one-dimensional case $p = 1$, the sampling procedure can be simply carried out by drawing the samples one by one in random order. However,

the procedure becomes more complex in the presence of multi-dimensional case $p > 1$, owing to the fact that the covering of all possible combinations lead to an exponential growth of the number of required samples. Therefore, keeping the number of samples as small as possible in this case is essential. For example, assume a two-dimensional random vector with uniform and independent distributions in the range of [0 1]. Figure 2.8 [38] illustrates how the LHS can be used to draw samples from this bidimensional parameter space. As shown in the figure, the samples are taken randomly from each subspace such that there is no repeat for drawing samples from the same subspace.

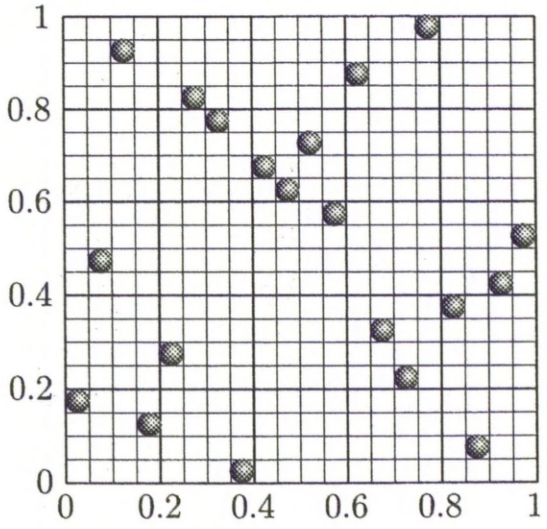

Figure 2.8: Latin hypercube sampling.

Kernel density estimation

The MCS and LHS provide a large number of response samples $[\ y_1 \quad y_2 \quad \cdots \quad y_{n_s}\ ]$ in which the statistical moments of the response can be directly estimated from the population, e.g. by Eqs. (2.20) and (2.21). In the situation where the detailed shape of the underlying density function is of interest, Kernel density estimation can be used [43]. Before explaining the Kernel density estimation, it may be useful to describe the histogram of response samples first. The histogram of the response samples can be constructed by dividing the sample space into a number of intervals and placing each observation over the appropriate interval. The histogram of response $f(y)$ may be expressed as

$$f(y) = \sum_{i=1}^{n_s} \breve{I}\left(y - y_i^{(c)}; h\right) \tag{2.42}$$

where $y_i^{(c)}$ denotes the centre of the interval in which y_i falls and $\breve{I}(\breve{z}; h)$ is the indicator function of the interval $[\ -h \quad h\ ]$ defined as

$$\breve{I}(\breve{z}; h) = \begin{cases} 1 & \text{if} \quad -h \leq \breve{z} \leq h \\ 0 & \text{if} \quad \breve{z} < -h \text{ or } \breve{z} > h \end{cases} \tag{2.43}$$

Further scaling is needed so that f integrates to 1. However, the drawbacks of histogram density function, e.g. (i) information is lost on replacing y_i by the central point of the interval in which it falls, (ii) the estimator is not smooth due the sharp edges of the boxes, and (iii) the behaviour of the estimator is affected by the choice of width of the intervals used, lead to the use of a smooth kernel function instead of a box. The Gaussian (normal) function is a common choice for the kernel function [43]. In this case, the PDF can be estimated using the kernel function with an h bandwidth (smoothing parameter) as

$$f(y) = \frac{1}{n_s} \sum_{i=1}^{n_s} kr(y - y_i; h) \tag{2.44}$$

where $kr(y - y_i; h)$ denotes the normal density function in $\breve{z} = (y - y_i)$ with mean 0 and standard deviation h. Since properties of kr are inherited by $f(y)$, choosing kr to be smooth will produce a density estimate which is also smooth [43].

In the presence of two or more responses, the kernel density estimation which is introduced in Eq. 2.44, is replaced by a multivariate Gaussian (normal) function with an $\mathbf{H}$ bandwidth matrix

$$kr_{\mathbf{H}}(\mathbf{y}) = |\mathbf{H}|^{-1} (2\pi)^{-p/2} e^{-\mathbf{y}^{\mathrm{T}}\mathbf{H}^{-1^{\mathrm{T}}}\mathbf{H}^{-1}\mathbf{y}/2} \tag{2.45}$$

The choice for the bandwidth matrix $\mathbf{H}$ is crucial and the following equation is recommended in [8, 44] for a better estimate

$$\mathbf{H} = n_s^{-1/(p+4)} \mathbf{V}_{\mathbf{y}}^{\frac{1}{2}} \tag{2.46}$$

where $\mathbf{V}_{\mathbf{y}}$ is the covariance matrix of the response samples, evaluated by Eq. (2.21). Eq. (2.46) is used when the number of parameters p is greater than the number

of responses n_r, $p > n_r$. However, in the case of $p < n_r$, $n_r + 4$ is replaced by $p + 4$ in Eq. (2.46).

2.3.2 The perturbation method

Consider a system with uncertain input parameters represented by $\Delta\mathbf{x}$ and uncertain outputs represented by $\Delta\mathbf{y}$. If the uncertain parameters follow a p-dimensional multivariate normal distribution $\Delta\mathbf{x} \in N_p(\widehat{\mathbf{x}}, \mathbf{V_x})$, response of the system can be expanded about the mean value of the uncertain parameters as,

$$\begin{aligned}\Delta\mathbf{y}(\Delta\mathbf{x}) =& \Delta\mathbf{y}(\widehat{\mathbf{x}}) + \sum_{i=1}^{p} \frac{\partial \Delta\mathbf{y}}{\partial \Delta x_i}|_{\Delta x_i = \widehat{x}_i} (\Delta x_i - \widehat{x}_i) \\ &+ \sum_{i=1}^{p}\sum_{j=1}^{p} \frac{\partial^2 \Delta\mathbf{y}}{\partial \Delta x_i \partial \Delta x_j}|_{\Delta x_i = \widehat{x}_i,\, \Delta x_j = \widehat{x}_j} (\Delta x_i - \widehat{x}_i)(\Delta x_j - \widehat{x}_j) + \ldots\end{aligned} \tag{2.47}$$

The assumption of normal distribution for uncertain parameters does not incur loss in generality as any set of non-Gaussian random parameters can be transformed into a set of uncorrelated Gaussian random parameters by using the 'Rosenblatt' transformation or the 'Nataf' transformation [45]. Truncating the series of Eq. (2.47) after the second order term leads to a quadratic form of response $\Delta\mathbf{y}$ as a function of uncertain parameters $\Delta\mathbf{x}$. The theory of Quadratic form in Gaussian random parameters has been extensively discussed in the literature [16, 46, 47]. This method can be used to determine the statistical moments of uncertain response from the truncated Taylor series expansion. It is done by evaluating a term called the moment generating function of each component of the response vector Δy_i, for any $s \in \Re$. The moment generating function can be obtained from

$$\breve{M}_{\Delta y_i}(s) = E\left(e^{s\Delta y_i(\Delta\mathbf{x})}\right) = \int_{\Re^p} e^v d\Delta\mathbf{x} \tag{2.48}$$

where

$$\begin{aligned}v =& s\widehat{y}_i + s\mathbf{g}^{\mathrm{T}}_{\Delta y_i}|_{\Delta\mathbf{x}=\widehat{\mathbf{x}}} (\Delta\mathbf{x} - \widehat{\mathbf{x}}) + \frac{s}{2}(\Delta\mathbf{x} - \widehat{\mathbf{x}})^{\mathrm{T}} \mathbf{G}_{\Delta y_i}|_{\Delta\mathbf{x}=\widehat{\mathbf{x}}} (\Delta\mathbf{x} - \widehat{\mathbf{x}}) \\ &- \frac{p}{2}\ln(2\pi) - \frac{1}{2}\ln|\mathbf{V_x}| - \frac{1}{2}(\Delta\mathbf{x} - \widehat{\mathbf{x}})^{\mathrm{T}} \mathbf{V}_{\mathbf{x}}^{-1} (\Delta\mathbf{x} - \widehat{\mathbf{x}})\end{aligned}$$

where $\widehat{y}_i = \Delta y_i(\widehat{\mathbf{x}})$, $\mathbf{g}_{\Delta y_i}|_{\Delta\mathbf{x}=\bullet} = \left\{\frac{\partial \Delta y_i}{\partial \Delta x_j}\right\}|_{\Delta\mathbf{x}=\bullet}$ is gradiant/sensitivity vector and $\mathbf{G}_{\Delta y_i}|_{\Delta\mathbf{x}=\bullet} = \left[\frac{\partial^2 \Delta y_i}{\partial \Delta x_j \partial \Delta x_k}\right]|_{\Delta\mathbf{x}=\bullet}$ is Hessian matrix. The integral in Eq. (2.48) can be evaluated exactly as [16]

$$\breve{M}_{\Delta y_i}(s) = \frac{e^{\left(s\widehat{y}_i + (s^2/2)\mathbf{g}^{\mathrm{T}}_{\Delta y_i}|_{\Delta\mathbf{x}=\widehat{\mathbf{x}}}\mathbf{V}_{\mathbf{x}}\left(\mathbf{I}-s\mathbf{V}_{\mathbf{x}}\mathbf{G}_{\Delta y_i}|_{\Delta\mathbf{x}=\widehat{\mathbf{x}}}\right)^{-1}\mathbf{g}_{\Delta y_i}|_{\Delta\mathbf{x}=\widehat{\mathbf{x}}}\right)}}{|\mathbf{I} - s\mathbf{V}_{\mathbf{x}}\mathbf{G}_{\Delta y_i}|_{\Delta\mathbf{x}=\widehat{\mathbf{x}}}|} \tag{2.49}$$

where $|\bullet|$ denotes the determinant of the matrix $\bullet$. The inverse Laplace transform of Eq. (2.49) gives the PDF of response $\Delta y_i(\Delta\mathbf{x})$. However, the exact closed-form expression of the PDF is not readily available. Pearson estimation, which is explained in Section 2.3.3, may be used to estimate the PDF of the response from its cumulants. The cumulants of the response can be obtained from

$$\kappa_i^{(r)} = \frac{d^r}{ds^r}\ln\breve{M}_{\Delta y_i}(s)|_{s=0} \tag{2.50}$$

with $\kappa_i^{(r)}$ is the r^{th}-order cumulant of i^{th} component of the response vector $\Delta\mathbf{y}$. According to Eq. (2.50) the cumulants of Δy_i may be expressed as

$$\kappa_i^{(1)} = \widehat{y}_i + \frac{1}{2}\mathrm{Trace}\left(\mathbf{G}_{\Delta y_i}|_{\Delta\mathbf{x}=\widehat{\mathbf{x}}}\mathbf{V}_{\mathbf{x}}\right) \tag{2.51}$$

$$\begin{aligned}\kappa_i^{(r)} =& \frac{r!}{2}\mathbf{g}^{\mathrm{T}}_{\Delta y_i}|_{\Delta\mathbf{x}=\widehat{\mathbf{x}}}\left[\mathbf{V}_{\mathbf{x}}\mathbf{G}_{\Delta y_i}|_{\Delta\mathbf{x}=\widehat{\mathbf{x}}}\right]^{r-2}\mathbf{V}_{\mathbf{x}}\mathbf{g}_{\Delta y_i}|_{\Delta\mathbf{x}=\widehat{\mathbf{x}}} \\ &+ \frac{(r-1)!}{2}\mathrm{Trace}\left(\left[\mathbf{G}_{\Delta y_i}|_{\Delta\mathbf{x}=\widehat{\mathbf{x}}}\mathbf{V}_{\mathbf{x}}\right]^r\right) \qquad r \geq 2\end{aligned} \tag{2.52}$$

The relationship between cumulants and the raw moment ($\mu'^{(r)}$) may be obtained from following recursion equation [16]

$$\kappa^{(r)} = \mu'^{(r)} - \sum_{k=1}^{r-1}\frac{(r-1)!}{(r-k)!\,(k-1)!}\kappa^{(k)}\mu'^{(r-k)} \tag{2.53}$$

It should be noted that for the mean-centred first order perturbation method, the Hessian matrix $\mathbf{G}_{\Delta y_i}|_{\Delta\mathbf{x}=\widehat{\mathbf{x}}}$ is $\mathbf{0}$ in Eq. (2.49). In this case the components of response $\Delta y_i(\Delta\mathbf{x})$ follow a Gaussian distribution with mean $\widehat{y}_i$ and variance $\mathbf{g}^{\mathrm{T}}_{\Delta y_i}|_{\Delta\mathbf{x}=\widehat{\mathbf{x}}}\mathbf{V}_{\mathbf{x}}\mathbf{g}_{\Delta y_i}|_{\Delta\mathbf{x}=\widehat{\mathbf{x}}}$.

2.3.3 The asymptotic integral

As mentioned in Section 2.3.2, in perturbation theory, there is a need for the assumption that the uncertain parameters must follow a Gaussian distribution. It is also mentioned that any non-Gaussian random parameter can be transformed to a Gaussian random parameter. However, using these transformations often makes the problem complicated. Adhikari and Friswell [16] proposed a method in which the moments of the response are obtained based on an asymptotic approximation of the multidimensional integral. The assumption of Gaussian distribution is generally not needed for the calculation of the moments. The raw moments of each component of response are defined by

$$\begin{aligned}\mu_i^{'(r)} =& E\left(\Delta y_i^r\left(\Delta\mathbf{x}\right)\right) = \int_{\Re^p} \Delta y_i^r\left(\mathbf{x}\right) f_{\Delta\mathbf{x}}\left(\mathbf{x}\right) d\mathbf{x} \\ =& \int_{\Re^p} e^{-\left(L_{\Delta\mathbf{x}}(\mathbf{x}) - r\ln\Delta y_i(\mathbf{x})\right)} d\mathbf{x}\end{aligned} \tag{2.54}$$

where $f_{\Delta\mathbf{x}}\left(\mathbf{x}\right)$ is the joint probability function of uncertain parameters and $L_{\Delta\mathbf{x}}\left(\mathbf{x}\right)$ is the log-likelihood function. It is now assumed that $u\left(\mathbf{x}\right) = L_{\Delta\mathbf{x}}\left(\mathbf{x}\right) - r\ln\Delta y_i\left(\mathbf{x}\right)$. The p-dimensional integral in Eq. (2.54) can now be written in the following form

$$\int_{\Re^p} e^{-u(\mathbf{x})} d\mathbf{x} \tag{2.55}$$

The p-dimensional integral in Eq. (2.55) is evaluated over unbounded domain $\Re^p$. However, the integral is dominated by the domain in the neighbourhood of $\mathbf{x}$ where $u\left(\mathbf{x}\right)$ reaches its global minimum. Assume that $u\left(\mathbf{x}\right)$ is minimum at a unique point $\vartheta \in \Re^p$. Therefore, at $\mathbf{x} = \vartheta$

$$\frac{\partial u\left(\mathbf{x}\right)}{\partial x_k} = 0 \quad \forall k \quad \text{or} \quad \mathbf{g}_{u(\mathbf{x})} = \mathbf{0} \tag{2.56}$$

Substituting $u\left(\mathbf{x}\right)$ by $L_{\Delta\mathbf{x}}\left(\mathbf{x}\right) - r\ln\Delta y_i\left(\mathbf{x}\right)$ in Eq. (2.56) leads to

$$\mathbf{g}_{\Delta y_i}\left|_{\mathbf{x}=\vartheta}\right. r = \Delta y_i\left(\vartheta\right) \mathbf{g}_{L_{\Delta\mathbf{x}}}\left|_{\mathbf{x}=\vartheta}\right. \tag{2.57}$$

Now $u\left(\mathbf{x}\right)$ in Eq. (2.55) is expanded in a Taylor series about ϑ and only the terms up to second-order are retained in this case, Eq. (2.55) may be approximated as

$$e^{-u(\vartheta)} \int_{\Re^p} -\frac{1}{2}\left(\mathbf{x}-\vartheta\right)^{\mathrm{T}} \mathbf{G}_u\left|_{\mathbf{x}=\vartheta}\right. \left(\mathbf{x}-\vartheta\right) d\mathbf{x} \tag{2.58}$$

The integral in Eq. (2.58) can be evaluated as [16]

$$e^{-u(\boldsymbol{\vartheta})} \int_{\Re^p} -\frac{1}{2} (\mathbf{x}-\boldsymbol{\vartheta})^{\mathrm{T}} \mathbf{G}_u \mid_{\mathbf{x}=\boldsymbol{\vartheta}} (\mathbf{x}-\boldsymbol{\vartheta})\, d\mathbf{x} = (2\pi)^{p/2} e^{-u(\boldsymbol{\vartheta})} \left| \mathbf{G}_u \mid_{\mathbf{x}=\boldsymbol{\vartheta}} \right|^{-1/2} \quad (2.59)$$

where

$$\mathbf{G}_u \mid_{\mathbf{x}=\boldsymbol{\vartheta}} = \mathbf{G}_{L_{\Delta\mathbf{x}}} \mid_{\mathbf{x}=\boldsymbol{\vartheta}} + \frac{1}{r} \mathbf{g}_{L_{\Delta\mathbf{x}}} \mid_{\mathbf{x}=\boldsymbol{\vartheta}} \mathbf{g}_{L_{\Delta\mathbf{x}}}^{\mathrm{T}} \mid_{\mathbf{x}=\boldsymbol{\vartheta}} - \frac{r}{\Delta y_i(\boldsymbol{\vartheta})} \mathbf{G}_{\Delta y_i} \mid_{\mathbf{x}=\boldsymbol{\vartheta}} \quad (2.60)$$

Using Eq. (2.54) and the approximation in Eq. (2.59), the r^{th} raw moment of response $\Delta y_i(\Delta\mathbf{x})$ can be calculated as

$$\begin{aligned} \mu_i^{'(r)} &= (2\pi)^{p/2} \Delta y_i^r(\boldsymbol{\vartheta}) \\ &\times e^{-L_{\Delta\mathbf{x}}(\boldsymbol{\vartheta})} \times \left| \mathbf{G}_{L_{\Delta\mathbf{x}}} \mid_{\mathbf{x}=\boldsymbol{\vartheta}} + \frac{1}{r} \mathbf{g}_{L_{\Delta\mathbf{x}}} \mid_{\mathbf{x}=\boldsymbol{\vartheta}} \mathbf{g}_{L_{\Delta\mathbf{x}}}^{\mathrm{T}} \mid_{\mathbf{x}=\boldsymbol{\vartheta}} - \frac{r}{\Delta y_i(\boldsymbol{\vartheta})} \mathbf{G}_{\Delta y_i} \mid_{\mathbf{x}=\boldsymbol{\vartheta}} \right|^{-1/2} \end{aligned} \quad (2.61)$$

where $\boldsymbol{\vartheta}$ is obtained from numerical solution of Eq. (2.57). The mean of the response $\widehat{y}_i$ can be obtained by substituting $r = 1$ into Eq. (2.61) and the central moments of the response can be evaluated in terms of the raw moments using Eq. (2.5).

If $\Delta\mathbf{x}$ follows a multivariate Gaussian distribution, the raw moments of the response may be approximated as

$$\mu_i^{'(r)} = \Delta y_i^r(\boldsymbol{\vartheta})\, e^{-\frac{1}{2}(\boldsymbol{\vartheta}-\widehat{\mathbf{x}})^{\mathrm{T}} \mathbf{V}_{\mathbf{x}}^{-1} (\boldsymbol{\vartheta}-\widehat{\mathbf{x}})} \left(\mathbf{I} + \tilde{\mathbf{G}}_u \mid_{\mathbf{x}=\boldsymbol{\vartheta}} \right)^{-1/2} \quad (2.62)$$

where

$$\tilde{G}_u \mid_{\mathbf{x}=\boldsymbol{\vartheta}} = \frac{1}{r} (\boldsymbol{\vartheta}-\widehat{\mathbf{x}}) (\boldsymbol{\vartheta}-\widehat{\mathbf{x}})^{\mathrm{T}} \mathbf{V}_{\mathbf{x}}^{-1} - \frac{r}{y_i(\boldsymbol{\vartheta})} \mathbf{V}_{\mathbf{x}} \mathbf{G}_{\Delta y_i} \mid_{\mathbf{x}=\boldsymbol{\vartheta}} \quad (2.63)$$

and the optimal point $\boldsymbol{\vartheta}$ can be obtained from following equation,

$$\boldsymbol{\vartheta} = \widehat{\mathbf{x}} + \frac{r}{\Delta y_i(\boldsymbol{\vartheta})} \mathbf{V}_{\mathbf{x}} \mathbf{g}_{\Delta y_i} \mid_{\mathbf{x}=\boldsymbol{\vartheta}} \quad (2.64)$$

It should be noted that the third and fourth moments, obtained from Eq. (2.61) (or Eq. (2.62), are more inaccurate than the first and second moments if a second-order perturbation is used to represent the response. In this case, if only the first two moments are considered, Eqs. (2.51) and (2.52) (or Eqs. (2.61) and (2.5))

may be used to estimate the PDF of the response. However, if the second-order model has a quite accurate description of the response in the region of uncertain parameter variation, then the accuracy of higher order moments will be increased. In this case, the PDF may be evaluated using Pearson's theory as reported in Refs. [48] and [49]. The PDF is expressed as a function of the mean and three central moments from 2[nd] order to 4[th] order as,

$$\frac{df\left(y_i\right)}{dy_i} = \frac{a + y_i}{b_0 + b_1 y_i + b_2 y_i^2} f\left(y_i\right) \quad \Rightarrow \quad f\left(y_i\right) = e^{\left(\int \frac{a+y_i}{b_0+b_1 y_i+b_2 y_i^2} dy_i\right)} \tag{2.65}$$

where the four unknown coefficients, a, b_0, b_1 and b_2, in Eq. (2.65) are determined as

$$\begin{bmatrix} 1 & 0 & 1 & 2\mu_i^{(1)} \\ 0 & 1 & \mu_i^{(1)} & \left(\mu_i^{(1)}\right)^2 + 3\mu_i^{(2)} \\ 0 & 0 & 2\mu_i^{(2)} & 4\left(\mu_i^{(1)}\mu_i^{(2)} + \mu_i^{(3)}\right) \\ 0 & 3\mu_i^{(2)} & 3\left(\mu_i^{(1)}\mu_i^{(2)} + \mu_i^{(3)}\right) & 3\left(\mu_i^{(1)}\right)^2\mu_i^{(2)} + 6\mu_i^{(1)}\mu_i^{(3)} + 5\mu_i^{(4)} \end{bmatrix} \times \begin{Bmatrix} a \\ b_0 \\ b_1 \\ b_2 \end{Bmatrix} = \begin{Bmatrix} \mu_i^{(1)} \\ \mu_i^{(2)} \\ \mu_i^{(3)} \\ \mu_i^{(4)} \end{Bmatrix} \tag{2.66}$$

2.3.4 Interval analysis

As mentioned in Section 2.2.3, the parameter uncertainty may be modelled using a range between lower and upper bounds. The aim of interval analysis is to evaluate the range of possible outputs considering all possible combinations of the uncertain inputs within their permissible range.

If each component of the response vector is generally represented by $y_i\left(\mathbf{x}\right)$, the interval analysis is a numerical procedure equivalent to solving the following equation

$$\overline{y}_i = \max\left(y_i\left(\mathbf{x}\right)\right), \quad \underline{y}_i = \min\left(y_i\left(\mathbf{x}\right)\right), \quad i = 1, ..., n_r \tag{2.67}$$

subject to,

$$\underline{\mathbf{x}} \leq \mathbf{x} \leq \overline{\mathbf{x}}$$

The operation on intervals, defined in interval arithmetic, may be used to solve Eq. (2.67) when the response function $y_i(\mathbf{x})$ has an analytical expression in a closed-form. Interval mathematics express the operations on interval for addition, subtraction, multiplication and division as

$$\left[\ \underline{x}_1 \quad \overline{x}_1\ \right] + \left[\ \underline{x}_2 \quad \overline{x}_2\ \right] = \left[\ \underline{x}_1 + \underline{x}_2 \quad \overline{x}_1 + \overline{x}_2\ \right] \tag{2.68}$$

$$\left[\ \underline{x}_1 \quad \overline{x}_1\ \right] - \left[\ \underline{x}_2 \quad \overline{x}_2\ \right] = \left[\ \underline{x}_1 - \underline{x}_2 \quad \overline{x}_1 - \overline{x}_2\ \right] \tag{2.69}$$

$$\begin{aligned}&\left[\ \underline{x}_1 \quad \overline{x}_1\ \right] \times \left[\ \underline{x}_2 \quad \overline{x}_2\ \right] = \\ &\left[\ \min\left(\underline{x}_1\underline{x}_2, \underline{x}_1\overline{x}_2, \overline{x}_1\underline{x}_2, \overline{x}_1\overline{x}_2\right) \quad \max\left(\underline{x}_1\underline{x}_2, \underline{x}_1\overline{x}_2, \overline{x}_1\underline{x}_2, \overline{x}_1\overline{x}_2\right)\ \right]\end{aligned} \tag{2.70}$$

$$\begin{aligned}&\left[\ \underline{x}_1 \quad \overline{x}_1\ \right] / \left[\ \underline{x}_2 \quad \overline{x}_2\ \right] = \\ &\left[\ \min\left(\underline{x}_1/\underline{x}_2, \underline{x}_1/\overline{x}_2, \overline{x}_1/\underline{x}_2, \overline{x}_1/\overline{x}_2\right) \quad \max\left(\underline{x}_1/\underline{x}_2, \underline{x}_1/\overline{x}_2, \overline{x}_1/\underline{x}_2, \overline{x}_1/\overline{x}_2\right)\ \right]\end{aligned} \tag{2.71}$$

The above basic operation can be implemented in a deterministic function to generate the corresponding interval of the function. For instance, assume that the response function is expressed as [3]

$$y_i\left(\widetilde{X}_1, \widetilde{X}_2\right) = 1 + \frac{\widetilde{X}_2}{\widetilde{X}_1} \tag{2.72}$$

where the uncertain input parameters $\widetilde{X}_1$ and $\widetilde{X}_2$ are defined as interval vector

$$\left\{ \begin{array}{c} \widetilde{X}_1 \\ \widetilde{X}_2 \end{array} \right\} = \left\{ \begin{bmatrix} 1 & 3 \\ 4 & 5 \end{bmatrix} \right\} \tag{2.73}$$

Applying the interval arithmetic gives the range of function $y_i\left(\widetilde{X}_1, \widetilde{X}_2\right)$ as

$$1 + \frac{\left[\ 4 \quad 5\ \right]}{\left[\ 1 \quad 3\ \right]} = 1 + \left[\ \tfrac{4}{3} \quad 5\ \right] = \left[\ \tfrac{7}{3} \quad 6\ \right] \tag{2.74}$$

The real range of function $y_i\left(\widetilde{X}_1, \widetilde{X}_2\right)$ is exactly similar to one obtained from Eq. (2.74). As can be seen in Eq. (2.74), the interval arithmetic is a very straightforward procedure to implement. However, the interval arithmetic operation often produces conservative results if the correlation between the operands is neglected. To illustrate the above example, the function $y_i\left(\widetilde{X}_1, \widetilde{X}_2\right)$, introduced in Eq. (2.72)), is rewritten in the format

[3] example is taken from [50]

$$y_i\left(\widetilde{X}_1, \widetilde{X}_2\right) = \frac{\widetilde{X}_1 + \widetilde{X}_2}{\widetilde{X}_1} \tag{2.75}$$

The range of function is now calculated by using the interval arithmetic as follows

$$\frac{[\ 1\ \ 3\ ] + [\ 4\ \ 5\ ]}{[\ 1\ \ 3\ ]} = \frac{[\ 5\ \ 8\ ]}{[\ 1\ \ 3\ ]} = [\ \tfrac{5}{3}\ \ 8\ ] \tag{2.76}$$

As previously mentioned, the exact range of the above function equals to $[\ \frac{7}{3}\ \ 6\ ]$. This shows that the result obtained from applying the arithmetic interval to the function with the form of Eq. (2.75) is conservative. This conservatism arises from the fact that the interval arithmetic does every arithmetical operation between interval numbers as an operation completely independent operands [50]. However, this assumption is not true in most cases.

The vertex method, originally developed by Dong and Shah [51], is considered as another tool for the solution of Eq. (2.67). In this case, the responses are either monotonically increased or decreased with the uncertain parameter variations. This implies that the solution of Eq. (2.67) can be sought in all possible combinations of the boundary values of the input intervals. For a system with p input intervals, 2^p analyses have to be carried out to find the boundary values of the output. The vertex solution is the simplest and most efficient method which is by far the most applied numerical procedure to calculate the output sets of interval analysis (e.g. [19]). However, the application of the vertex method is only valid for a restricted class of numerical problems, i.e. when there is a monotonic relationship between the inputs and outputs.

A global optimisation procedure may be considered as the most general solution of the Eq. (2.67). The optimisation is carried out independently on every component of the response vector $\mathbf{y}$. For example, using the global optimisation technique, the range of the function in Eq. (2.72) is achieved as $[\ \frac{7}{3}\ \ 6\ ]$ which is the exact range. Different optimisation procedures have been proposed in the literature, e.g. [52–54]. The solution from optimisation procedure gives the upper and lower bounds for each component of response. The interval vector of the response is then assembled from the interval scalars of each element $\{[\ \underline{y}_i\ \ \overline{y}_i\ ]\}$. The interval responses in this way will be described by a hypercube. However,

the elements of response are often interdependent and the exact region of their variation in the space is not hypercube. Figure 2.9 [21] shows a particular case of a two-dimensional response. As can be seen in the figure, the true region of possible variation of outputs is not often a hypercube due to interdependency of the response elements. The meta-model (Section 2.3.6) may be used to overcome this issue.

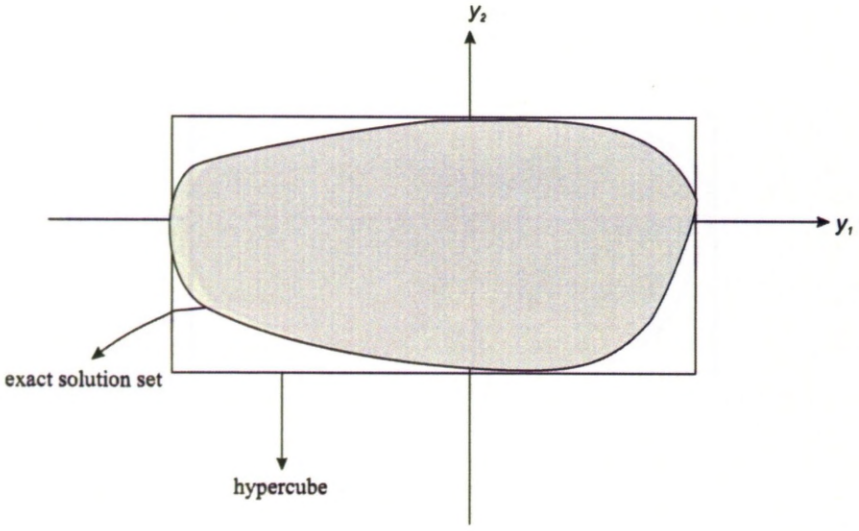

Figure 2.9: Hypercubic approximations of a two-dimensional output set of an interval analysis.

2.3.5 Fuzzy method

The purpose of fuzzy analysis is to determine the fuzzy description of outputs when the inputs are modelled using fuzzy sets as described in Section 2.2.4. As mentioned in Section 2.2.4, the fuzzy set model uses the membership function to describe the uncertainty in the input parameters. The fuzzy method consequently aims to derive the fuzzy membership function of output data. The fuzzy method involves the application of a numerical procedure of interval analysis at a number of α-levels as illustrated in Figure 2.10 (reproduced from Moens and Vandepitte [21]). The figure shows specifically the procedure for a function of two triangular fuzzy parameters with four α-levels. The range of the response vector components y_i on a specific level of membership function α is searched within the same α-level on the input domain, which means that the analysis at each α-cuts corresponds

to an interval analysis for the system as described in Section 2.3.4. The interval analysis is performed for all α-levels and the fuzzy membership function of the outputs can be constructed by connecting the upper bounds and the lower bounds of response at different α-levels by a straight line. The meta-model can also be used for the construction of fuzzy membership functions of the output data. It is shown in Chapter 4 that a combination of the fuzzy method and the meta-model can lead to a more efficient procedure for fuzzy analysis.

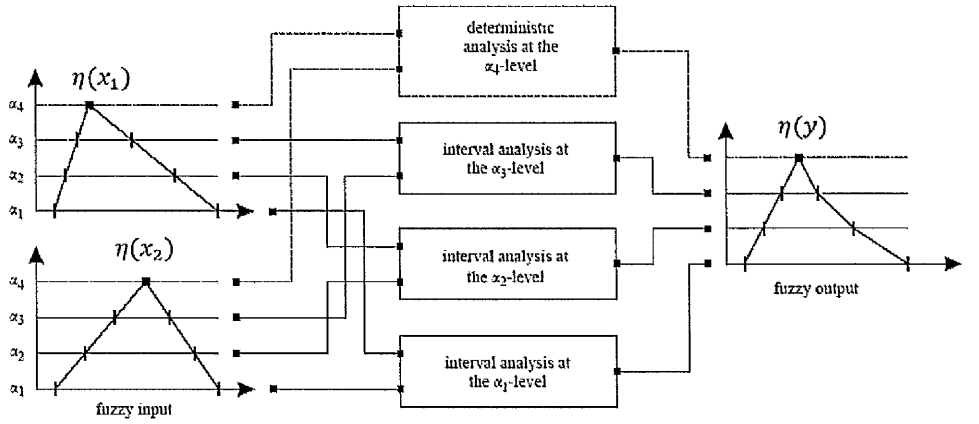

Figure 2.10: α-Level strategy, with 4 α-levels, for a function of two triangular fuzzy parameters.

2.3.6 Meta model

In this thesis, a meta-model is used for the purposes of efficient and optimal uncertainty propagation by interval and fuzzy methods as described in Chapter 4. It is also used for the solution of the interval model updating problem which is described in Chapter 6. The meta-model acts as a surrogate for the full finite-element or mathematical model in which a region of input data (e.g. structural parameters) is mapped to a region of output data (e.g. eigenvalues or flutter speeds) with parameters obtained by regression analysis. Selection of the meta-model is a crucial step in that it influences the performance of the procedure to a very significant degree. Conventional Response Surface Method (RSM) based on some low order polynomial functions and a more recent method, the Kriging estimator, are discussed in the following sections.

Response Surface Method

In the Response Surface Method (RSM), it is assumed that n_s vectors of independent input parameters $\mathbf{X} = \left[\begin{array}{cccc} \mathbf{x}^{(1)} & \mathbf{x}^{(2)} & \ldots & \mathbf{x}^{(n_s)} \end{array} \right]^{\mathrm{T}}$ with $\mathbf{x}^{(k)} \in \Re^p$ are selected using a sampling method and the corresponding output parameters $\mathbf{Y} = \left[\begin{array}{cccc} \mathbf{y}^{(1)} & \mathbf{y}^{(2)} & \ldots & \mathbf{y}^{(n_s)} \end{array} \right]^{\mathrm{T}}$ with $\mathbf{y}^{(k)} \in \Re^{n_r}$ are obtained from n_s deterministic analysis of the system. Then, each component of response variable y_i may be defined as the summation of functions of uncertain structural parameters with regression coefficients $\beta_{.,i}$ as,

$$y_i(\mathbf{x}) = \sum_{k=0}^{n} \beta_{k,i} u_{k,i}(\mathbf{x}) \tag{2.77}$$

where $\mathbf{x} \in \Re^p$ is the vector of uncertain input parameters. The method of least squares may be used to estimate the regression coefficients in Eq. (2.77) as will be described later in this section. For small uncertainties in input parameters some low-order polynomial form may be chosen for the functions in Eq. (2.77). For example, the quadratic response surface may be used for the numerical model with p paramers as:

$$\begin{aligned} y_i =& \beta_{0,i} + \sum_{k=1}^{p} \beta_{k,i} x_k + \sum_{k=1}^{p} \beta_{kk,i} x_k^2 + \sum_{k<l} \sum_{l=2}^{p} \beta_{kl,i} x_k x_l + \epsilon_i \\ =& \beta_{0,i} + \mathbf{b}_i^{\mathrm{T}} \mathbf{x} + \frac{1}{2} \mathbf{x}^{\mathrm{T}} \mathbf{B}_i \mathbf{x} + \epsilon_i \end{aligned} \tag{2.78}$$

where $\beta_{.,i}$ are regression coefficients, $\mathbf{b}_i = \left[\begin{array}{cccc} \beta_{1,i} & \beta_{2,i} & \ldots & \beta_{p,i} \end{array} \right]_{p \times 1}^{\mathrm{T}}$,

$$\mathbf{B}_i = \begin{bmatrix} 2\beta_{11,i} & \beta_{12,i} & \cdots & \beta_{1p,i} \\ & 2\beta_{22,i} & \cdots & \beta_{2p,i} \\ & & \ddots & \vdots \\ & & & \vdots \\ \text{sym.} & & & 2\beta_{pp,i} \end{bmatrix}_{p \times p}$$

and ϵ_i represents the fitting error. In the RSM, it is assumed that the above equation is valid for the input parameters $\mathbf{x}$ which are located within the interval of $[\underline{\mathbf{x}}\ \overline{\mathbf{x}}]$ ($\underline{\mathbf{x}} \leq \mathbf{x} \leq \overline{\mathbf{x}}$). The quadratic model includes $(p+1)(p+2)/2$ regression coefficients. Therefore the number of samples n_s, taken from the space of input

parameters, should be greater than $(p+1)(p+2)/2$ for an over-determined least-squares solution. As previously mentioned, the response data may be obtained by solving the deterministic equation for samples selected from the space of uncertain input parameters. Therefore Eq. (2.78) can be rearranged to provide a system of overdetermined linear equations as,

$$\mathbf{Y}_{:,i} = \Xi\boldsymbol{\beta}_{:,i} + \boldsymbol{\epsilon}_i \tag{2.79}$$

where $\boldsymbol{\beta}_{:,i} = \left[\ \beta_{0,i} \quad \beta_{1,i} \quad \beta_{2,i} \quad \cdots \quad \beta_{p,i} \quad \beta_{11,i} \quad \beta_{22,i} \quad \cdots \quad \beta_{pp,i} \quad \beta_{12,i} \quad \cdots \quad \beta_{p(p-1),i}\ \right]^{\mathrm{T}}$,

$$\Xi = \begin{bmatrix} 1 & x_1^{(1)} & \cdots & x_p^{(1)} & x_1^{2(1)} & \cdots & x_p^{2(1)} & x_1^{(1)}x_2^{(1)} & \cdots & x_{p-1}^{(1)}x_p^{(1)} \\ 1 & x_1^{(2)} & \cdots & x_p^{(2)} & x_1^{2(2)} & \cdots & x_p^{2(2)} & x_1^{(2)}x_2^{(2)} & \cdots & x_{p-1}^{(2)}x_p^{(2)} \\ \vdots & \vdots & \cdots & \vdots & \vdots & \cdots & \vdots & \vdots & \cdots & \vdots \\ \vdots & \vdots & \cdots & \vdots & \vdots & \cdots & \vdots & \vdots & \cdots & \vdots \\ \vdots & \vdots & \cdots & \vdots & \vdots & \cdots & \vdots & \vdots & \cdots & \vdots \\ 1 & x_1^{(n_s)} & \cdots & x_p^{(n_s)} & x_1^{2(n_s)} & \cdots & x_p^{2(n_s)} & x_1^{(n_s)}x_2^{(n_s)} & \cdots & x_{p-1}^{(n_s)}x_p^{(n_s)} \end{bmatrix}$$

and $\mathbf{Y}_{:,i} = \left[\ y_i^1 \quad y_i^2 \quad \cdots \quad y_i^{n_s}\ \right]$. Minimising the vector of residuals $\boldsymbol{\epsilon}_i$ with respect to coefficients $\boldsymbol{\beta}_{:,i}$ leads to:

$$\boldsymbol{\beta}_{:,i} = \left(\Xi^{\mathrm{T}}\Xi\right)^{-1}\Xi^{\mathrm{T}}\mathbf{Y}_{:,i} \tag{2.80}$$

Model adequacy checking is a crucial step in Response Surface Analysis (RSA). The residuals from the least-square fit can be used to judge the model adequacy. If the residuals show that the fitted model cannot represent the true function values, then a higher order model or different type of functions may be needed. Another option might be to divide the space of uncertain parameters into regions and consider a quadratic model for each region. It should be noted that the higher order model includes a greater number of regression coefficients and therefore leads to increased computational time. Therefore more efficient method is needed to improve the accuracy of fitting. Kriging predictor may be used for this purpose as explained in the next section.

The Kriging Predictor

In The Kriging predictor, a similar polynomial expansion to the one given by Eq. 2.78, is used. The only difference is that the error term ϵ_i is assumed to be a random function of uncertain input parameters ($\epsilon_i = \epsilon_i(\mathbf{x})$). This assumption can be used when the application is to fit a regression model on a numerical computer code where any lack of fit will be due entirely to the modeling error (incomplete set of regression terms), not measurement error or noise [55]. The error function $\epsilon_i(\mathbf{x})$ represents the errors of the fitting as a random field having zero-mean and covariance

$$\mathrm{Cov}\left(\epsilon_i(\mathbf{x}), \epsilon_i\left(\mathbf{x}^{(h)}\right)\right) = \sigma_i^2 C_i\left(\mathbf{x}, \mathbf{x}^{(h)}\right) \tag{2.81}$$

where σ_i^2 is the variance of the i^{th} output data and C is the correlation function between untried input parameters $\mathbf{x}$ and one of the design samples $\mathbf{x}^{(h)}$, $h = 1 : n_s$. A suitably chosen correlation function may improve the quality of fit as explained below.

As previously mentioned, the random function in Eq. (2.78) becomes a function of the system parameters $\mathbf{x}$. Hence the errors of the output predictor in Eq. (2.78) are correlated. The correlation function of the prediction errors is assumed to be related inversely to the distance between the corresponding points in the output [55]. The closer the points in space, the greater the correlation between the error terms. Because the components of input parameters are statistically independent (for example the parameters of a Finite Element model chosen for updating), one may calculate the correlation function between the input parameters as [56],

$$C_i\left(\mathbf{x}, \mathbf{x}^{(h)}\right) = \prod_{j=1}^{p} C_{j,i}\left(x_j, x_j^{(h)}\right) \tag{2.82}$$

Different types of correlation functions have been introduced in [57] and [58]. As mentioned in Section 2.2.2, the choice of correlation function depends on the underlying behavior of the true response. The following correlation function which is almost analogous to Eq. (2.26) (but with one more parameter) may be used,

$$C_{j,i}\left(x_j, x_j^{(h)}\right) = \exp\left(-\zeta_{j,i}\left|x_j - x_j^{(h)}\right|^{\nu_i}\right) \quad 1 \leq \nu_i \leq 2 \tag{2.83}$$

$\zeta_{j,i}$ (the j^{th} term of the vector $\boldsymbol{\zeta}_i$) and ν_i are parameters of the correlation function at the i^{th} output. $\nu_i = 1$ (Eq. (2.26)) gives an Ornstein-Uhlenbeck process which produces continuous (but not very smooth) paths. The case of $\nu_i = 2$ produces infinity differentiable paths. Therefore, the parameter ν_i is related to the smoothness of the function in the x_j coordinate. As it can be seen from Eq. (2.83), the correlation function is 1 when $x_j = x_j^h$ and its value reduces as the untried point x_j goes away from the h^{th} design sample x_j^h. Since the predictor is unbiased at the observation point, a high level of confidence in the prediction of the outputs for the points which are close to the design samples can be achieved. The level of confidence of the predictions at untried points can be assessed by evaluating the mean squared error MSE, to be discussed in the following section. The parameter $\zeta_{j,i}$ controls the importance of the j^{th} component. The calculation of correlation parameters is discussed below.

To compute the Kriging model for the i^{th} output, the regression coefficients $\beta_{:,i}$, in Eq. (2.78) and correlation parameters $\boldsymbol{\zeta}$ and ν in Eq. (2.83) must be estimated. When the correlation parameters are given, the regression coefficients $\beta_{:,i}$ and variance of output data σ_i^2 can be estimated using a weighted least-square technique as,

$$\boldsymbol{\beta}_{:,i} = \left(\Xi^{\mathrm{T}}\mathbf{R}_i\Xi\right)^{-1}\Xi^{\mathrm{T}}\mathbf{R}_i^{-1}\mathbf{Y}_{:,i} \tag{2.84}$$

$$\sigma_i^2 = \frac{1}{n_s}\left[\mathbf{Y}_{:,i} - \Xi\boldsymbol{\beta}_{:,i}\right]^{\mathrm{T}}\mathbf{R}_i^{-1}\left[\mathbf{Y}_{:,i} - \Xi\boldsymbol{\beta}_{:,i}\right] \tag{2.85}$$

where $\mathbf{R}_i \in \Re^{n_s \times n_s}$ is the correlation matrix between samples with components $R_{hq,i} = C_i\left(\mathbf{x}^{(h)}, \mathbf{x}^{(q)}\right)$. The number of regression coefficients is equal to 1 for a zero-order polynomial model, $p+1$ for a first-order polynomial model and $\frac{1}{2}(p+1)(p+2)$ for a second-order polynomial model. Minimising the mean square error (MSE) then leads to the mean value of Kriging predictor expressed as,

$$y_i = \beta_{0,i} + \mathbf{b}_i^{\mathrm{T}}\mathbf{x} + \frac{1}{2}\mathbf{x}^{\mathrm{T}}\mathbf{B}\mathbf{x} + \boldsymbol{\iota}_i^{\mathrm{T}}\mathbf{r}_i(\mathbf{x}) \tag{2.86}$$

where $\mathbf{r}_i(\mathbf{x}) \in \Re^{n_s}$,

$$\mathbf{r}_i(\mathbf{x}) = \left[\begin{array}{cccc} C_i\left(\mathbf{x}, \mathbf{x}^{(1)}\right) & C_i\left(\mathbf{x}, \mathbf{x}^{(2)}\right) & \ldots & C_i\left(\mathbf{x}, \mathbf{x}^{(n_s)}\right) \end{array} \right]^{\mathrm{T}}$$

and $\iota_i = \mathbf{R}_i^{-1}\left(\mathbf{Y}_{:,i} - \Xi\boldsymbol{\beta}\right)$. The predictor is unbiased at the observation points. Further detail on the derivation of Eq. (2.86) can be found in [55, 56]. If a Gaussian process is assumed the maximum likelihood estimate $\boldsymbol{\beta}_{:,i}$, σ_i^2 when the values of the correlation parameters are known, is the generalized least square solution given in Eqs. (2.84) and (2.85). The updated correlation parameters are then estimated by minimising the following objective function [56],

$$\min_{\boldsymbol{\zeta},\, \boldsymbol{\nu}} |\mathbf{R}_i|^{\frac{1}{n_s}} \sigma_i^2 \tag{2.87}$$

Therefore an iterative procedure can be defined for evaluation of regression coefficients $\beta_{\bullet,i}$ and correlation parameters $\boldsymbol{\zeta}$ and $\boldsymbol{\nu}$ as follows:

1. Estimate initial values of correlation parameters $\boldsymbol{\zeta}$ and $\boldsymbol{\nu}$.
2. Evaluate $\beta_{\bullet,i}$ and σ_i^2 using the generalized least square solution given in Eqs. (2.84) and (2.85).
3. Update the correlation parameters to minimise the objective function given by Eq. (2.87).
4. If a minimum is found then go to the next step 5. Otherwise go to step 2.
5. End.

Sampling for the RSM and the Kriging Predictor

Different types of sampling methods may be used to generate the data for the RSM approximation. Central Composite Design (CCD) [59], the most popular class of second-order designs, is used in this study. The method was introduced by Box and Wilson [60]. The solid circle points, shown in Figure 2.11, indicate the design points in the CCD. As it is seen in the figure, the CCD generates $2^p + 2p + 1$ samples and consequently $2^p + 2p + 1$ deterministic analyses are needed. The design involves the use of a two-level factorial design 2^p combined

with $2p$ axial points. It also includes one centre point. Parameter α in Figure 2.11 represents the distance of axial point from the centre. It is common to assume that $\alpha = \sqrt{2}$. However $\alpha = 1$ gives the samples on the face of the hypercube. Note that this is for nondimensional input parameters with values in the range of -1 and +1. It can be readily seen that as the number of parameters p in a 2^p factorial design increases, the number of numerical runs rapidly increases. This increases the computational time considerably, especially for industrial-sized problems. Fractional factorial design may be used in this case to reduce the number of samples. As shown in Figure 2.12, any fractional factorial design of resolution p includes complete factorial designs in any subset of $p-1$ parameters. This concept can be used to reduce the number of runs from 2^p to 2^{p-1}. This is called half fraction design. Suppose a system with seven parameters in which full factorial designs requires 128 analyses. The number of samples can be reduced to 64 using half-fraction design. More details about the fraction analysis can be found in [59].

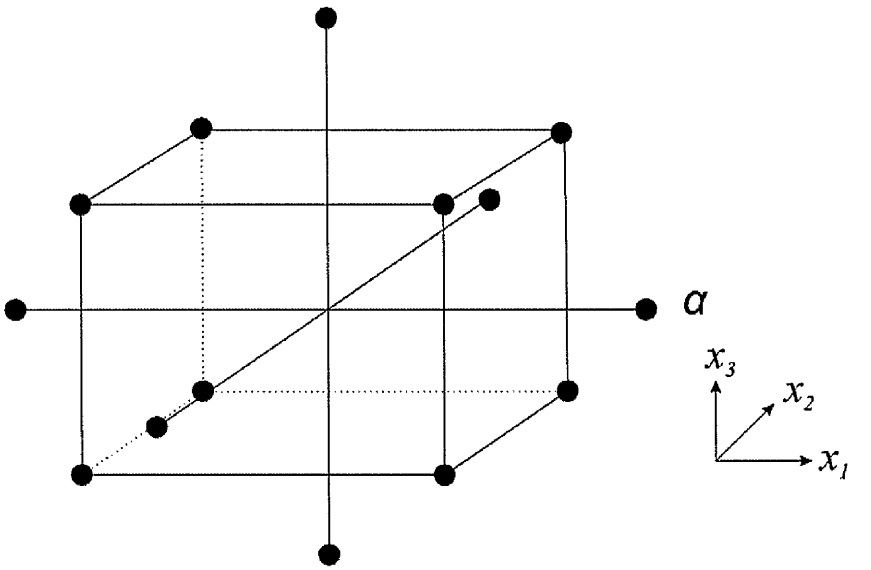

Figure 2.11: Central Composite Design (CCD) for 3 parameters.

For the Kriging predictor a systematic method for the generation of samples can be used to ensure that the uncertainty in the prediction of the target function is minimized. This also has a significant effect on the accuracy of the inverse problem which will be discussed in Chapter 6. The method is presented in [61].

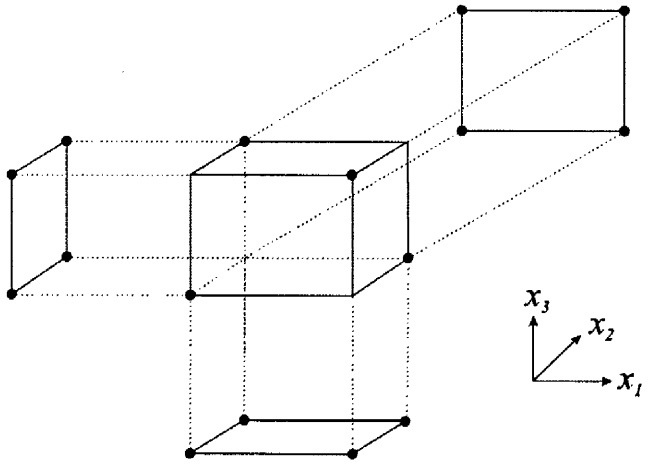

Figure 2.12: Projection of three dimensional design to two dimensional.

To minimize the uncertainty on the Kriging predictor in representing output data, the Kriging-predicted mean squared error (MSE) can be used as the criterion for the sample generation. The Kriging predictor provides an estimation of the MSE [56] as,

$$\mathrm{MSE}(\mathbf{x}) = \sigma_i^2 \left[1 - \mathbf{u}^{\mathrm{T}}\mathbf{P}\mathbf{u}\right] \tag{2.88}$$

where $\mathbf{u} = \left[1 \; x_1 \; x_2 \; \ldots \; x_p \; x_1^2 \; x_2^2 \; \ldots \; x_p^2 \; x_1x_2 \; \ldots \; x_{p-1}x_p \; \mathbf{r}_i^{\mathrm{T}}(\mathbf{x})\right]^{\mathrm{T}}$ and

$$\begin{aligned}\mathbf{P} &= \begin{bmatrix} \mathbf{O} & \boldsymbol{\Xi}^{\mathrm{T}} \\ \boldsymbol{\Xi} & \mathbf{R}_i \end{bmatrix}^{-1} \\ &= \begin{bmatrix} -\left(\boldsymbol{\Xi}^{\mathrm{T}}\mathbf{R}_i^{-1}\boldsymbol{\Xi}\right)^{-1} & \left(\boldsymbol{\Xi}^{\mathrm{T}}\mathbf{R}_i^{-1}\boldsymbol{\Xi}\right)^{-1}\boldsymbol{\Xi}^{\mathrm{T}}\mathbf{R}_i^{-1} \\ \mathbf{R}_i^{-1}\boldsymbol{\Xi}\left(\boldsymbol{\Xi}^{\mathrm{T}}\mathbf{R}_i^{-1}\boldsymbol{\Xi}\right)^{-1} & \mathbf{R}_i^{-1}\left(\mathbf{I} - \boldsymbol{\Xi}\left(\boldsymbol{\Xi}^{\mathrm{T}}\mathbf{R}_i^{-1}\boldsymbol{\Xi}\right)^{-1}\boldsymbol{\Xi}^{\mathrm{T}}\mathbf{R}_i^{-1}\right) \end{bmatrix}\end{aligned}$$

It should be recalled that the predictor is unbiased at the observed points and therefore the MSE is zero at these points.

The following procedure may be defined for sampling:

1. Generate a central composite design (CCD) with one centre point [59] as the initial sample.

2. Generate further samples at the locations where the MSE is a maximum.

3. If the maximum MSE is smaller than a threshold go to the next step; otherwise go to step 2.

4. End.

To illustrate the sampling methods and fitting using a Kriging predictor, a three degree of freedom mass-spring system with close eigenvalues is considered. The system shown in Figure 2.13, is based on the example used by Friswell et al. [62]. The parameters are,

$$\begin{aligned} &m_1 = 1\,\text{kg}, \quad m_2 = 4\,\text{kg}, \quad m_3 = 1\,\text{kg}, \\ &k_1 = k_3 = 0. \quad k_4 = 2.0\,\text{N/m}, \quad k_5 = 2\,\text{N/m}, \quad k_6 = 1\,\text{N/m} \end{aligned} \tag{2.89}$$

and it is assumed that the stiffness parameter k_2 is uncertain within the interval [6.5 9.5]. Now the third eigenvalue of the system is assumed to be an unknown function of the uncertain parameter k_2. Figure 2.14 shows the sampling procedure for this example. Figures 2.14(a) and 2.14(b) show the initial and final selected samples, the target function (solid line) and Kriging approximations (dashed line). The initial and final values of MSE function against the uncertain parameter k_2 are shown in Figures 2.14(c) and 2.14(d). As can be seen from Figure 2.14(d), the sampling stops because the maximum value of MSE falls below a specified tolerance. Figure 2.14(d) also shows that by increasing the number of samples the Kriging approximation produces a more accurate representation of the target function. Figure 2.14(b) shows that the Kriging model represents the true function very accurately indeed.

The procedure is also applied to the three degree of freedom mass-spring system with well separated modes. The eigenvalues of the system shown in Figure 2.13 are well separated if the parameters are:

$$\begin{aligned} &m_2 = 1\,\text{kg}, \quad m_3 = 1\,\text{kg}, \\ &k_1 = k_2 = k_3 = k_4 = k_5 = 1\,\text{N/m} \quad k_6 = 3\,\text{N/m} \end{aligned} \tag{2.90}$$

The mass parameter m_1 is assumed to be uncertain and can be changed within the interval $[\ 0.6 \quad 0.9\ ]$. The first component of the first eigenvector (mode shape) is assumed to be an unknown function. Figure 2.15 shows the Kriging model and target function together with the mean square error estimate with initial samples. It can be seen from Figure 2.15 that the Kriging model is in very good agreement with the target function and the MSE is sufficiently small.

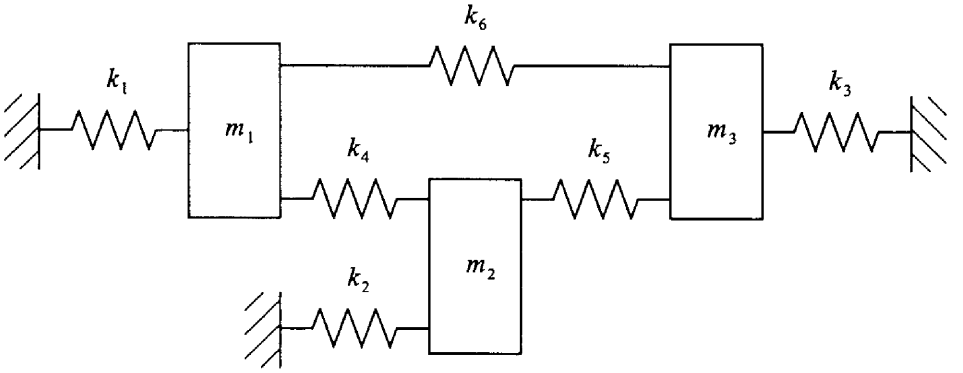

Figure 2.13: Three degree of freedom system.

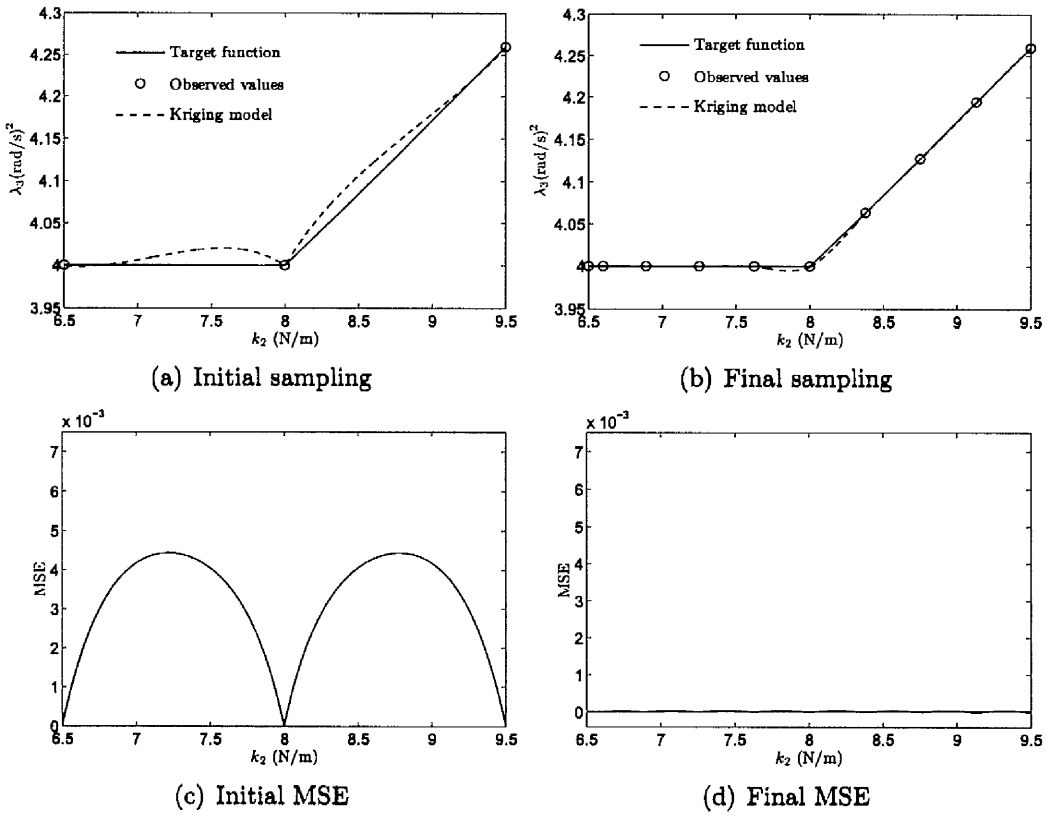

(a) Initial sampling

(b) Final sampling

(c) Initial MSE

(d) Final MSE

Figure 2.14: Kriging approximation and MSE of the third eigenvalue λ_3 versus uncertain stiffness parameter k_2.

Figure 2.15(a) also shows that the vertex solution, described in section (2.3.4), is invalid in this case because the relationship between input and output is not monotonic.

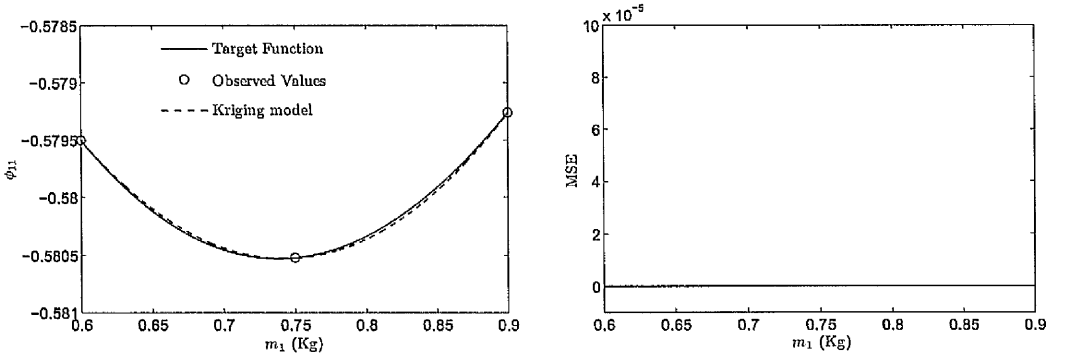

(a) (b)

Figure 2.15: (a)Kriging approximation and (b)MSE of the first component of first mode shape (3 DOFs system with well separated modes) against the uncertain mass parameter m_1.

2.4 Closure

Necessary information about the mathematical tools used in this thesis, have been provided in this chapter. Firstly, the methods for modelling uncertainty in input parameters are described. The models are generally categorised into two groups, i.e., probabilistic and non-probabilistic models. Probability theory and random fields are explained for the probabilistic models, while interval and fuzzy sets are described for the non-probabilistic models. The methods for quantifying the uncertainty in the outputs of a numerical model due to uncertainty in the input parameters are also introduced. The MCS, perturbation, asymptotic integral, interval analysis, fuzzy method and meta-model are considered and discussed.

The subject of uncertainty in the engineering problems has been extensively investigated in the literature (e.g. [9]). The application of the forward uncertainty propagation methods to non-deterministic analysis of aeroelasticity which has received less attention (in comparison with non-deterministic dynamic analysis) in the literature will be discussed in Chapter 4. However, propagation of structural uncertainty through a deterministic analysis requires the information on the range/distribution of uncertain parameters. The structural uncertain parameters are often not measurable and have to be identified from the information on the output test data. This requires the solution of an inverse problem. A review of the inverse problem of uncertainty identification in structural dynamics

is carried out in the following chapter and new methods developed in this work, are discussed in Chapters 5 and 6.

Chapter 3

Literature review of model updating in structural dynamics

3.1 Introduction

Comparison between measured data from prototype structures and predicted results from a corresponding analytical or numerical model is a very important step in the design of structures. Once the comparison is carried out, the quality of the numerical model can be evaluated. If the results from the numerical model agree well with their experimental counterparts, one may rely on the numerical model for the purposes of design. However, in most cases the agreement is not good enough due to different sources of errors in the numerical model such as model structure errors, model parameter errors and model order errors. These errors can be overcome by different methods such as those presented in [2–5].

Model updating [3, 4] is the tool that deals with parameterisation and the model parameter errors. In the model updating procedure, inaccurate parameters are often chosen by the analyst and are corrected by means of available measured data. However, the measured data are not often accurate and variability may exist in the data. The performance of model updating methods may be improved by implementing statistical techniques in which the inaccurate numerical model is corrected by using uncertain measured data. The measured data often include modal data (natural frequencies and mode shapes) and Frequency Response Functions (FRFs), obtained from experimental modal analysis [63–65].

Parameterisation in model updating (the choice of updating parameters) is very important and requires considerable physical insight. The parameterisation

of the numerical model which is commonly used in deterministic/stochastic model updating methods have been extensively studied in the literature such as those presented in [32, 66–71]. However, this topic is of no direct concern of this thesis and can be investigated in future work.

In this chapter, a brief description of the comparison techniques and the problem of model updating when the measured data are assumed to be accurate are given. A comprehensive review of the model updating techniques in the presence of uncertain measured data with reducible and irreducible uncertainty is then presented. Finally, the performance of some of the methods is evaluated in a simple numerical example.

3.2 Comparison methods in model updating

Comparing predictions from numerical model with test data is a necessary stage in the model updating procedure. The purpose of this comparison is to evaluate the closeness of the experimental model and corresponding numerical counterpart. The comparison is often carried out in the modal domain between the natural frequencies and the mode shape vectors. Determining the degree of correlation between the measured and predicted natural frequencies is quite straightforward. On the other hand, due to the fact that experimental mode shapes are often incomplete and complex[1], different indicators for the comparison between the experimental and analytical mode shapes have to be introduced. The Modal Assurance Criterion (MAC) [75] is the most popular indicator that has been frequently used in the literature. In order to calculate the MAC value, the mode shapes obtained from numerical/analytical models are paired with those achieved experimentally and the following equation can then be used,

[1]In practice the dimensions of the eigenvectors obtained from numerical model $\boldsymbol{\phi}_i^{(a)}$ is greater than the dimensions of the experimental eigenvector counterparts $\boldsymbol{\phi}_i^{(m)}$. This is due to the fact that the responses can only be measured at limited number of locations on physical structures. Furthermore, measuring the rotational degree of freedom is not straightforward and they are often not measured. The reduction techniques (e.g. [72, 73]) can be used to reduce the size of numerical eigenvector to the size of measured eigenvector. Alternatively, the expansion method (e.g. [74]) may be utilized to expand the size of measured eigenvector to the size of numerical eigenvector.

$$\mathrm{MAC}\left(\boldsymbol{\phi}_i, \boldsymbol{\phi}_j\right) = \frac{\left|\boldsymbol{\phi}_i^{\mathrm{T}} \boldsymbol{\phi}_j^*\right|^2}{\left(\boldsymbol{\phi}_i^{\mathrm{T}} \boldsymbol{\phi}_i^*\right)\left(\boldsymbol{\phi}_j^{\mathrm{T}} \boldsymbol{\phi}_j^*\right)} \tag{3.1}$$

where $\boldsymbol{\phi}_i$ and $\boldsymbol{\phi}_j$ are the i^{th} and j^{th} structural normal mode and $\bullet^*$ represents the complex conjugate. The MAC value varies between 0 and 1; The value of 1 shows a perfect correlation, while zero value indicates no correlation between analytical and experimental mode shapes. Some of the advantages of using the MAC indicator include: (i) direct utilisation of complex modes from measurement, and (ii) straightforward implementation of reduced numerical/analytical mode shape. However, there are also some disadvantages in using the MAC indicator as: (i) it does not work well in dealing with local modes, and (ii) it does not include any explicit information on shape features. In order to overcome the first disadvantage, an error location technique namely Coordinate Modal Assurance Criteria (COMAC) [76] can be applied to measure the degree of correlation at each degree of freedom by averaging the set of correlation between mode pairs. The second disadvantage can be overcome using new methods [77] based upon the concepts of image processing and pattern recognition which have been developed to determine the degree of correlation between the displacements of the mode shape vectors together with their shape features.

3.3 Deterministic model updating

A general procedure of model updating technique is shown in Figure 3.1. As shown in this figure, the objective of model updating is to improve the correlation between the experimental and analytical/numerical model. Various methods have emerged for this purpose and they can be generally categorised into three groups: (i) direct methods using modal data, (ii) iterative methods using modal data, and (iii) iterative methods using FRF data [3].

In the direct methods, a 'representational' model including the updated global mass and stiffness matrices that are capable of reproducing the measured data exactly are determined. These matrices are obtained by minimising an objective function (i.e., the difference between the measured data and predicted data using a suitable norm) subject to exact constraints on the independent variables. How-

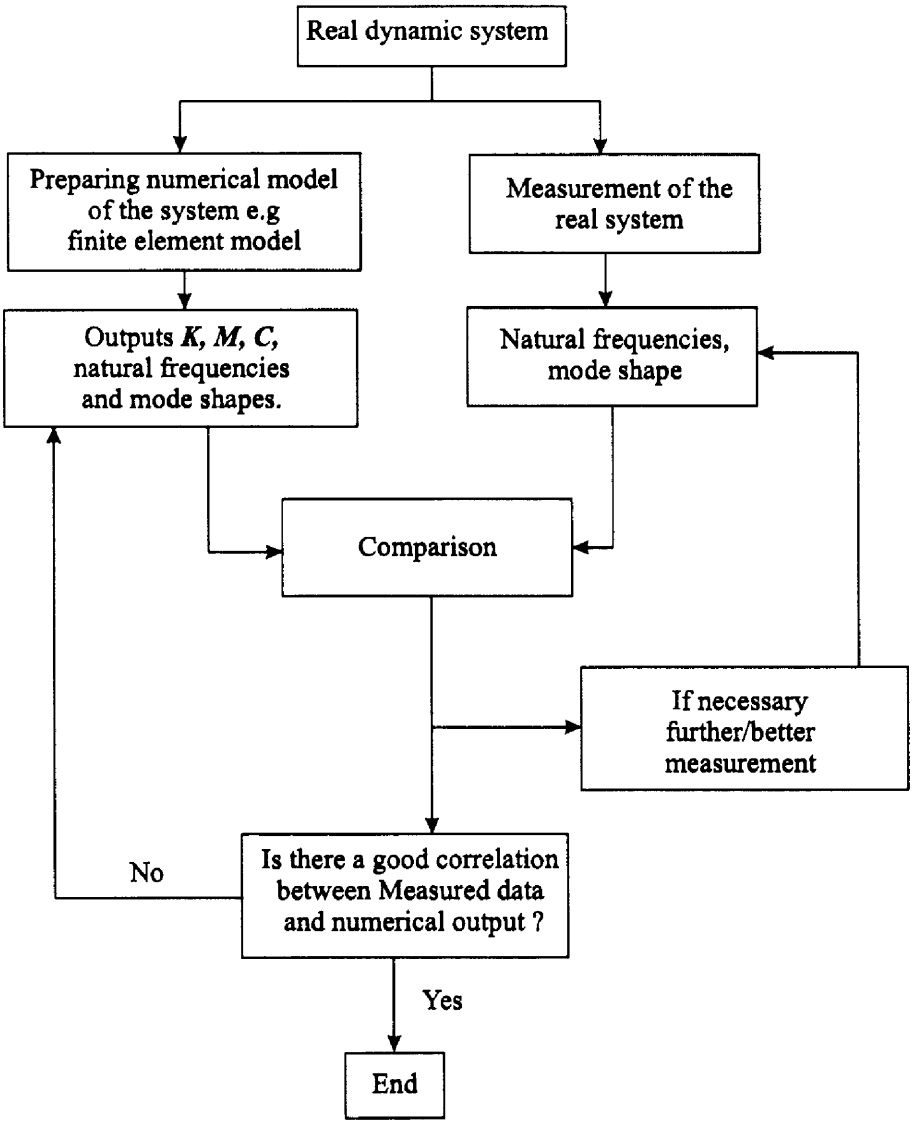

Figure 3.1: Procedure of model updating.

ever, these methods have received less attention in the industry due to the lack of insight into the modelling errors and lack of confidence about the connectivity of the nodes. The work presented in [78–83] are examples of the direct methods for model updating.

In the iterative methods for model updating, physical parameters such as joint stiffness and damping are chosen and adjusted based on sensitivity analysis so that the difference between the measured data and predicted modal/FRF data is minimised. In these methods, the experimental model is treated as a perturbation method in updating parameters about the initial numerical model. In the iterative

methods using modal data, the perturbation equation may be written as follows:

$$\mathbf{z}_m = \mathbf{z}_j + \mathbf{S}_j \left(\boldsymbol{\theta}_{j+1} - \boldsymbol{\theta}_j\right) \tag{3.2}$$

where

$$\mathbf{z}_m = \left[\begin{array}{cccccccc} \lambda_1^{(\mathrm{m})} & \lambda_2^{(\mathrm{m})} & \cdots & \lambda_{r_1}^{(\mathrm{m})} & \boldsymbol{\phi}_1^{\mathrm{T}(\mathrm{m})} & \boldsymbol{\phi}_2^{\mathrm{T}(\mathrm{m})} & \cdots & \boldsymbol{\phi}_{r_2}^{\mathrm{T}(\mathrm{m})} \end{array} \right]^{\mathrm{T}} \in \Re^{n_r} \tag{3.3}$$

is the assembled vector of measured data,

$$\mathbf{z}_j = \left[\begin{array}{cccccccc} \lambda_1^{(\mathrm{a})} & \lambda_2^{(\mathrm{a})} & \cdots & \lambda_{r_1}^{(\mathrm{a})} & \boldsymbol{\phi}_1^{\mathrm{T}(\mathrm{a})} & \boldsymbol{\phi}_2^{\mathrm{T}(\mathrm{a})} & \cdots & \boldsymbol{\phi}_{r_2}^{\mathrm{T}(\mathrm{a})} \end{array} \right]^{\mathrm{T}} \in \Re^{n_r} \tag{3.4}$$

is the j^{th} assembled vector of the predicted outputs from analytical/numerical model, $\lambda_i = \omega_i^2$ is the i^{th} eigenvalue of dynamic system, $\boldsymbol{\phi}_i^{(\mathrm{a})}$ and $\boldsymbol{\phi}_i^{(\mathrm{m})}$ are the i^{th} numerical/analytical and experimental eigenvector (mode shape) respectively, n_r is the number of responses, $\boldsymbol{\theta}_j \in \Re^p$ is the vector of updating parameter at j^{th} iteration and $\mathbf{S}_j$ is the sensitivity matrix at j^{th} iteration which is defined as

$$\mathbf{S}_j = \left[\begin{array}{cccc} \frac{\partial z_{j_1}}{\partial \theta_1} & \frac{\partial z_{j_1}}{\partial \theta_2} & \cdots & \frac{\partial z_{j_1}}{\partial \theta_p} \\ \frac{\partial z_{j_2}}{\partial \theta_1} & \frac{\partial z_{j_2}}{\partial \theta_2} & \cdots & \frac{\partial z_{j_2}}{\partial \theta_p} \\ \cdot & \cdot & \cdots & \cdot \\ \cdot & \cdot & \cdots & \cdot \\ \cdot & \cdot & \cdots & \cdot \\ \frac{\partial z_{j_{n_r}}}{\partial \theta_1} & \frac{\partial z_{j_{n_r}}}{\partial \theta_2} & \cdots & \frac{\partial z_{j_{n_r}}}{\partial \theta_p} \end{array} \right] \in \Re^{n_r \times p} \tag{3.5}$$

The eigenvalue derivatives of the system with respect to the updating parameters are given by [84],

$$\frac{\partial \lambda_i}{\partial \theta_j} = \frac{\boldsymbol{\phi}_i^{\mathrm{T}} \frac{\partial \mathbf{K}}{\partial \theta_j} \boldsymbol{\phi}_i - \lambda_i \boldsymbol{\phi}_i^{\mathrm{T}} \frac{\partial \mathbf{M}}{\partial \theta_j} \boldsymbol{\phi}_i}{\boldsymbol{\phi}_i^{\mathrm{T}} \mathbf{M} \boldsymbol{\phi}_i} \tag{3.6}$$

where $\mathbf{M}$ is the global mass matrix, $\mathbf{K}$ is the global stiffness matrix and the eigenvector derivatives of the dynamic system with respect to the updating parameters can be written as [84]:

$$\frac{\partial \boldsymbol{\phi}_i}{\partial \theta_j} = \sum_{k=1}^{n} \alpha_{ik} \boldsymbol{\phi}_k \tag{3.7}$$

where

$$\alpha_{ik} = \begin{cases} \frac{\boldsymbol{\phi}_k^{\mathrm{T}} \left[\frac{\partial \mathbf{K}}{\partial \theta_j} - \lambda_i \frac{\partial \mathbf{M}}{\partial \theta_j} \right] \boldsymbol{\phi}_i}{\lambda_i - \lambda_k} & \text{if } i \neq k \\ -\frac{1}{2} \boldsymbol{\phi}_i^{\mathrm{T}} \frac{\partial \mathbf{M}}{\partial \theta_j} \boldsymbol{\phi}_i & \text{if } i = k \end{cases}$$

In practice, there are three major issues related to the measured data and numerical/analytical predictions introduced in Eq. (3.2) [3]. The first is mode pairing. The measured natural frequencies/mode shapes should be paired with those obtained from numerical model. The MAC value, explained in Section 3.2, is a tool for the solution of mode pairing.

The second concerns mode shape scaling. The numerical/analytical and experimental mode shapes have different scales due to the difference between the mass distribution of the numerical model and physical structure. The Modal Scale Factor (MSF) may be used to scale the measured mode shape to the analytical mode shape as described in [85].

Extracting the real mode shapes from experimental complex mode shape is the third issue in the model updating. Structural damping is not often included in the numerical/analytical model and therefore the numerical/analytical mode shapes are real. However, due to the presence of actual damping in the physical structure, the experimental mode shapes are complex. For lightly damped system, the complex eigenvector terms are converted to real values by multiplying the modulus of each term of complex eigenvector by the sign of the cosine of its phase angle [3]. This method is the most common method which deals with the issue of the complexity of the measured mode shape.

The perturbation approach, described by Eq. (3.2), is limited to small variation of the updating parameters. Therefore, Eq. (3.2) has to be applied iteratively so that the restriction applies step-by-step. The issues of convergence and ill-conditioning of the matrices are associated with the iterative methods in the model updating problem. When the matrix $\mathbf{S}_j$ in Eq. (3.2) is close to being rank deficient, the updating parameters, $\boldsymbol{\theta}_j$, will have large deviations at each iteration. This usually results in fluctuation of the updating parameters without achieving convergence. In this case, the system of equations in model updating is said to be unstable and Eq. (3.2) is ill-conditioned. Different methods, namely the regularisation methods [6], for the treatment of ill-conditioned systems of equations in the model updating problem have been introduced. The Tikhonov's regularisation technique [86] is the most popular method and has received considerable attention in the literature. In the application of Tikhonov's regularisation

technique, the parameter change at each iteration is limited by introducing a positive definite weighting matrix, $\mathbf{W}_2$, which gives the new constrained optimisation problem as

$$\text{Minimise} \qquad (\boldsymbol{\theta}_{j+1} - \boldsymbol{\theta}_j)^{\mathrm{T}} \mathbf{W}_2 (\boldsymbol{\theta}_{j+1} - \boldsymbol{\theta}_j) \tag{3.8}$$

subject to Eq. (3.2). The solution of above constrained minimisation problem leads to the following recursive equation for estimation of updating parameters (presented in [87]).

$$\boldsymbol{\theta}_{j+1} = \boldsymbol{\theta}_j + \left[\mathbf{S}_j^{\mathrm{T}} \mathbf{W}_1 \mathbf{S}_j + \mathbf{W}_2\right]^{-1} \left\{\mathbf{S}_j^{\mathrm{T}} \mathbf{W}_1 (\mathbf{z}_m - \mathbf{z}_j)\right\} \tag{3.9}$$

where the minimum-norm regularised solution is obtained when $\mathbf{W}_2 = r_g \mathbf{I}$ and r_g is the regularisation parameter that locates the corner of an L-curve obtained by plotting the norms $\|\mathbf{W}_2 (\boldsymbol{\theta}_{j+1} - \boldsymbol{\theta}_j)\|$ vs $\|\mathbf{S}_j (\boldsymbol{\theta}_{j+1} - \boldsymbol{\theta}_j) - (\mathbf{z}_m - \mathbf{z}_j)\|$ as r_g is varied [6].

Friswell and Mottershead [3] derived the following iterative equation by changing the constraint in Eq. (3.8) to $(\boldsymbol{\theta}_{j+1} - \boldsymbol{\theta}_0)^{\mathrm{T}} \mathbf{W}_2 (\boldsymbol{\theta}_{j+1} - \boldsymbol{\theta}_0)$.

$$\boldsymbol{\theta}_{j+1} = \boldsymbol{\theta}_j + \left[\mathbf{S}_j^{\mathrm{T}} \mathbf{W}_1 \mathbf{S}_j + \mathbf{W}_2\right]^{-1} \left\{\mathbf{S}_j^{\mathrm{T}} \mathbf{W}_1 (\mathbf{z}_m - \mathbf{z}_j) - \mathbf{W}_2 (\boldsymbol{\theta}_j - \boldsymbol{\theta}_0)\right\} \tag{3.10}$$

By doing so the regulation parameter at each iteration is decreased. The reduction of regulation parameter results in making the weighting matrix smaller at each iteration which is somehow equivalent to the minimum variance method which will be explained later in this chapter.

The iterative model updating techniques using modal data have been frequently and successfully used in the application to industrial-scale structure such as those presented in [71, 88–90].

The iterative model updating methods which minimise the difference between measured and analytical FRF data have been also studied [91,92]. These methods are particularly useful for the model updating of damped structural systems. However, modal data including natural frequencies and mode shapes are sufficient when interest is mostly correcting stiffness and mass terms, where is usually the case.

In the above discussion, it is assumed that the measured data are accurate. However, variability inevitably exists in the measured data and has to be considered in the model updating procedure. The next section discusses the problem of model updating in the presence of uncertain measured data.

3.4 Model updating methods in the presence of uncertain measured data

In practical model updating the measured data are often imprecise, incomplete and variable. Therefore, it is very important to include statistical techniques to improve performance. However, care should be taken about the type of variability that exists in the experimental data.

Variability in experimental results can be categorised in two groups; reducible and irreducible. Measurement noise and the use of sensors that affect the measurement or signal processing that might introduce bias are some examples of reducible uncertainty which can be minimised by gathering more/further information (e.g. repeating the measurement). Statistical methods for the treatment of measurement noise in model updating were established in 1974 by Collins et al. [26] and more recently by Friswell [93]. In these approaches, randomness arises only from the measurement noise. The updating parameters take unique values, found by iterative correction to the estimated means, whilst the variances are minimised. Beck and Katafygiotis [94] developed a Bayesian probabilistic framework for robust finite element model updating, which was later employed by Beck and Au [95], to correct a two degree-of-freedom mass-spring system by using Markov Chain Monte-Carlo Simulation (MCMCS). They demonstrated that the method is capable of identifying multiple non-unique solutions. Other model updating approaches that incorporate Bayesian theory are presented in [96–98]. Soize et al. [99] presented a methodology for robust model updating by using a nonparametric probabilistic approach. The method leads to the solution of a mono-objective optimisation problem with inequality probabilistic constraints. Haag et al. [100] proposed an inverse approach based on the fuzzy arithmetic for the model updating. The method utilises the transformation method, introduced

in [50] for the purpose of forward propagation method, to identify the epistemic uncertainties inherent to numerical model of physical structure. Although statistics have been incorporated into the above methods, only one value is identified for each of the updating parameters, and the estimates of distributions/ranges of updating parameters are indicators of the uncertainty in the identified parameters due to measurement noise and do not represent a physical variability (e.g. due to manufacturing tolerances).

On the other hand, the model updating methods in the presence of the irreducible uncertain measured data require different mathematical approaches as the distribution/ranges of updating parameters and measured data become physically meaningful in this situation. Uncertain parameters such as damping and stiffness in mechanical joints are chosen for updating. In this case, it is assumed that multiple sets of modal test data (e.g. from nominally identical test structures built in the same way from the same materials), are available. The distributions of the updating parameters are then modified in order to improve the correlation between model-predicted distributions and distributions of measured data. This is called stochastic model updating or uncertainty identification. Note that the stochastic model updating problem includes not only the variability in measurement signals due to noise, but also the variability that exists between nominally identical test structures, built in the same way from the same materials but with manufacturing and material variability [25, 101]. Similar variability is known to result from environmental erosion, damage [27, 102, 103], or disassembly and reassembly of the same structure [104, 105]. Very few papers have considered the problem of stochastic model updating or uncertainty identification in the literature. However, the distribution or range of uncertain parameters is very important for numerous practical applications and is required for forward propagation to estimate the distributions of the outputs of dynamic system (e.g. natural frequencies, mode shapes, frequency response functions, flutter speed etc).

As previously mentioned, in a small number of research papers the problem of stochastic model updating is considered. Fonseca et al. [24] proposed an optimisation procedure for the purpose of stochastic model updating based on maximising a likelihood function and applied it to a cantilever beam with a point mass at

an uncertain location. Mares et al. [25] adapted the method of Collins et al. [26] within a gradient-regression formulation for the treatment of test-structure variability. Hua et al. [27] used perturbation theory in the problem of test-structure variability. The predicted output mean values and the matrix of predicted covariances were made to converge upon measured values and in so doing the first two statistical moments of the uncertain updating parameters were determined. In the following sections, methods proposed by Collins et al. [26], Friswell [93], Beck and Au [95], Fonseca et al. [24] and Hua et al. [27] are considered and explained. A comparative study on the performance of these methods is also carried out on a three-degree-of-freedom mass-spring system.

3.4.1 Minimum variance methods

Collins et al. [26] formulated a method in which the updating parameters are estimated in an iterative way from experimental data. The method incorporated statistical techniques to treat the test measurement errors as well as uncertainty in the estimation of updating parameters. In other words, it is assumed that both measured data and updating parameters have errors which may be described by their variances. An advantage of this method is that it enables the structural analyst to assess the quality of updated parameters through their estimated variances [3]. However, the method works well in the presence of large amount of test data. In the minimum variance method, the unknown structural parameters (updating parameters) are assumed to be normally distributed with mean values

$$E(\boldsymbol{\theta}_j) = \widehat{\boldsymbol{\theta}}_j \tag{3.11}$$

and covariance matrix

$$\mathrm{Cov}(\boldsymbol{\theta}_j, \boldsymbol{\theta}_j) = \mathbf{V}_{\boldsymbol{\theta}_j} \tag{3.12}$$

It is also assumed that an estimate $\boldsymbol{\theta}_{j+1}$ may be updated by using a prior estimate $\boldsymbol{\theta}_j$ as

$$\boldsymbol{\theta}_{j+1} = \boldsymbol{\theta}_j + \mathbf{T}(\mathbf{z}_m - \mathbf{z}_j) \tag{3.13}$$

where $\mathbf{T}$ is an unknown transformation matrix. Another assumption, made in Collins's method, is that the errors vector $\epsilon = \mathbf{z}_m - \widehat{\mathbf{z}}$ ($\widehat{\mathbf{z}}$ is the expected (mean)

value of predicted output from analytical/numerical model) follows a joint normal distribution with mean

$$E(\epsilon) = \{0\} \tag{3.14}$$

and covariance matrix

$$\mathrm{Cov}(\epsilon, \epsilon) = E\left(\epsilon^{\mathrm{T}}\epsilon\right) = \mathbf{V}_{\epsilon} \tag{3.15}$$

Since the transformation matrix $\mathbf{T}$ in Eq. (3.13) is deterministic, the following equation can be written

$$E(\theta_{j+1} - \theta_j) = TE(\mathbf{z}_m - \mathbf{z}_j) = \{0\} \quad \Rightarrow \quad E(\theta_{j+1}) = E(\theta_j) = \widehat{\theta} \tag{3.16}$$

Therefore the mean values of the parameter estimates give the solution of the inverse problem. The best estimate of the mean will occur when the variance estimate is minimised. In other words, the scattering around the mean will be minimised and the solution is more likely to be closer to the mean value. In order to obtain the parameter estimates with minimum variances, the covariance estimates at $j+1^{\mathrm{th}}$ iteration can be calculated as [2]

$$\begin{aligned}\mathbf{V}_{\theta_{j+1}} =& \mathbf{V}_{\theta_j} + \mathrm{Cov}(\theta_j, \mathbf{z}_m)\,\mathbf{T}^{\mathrm{T}} - \mathrm{Cov}(\theta_j, \mathbf{z}_j)\,\mathbf{T}^{\mathrm{T}} \\ &+ \mathbf{T}\,\mathrm{Cov}(\mathbf{z}_m, \theta_j) + \mathbf{T}\,\mathbf{V}_{\epsilon}\mathbf{T}^{\mathrm{T}} - \mathbf{T}\,\mathrm{Cov}(\mathbf{z}_m, \mathbf{z}_j) \\ &- \mathbf{T}\,\mathrm{Cov}(\mathbf{z}_j, \theta_j) - \mathbf{T}\,\mathrm{Cov}(\mathbf{z}_j, \mathbf{z}_m)\,\mathbf{T}^{\mathrm{T}} + \mathbf{T}\,\mathrm{Cov}(\mathbf{z}_j, \mathbf{z}_j)\,\mathbf{T}^{\mathrm{T}}\end{aligned} \tag{3.17}$$

where $\mathbf{V}_{\theta} = \mathrm{Cov}(\theta, \theta)$ and $\mathbf{V}_{\epsilon} = \mathrm{Cov}(\mathbf{z}_m, \mathbf{z}_m)$. For the mean-centred first order perturbation method the mean value of predicted output data $\widehat{\mathbf{z}}$ may be expanded around the mean values of updating parameters $\widehat{\theta}$ as

$$\mathbf{z}_j = \widehat{\mathbf{z}} + \mathbf{S}_j\left(\theta_j - \widehat{\theta}\right) \quad \Rightarrow \quad \mathbf{z}_j - \widehat{\mathbf{z}} = \mathbf{S}_j\left(\theta_j - \widehat{\theta}\right) \tag{3.18}$$

Eq. (3.18) results in

$$\mathrm{Cov}(\theta_j, \mathbf{z}_j) = E\left(\left(\theta_j - \widehat{\theta}\right)(\mathbf{z}_j - \widehat{\mathbf{z}})^{\mathrm{T}}\right) = E\left(\left(\theta_j - \widehat{\theta}\right)\left(\theta_j - \widehat{\theta}\right)^{\mathrm{T}}\right)\mathbf{S}_j^{\mathrm{T}} \tag{3.19}$$

[2]Note: the proof which is given here is slightly different from those presented in [3, 26, 93], however the final equations are the same.

and therefore

$$\mathrm{Cov}\left(\boldsymbol{\theta}_j, \mathbf{z}_j\right) = \mathbf{V}_{\boldsymbol{\theta}_j}\mathbf{S}_j^{\mathrm{T}} \tag{3.20}$$

$$\mathrm{Cov}\left(\mathbf{z}_j, \boldsymbol{\theta}_j\right) = \mathbf{S}_j\mathbf{V}_{\boldsymbol{\theta}_j} \tag{3.21}$$

$$\mathrm{Cov}\left(\mathbf{z}_j, \mathbf{z}_j\right) = \mathbf{S}_j\mathbf{V}_{\boldsymbol{\theta}_j}\mathbf{S}_j^{\mathrm{T}} \tag{3.22}$$

In the Collins's method the correlation between measurements $\mathbf{z}_m$ and updating parameters $\boldsymbol{\theta}$ is omitted. Therefore $\mathrm{Cov}\left(\boldsymbol{\theta}_j, \mathbf{z}_m\right)$ and $\mathrm{Cov}\left(\mathbf{z}_j, \mathbf{z}_m\right)$ vanish under the Collins's assumption. Substituting Eqs. (3.20), (3.21) and (3.22) into Eq. (3.17) and considering Collins's assumption leads to:

$$\mathbf{V}_{\boldsymbol{\theta}_{j+1}} = \mathbf{V}_{\boldsymbol{\theta}_j} - \mathbf{V}_{\boldsymbol{\theta}_j}\mathbf{S}_j^{\mathrm{T}}\mathbf{T}^{\mathrm{T}} + \mathbf{T}\mathbf{V}_{\boldsymbol{\epsilon}}\mathbf{T}^{\mathrm{T}} - \mathbf{T}\mathbf{S}_j\mathbf{V}_{\boldsymbol{\theta}_j} + \mathbf{T}\mathbf{S}_j\mathbf{V}_{\boldsymbol{\theta}_j}\mathbf{S}_j^{\mathrm{T}}\mathbf{T}^{\mathrm{T}} \tag{3.23}$$

Minimising the covariance matrix $\mathbf{V}_{\boldsymbol{\theta}_{j+1}}$ with respect to components of transformation matrix T_{ik} gives the transformation matrix. A necessary condition for this minimising is that

$$\frac{\partial \mathbf{V}_{\boldsymbol{\theta}_{j+1}}}{\partial T_{ik}} = 0 \qquad \forall\ i = 1...p,\ k = 1...n_r \tag{3.24}$$

which leads to

$$\mathbf{T} = \mathbf{V}_{\boldsymbol{\theta}_j}\mathbf{S}_j^{\mathrm{T}}\left[\mathbf{S}_j\mathbf{V}_{\boldsymbol{\theta}_j}\mathbf{S}_j^{\mathrm{T}} + \mathbf{V}_{\boldsymbol{\epsilon}}\right]^{-1} \tag{3.25}$$

Hence two recursive systems of equations having the following form for the estimation of updating parameters and their covariance matrix are obtained,

$$\boldsymbol{\theta}_{j+1} = \boldsymbol{\theta}_j + \mathbf{V}_{\boldsymbol{\theta}_j}\mathbf{S}_j^{\mathrm{T}}\left[\mathbf{S}_j\mathbf{V}_{\boldsymbol{\theta}_j}\mathbf{S}_j^{\mathrm{T}} + \mathbf{V}_{\boldsymbol{\epsilon}}\right]^{-1}\left(\mathbf{z}_m - \mathbf{z}_j\right) \tag{3.26}$$

$$\mathbf{V}_{\boldsymbol{\theta}_{j+1}} = \mathbf{V}_{\boldsymbol{\theta}_j} - \mathbf{V}_{\boldsymbol{\theta}_j}\mathbf{S}_j^{\mathrm{T}}\left[\mathbf{S}_j\mathbf{V}_{\boldsymbol{\theta}_j}\mathbf{S}_j^{\mathrm{T}} + \mathbf{V}_{\boldsymbol{\epsilon}}\right]^{-1}\mathbf{S}_j\mathbf{V}_{\boldsymbol{\theta}_j}^{\mathrm{T}} \tag{3.27}$$

Friswell [93] corrected the assumption of omitted correlation between $\mathbf{z}_m$ and $\boldsymbol{\theta}$, made by Collins [26], by including the correlation after the first iteration. In the Friswell's approach, the correlation between measured data and updating parameters is defined as

$$\mathrm{Cov}\left(\theta_j, \mathbf{z}_m\right) = \begin{cases} 0 & \text{if} \quad j = 1 \\ \mathbf{D}_j & \text{if} \quad j = 2, 3, 4, \ldots \end{cases} \tag{3.28}$$

Using the mean-centred first order perturbation method, given in Eq. (3.18), produces the following equation

$$\mathrm{Cov}\left(\mathbf{z}_j, \mathbf{z}_m\right) = \mathbf{S}_j \mathbf{D}_j \tag{3.29}$$

It is evident that $\mathrm{Cov}\left(\mathbf{z}_m, \theta_j\right) = \mathbf{D}_j^{\mathrm{T}}$ and $\mathrm{Cov}\left(\mathbf{z}_m, \mathbf{z}_j\right) = \mathbf{D}_j^{\mathrm{T}} \mathbf{S}_j^{\mathrm{T}}$. In this case, Eq. (3.17) is now written in the format

$$\begin{aligned} \mathbf{V}_{\theta_{j+1}} =& \mathbf{V}_{\theta_j} + \mathbf{D}_j \mathbf{T}^{\mathrm{T}} - \mathbf{V}_{\theta_j} \mathbf{S}_j^{\mathrm{T}} \mathbf{T}^{\mathrm{T}} + \mathbf{T} \mathbf{D}_j^{\mathrm{T}} + \mathbf{T} \mathbf{V}_{\epsilon} \mathbf{T}^{\mathrm{T}} - \mathbf{T} \mathbf{D}_j^{\mathrm{T}} \mathbf{S}_j^{\mathrm{T}} \\ & - \mathbf{T} \mathbf{S}_j \mathbf{V}_{\theta_j} - \mathbf{T} \mathbf{S}_j \mathbf{D}_j \mathbf{T}^{\mathrm{T}} + \mathbf{T} \mathbf{S}_j \mathbf{V}_{\theta_j} \mathbf{S}_j^{\mathrm{T}} \mathbf{T}^{\mathrm{T}} \end{aligned} \tag{3.30}$$

The transformation matrix can now be obtained by minimising the covariance matrix $\mathbf{V}_{\theta_{j+1}}$ with respect to components of transformation matrix T_{ik} as

$$\mathbf{T} = \left(\mathbf{V}_{\theta_j} \mathbf{S}_j^{\mathrm{T}} - \mathbf{D}_j\right) \left[\mathbf{S}_j \mathbf{V}_{\theta_j} \mathbf{S}_j^{\mathrm{T}} - \mathbf{S}_j \mathbf{D}_j - \mathbf{D}_j^{\mathrm{T}} \mathbf{S}_j^{\mathrm{T}} + \mathbf{V}_{\epsilon}\right]^{-1} \tag{3.31}$$

Now three recursive systems of equations having the following forms for the estimation of updating parameters, their covariance matrix and the correlation matrix are obtained,

$$\theta_{j+1} = \theta_j + \left(\mathbf{V}_{\theta_j} \mathbf{S}_j^{\mathrm{T}} - \mathbf{D}_j\right) \mathbf{V}_{zj}^{-1} \left(\mathbf{z}_m - \mathbf{z}_j\right) \tag{3.32}$$

$$\mathbf{V}_{\theta_{j+1}} = \mathbf{V}_{\theta_j} - \left(\mathbf{V}_{\theta_j} \mathbf{S}_j^{\mathrm{T}} - \mathbf{D}_j\right) \mathbf{V}_{zj}^{-1} \left(\mathbf{V}_{\theta_j} \mathbf{S}_j^{\mathrm{T}} - \mathbf{D}_j\right)^{\mathrm{T}} \tag{3.33}$$

$$\mathbf{D}_{j+1} = \mathbf{D}_j - \left(\mathbf{V}_{\theta_j} \mathbf{S}_j^{\mathrm{T}} - \mathbf{D}_j\right) \mathbf{V}_{zj}^{-1} \left(\mathbf{S}_j \mathbf{D}_j - \mathbf{V}_{\epsilon}\right) \tag{3.34}$$

where $\mathbf{V}_{zj} = \mathbf{S}_j \mathbf{V}_{\theta_j} \mathbf{S}_j^{\mathrm{T}} - \mathbf{S}_j \mathbf{D}_j - \mathbf{D}_j^{\mathrm{T}} \mathbf{S}_j^{\mathrm{T}} + \mathbf{V}_{\epsilon}$.

As can be seen in Eqs. (3.27) and (3.33) the second term of the covariance estimate in both Collins and Friswell approaches has a quadratic form. This means that the procedure always gives the minimum parameter variance estimate, hence these methods are called minimum variance estimators. The application of the above methods to a simple three degree of freedom system having irreducible uncertain parameters is presented in Section (3.5).

3.4.2 Bayesian updating methods

Bayes' theorem (rule), named after the Reverend Thomas Bayes (1702-1761), utilizes the definition of conditional probability $P(X|Y)$ as

$$P(X|Y) = \frac{P(X,Y)}{P(Y)} \tag{3.35}$$

and by symmetry,

$$P(Y|X) = \frac{P(Y,X)}{P(X)} \tag{3.36}$$

where $P(X,Y)$ is the joint probability of X and Y and $P(X)$ and $P(Y)$ are the probability of X and Y respectively. The following equation may then be written from Eqs. (3.35) and (3.36),

$$P(Y|X) = \frac{P(X|Y)P(Y)}{P(X)} \tag{3.37}$$

which represents Bayes' rule. The dominator $P(X)$ acts as a normalising constant. According to Eq. (3.37), the conditional probability of event Y given X depends on the the conditional probability of event X given Y, and the prior probabilities of Y and X. This equation can be used for updating of the probability of Y using available information on X and the prior probability of Y.

The Bayes' theorem can be used for the model updating procedure in structural dynamics. Beck and his colleagues [94, 95] introduced the application of this theorem into updating problem. In this method, the initial joint probability distribution of unknown structural parameters $f_{\theta_0}(\boldsymbol{\theta})$ is chosen so that the predictions of a whole set of possible structural models are covered. The prior joint probability distribution is then updated using structural test data. In mathematical language, the updated joint probability distribution $f_{\boldsymbol{\theta}}(\boldsymbol{\theta})$ is obtained using the Bayes' theorem as follows:

$$f_{\boldsymbol{\theta}}(\boldsymbol{\theta}) = \frac{f_D(D|\boldsymbol{\theta})\, f_{\theta_0}(\boldsymbol{\theta})}{f_D(D)} \tag{3.38}$$

where D is a function representing the 'measure-of-fit' [95] given structural parameters $\boldsymbol{\theta}$, $f_D(D) = \int_{\Re^p} f_D(D|\boldsymbol{\theta})\, f_{\theta_0}(\boldsymbol{\theta})\, d\boldsymbol{\theta}$ is a normalising constant which is

a p-dimensional integral over unbounded domain $\Re^p$ and $f_D(D|\boldsymbol{\theta})$ describes the probability distribution of the data D based on model specified by the model parameters $\boldsymbol{\theta}$. The probability distribution of the data D describes the degree-of-correlation between predictions from the numerical model and the actual test data.

In many applications, the multi-dimensional integral for calculation of normalising constant, may not be tractable. In this case, sampling methods such as the Marcov Chain Monte Carlo (MCMC) method may be used to approximate this integral. In MCMC, the sample $\boldsymbol{\theta}^{(k)}$ is simulated from Markov chain samples $\left\{\boldsymbol{\theta}^{(1)}, \boldsymbol{\theta}^{(2)}, ..., \boldsymbol{\theta}^{(k)}\right\}$ in a way that the PDF of the Markov chain tends to the target PDF ($f_D(D)$) as $k \rightarrow \infty$. More details about the MCMC method and its application in Bayesian methods can be found in [106, 107].

To illustrate the Bayesian updating framework presented in [94], a simple numerical example (taken from [95]) is considered. It is a two-degree-of-freedom shear building model with the story masses of 16.5×10^3 kg for the first story and 16.1×10^3 kg for the second story. The interstory stiffnesses are assumed to be given by the following equations: $k_1 = 29.7 \times 10^6 \theta_1$ N/m and $k_2 = 29.7 \times 10^6 \theta_2$ N/m respectively where θ_1 and θ_2 are the unknown structural parameters. Since the structural parameters are statistically independent from each other, the joint PDF $f_{\theta_0}(\theta_1, \theta_2)$ for θ_1 and θ_2 are given by

$$f_{\boldsymbol{\theta}}(\theta_1, \theta_2) = f_{\theta_1}(\theta_1) \times f_{\theta_2}(\theta_2) \tag{3.39}$$

Log-normal PDFs with most probable values (MPVs) of 1.3 (30% overestimation relative to its nominal value) and 0.8 (20% underestimation relative to its nominal value) are chosen for θ_1 and θ_2, respectively. The 'measure-of-fit' function D between experimental and predicted outputs is defined by the following objective function [108]

$$J(\boldsymbol{\theta}) = \sum_{k=1}^{2} w_i^2 \left(\frac{\omega_k^2(\boldsymbol{\theta})}{\omega_{m_k}^2} - 1 \right)^2 \tag{3.40}$$

where the weights set to unity, $w_i = 1,\ i = 1, 2$, ω_k is the k^{th} predicted frequency and $\omega_{m_1} = 3.13$ Hz and $\omega_{m_2} = 9.83$ Hz are the first and second simulated mea-

sured frequency. A Gaussian distribution function with mean zero and standard deviation σ is chosen for $f_D(D|\boldsymbol{\theta})$ i.e., $f_D(D|\boldsymbol{\theta}) = \exp(-J(\boldsymbol{\theta})/(2\sigma^2))/\sqrt{2\pi\sigma^2}$. Eq. (3.38) is now written in the format

$$f_{\boldsymbol{\theta}}(\boldsymbol{\theta}) = c \exp\left(-\frac{J(\boldsymbol{\theta})}{2\epsilon^2}\right) f_{\boldsymbol{\theta}_0}(\boldsymbol{\theta}) \tag{3.41}$$

where the updated marginal PDFs can be calculated according to Eq. (2.10) as follows,

$$f_{\theta_i}(\theta_i) = \int_{-\infty}^{+\infty} f_{\boldsymbol{\theta}}(\boldsymbol{\theta})\, d\theta_j \quad i,j = 1,2 \quad i \neq j \tag{3.42}$$

The updated marginal PDFs ($f_{\theta_1}(\theta_1)$ and $f_{\theta_2}(\theta_2)$) of structural parameters are obtained by decreasing prediction error levels as $\sigma_i^2 = 1/2^{i-1}$ for successive simulation levels. The updated marginal PDF of the structural parameters ($f_D(\boldsymbol{\theta})$), shown in Figure 3.2, are achieved by substituting the sequence of values $\sigma_i^2 = 1/2^{i-1}$ into Eq. (3.41). The normalised constant c is calculated using direct numerical integration in this case. As can be seen in the figure, the updated PDFs bifurcate into two peaks as σ decreases. This is due to the fact that two optimal model exist that give the identified frequencies. This shows the capability of the method to identify a class of models rather than one model. This is an advantage over the minimum variance method which converges to one of the possible model parameters (depending on the initial selection of parameters).

By looking at the updated PDF in Figure 3.2, it can be readily implied that the Bayesian method attempts to minimise the variance of distribution around the peaks (identified parameters). This means that the standard deviations identified by this method are not physically meaningful as are in the minimum variance methods (in Section 3.4.1). In the following section, methods for irreducible uncertainty identification are described.

3.4.3 Maximum likelihood method

In the application of the stochastic model updating (identification of uncertain structural parameters from irreducible uncertain modal test data), Fonseca et al. [24] proposed a method based on maximising the likelihood of the measurements.

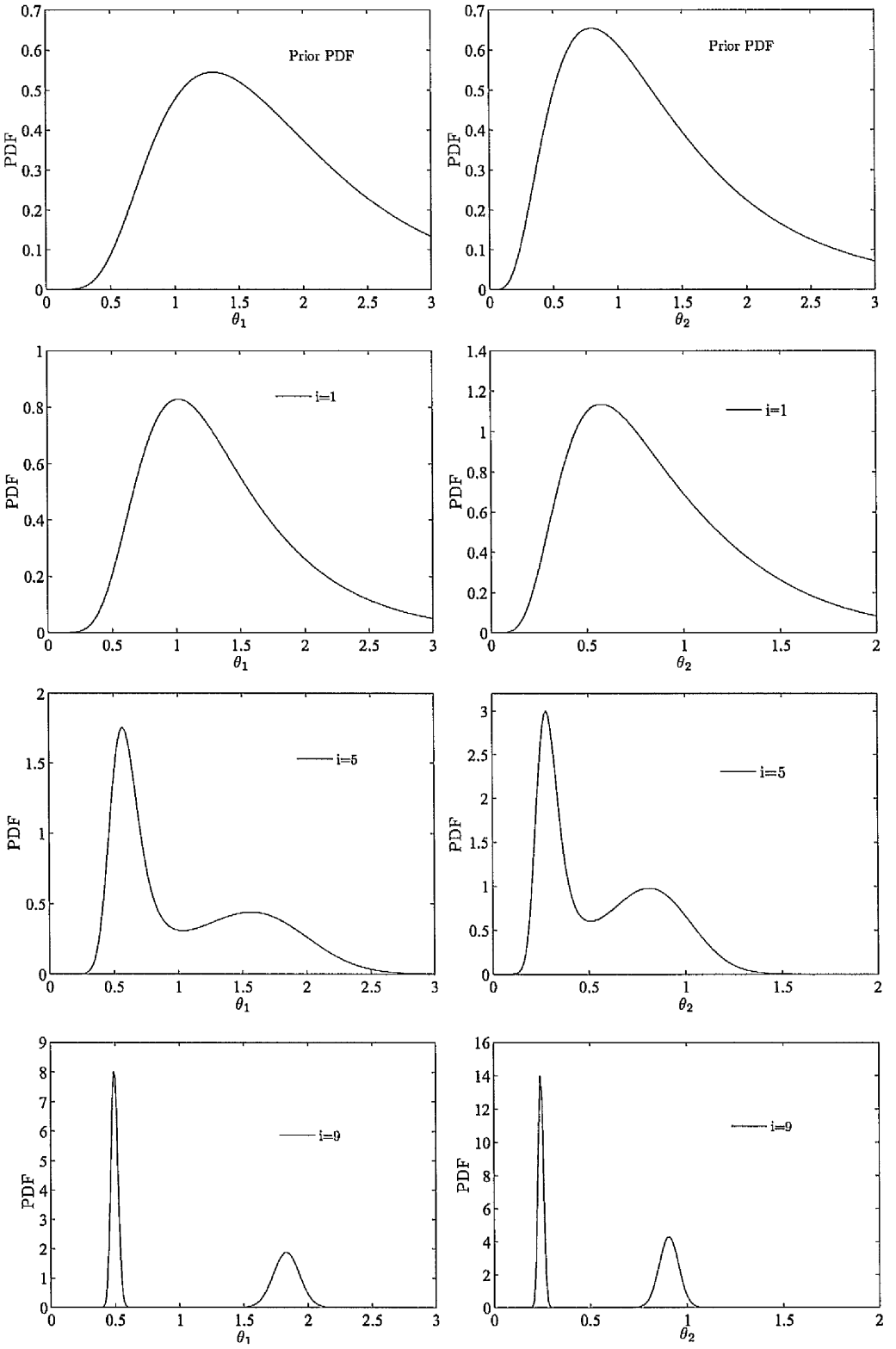

Figure 3.2: Initial and updated marginal PDF for θ_1 and θ_2 at iterations $i = 1, 5, 9$.

If n_s vectors of measured data $\mathbf{Z}_m = \left[\begin{array}{cccc} \mathbf{z}_m^{(1)} & \mathbf{z}_m^{(2)} & \ldots & \mathbf{z}_m^{(n_s)} \end{array} \right]$ are assumed to be statistically independent from each other, the log-likelihood function of them may be defined by

$$L_{\mathbf{z}_m}\left(\mathbf{z}_m \left| \boldsymbol{\theta} \right.\right) = \sum_{i=1}^{n_s} L_{\mathbf{z}_m^{(i)}}\left(\mathbf{z}_m^{(i)} \left| \boldsymbol{\theta} \right.\right) \tag{3.43}$$

where $\boldsymbol{\theta} \in \Re^p$ is the vector of uncertain structural parameters that should be identified (updated), $\mathbf{z}_m^{(i)}$ is the i^{th} samples of measured data and n_s is the number of samples of measured data. Fonseca et al. [24] formulated Eq. (3.43) for estimating the mean and standard deviation of uncertain updating parameters using experimental modal data. They implemented the mean-centred first order perturbation and the MCS methods for the formulation. The formulation obtained by the mean-centred perturbation method is discussed in this section.

In Fonseca's approach, the uncertain updating parameters are assumed to follow a Gaussian distribution with mean $\widehat{\boldsymbol{\theta}}$ and covariance matrix $\mathbf{V}_{\boldsymbol{\theta}}$ i.e., $\boldsymbol{\theta} \in N_p\left(\widehat{\boldsymbol{\theta}}, \mathbf{V}_{\boldsymbol{\theta}}\right)$. Implementing the mean-centred first order perturbation method for the formulation of log-likelihood function leads to:

$$L_{\mathbf{z}_m}\left(\mathbf{z}_m \left| \left(\widehat{\boldsymbol{\theta}}, \mathbf{V}_{\boldsymbol{\theta}}\right)\right.\right) = -\frac{1}{2}\left(n_s p \ln 2\pi + n_s \ln\left|\mathbf{V}_{\mathbf{z}}\right| + \sum_{i=1}^{n_s}\left(\mathbf{z}_m^{(i)} - \widehat{\mathbf{z}}\right)^{\mathrm{T}} \mathbf{V}_{\mathbf{z}}^{-1}\left(\mathbf{z}_m^{(i)} - \widehat{\mathbf{z}}\right)\right) \tag{3.44}$$

where $\widehat{\mathbf{z}}$ and $\mathbf{V}_{\mathbf{z}}$ are the mean vector and covariance matrix of the predicted outputs. They can be calculated using the mean-centred first order perturbation method as follows

$$\widehat{\mathbf{z}} = \mathbf{z}\left(\widehat{\boldsymbol{\theta}}\right) \tag{3.45}$$

$$\mathbf{V}_{\mathbf{z}} = \widehat{\mathbf{S}}^{\mathrm{T}} \mathbf{V}_{\boldsymbol{\theta}} \widehat{\mathbf{S}} \tag{3.46}$$

where $\widehat{\mathbf{S}}$ denotes the sensitivity matrix (obtained from Eq. (3.5)) at the parameters mean, $\widehat{\mathbf{S}} = \mathbf{S}\left(\widehat{\boldsymbol{\theta}}\right)$. The unknown parameters in Eq. (3.44) are the mean and standard deviation of the structural parameters. The solution of the unknown parameters is obtained by using a global optimisation technique.

Fonseca et al. [24] derived another equation for the estimation of the likelihood function using the MCS. Regardless of the type of propagation method (MCS or perturbation), the correlation between components of measured modal parameters (e.g. the correlation between the first and second natural frequencies) cannot be included in Fonseca's approach and this may result in poor estimation of standard deviations of updating parameters as will be shown in Section 3.5.

3.4.4 Perturbation methods

Hua et al. [27] considered the problem of stochastic model updating by a perturbation method. In Hua's approach, the predicted mean values and the matrix of predicted covariances are converged upon measured values and in so doing the first two statistical moments of the uncertain updating parameters are determined. To account for uncertainty in the model updating procedure, Hua et al. [27] assumed that the measured vector $\mathbf{z}_m$ was defined by the summation of a deterministic part (mean value) $\widehat{\mathbf{z}}_m \in \Re^{n_r}$ and a random part $\Delta\mathbf{z}_m$, i.e.

$$\mathbf{z}_m = \widehat{\mathbf{z}}_m + \Delta\mathbf{z}_m \tag{3.47}$$

where the term $\Delta\mathbf{z}_m \in \Re^{n_r}$ (with zero mean) represents the uncertainty in measured data. Now the structural parameters $\boldsymbol{\theta} \in \Re^{p}$, the sensitivity matrix $\mathbf{S} \in \Re^{n_r \times p}$ and the predictions $\mathbf{z} \in \Re^{n_r}$ introduced in Eq. (3.2), can be expanded about the mean value of the vector of the parameters $\widehat{\boldsymbol{\theta}}$ as follows,

$$\boldsymbol{\theta} = \widehat{\boldsymbol{\theta}} + \sum_{i=1}^{n_r} \frac{\partial \boldsymbol{\theta}}{\partial \Delta z_{m_i}} \Delta z_{m_i} \tag{3.48}$$

$$\mathbf{S} = \widehat{\mathbf{S}} + \sum_{i=1}^{n_r} \frac{\partial \mathbf{S}}{\partial \Delta z_{m_i}} \Delta z_{m_i} \tag{3.49}$$

$$\mathbf{z} = \widehat{\mathbf{z}} + \sum_{i=1}^{n_r} \frac{\partial \mathbf{z}}{\partial \Delta z_{m_i}} \Delta z_{m_i} \tag{3.50}$$

where the subscript j (iteration number) on $\mathbf{S}$, $\boldsymbol{\theta}$ and $\mathbf{z}$ is omitted in Eqs. (3.48), (3.49) and (3.50). Replacing Eqs. (3.48), (3.49) and (3.50) in Eq. (3.2) together with the application of the perturbation method leads to,

$$\widehat{\mathbf{z}}_m = \widehat{\mathbf{z}}_j + \widehat{\mathbf{S}}_j \left(\widehat{\boldsymbol{\theta}}_{j+1} - \widehat{\boldsymbol{\theta}}_j \right) \tag{3.51}$$

$$\widehat{\mathbf{S}}_j \frac{\partial \boldsymbol{\theta}_{j+1}}{\partial \Delta z_{m_i}} = \widehat{\mathbf{S}}_j \frac{\partial \boldsymbol{\theta}_j}{\partial \Delta z_{m_i}} + \left(\mathbf{e} - \frac{\partial \mathbf{z}_j}{\partial \Delta z_{m_i}} - \frac{\partial \mathbf{S}_j}{\partial \Delta z_{m_i}} \right) \left(\widehat{\boldsymbol{\theta}}_{j+1} - \widehat{\boldsymbol{\theta}}_j \right) \quad i = 1, 2, ..., n_r \tag{3.52}$$

where $\mathbf{e} = \begin{bmatrix} 0 & \dots & 0 & 1 & 0 & \dots & 0 \end{bmatrix}$ is a vector with all components equal to zero except at position i in which $e_i = 1$ and

$$\frac{\partial \mathbf{z}_j}{\partial \Delta z_{m_i}} = \mathbf{S}_j \frac{\partial \boldsymbol{\theta}_j}{\partial \Delta z_{m_i}} \tag{3.53}$$

$$\frac{\partial \mathbf{S}_j}{\partial \Delta z_{m_i}} = \sum_{k=1}^{p} \frac{\partial \mathbf{S}_j}{\partial \theta_k} \frac{\partial \theta_k}{\partial \Delta z_{m_i}} \tag{3.54}$$

Eq. (3.51) leads to the estimate of the mean of the parameters and the system of n_r equations given by Eq. (3.52), is used in the determination of the covariance matrix by using the following equation

$$\mathbf{V}_{\boldsymbol{\theta}_j} = \boldsymbol{\Theta}_{j,\Delta \mathbf{z}_m} \mathbf{V}_{\mathbf{z}_m} \boldsymbol{\Theta}^{\mathrm{T}}_{j,\Delta \mathbf{z}_m} \tag{3.55}$$

where $\mathbf{V}_{\mathbf{z}_m}$ is the covariance of measured data and

$$\boldsymbol{\Theta}_{j,\Delta \mathbf{z}_m} = \begin{bmatrix} \frac{\partial \theta_{j_1}}{\partial \Delta z_{m_1}} & \frac{\partial \theta_{j_1}}{\partial \Delta z_{m_2}} & \cdots & \frac{\partial \theta_{j_1}}{\partial \Delta z_{m_{n_r}}} \\ \frac{\partial \theta_{j_2}}{\partial \Delta z_{m_1}} & \frac{\partial \theta_{j_2}}{\partial \Delta z_{m_2}} & \cdots & \frac{\partial \theta_{j_2}}{\partial \Delta z_{m_{n_r}}} \\ \cdot & \cdot & \cdots & \cdot \\ \cdot & \cdot & \cdots & \cdot \\ \cdot & \cdot & \cdots & \cdot \\ \frac{\partial \theta_{j_p}}{\partial \Delta z_{m_1}} & \frac{\partial \theta_{j_p}}{\partial \Delta z_{m_2}} & \cdots & \frac{\partial \theta_{j_p}}{\partial \Delta z_{m_{n_r}}} \end{bmatrix} \tag{3.56}$$

$\frac{\partial \boldsymbol{\theta}_{j+1}}{\partial \Delta z_{m_i}}$ can be estimated from Eq. (3.52). Note that the starting estimate for the $\frac{\partial \boldsymbol{\theta}_0}{\partial \Delta z_{m_i}}$ is zero at the first iteration.

As will be seen in the following section, although Hua's method is applicable to the problem of model updating in the presence of irreducible uncertainty, it requires the calculation of the second order sensitivity matrix (as can be seen in Eq. (3.54)). This is computationally intensive.

3.5 Comparison of the uncertainty identification methods

In this section, the methods introduced in Sections 3.4.1 to 3.4.4 are applied to a simple numerical example to investigate their performance and range of applications. The three degree-of-freedom mass-spring system, shown in Figure 2.13, is considered having known its deterministic parameters,

$$m_i = 1.0\,\text{kg} \quad (i = 1,2,3)\,, \quad k_i = 1.0\,\text{N/m} \quad (i = 3,4)\,, \quad k_6 = 3.0\,\text{N/m} \quad (3.57)$$

while the other parameters are represented as unknown Gaussian random variables with nominal mean values and standard deviations given by

$$\widehat{k}_i = 1.0\,\text{N/m} \quad (i = 1,2,5)\,, \quad \sigma_{k_i} = 0.20\,\text{N/m}\,(i = 1,2,5) \qquad (3.58)$$

The measured data, $\mathbf{z}_m$ and $\mathbf{V}_{\mathbf{z}_m}$, are obtained by using the MCS with 10,000 samples. This number of measurements is unrealistic but is used here to demonstrate the asymptotic properties of the methods. The initial estimates of the unknown random parameters are

$$\widehat{k}_i = 2.0\,\text{N/m} \quad (i = 1,2,5)\,, \quad \sigma_{k_i} = 0.30\,\text{N/m}\,(i = 1,2,5) \qquad (3.59)$$

so that a 100% initial error in mean values and a 50% initial error in standard deviations is represented.

Results obtained by the minimum variance estimators of Collins et al. [26] and Friswell [93], the Bayesian method of Beck et al. [94,95], the maximum likelihood method (Fonseca et al. [24]) and the perturbation method of Hua et al. [27] are shown in Table 3.1. The numbers, (1)-(5) in the table denote the following methods:

1. The minimum variance method of Collins et al. [26].

2. The minimum variance method of Friswell [93].

3. Bayesian method of Beck et al. [94,95]

4. The maximum likelihood method of Fonseca et al. [24]

5. The perturbation method of Hua et al. [27]

Table 3.1: Updating results obtained by various methods (10,000 samples)

Parameters	Initial error %	Error (1)%	Error (2)%	Error (3)%	Error (4)%	Error (5)%
k_1	100.00	2.10	17.40	6.00	0.00	1.30
k_2	100.00	-2.25	36.70	-6.00	0.70	-2.80
k_5	100.00	1.30	59.20	3.00	-2.72	0.60
σ_{k_1}	50.00	-89.00	-14.25	-25.00	46.50	0.00
σ_{k_2}	50.00	-89.50	-13.05	-30.00	40.00	-0.40
σ_{k_5}	50.00	-89.50	-59.50	-72.00	39.80	0.00

It is seen that the minimum variance methods (1) and (2) and the Bayesian method (3) are really not intended for the estimation of randomised parameters to represent test-piece variability. These methods work well when the variability is limited to the measurement noise from a single test piece. On the other hand, the maximum likelihood method (4) and perturbation method (5) are capable of estimating the standard deviation. Nevertheless, large errors in the estimation of standard deviation is observed in the Fonseca' approach (method 4), which may be due to the method's assumption of ignoring the correlation between the components of modal test data.

Table 3.2: Updating results obtained by Hua's approach (method (5)) when the correlation between the components of modal test data are ignored (10,000 samples)

Parameters	k_1	k_2	k_5	σ_{k_1}	σ_{k_2}	σ_{k_5}
Error %	1.40	-2.60	0.70	45.20	63.25	1.85

By doing so (i.e., ignoring the modal data correlation) using Hua's approach, large errors are also obtained (see Table 3.2) in the estimation of standard deviations of updating parameters. The correlation of modal data is removed by setting the off-diagonal terms of the covariance matrix of measured data to zero. The errors shown in the table, have the same level of errors with those obtained by the Fonseca' approach. However, the correlation terms between measured

modal data cannot be easily incorporated in Fonseca's approach. Finaly, convergences of the parameter estimates by each of the different methods are shown in Figures 3.3 to 3.7. It can be seen from Figure 3.3 that method (1) is slow to converge. The convergence of marginal PDFs of updating parameters obtained by Bayesian method is also shown in Figure 3.8.

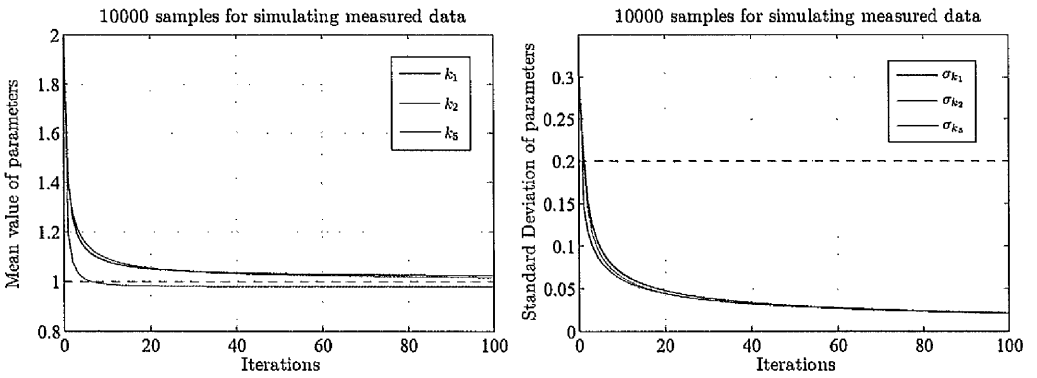

Figure 3.3: Convergence of parameter estimates by method (1).

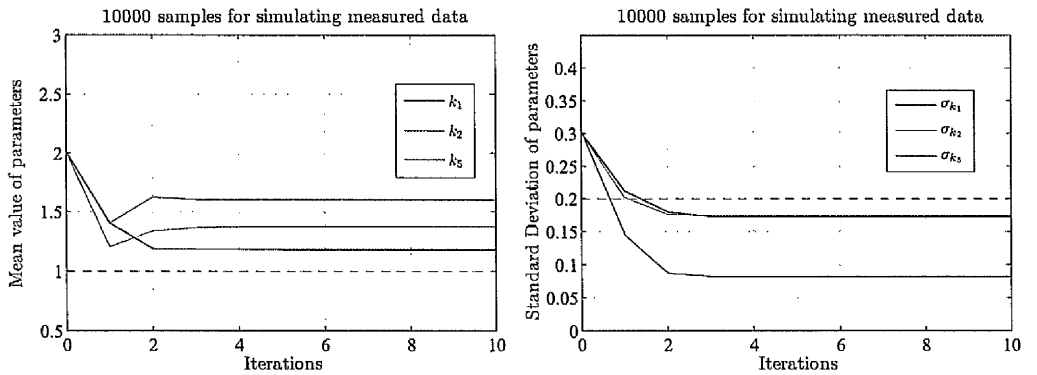

Figure 3.4: Convergence of parameter estimates by method (2).

3.6 Closure

A review of the deterministic model updating approaches is presented and the advantages and disadvantages of the methods are discussed. The earlier model updating approaches are categorised into three groups: (i) direct method, (ii) iterative methods using modal data and (iii) iterative method using FRF data. It is found that the iterative method using modal data have become most popular

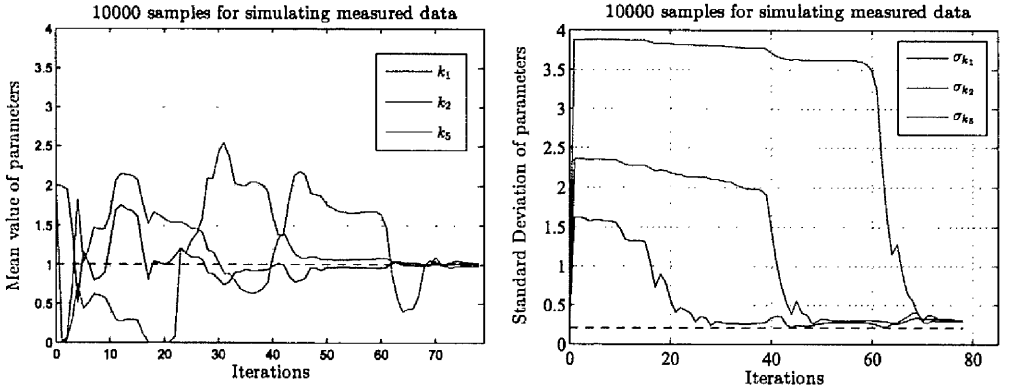

Figure 3.5: Convergence of parameter estimates by method (4).

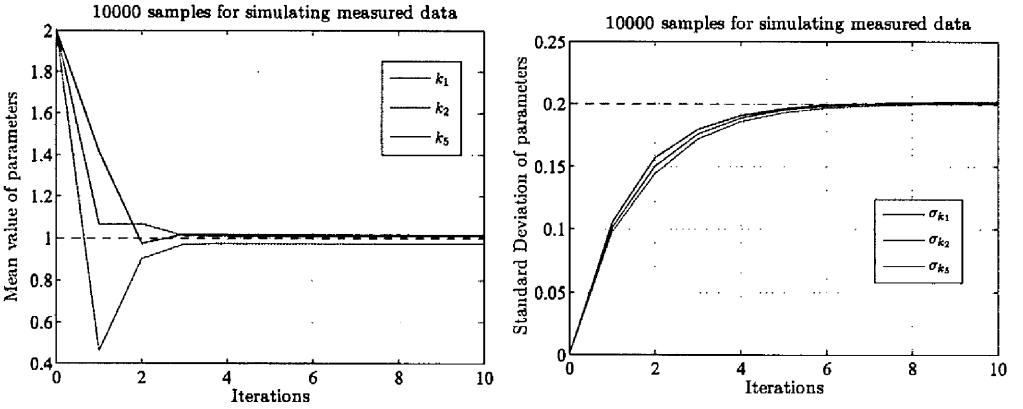

Figure 3.6: Convergence of parameter estimates by method (5) (including correlation terms between measured data).

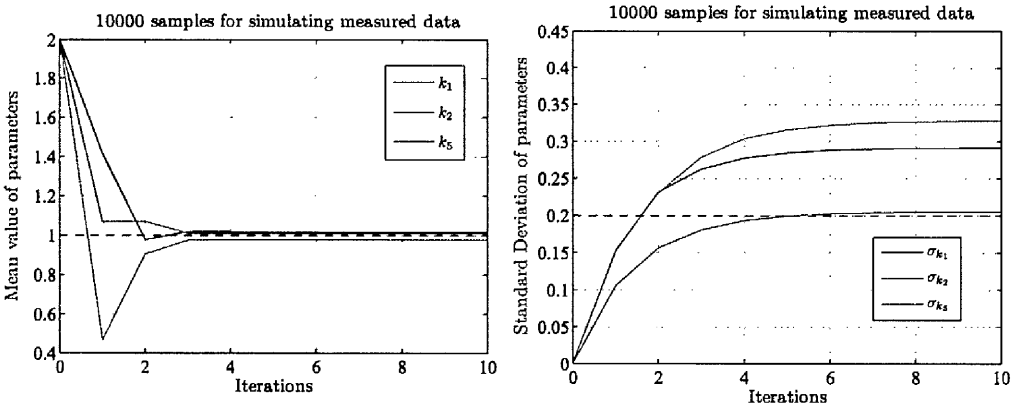

Figure 3.7: Convergence of parameter estimates by method (5) (ignoring correlation terms between measured data).

in the application to industrial problem. However, this method can be improved by using statistical techniques.

Statistical methods can be utilised to treat the uncertainty in the measured data. From the statistical point of view, the uncertainty in the measured data can be categorised into two groups: reducible and irreducible. The most popular existing updating methods that incorporate statistics namely minimum variance methods, Bayesian updating method and uncertainty identification/stochastic model updating methods, are considered and explained in detail. Their performance and range of application are discussed by applying the methods to a simple numerical example. It is found that the methods proposed by Hua et al. [27] and Fonseca et al. [24] are applicable to the problem of model updating in the presence of irreducible uncertainty whereas the minimum variance methods and Bayesian updating methods described in Sections 3.4.2 and 3.4.1, are not. It appears that the development of the uncertainty identification methods in the presence of irreducible uncertain measured data have received less attention in the literature.

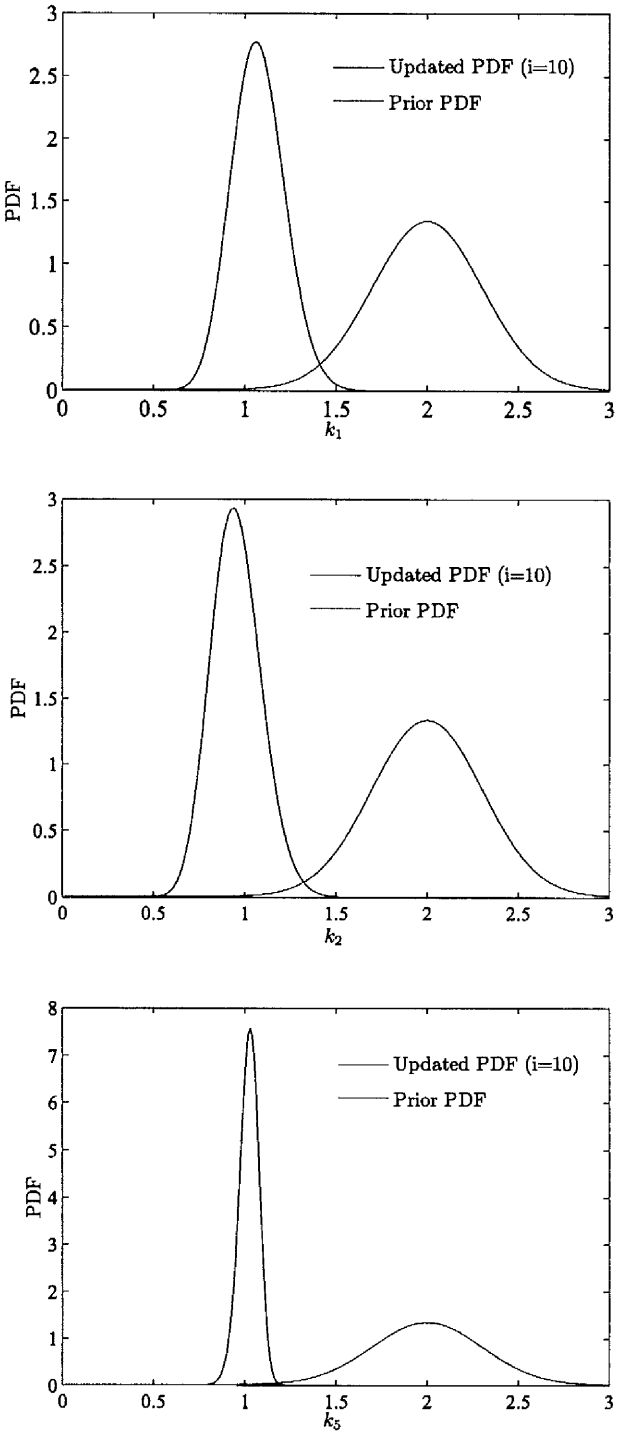

Figure 3.8: Initial and updated marginal PDF for k_1, k_2 and k_5 (method (3)).

Chapter 4

Propagation of structural uncertainty to linear and CFD based aeroelastic stability

4.1 Introduction

Flutter, the most important phenomenon in aeroelasticity [109], is an unstable self-excited vibration where energy is transferred from the air stream to the structure and often leads to catastrophic structural failure. This phenomenon can be triggered by the altitude or velocity of aircraft. The velocity of the aircraft at where flutter happens is known as the flutter speed, where the structure maintains oscillations following some initial disturbance. Below this speed the structure is stable since the oscillations are damped, while it becomes unstable above the flutter speed with a negative damping effect. The flutter speed can be determined by aeroelastic analysis.

The aeroelastic analysis requires the solution of a coupled fluid-structure system. The structure can be modelled using FEM tools, while the fluid (aerodynamic) model depends on the altitude and velocity of the aircraft so different aerodynamic models can be used to describe the fluid behaviour. The accuracy of the aerodynamic model is not the aim of this thesis, however, the feasibility of flutter analysis in the presence of uncertain structural parameters is demonstrated in this chapter for both linear (panel methods) and CFD based aeroelasticity (when CFD is used for the aerodynamics).

In this chapter, firstly a brief review of flutter analysis in the presence of structural uncertainty is carried out. Secondly, the aeroelastic stability formula-

tion for the linear and CFD aerodynamic models is presented. The aeroelastic equations in both cases are based on an eigenvalue stability method. Thirdly, the response surface method is used to evaluate the sensitivity of aeroelastic damping to a number of uncertain structural parameters. Then the critical structural parameters for influencing aeroelastic stability are identified based on sensitivity values. Finally, the forward propagation methods, introduced in Chapter 2, are applied to both linear and CFD-based aeroelastic analysis for several test cases. Results are presented for the Goland wing with and without damping and for a generic fighter configuration.

4.2 Flutter analysis in the presence of uncertain structural parameters

The accurate estimation of flutter boundaries is an important problem in aircraft certification. When the structural model includes parameter uncertainties, represented by intervals, fuzzy membership functions or probability density functions, then this uncertainty may be propagated through the aeroelastic model resulting in uncertain flutter boundaries, described correspondingly in terms of intervals, fuzzy memberships and probability densities. The review paper by Pettit [110] and references therein show the considerable attention that has already been paid to this subject. Structural variability, an important source of the variability in aircraft, arises from several sources, such as manufacturing tolerances, material differences, and wear. For example, a study of the McDonnell Douglas F-4 Phantom II [111] quantified the weight and inertia variability for this aircraft, showing changes in mass and inertias of control surfaces of up to 15%.

The characterisation of structural variability is crucial and the first step in achieving this is to discover which of the uncertain structural parameters have a significant effect on the aeroelastic analysis. The distribution or range of these parameters must be estimated. This variability may then be propagated through the model to determine a distribution or range of flutter speeds. In a small number of research papers flutter speed estimates are determined in the presence of parameter uncertainty. Poirion [112] used a first-order perturbation method to

calculate the probability of flutter for given uncertainty in structural properties. The estimated flutter probability density function obtained by the perturbation method was found not to be in good agreement with MCS results. Kuttenkeuler and Ringertz [113] explored the robust aeroelastic design optimization with respect to uncertainties in material and structural properties. Three different configurations of thin orthotropic composite are considered to find the maximum critical airspeed. Kurdi et al. [114] used MCS to propagate the variation in dimensional properties of the structural parameters of the Goland wing in order to quantify the flutter-speed probability density function. Results showed the flutter speed to be highly sensitive to small changes in the structure. Beran et al. [115] studied the effect of uncertainties in the cubic coefficient of the torsional spring and also in the initial pitch angle of the airfoil on the limit cycle oscillation of a rigid pitch-plunge airfoil. The LCO behaviour and flutter boundary of a metallic wing was investigated in terms of stiffness uncertainties by Catravete and Ibrahim [116]. They utilized the Karhunen-Loeve (KL) expansion to represent the stiffness uncertainties along the span of the wing. The perturbation theory was then applied to quantify the response variability. Attar and Dowell [117] used a response surface method to identify the effect of uncertainty on the response of a nonlinear aeroelastic system. Results were found to be in good agreement with those obtained by MCS. Wang et al. [118] considered the problem of flutter analysis in the presence of structural uncertainty using a CFD-based aerodynamic reduced-order model. They evaluated probability density functions for the flutter speeds of the Goland wing by randomizing the stiffness matrix. The problem of design of composite wings including the uncertainties in the material properties, fiber-direction angle, and ply thickness is considered by Manan and Cooper [119]. They developed a probabilistic design approach based on polynomial chaos expansions and showed that the PDFs obtained by second- and third-order expansions are in good agreement with those generated by MCS. Based on PDFs calculated by polynomial chaos, they found a reliability criterion which indicates the probability of failure due to flutter. This criterion is then used to determine the optimal robust design of composite wing. Willcox and Peraire [120] applied a two-dimensional time domain Euler CFD code to assess the impact of

variability in structural frequencies of bladed disks and the effects in the tuning of cascades. Blade structural variability was translated into a frequency PDF and the coupled aeroelastic system was solved making use of reduced order models. Verhoosel et al. [121] used a monolithic fluid-structure interaction (FSI) code to model panel flutter with variability in the Young's modulus. In this case, the fluid flow was described by a two-dimensional unsteady linearized potential equation, and the structure was modelled by the Euler-Bernoulli beam equation. The parameter variability was represented by a Gaussian distribution obtained from a Karhunen-Loeve expansion and used perturbation methods. They found the sensitivity-based methods capable of characterising the statistical moments of the aeroelastic response. Rao and Majumder [122] applied interval analysis to a structural optimization problem under atmospheric uncertainty.

In this work, a sensitivity study is carried out to select those uncertain structural parameters that influence the aeroelastic responses (such as damping, frequency or flutter speed) considerably. Then three different approaches are considered for the characterisation of flutter-speed uncertainty. In the first approach, an interval flutter analysis is used. The interval flutter analysis requires a minimisation and a maximization of the aeroelastic response. The second approach makes use of fuzzy logic so that the uncertainty is defined according to a membership function. The fuzzy method is implemented within a number of α-levels for the numerical solution of the underlying interval finite element problem. Efficient optimisation procedures make use of the Response Surface Method (RSM) [59], which generally produces more accurate estimates of the gradient and Hessian than numerical estimation by finite differences. The third procedure is a probabilistic perturbation approach that makes use of the theory of quadratic forms [16, 47]. Each solution of the flutter equation is perturbed about the mean values of the uncertain parameters through a truncated Taylor series expansion. Then the statistical moments of the aeroelastic responses are calculated. The procedure requires the calculation of the gradient and Hessian, which is estimated using RSM. When the perturbation is limited to the first-order terms of the Taylor series there is no need to calculate the Hessian matrix. The methods are firstly applied to the problem of flutter analysis using linearized aerodynamic potential

theory. The practicality of using CFD-derived aerodynamics when these methods are used is also investigated.

4.3 Eigenvalue-based stability formulation for the linear flutter analysis

Different aerodynamic models can be used for the solution of flutter problem in aeroelasticity. The Doublet-Lattice Method (DLM), introduced by Albano and Rodden [123], has received considerable attention in both research and industrial applications. This method is based on linearized aerodynamic potential theory and its main advantage is speed of computation. In this method it is assumed that the undistributed flow is uniform and is either steady or varying harmonically. The lifting surfaces (panels) are supposed to be parallel with the flow and each panel is divided into small trapezoidal lifting elements. Then the lifting pressure is evaluated across the one-quarter chord line of each panel using potential theory. The panel methods has been extensively explained in the reference books such as [124].

In this section, the DLM, available in the aeroelastic module of MSC-NASTRAN [125], is exploited to carry out linear flutter analysis. The standard linear aeroelastic equation for modal linear flutter analysis by the PK-method (in MSC-NASTRAN) may be expressed as follows,

$$\left[\mathbf{M}_\phi \lambda^2 + \left(-\frac{1}{4}\rho \bar{c} V \mathbf{B}_\phi / r_f + \mathbf{C}_\phi\right)\lambda + \left(-\frac{1}{2}\rho V^2 \mathbf{Q}_\phi + \mathbf{K}_\phi\right)\right](\mathbf{u}) = 0 \qquad (4.1)$$

where r_f is the reduced frequency which is a function of frequency ω, mid-chord $\bar{c}$ and air velocity V as $r_f = \bar{c}\omega/2V$, $\mathbf{M}_\phi \in \Re^{n_m \times n_m}$, $\mathbf{B}_\phi \in \Re^{n_m \times n_m}$, $\mathbf{Q}_\phi \in \Re^{n_m \times n_m}$, $\mathbf{C}_\phi \in \Re^{n_m \times n_m}$, $\mathbf{K}_\phi \in \Re^{n_m \times n_m}$ (n_m is the number of the normal structural modes which are retained for the analysis) are respectively the modal mass, modal aerodynamic damping, modal aerodynamic stiffness, modal structural damping and modal structural stiffness matrices. Eq. (4.1) may be cast in state-space form as

$$[\mathbf{A}_l(\omega) - \lambda \mathbf{I}]\{\mathbf{u}\} = \mathbf{0} \qquad (4.2)$$

where

$$\mathbf{A}_l(\omega) = \begin{bmatrix} \mathbf{0} & \mathbf{I} \\ -\mathbf{M}_\phi^{-1}\left[-\frac{1}{2}\rho V^2 \mathbf{Q}_\phi + \mathbf{K}_\phi\right] & -\mathbf{M}_\phi^{-1}\left[-\frac{1}{4}\rho \bar{c} V \mathbf{B}_\phi / r_f + \mathbf{C}_\phi\right] \end{bmatrix}$$

$\mathbf{B}_\phi$ and $\mathbf{Q}_\phi$ in the above equation are functions of the Mach number 'Mach' (the ratio of the speed of the aircraft to the speed of sound in air) and reduced velocity r_f. Eq. (4.1) describes a nonlinear eigenvalue problem. The eigenvalue λ may be expressed as $\lambda = \omega(\gamma \pm i)$ where ω is frequency and γ is transient decay rate coefficient, or aeroelastic damping (which is referred to as damping for simplicity).

4.4 CFD based Aeroelastic Stability Formulation

The semi-discrete form of the coupled CFD-FEM system is written as [1]

$$\frac{d\mathbf{w}}{dt} = \mathbf{R}_c(\mathbf{w}, b_f) \tag{4.3}$$

where

$$\mathbf{w} = [\mathbf{w}_f, \mathbf{w}_s]^{\mathrm{T}} \tag{4.4}$$

is a vector containing the fluid unknowns ($\mathbf{w}_f$) and the structural unknowns ($\mathbf{w}_s$), and

$$\mathbf{R}_c = [\mathbf{R}_f, \mathbf{R}_s]^{\mathrm{T}} \tag{4.5}$$

is a vector containing the fluid residual ($\mathbf{R}_f$) and the structural residual ($\mathbf{R}_s$). The residual also depends on a parameter b_f (b_f is altitude for CFD based aeroelastic analysis) which is independent of $\mathbf{w}$. An equilibrium $\mathbf{w}_0$ of this system satisfies $\mathbf{R}_c(\mathbf{w}_0, b_f) = \mathbf{0}$.

The linear stability of equilibria of Eq. (4.3) is determined by eigenvalues of the Jacobian matrix $\mathbf{A}_c = \partial\mathbf{R}/\partial\mathbf{w}$. In the current work a stability analysis is done based on the coupled system Jacobian matrix which includes the Jacobian of the CFD residual with respect to the CFD and structural unknowns. The calculation of the Jacobian $\mathbf{A}_c$ is most conveniently done by partitioning the matrix as

[1] This work is done in collaboration with Prof Badcock (my second supervisor) and Dr Simao Marques in CFD laboratory of Flight Science and Technology of University of Liverpool.

$$\mathbf{A}_c = \begin{bmatrix} \frac{\partial \mathbf{R}_f}{\partial \mathbf{w}_f} & \frac{\partial \mathbf{R}_f}{\partial \mathbf{w}_s} \\ \frac{\partial \mathbf{R}_s}{\partial \mathbf{w}_f} & \frac{\partial \mathbf{R}_s}{\partial \mathbf{w}_s} \end{bmatrix} = \begin{bmatrix} \mathbf{A}_{ff} & \mathbf{A}_{fs} \\ \mathbf{A}_{sf} & \mathbf{A}_{ss} \end{bmatrix} \tag{4.6}$$

The details of the Jacobian calculation are given in references [126] and [127].

In the current work, and as is conventional in aircraft aeroelasticity, the structure is modelled by a small number of modes, and so the number of the fluid unknowns is far higher than the structural unknowns. This means that the Jacobian matrix has a large, but sparse, block $\mathbf{A}_{ff}$ surrounded by thin strips for $\mathbf{A}_{fs}$ and $\mathbf{A}_{sf}$. As described in reference [128] the stability calculation is formulated as an eigenvalue problem, focussing on eigenvalues of the coupled system that originate from the uncoupled block $\mathbf{A}_{ss}$.

The coupled-system eigenvalue problem may be written as

$$\begin{bmatrix} \mathbf{A}_{ff} & \mathbf{A}_{fs} \\ \mathbf{A}_{sf} & \mathbf{A}_{ss} \end{bmatrix} \mathbf{p} = \lambda \mathbf{p} \tag{4.7}$$

where $\mathbf{p} = [\mathbf{p}_f, \mathbf{p}_s]^{\mathrm{T}}$ and λ are the complex eigenvector and eigenvalue respectively. The eigenvalue λ (assuming it is not an eigenvalue of $\mathbf{A}_{ff}$) satisfies [129] the nonlinear eigenvalue problem

$$S(\lambda)\,\mathbf{p}_s = \lambda \mathbf{p}_s \tag{4.8}$$

where $\mathbf{S}(\lambda) = \mathbf{A}_{ss} - \mathbf{A}_{sf}(\mathbf{A}_{ff} - \lambda \mathbf{I})^{-1}\mathbf{A}_{fs}$.

The nonlinear equation (4.8) may be solved using Newton's method. Each iteration requires the formation of the residual, $\mathbf{S}(\lambda)\,\mathbf{p}_s - \lambda \mathbf{p}_s$ and its Jacobian matrix. The calculation of the correction matrix, $\mathbf{A}_{sf}(\mathbf{A}_{ff} - \lambda \mathbf{I})^{-1}\mathbf{A}_{fs}$, is required to form the Jacobian matrix with respect to $\mathbf{p}_s$ and λ. This can be achieved through $2n_m$ solutions of a linear system against $\mathbf{A}_{ff} - \lambda \mathbf{I}$, one for each column of $\mathbf{A}_{fs}$ with n_m being the number of normal modes retained. These solutions are then multiplied against $\mathbf{A}_{sf}$. Now, for each value of the bifurcation parameter, there are multiple solutions of the nonlinear system in equation (4.8), and so the cost of forming the correction matrix at each Newton step, for each solution and for a range of structural parameters becomes high. To overcome this the expansion

$$(\mathbf{A}_{ff} - \lambda \mathbf{I})^{-1} = \mathbf{A}_{ff}^{-1} + \lambda \mathbf{A}_{ff}^{-2} + \lambda^2 \mathbf{A}_{ff}^{-3} + \ldots\ldots \tag{4.9}$$

is used where λ must be small for the series to converge. Note that this assumption is not restrictive since it is assumed that the calculated eigenvalue is a small change from the eigenvalue λ_0 of $\mathbf{A}_{ss}$. Then λ_0 can be used as a shift to the full system eigenvalue problem by replacing $\mathbf{A}_{ff}$ by $\mathbf{A}_{ff} - \lambda_0\mathbf{I}$ and $\mathbf{A}_{ss}$ by $\mathbf{A}_{ss} - \lambda_0\mathbf{I}$. This modifies the nonlinear eigenvalue problem in equation (4.8) by redefining $\mathbf{S}(\lambda) = (\mathbf{A}_{ss} - \lambda_0\mathbf{I} - \lambda\mathbf{I}) - \mathbf{A}_{sf}(\mathbf{A}_{ff} - \lambda_0\mathbf{I} - \lambda\mathbf{I})^{-1}\mathbf{A}_{fs}$. The series approximation then becomes

$$(\mathbf{A}_{ff}-\lambda_0\mathbf{I}-\lambda\mathbf{I})^{-1} = (\mathbf{A}_{ff}-\lambda_0\mathbf{I})^{-1}+\lambda(\mathbf{A}_{ff}-\lambda_0\mathbf{I})^{-2}+\lambda^2(\mathbf{A}_{ff}-\lambda_0\mathbf{I})^{-3}+..... \quad (4.10)$$

When the shifted problem is solved for λ, the eigenvalue of the original system is then $\lambda_0 + \lambda$. The terms $(\mathbf{A}_{ff} - \lambda_0\mathbf{I})^{-1}\mathbf{A}_{fs}, \lambda(\mathbf{A}_{ff} - \lambda_0\mathbf{I})^{-2}\mathbf{A}_{fs}$ can be pre-computed to yield the series approximation which can then be evaluated for any λ at virtually no computational cost.

This method is referred to as the Schur method. Two forms are available. In both cases the series approximation is used for approximating the Jacobian matrix of the residual from equation (4.8). For the residual the evaluation of $\mathbf{S}(\lambda)\mathbf{p}_s - \lambda\mathbf{p}_s$ can be made based on an exact evaluation (referred to as *full* in this work) which requires the solution of one linear system against the right hand side $\mathbf{A}_{fs}\mathbf{p}_s$, or can use the series approximation (referred to as *series*) at virtually no additional cost after the series matrices are formed.

4.5 Flutter sensitivity analysis using the response surface method (RSM)

As shown in the previous sections, the flutter analysis requires the solution of a complex eigenvalue problem. To investigate the flutter analysis of the stochastic system in the presence of uncertain structural parameters, one may consider the solution of a complex stochastic eigenvalue problem [130] which usually relies upon the availability of the gradient (or sensitivity) and the Hessian. Sensitivity analysis may be used to select those uncertain structural parameters that are most significant. The flutter sensitivity is the rate of change of the eigenvalue real part or damping, both represented by γ, with respect to changes in the

structural parameters $\boldsymbol{\theta}$. For linear flutter analysis, the sensitivity values may be computed by using MSC-NASTRAN. In this case, Eq. (4.2) is differentiated with respect to parameters and the quantity $\partial\gamma_i/\partial\theta_j$ determined. The solution is semi-analytical with derivatives approximated using forward differences [125]. However, the rate of change of the frequency ω_i and flutter speed with respect to changes in the structural parameters $\boldsymbol{\theta}$ and the second-order sensitivities, not available in MSC-NASTRAN, may be calculated using forward finite differences or alternatively, and usually more accurately, by RSM [59] (Section 2.3.6) as will now be described. The RSM can also be used for evaluation of sensitivities and the Hessian matrix when CFD is used for aerodynamics.

Since this work is concerned with the problem of flutter analysis under the influence of structural variability, the RSM may be used to approximate the aeroelastic responses such as eigenvalues or flutter speeds versus uncertain structural parameters within the region of their variation. The quadratic response surface, given by Eq. (2.78), may now be used for the aeroelastic model with p uncertain structural paramers $\boldsymbol{\theta}$ as

$$y = \beta_0 + \mathbf{b}^{\mathrm{T}}\boldsymbol{\theta} + \frac{1}{2}\boldsymbol{\theta}^{\mathrm{T}}\mathbf{B}\boldsymbol{\theta} \tag{4.11}$$

where $\underline{\boldsymbol{\theta}} \leq \boldsymbol{\theta} \leq \overline{\boldsymbol{\theta}}$, β_0, $\mathbf{b}$ and $\mathbf{B}$ are introduced in Section 2.3.6. The sensitivity vector, $\mathbf{g}_{y(\boldsymbol{\theta})} = \left[\frac{\partial y(\boldsymbol{\theta})}{\partial \theta_j}\right]$, and the Hessian matrix, $\mathbf{G}_{y(\boldsymbol{\theta})} = \left[\frac{\partial^2 y(\boldsymbol{\theta})}{\partial \theta_j \theta_k}\right]$, may now be estimated by differentiating Eq. (4.11) with respect to structural parameters,

$$\mathbf{g}_{y(\boldsymbol{\theta})} = \mathbf{b} + \mathbf{B}\boldsymbol{\theta} \tag{4.12}$$

$$\mathbf{G}_{y(\boldsymbol{\theta})} = \mathbf{B} \tag{4.13}$$

For sampling, a hybrid sampling method consists of Central Composite Design (CCD) and LHS (explained in Sections (2.3.6) and (2.3.1) respectively) may be used for higher order models. The CCD [59], the most popular class of second-order designs, is used in this study.

4.6 Propagation methods in flutter analysis

In this section, propagation methods which are explained in Section (2.3) (Chapter (2)) are used for the solution of the problem of flutter analysis in the presence of uncertain structural parameters. The solutions are made available in two forms; probabilistic and non-probabilistic. For the probabilistic flutter analysis, the perturbation approach based on the theory of quadratic forms (explained in Section (2.3.2)) are implemented and described in Section (4.6.1). The problem of interval flutter analysis is also introduced and described in Section (4.6.2). Finally, the application of fuzzy logic methods to flutter problems are described in Section (4.6.3).

4.6.1 Probabilistic flutter analysis in the presence of uncertain structural parameters

In the presence of random structural parameters, represented by $\boldsymbol{\theta} \in \Re^p$, the mass, damping and stiffness matrices ($\mathbf{M}_\phi$,$\mathbf{C}_\phi$ and $\mathbf{K}_\phi$) in Eq. (4.1) and $\mathbf{A}_{ss}$, $\mathbf{A}_{sf}$ and $\mathbf{A}_{fs}$ in Eq. (4.6) becomes random matrices. This results in random aeroelastic responses which are obtained from these equations. As explained in Section (2.3.2), the aeroelastic response can be expanded about the mean value of the uncertain parameters $\widehat{\boldsymbol{\theta}}$ as,

$$y = \widehat{y} + \sum_{i=1}^{p} \frac{\partial y}{\partial \theta_i}|_{\theta_i=\widehat{\theta}_i} \left(\theta_i - \widehat{\theta}_i\right) + \sum_{i=1}^{p}\sum_{j=1}^{p} \frac{\partial^2 y}{\partial \theta_i \partial \theta_j}|_{\theta_i=\widehat{\theta}_i,\, \theta_j=\widehat{\theta}_j} \left(\theta_i - \widehat{\theta}_i\right)\left(\theta_j - \widehat{\theta}_j\right) \tag{4.14}$$

where $\widehat{y} = y\left(\widehat{\boldsymbol{\theta}}\right)$, $\widehat{\bullet}$ denotes the mean value of $\bullet$ and $\boldsymbol{\theta}$ is the vector of uncertain structural parameter. In the above equation, y denotes the aeroelastic response such as real, imaginary parts of the solution of eigenvalue problem or the flutter speed/altitude and the partial derivatives are evaluated at the mean values of the structural parameters using Eqs. (4.12) and (4.13). The cumulants of y may be obtained based on quadratic theory (explained in Section (2.3.2)) as,

$$\kappa^{(1)} = \widehat{y} + \frac{1}{2}\text{Trace}\left(\mathbf{G}_y\left|_{\theta=\widehat{\theta}}\,\mathbf{V}_\theta\right.\right) \tag{4.15}$$

$$\begin{aligned}\kappa^{(r)} =& \frac{r!}{2}\mathbf{g}_y^{\mathrm{T}}\left|_{\theta=\widehat{\theta}}\left[\mathbf{V}_\theta\mathbf{G}_y\left|_{\theta=\widehat{\theta}}\right.\right]^{r-2}\mathbf{V}_\theta\mathbf{g}_y\right|_{\theta=\widehat{\theta}} \\ &+ \frac{(r-1)!}{2}\text{Trace}\left(\left[\mathbf{G}_y\left|_{\theta=\widehat{\theta}}\,\mathbf{V}_\theta\right.\right]^r\right) \qquad r \geq 2\end{aligned} \tag{4.16}$$

where $\mathbf{g}_y\left|_{\theta=\widehat{\theta}}\right.$ and $\mathbf{G}_y\left|_{\theta=\widehat{\theta}}\right.$ are the gradient vector and Hessian matrix respectively evaluated by RSM at the mean values of structural parameters $\widehat{\boldsymbol{\theta}}$. If only the first-order terms are retained then $\kappa^{(1)} = \widehat{y} = y\left(\widehat{\boldsymbol{\theta}}\right)$, $\kappa^{(2)} = \mathbf{g}_y^{\mathrm{T}}\left|_{\theta=\widehat{\theta}}\,\mathbf{V}_\theta\mathbf{g}_y\right|_{\theta=\widehat{\theta}}$. Therefore the PDFs of aeroelastic responses, may be assumed to be normally distributed,

$$f(y) = \frac{1}{\sqrt{2\pi\kappa^{(2)}}}\quad \exp\left(-\frac{\left(y-\kappa^{(1)}\right)^2}{2\kappa^{(2)}}\right) \tag{4.17}$$

If the Hessian matrix is retained then the first four moments of the aeroelastic responses can be determined using Eqs. (4.15) and (4.16). It should be noted that the third and fourth moments are more inaccurate than the first and second moments because of the second-order perturbation used to represent the aeroelastic response. In this case if only the first two moments are considered, Eq. (4.17) may be used to estimate the PDF of the aeroelastic response. However if the second-order model is a quite accurate description of the aeroelastic response in the region of structural parameter variation, then the accuracy of higher order moments will be increased. In this case the probability density function may be evaluated using Pearson's theory ([48] and [49]) as explained in Section (2.3.3) of Chapter (2).

4.6.2 Interval flutter analysis

The parameter vertex solution [19] is the simplest and most efficient method for interval analysis, but its application is only valid for a restricted class of eigenvalue problems. In particular the eigenvalue problem must be symmetric and linear. As stated before, the eigenvalue problems in Eqs. (4.1) and (4.7) are nonlinear. In addition the matrices $\mathbf{A}_l$ and $\mathbf{A}_c$ are asymmetric. Therefore it is necessary to apply global optimisation procedures in search of the maximum and minimum

damping, frequency or flutter speed/altitude. The optimisation problem may be expressed by the following statement.

Determine,

$$[\underline{y}, \overline{y}] = [\min(y), \max(y)] \tag{4.18}$$

subject to,

$$\underline{\boldsymbol{\theta}} \leq \boldsymbol{\theta} \leq \overline{\boldsymbol{\theta}}$$

where $\underline{\bullet}$ and $\overline{\bullet}$ represent the lower and upper bounds of $\bullet$ respectively, y is an aeroelastic response and $\boldsymbol{\theta} \in \Re^p$ is the vector of uncertain system parameters. Different optimisation methods may be used in Eq. (4.18). The method of Feasible Directions (FD) based on Newton's approach [131] is used for global optimisation in this study. However it is important to choose an efficient optimisation method. The response surface method can also be used for reducing the computational time of optimisation. As mentioned earlier, a quadratic function is used to approximate the aeroelastic response in this work. Therefore a quadratic optimisation method may be used to evaluate the upper bound and lower bound of aeroelastic responses in Eq. (4.18). The reflective Newton method [132] for minimisation/maximization of a quadratic function subject to bounds on variables is used here. The method is available in the optimisation toolbox of MATLAB. Figure 4.1 shows a typical graph of the interval results for the eigenvalue real part of an unstable mode and flutter speed/altitude. 'LB' denotes the lower bound and 'UB' denotes the upper bound in the figure. The procedure for interval flutter analysis may be described according to the following steps,

1. Select uncertain structural parameters from sensitivity analysis and define their intervals.
2. Generate samples from the space of structural parameters using CCD.
3. Evaluate the aeroelastic responses at these samples.
4. Fit a second-order model using the least-square technique.
5. Find the upper and lower aeroelastic responses using quadratic programming optimisation.

4.6.3 Fuzzy method in flutter analysis

The fuzzy finite element method, explained in Section (2.3.5), is now used for the solution of the problem of flutter analysis in the presence of uncertain structural parameters. In this particular application the fuzzy-output membership function is the aeroelastic responses, typically the flutter speed. The procedure for a function of two triangular fuzzy variables with four α-levels was shown in Figure 2.10. The response surface method can be used for construction of fuzzy membership functions of the output data. In the numerical example in this work, it is observed that an adequate RSM approximation can be obtained by using a CCD (Central Composite Design) at the mid-level of the fuzzy diagram of input parameters. If the samples from axial points of this design are chosen to coincide with the bounds of the lowest α-level of the fuzzy diagram of input parameters then only one response surface at the mid-level is estimated and this model will be used for interval analysis at all the α-levels considered. The computational time for propagation using fuzzy methods is then reduced considerably.

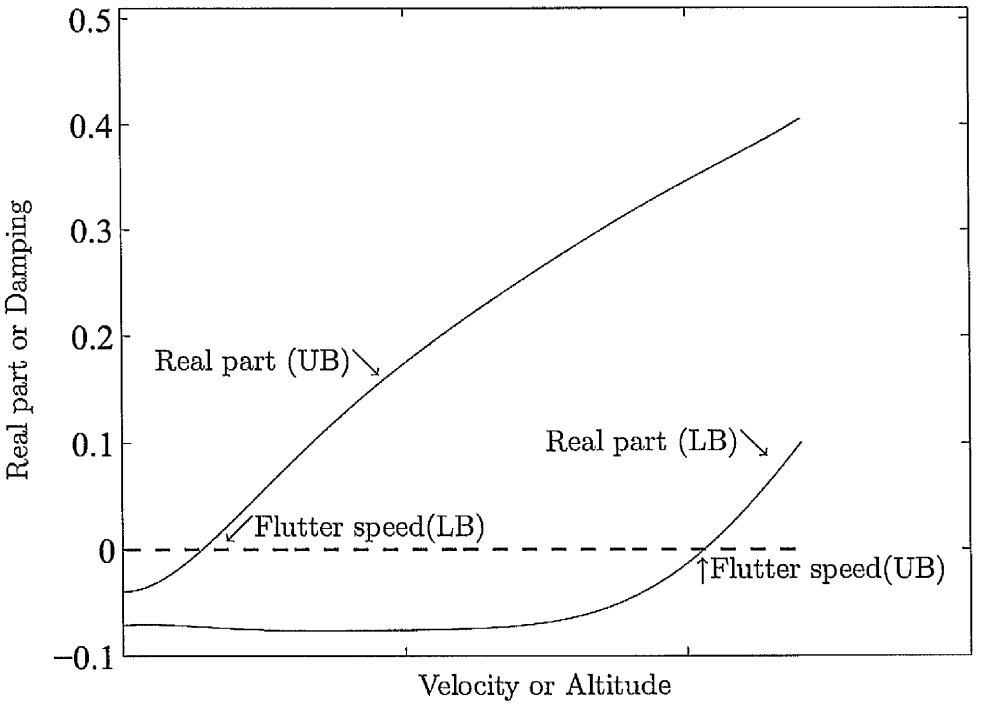

Figure 4.1: Flutter speeds bounds and real parts of the flutter mode bounds.

4.7 Numerical examples for linear flutter analysis

4.7.1 Goland wing without structural damping

The Goland wing, shown in Figure 4.2, has a chord of 6 feet and a span of 20 feet. It is a rectangular cantilevered wing with a 4%-thick parabolic section. The structural model is built based on the description given in [133] and is shown in Figure 4.3. The wing is composed of upper and lower skins, three spars, eleven ribs, three spar caps, eleven rib caps and 33 posts (1D elements) with nominal, but uncertain, thicknesses and areas as defined in Table 4.1. These components of the wing are shown in Figure 4.4. Four mode shapes, shown in Figure (4.5) were retained for the aeroelastic simulation. Flutter analysis was carried out using the aerodynamic module of MSC-NASTRAN, exploiting the double-lattice subsonic lifting surface theory (DLM). The standard linear aeroelastic equation for modal flutter analysis by the PK-method (Eq. (4.1)), available in the aeroelastic module of MSC-NASTRAN [125], is used in this section.

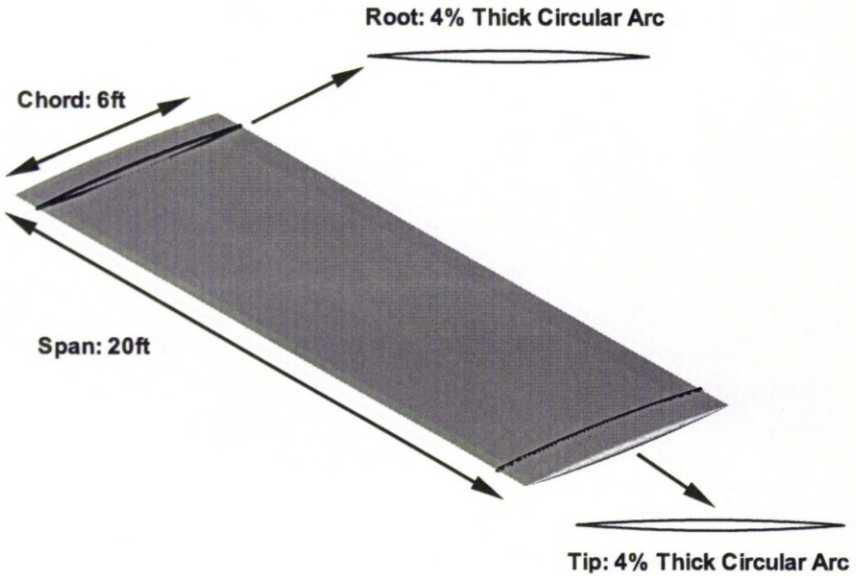

Figure 4.2: Geometry of the Goland wing.

Sensitivity analysis was carried out in order to find the random parameters having most affect on the damping of the aeroelastic modes. The sensitivities of damping with respect to the normalised structural parameters were evaluated

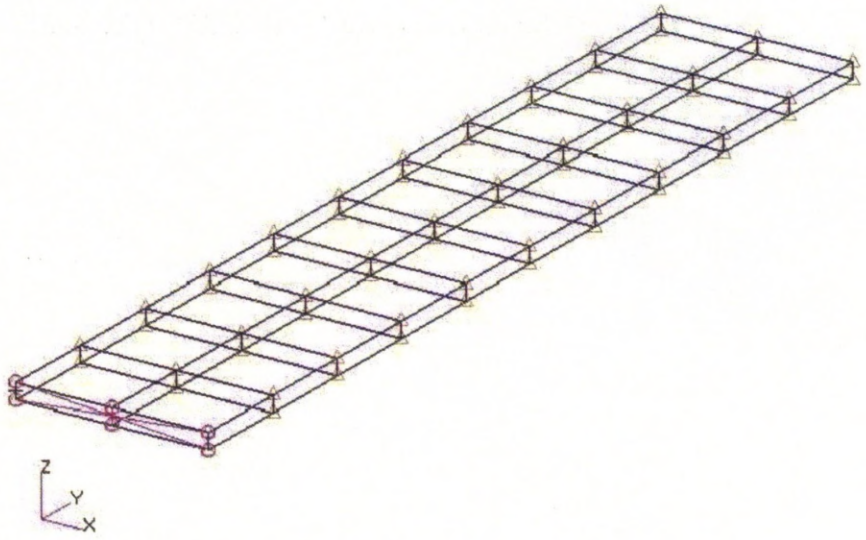

Figure 4.3: Finite element model of the Goland wing.

Table 4.1: Nominal values of thicknesses and areas for the Goland wing finite element model.

Parameter	Thickness ft (m)	Parameter	Area ft^2 (m^2)
Upper and lower wing skins	0.0155 (0.0047)	Leading and trailing edge spar caps	0.0416 (0.003865)
Leading and trailing edge spars	0.0006 (0.00018)	Centre spar cap	0.1496 (0.013898)
Centre spar	0.0889 (0.0271)	Rib caps	0.0422 (0.003921)
Ribs	0.0347 (0.01058)	Posts	0.0008 (0.000074)

at four velocities close to the flutter speed at different Mach numbers. Solving the deterministic flutter equation at the mean values of the random parameters showed that flutter occurred in the first mode for the complete range of Mach numbers chosen. The sensitivities, scaled to avoid ordering effects. Figure 4.6 shows the values of the sensitivities for the Mach number of 0.7, where it is seen that among the 63 random parameters, just seven are capable of significantly changing the damping and the flutter speed. The damping ratios were found to be most sensitive to the same seven parameters at different Mach numbers.

For interval analysis, the selected random parameters were considered to be in intervals defined by $\pm 5\%$ of the mean values given in Table 4.1. The damping and frequency of modes 1 and 2 are shown in Figures 4.7(a) and 4.7(b). MCS was used to verify the results obtained by interval analysis using samples generated from uniform distributions. Figure 4.7 shows that a good agreement between results obtained from interval analysis and MCS is achieved. It is also seen

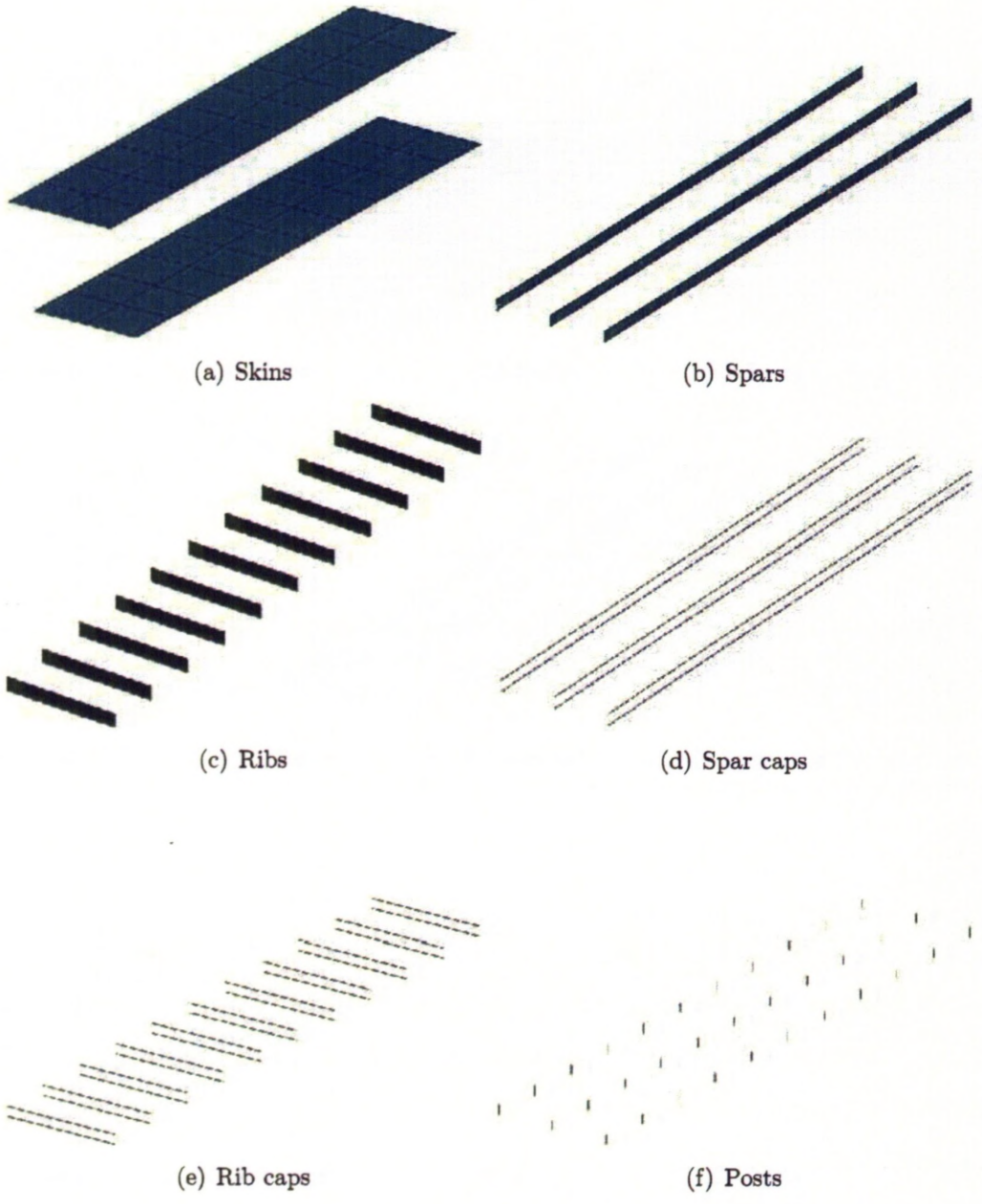

(a) Skins (b) Spars

(c) Ribs (d) Spar caps

(e) Rib caps (f) Posts

Figure 4.4: Views of the main structural model components for the Goland wing.

in Figure 4.7 that the results achieved by RSM optimisation match with those obtained from global optimisation using the method of feasible direction (FD). Also from Figure 4.7(a) it is observed that the flutter speed is defined within the interval from 410 ft/s (125 m/s) to 440 ft/s (134 m/s) at Mach 0.7. Modes 3 and 4 remained stable at all the velocities considered. The flutter-speed bounds versus Mach number are shown in Figure 4.8 where it is seen that the interval-analysis

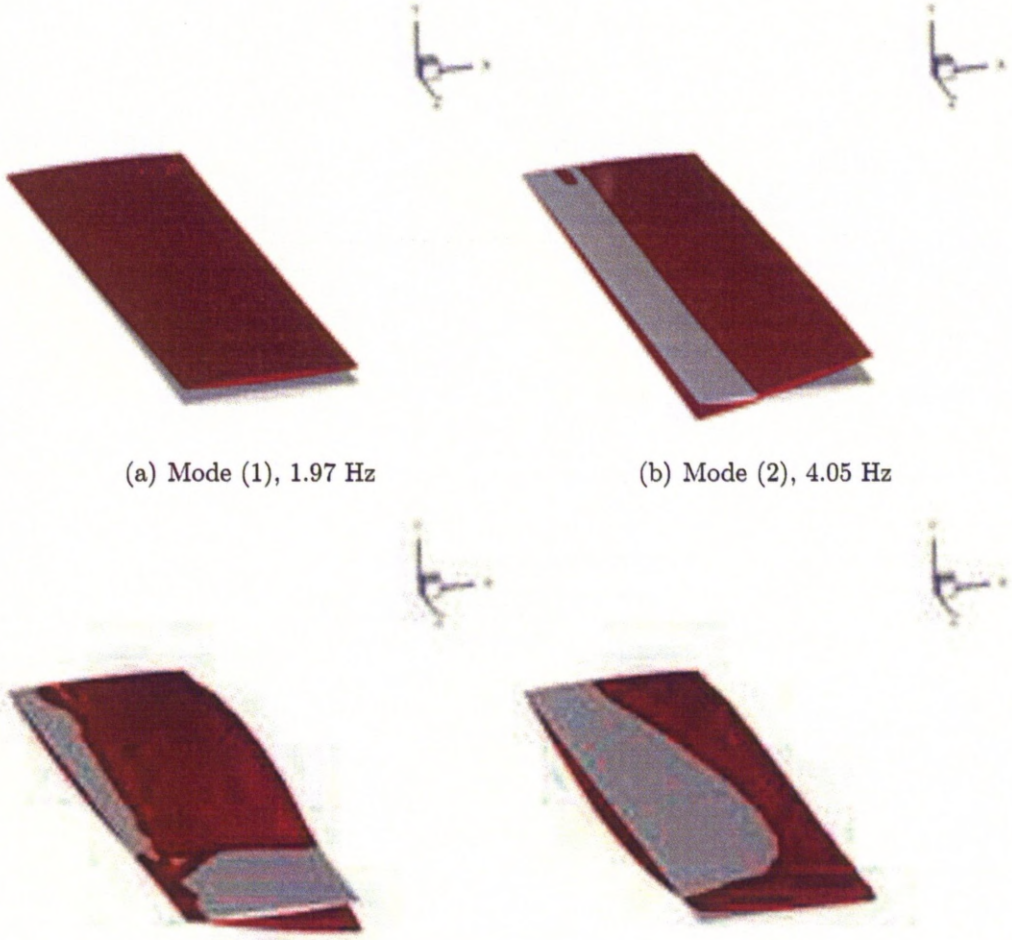

(a) Mode (1), 1.97 Hz

(b) Mode (2), 4.05 Hz

(c) Mode (3), 9.65 Hz

(d) Mode (4), 13.45 Hz

Figure 4.5: The first four mode shapes of Goland wing.

and MCS results are in good agreement.

From Figures 4.7(a) and 4.7(b) it can be also seen that whereas the variability of the frequency remains unchanged throughout the velocity range, the damping becomes sensitive as the flutter speed is approached and at higher velocities the damping variability becomes similar in extent to the frequency variability. This result demonstrates how the damping becomes dependent upon the mass and stiffness structural parameters at the flutter speed and beyond. At low speeds the damping ratios are mostly unaffected by mass and stiffness variability so that in this range the behaviour is similar to normal-mode structural behaviour. This can be easily shown by calculating the MAC matrix [64] between normal-mode and aeroelastic mode using Eq. (3.1). At low velocities, e.g. 300 ft/s (91.44 m/s),

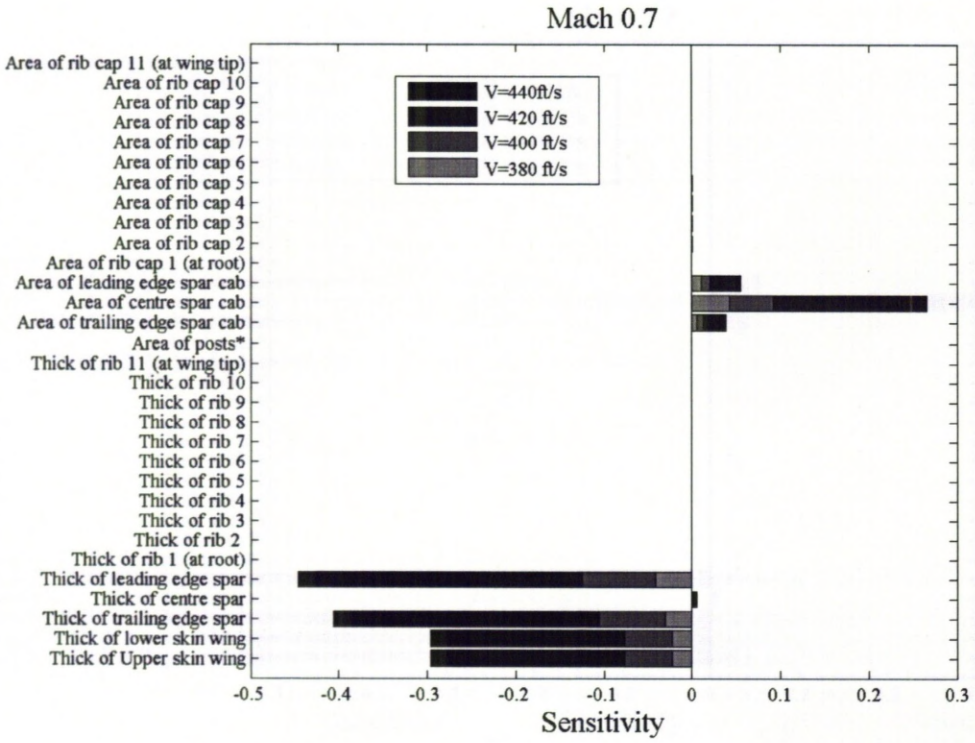

Figure 4.6: Aeroelastic damping sensitivity at different velocities (mode 1) *only the greatest sensitivity among 33 posts is shown.

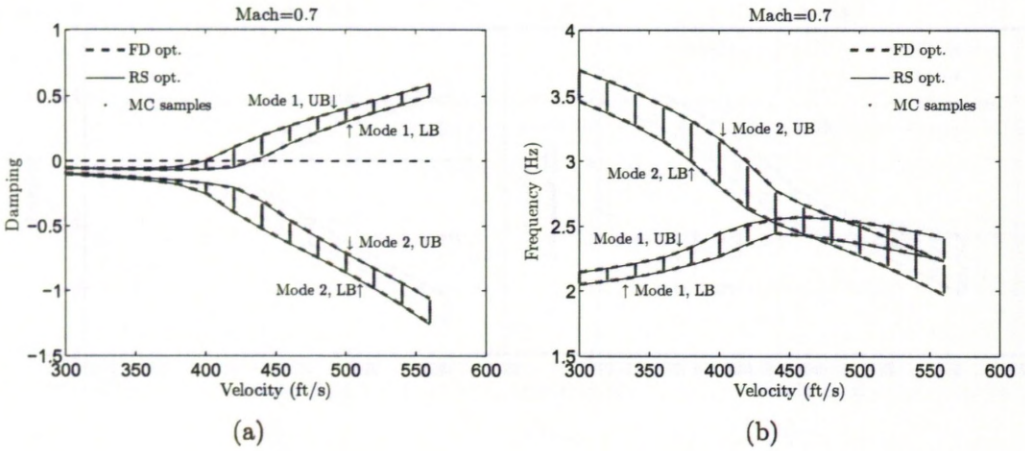

Figure 4.7: Interval and MCS results for (a) damping and (b) frequency for modes 1 and 2.

the MAC matrix is,

$$\text{MAC} = \begin{bmatrix} 0.995 & 0.004 \\ 0.062 & 0.931 \end{bmatrix} \tag{4.19}$$

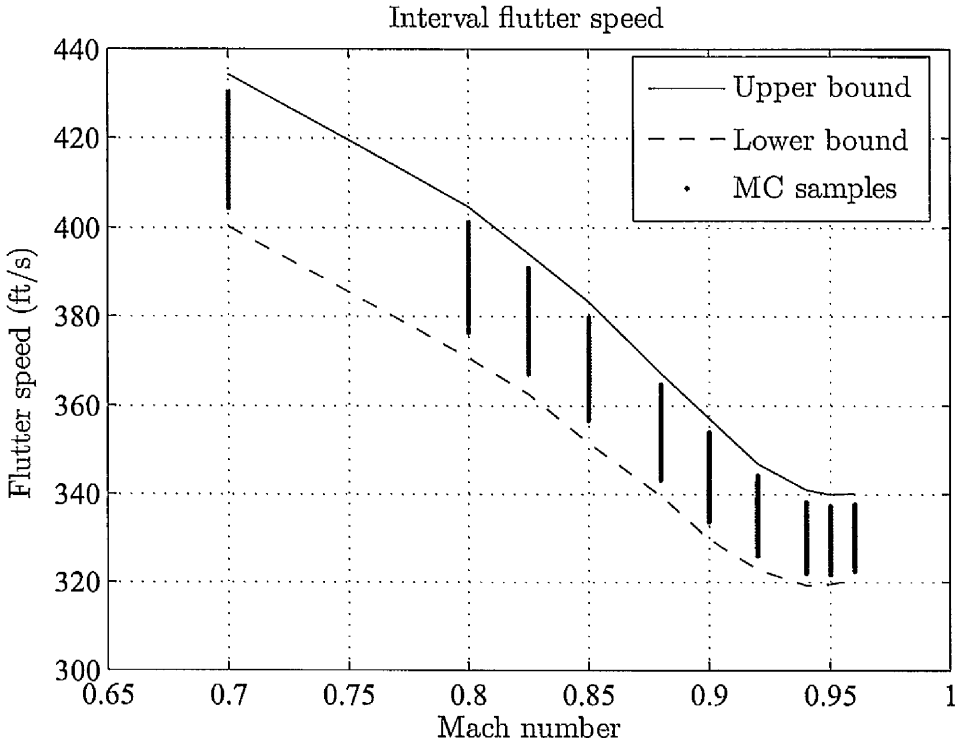

Figure 4.8: Interval and MCS results showing flutter speeds versus Mach values.

and at high velocity, e.g. 420 ft/s (128 m/s), the MAC is found to be,

$$\text{MAC} = \begin{bmatrix} 0.897 & 0.013 \\ 0.530 & 0.223 \end{bmatrix} \tag{4.20}$$

According to the MAC matrices, given in Eqs. (4.19) and (4.20), the aeroelastic eigenvalues may be expressed as a complex linear combination of the structural normal-mode eigenvalues. Therefore, the first and second complex aeroelastic eigenvalues can be approximately written as,

$$\lambda_1(\boldsymbol{\theta}) \approx \alpha_1 \lambda_1^{(n)}(\boldsymbol{\theta}) + \alpha_2 \lambda_2^{(n)}(\boldsymbol{\theta}) \tag{4.21}$$

$$\lambda_2(\boldsymbol{\theta}) \approx \beta_1 \lambda_1^{(n)}(\boldsymbol{\theta}) + \beta_2 \lambda_2^{(n)}(\boldsymbol{\theta}) \tag{4.22}$$

where α_1, α_2, β_1, β_2 are complex functions of velocity and the superscript (n) distinguishes a real structural normal-mode eigenvalue from an aeroelastic eigenvalue. At low velocities $\alpha_2, \beta_1 \to 0$, $\alpha_1, \beta_2 \to 1$ (according to MAC matrix given in Eq. (4.19)) so that the aeroelastic damping values are close to the normal-mode

eigenvalues. At higher speeds the complex constants are given more generally by $0 \leq |\alpha_1|, |\alpha_2|, |\beta_1|, |\beta_2| \leq 1$ (according to MAC matrix given in Eq. (4.20) so that the damping values include structural mass- and stiffness-variability present in the normal mode eigenvalues.

Figures 4.9(a) and 4.9(b) shows the sensitivity of damping ratio and frequency of the first two eigenvalues (crossing modes) with respect to thickness of leading edge spar, the most effective parameter from Figure 4.6, at different velocities and Mach number 0.7. As it can be seen from Figure 4.9(a), the damping ratios of both modes are insensitive to the uncertain parameter at low velocities and they reach their maximum value at flutter speed regardless of sign. The sensitivity values decrease when the flutter speed is exceeded. Figure 4.9(b) shows that the sensitivities of frequencies of both modes reach a maximum at flutter speed. Sensitivity curves of similar symmetric form to Figures 4.9(a) and 4.9(b) were found for the sensitivities of both modes to the other randomised parameters. This verifies the observation shown in the previous paragraph which are justified by Eqs. 4.21 and 4.22.

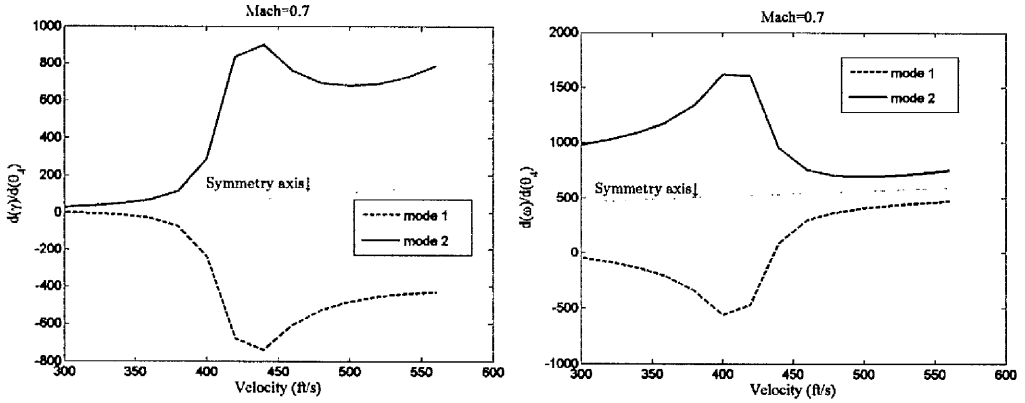

Figure 4.9: The sensitivities of (a) damping and (b) frequency for modes 1 and 2 with respect to thickness of leading spar edge.

Gaussian distributions were chosen for the probability perturbation analysis using seven randomised parameters with mean values as in Table 4.1 and coefficients of variation COV = 0.05 (as in Ref. [114]). Other parameters were taken to be deterministic with values as in Table 4.1. Propagation methods were applied to the Goland wing to estimate the output PDFs. In MCS, 1000 samples

were taken from the parameter PDFs. For propagation by the fuzzy method, the Gaussian probability density functions of system parameters were approximated by triangular membership functions as explained in Section 2.2.4. The maximum variation of the parameters (i.e. at level α_1) was given by Eq. (2.38). First eigenvalue damping distributions by first- and second-order probabilistic perturbation using normal distribution (Eq. (4.17)) and Pearson's theory (Section 2.3.3), and MCS are shown together in Figure 4.10(a) at velocity 400 ft/s (121.9 m/s) and Mach number 0.7. Although the first-order perturbation and second-order perturbation using normal distribution accurately captures most of the PDF generated by MCS, it is clear that there are differences at the tails that might be important from a practical engineering point of view. The tails are better represented by the second-order perturbation using Pearson's theory, which is close to the MCS result at the tails. Figure 4.10(b) shows the fuzzy membership function for the damping (first eigenvalue) at velocity 400 ft/s (121.9 m/s) using FD optimisation and RS optimisation. There is a good agreement between results obtained by the two optimisation methods. Significantly, it is seen from Figures 4.10(a) and 4.10(b) that the fuzzy membership function captures the nonlinearity in the tails of the MCS distributions. In fact the range of variability of aeroelastic-damping variability obtained from the fuzzy method exceeds that determined from MCS.

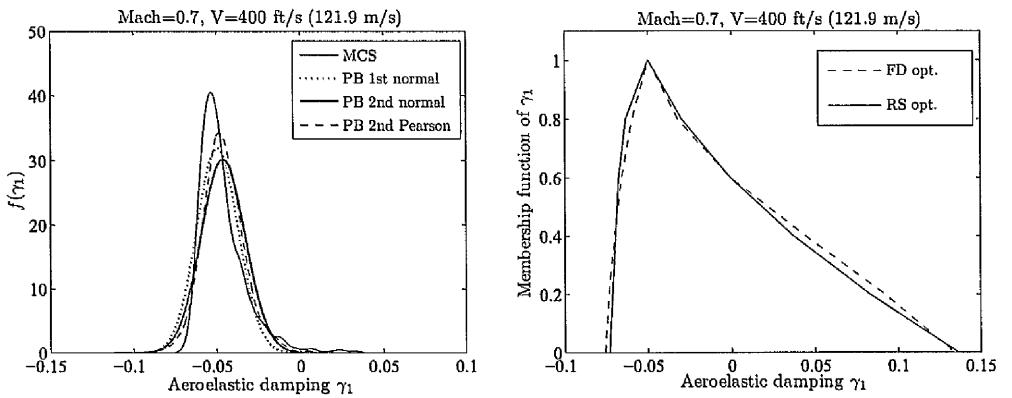

(a) (b)

Figure 4.10: Aeroelastic damping at velocity 400 ft/s (121.9 m/s): (a) PDFs obtained by 1st and 2nd order perturbation and MCS (b) membership function obtained by RSM and FD optimisation.

The flutter speed distributions by first- and second-order probabilistic perturbation using normal distribution (Eq. (4.17)) and Pearson's theory (Section 2.3.3), and MCS are shown together in Figure 4.11(a) at Mach 0.7. Two fuzzy membership functions of flutter speed at Mach 0.7 obtained from optimisation method using the method of feasible direction (FD) and RS optimisation are also shown in Figure 4.11(b). Generally there is a good agreement between the PDFs obtained by perturbation method and PDF generated by MCS. However the second-order perturbation method using Pearsons theory is slightly in better agreement with PDF generated by MCS. From Figure 4.11(b), it can be seen that the membership function of flutter speed estimated by RS optimisation matches well with membership function of flutter speed achieved by global optimisation using the method of feasible direction (FD).

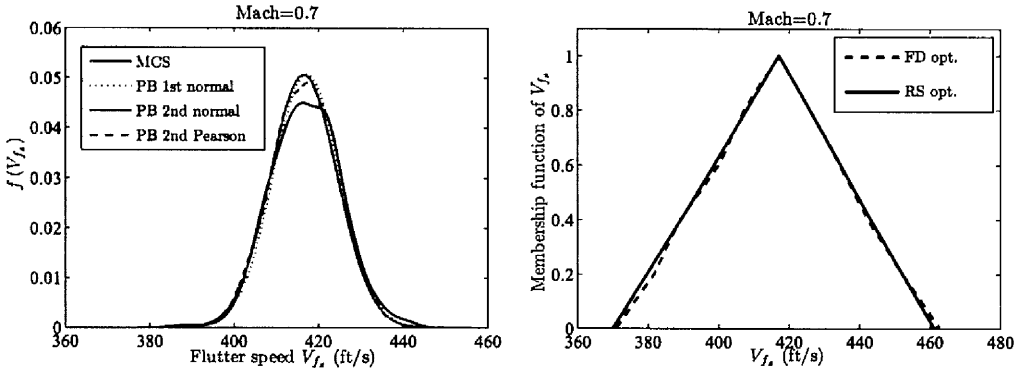

Figure 4.11: Flutter speed: (a) PDFs obtained by 1st and 2nd order perturbation and MCS (b) membership function obtained by RSM and FD optimisation.

Table 4.2 shows the lower and upper bounds of flutter speed obtained from cumulative distribution function of flutter speed from the range of 0.1% to 99.9% at different Mach numbers. The bounds of zero levels of membership function of flutter speed and the mean values of flutter speed are also shown in the table. Generally the bounds achieved by perturbation method are in good agreement with bounds generated by MCS. However, as it can be seen in this table the bounds obtained from second-order perturbation using Pearson's theory are in better agreement with the bounds achieved by MCS at Mach numbers 0.7, 0.8,

0.85 and 0.9. It may be noted, from an engineering point of view, that the bounds of flutter speed from fuzzy membership functions looks greater than those obtained from probabilistic distributions.

The correlation coefficients between the real parts and the imaginary parts of crossing modes at different velocities can be directly calculated from the population which has been generated by MCS. However this needs large number of samples and is computationally expensive. Another alternative method that is computationally more efficient than the MCS is asymptotic integral as explained in Section (2.3.3). According to Eq. (2.17), the correlation coefficient between the real parts of two crossing eigenvalues can be expressed as,

$$\rho_{\gamma_i,\gamma_j} = \frac{\mathrm{Cov}\left(\gamma_i,\gamma_j\right)}{\sigma_{\gamma_i}\sigma_{\gamma_j}} = \frac{\mathrm{E}\left(\gamma_i\gamma_j\right) - \mathrm{E}\left(\gamma_i\right)\mathrm{E}\left(\gamma_j\right)}{\sqrt{\mathrm{E}\left(\gamma_i^2\right) - \left(\mathrm{E}\left(\gamma_i\right)\right)^2}\sqrt{\mathrm{E}\left(\gamma_j^2\right) - \left(\mathrm{E}\left(\gamma_j\right)\right)^2}} \tag{4.23}$$

where $\mathrm{E}\left(\gamma_i^r\right)$ and $\mathrm{E}\left(\gamma_j^r\right)$ may be estimated by using Eq. (2.62) as follows:

$$\mathrm{E}\left(\gamma_i^r\right) = \gamma_i^r\left(\vartheta_{ir}\right)\exp\left\{-\frac{1}{2}\left(\vartheta_{ir}-\widehat{\theta}\right)^{\mathrm{T}}\mathbf{V}_\theta^{-1}\left(\vartheta_{ir}-\widehat{\theta}\right)\right\}\left|\mathbf{I}+\widetilde{\mathbf{G}}_{\gamma_i}\right|^{-\frac{1}{2}} \quad r=1,2 \tag{4.24}$$

where the vector of uncertain parameter θ follows a joint normal distribution with mean vector $\widehat{\theta}$ and covariance matrix $\mathbf{V}_\theta$, $|\bullet|$ shows the determinant of matrix $\bullet$, and

$$\widetilde{\mathbf{G}}_{\gamma_i} = \frac{r}{\gamma_i^2\left(\vartheta_{ir}\right)}\mathbf{V}_\theta\mathbf{g}_{\gamma_i}\left|_{\theta=\vartheta_{ir}}\right.\mathbf{g}_{\gamma_i}^{\mathrm{T}}\left|_{\theta=\vartheta_{ir}}\right. - \frac{r}{\gamma_i\left(\vartheta_{ir}\right)}\mathbf{V}_\theta\mathbf{G}_{\gamma_i}\left|_{\theta=\vartheta_{ir}}\right. \tag{4.25}$$

In the above equation, $\mathbf{g}$ and $\mathbf{G}$ are gradient vector and Hessian matrix and ϑ_{ir} may be obtained according to

$$\vartheta_{ir} = \widehat{\theta} + \frac{r}{\gamma_i\left(\vartheta_{ir}\right)}\mathbf{V}_\theta\mathbf{g}_{\gamma_i}\left|_{\theta=\vartheta_{ir}}\right. \tag{4.26}$$

By using the same approach, $\mathrm{E}\left(\gamma_i\gamma_j\right)$ may be calculated using the following expression:

$$\mathrm{E}\left(\gamma_i\gamma_j\right) = \gamma_i\left(\vartheta_{ij}\right)\gamma_j\left(\vartheta_{ij}\right)\exp\left\{-\frac{1}{2}\left(\vartheta_{ij}-\widehat{\theta}\right)^{\mathrm{T}}\mathbf{V}_\theta^{-1}\left(\vartheta_{ij}-\widehat{\theta}\right)\right\}\left|\mathbf{I}+\widetilde{\mathbf{G}}_{\gamma_{ij}}\right|^{-\frac{1}{2}} \tag{4.27}$$

Table 4.2: Flutter speed bounds from different methods.

Mach	Lower bound of flutter speed ft/s (×0.3048 m/s)					Mean flutter speed ft/s (×0.3048 m/s)					Upper bound of flutter speed ft/s (×0.3048 m/s)				
	MCS	Pb 1st	Pb 2nd n	Pb 2nd p	Fuzzy	MCS	Pb 1st	Pb 2nd n	Pb 2nd p	Fuzzy	MCS	Pb 1st	Pb 2nd n	Pb 2nd p	Fuzzy
0.7	387.0	393.5	392.8	390.9	374.0	417.1	417.1	416.5	416.5	417.1	443.4	440.8	440.2	440.6	463.0
0.8	365.5	366.0	366.3	366.5	349.3	388.7	387.4	387.8	387.8	387.4	415.2	408.9	409.2	411.9	430.9
0.825	357.8	357.7	356.6	354.1	340.1	379.2	379.0	378.0	378.0	379.0	401.6	400.2	399.3	400.2	419.8
0.85	346.3	347.1	347.4	346.2	331.1	368.2	366.9	367.2	367.2	366.9	390.7	386.7	387.0	388.0	407.4
0.88	334.7	333.5	333.7	332.3	319.3	353.8	352.7	353.0	353.0	352.7	375.0	372.0	372.3	373.4	390.6
0.90	321.3	326.0	325.4	323.9	312.1	343.6	343.4	342.9	342.9	343.4	363.5	360.9	360.3	360.7	378.6
0.92	318.2	317.9	317.5	316.2	306.1	335.1	334.6	334.3	334.3	334.6	355.4	351.4	351.1	351.6	366.9
0.94	314.8	314.4	314.4	314.2	304.1	330.1	329.1	329.1	329.1	329.1	346.2	343.8	343.9	345.6	358.0
0.95	315.5	314.8	314.8	314.2	306.0	329.7	328.7	328.7	328.7	328.7	344.8	342.6	342.7	343.8	355.5
0.96	316.2	316.0	315.9	315.9	307.7	330.5	329.6	329.6	329.6	329.6	344.6	343.1	343.2	343.6	354.9

Pb 1st: First order perturbation method

Pb 2nd n: Second order perturbation method using normal PDF

Pb 2nd p: Second order perturbation method using Pearson's theory for determining PDF

where

$$\begin{aligned}\widetilde{\mathbf{G}}_{\gamma_{ij}} =& \frac{1}{\gamma_i^2(\vartheta_{ij})}\mathbf{V}_{\theta}\mathbf{g}_{\gamma_i}|_{\theta=\vartheta_{ir}}\,\mathbf{g}_{\gamma_i}^{\mathrm{T}}|_{\theta=\vartheta_{ir}} - \frac{1}{\gamma_i(\vartheta_{ij})}\mathbf{V}_{\theta}\mathbf{G}_{\gamma_i}|_{\theta=\vartheta_{ir}} \\ & \frac{1}{\gamma_j^2(\vartheta_{ij})}\mathbf{V}_{\theta}\mathbf{g}_{\gamma_j}|_{\theta=\vartheta_{ir}}\,\mathbf{g}_{\gamma_j}^{\mathrm{T}}|_{\theta=\vartheta_{ir}} - \frac{1}{\gamma_j(\vartheta_{ij})}\mathbf{V}_{\theta}\mathbf{G}_{\gamma_j}|_{\theta=\vartheta_{ir}}\end{aligned} \tag{4.28}$$

and ϑ_{ij} is found by solving the following equation numerically,

$$\vartheta_{ij} = \widehat{\theta} + \frac{1}{\gamma_i(\vartheta_{ij})}\mathbf{V}_{\theta}\mathbf{g}_{\gamma_i}|_{\theta=\vartheta_{ir}} + \frac{1}{\gamma_j(\vartheta_{ij})}\mathbf{V}_{\theta}\mathbf{g}_{\gamma_j}|_{\theta=\vartheta_{ir}} \tag{4.29}$$

Substituting Eqs. (4.27) and (4.24) into (4.23) gives the correlation coefficient. The procedure for the calculation of the correlation coefficient between frequencies is similar to the above procedure (Eqs. (4.23) to (4.29)).

Figure 4.12 shows the correlation coefficient between the damping ratios and the frequencies of the crossing modes in Goland wing. There is excellent agreement between the results obtained by the asymptotic integral and the MCS. A very interesting observation in this figure is that there is a velocity in which the correlation coefficient between the first and second damping ratios and the correlation coefficient between the first and second frequencies of crossing modes become zero. This happens at velocity 327 ft/s which is referred to as zero correlation velocity. It can be seen from the figure that the correlation coefficient of the damping ratios of the crossing modes decreases after the zero correlation speed and becomes -1 at flutter speed and beyond. However, the correlation coefficient of the frequencies also decreases after the zero correlation speed but starts increasing after flutter speed and goes to 1 at velocity 500 ft/s. This shows that after flutter speed two crossing modes tend to behave as a pair of complex conjugate modes.

In order to visualise the extreme values (-1 and 1) of the correlation coefficients that are shown in Figure 4.12, the scatter diagrams that show the variability in the aeroelastic damping and frequency at 420 ft/s (128.02 m/s) (for damping) and 520 ft/s (158.5 m/s) (for frequency) are plotted and shown in Figure 4.13. An ellipse at two standard deviations is superimposed upon the scatter in the figures. As can be seen in the figure, the scatter diagrams for the damping and frequency have a particular structure close to a -45° line and +45° respectively. Figure 4.13(a)

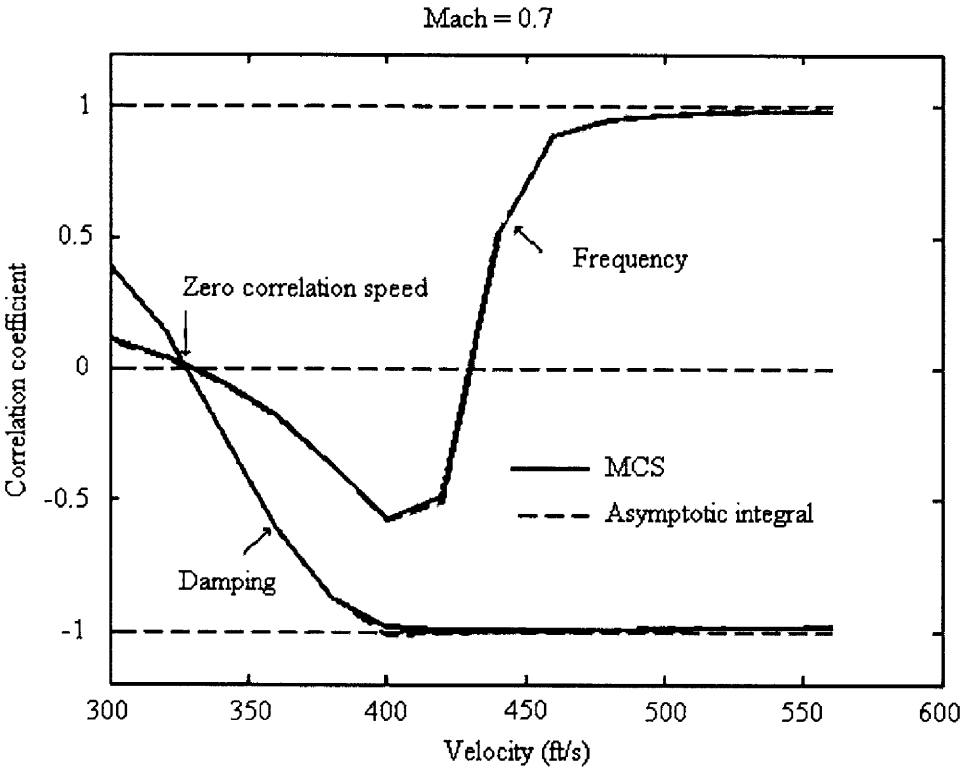

Figure 4.12: The correlation coefficients between the first and second damping ratios and the first and second frequencies.

shows that at the flutter boundary the uncertainty in the damping has a particular structure that renders the unstable mode less damped while the stable mode is rendered more damped to a similar degree, and vice versa. Figure 4.13(b) shows that if a scatter point is chosen that corresponds to increased frequency in aeroelastic mode 1 then the frequency in mode 2 is increased to a similar degree and vice-versa. These observations confirm the correlation coefficients which are shown in Figure 4.12.

4.7.2 Goland wing with structural damping

The effect of structural damping on the flutter stability boundaries by adding twelve dashpot elements, uniformly located along the length of the Goland wing from tip to root, is considered in this section. Complex eigenvalue analysis was carried out, resulting in modal damping parameters for the first four modes as: 3.403772×10^{-2}, 1.345800×10^{-2}, 4.506277×10^{-2} and 4.539254×10^{-2}, being representative of structural damping in an aircraft wing. The damping of the aeroe-

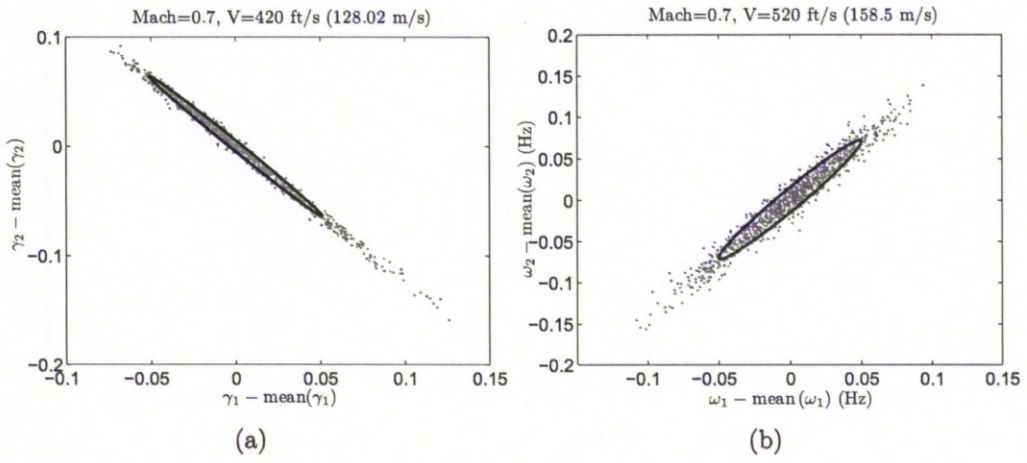

Figure 4.13: Scatter of the aeroelastic eigenvalues (a) Damping at 400 ft/s (121.92 m/s), and (b) frequency at 520 ft/s (158.5 m/s).

lastic eigenvalues for the damped and undamped system is shown at different velocities in Figure 4.14. It can be seen in the figure that a small but significant increase in the flutter speed is observed when structural damping is included. It was also observed that the frequencies of the aeroelastic modes are not affected by structural damping at lower velocities but they changed as flutter occurs. Gaussian distributions were chosen for the twelve damping parameters with mean values of 200 lbs/ft (2919 Ns/m) and coefficients of variation COV = 0.05.

Probabilistic perturbation and MCS was found to result in very narrow bands of variation for the damping, frequency and flutter speed. This shows that structural damping variability has virtually no effect upon the flutter intervals.

The results obtained by different methods from numerous test cases, with and without structural damping, show that reliable flutter boundary estimates may be obtained by a combination of interval analysis and RSM. Therefore it was decided to use interval analysis for the test case described in the following section.

4.7.3 Generic fighter FE model

Having demonstrated the approach on a model wing, a second case is computed to show feasibility on a realistically sized aircraft model. The intention here is to show that the method can scale to models of the size required for the analysis

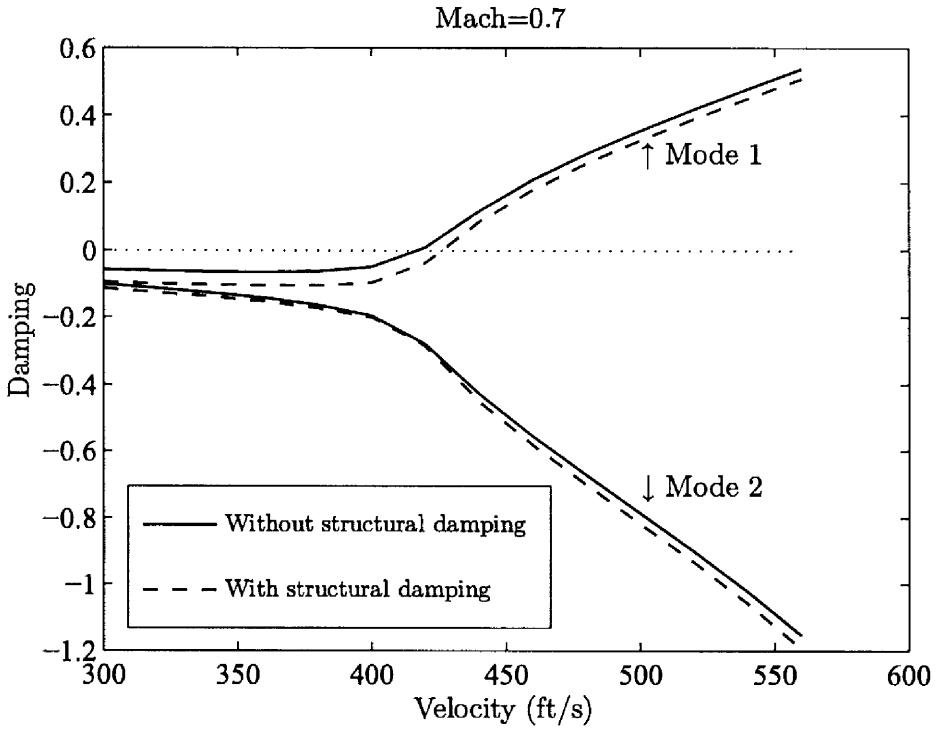

Figure 4.14: Damping ratios for modes 1 and 2 with and without damping.

of aircraft. The generic fighter was built on data publically available for the F-16 aircraft, since this has been the subject of much interest from an aeroelastic viewpoint.

The finite element model of the generic fighter wing, based on the model described by Cattarius [134], consists of a fuselage, wings, pylon and stores, all modelled using MSC-NASTRAN QUAD4 elements. The fuselage, pylon and stores were considered to be effectively rigid, having very large values for the elastic modulus assigned to them. The mass properties of the pylon and stores were represented by lumped masses, the masses of the pylon and stores being 161 kg and 1027.5 kg respectively and the principal moments of inertias of the stores, $I_{xx} = 27.5$ kg×m^2, $I_{yy} = I_{zz} = 1000$ kg×m^2. The wing-pylon connection was assumed to be rigid and each store was connected to a pylon by six springs (three translational and three rotational). The wings were divided into three regions, root, pylon and tip as shown in Figure 4.15. The Young's modulus and density of each region of the wing was adjusted in order to match the normal mode frequencies with data from a Ground Vibration Test (GVT). Table 4.3

shows updated wing-model properties. Table 4.4 shows the first five symmetric natural frequencies from the updated finite element model and the GVT [135,136]. Figure 4.16 and 4.17 show the first and second structural normal-mode shapes and aeroelastic mode shapes of the full model respectively. It can be seen from Figure 4.17 that both first and second aeroelastic mode shapes at the flutter speed are a combination of the bending mode and store pitch.

Table 4.3: Updated wing-model properties.

Parameter	Root	Pylon	Tip
E (Gpa)	157.3	96.7	95.6
G (Gpa)	62.92	38.68	38.24
ρ (kg/m^3)	5680	3780	3780
ν	0.25	0.25	0.25
t (m)	0.075	0.03	0.03

Table 4.4: Symmetric mode frequencies (Hz).

	Mode 1 (Hz)	Mode 2 (Hz)	Mode 3 (Hz)	Mode 4 (Hz)	Mode 5 (Hz)
Updated FE	3.74	5.91	8.12	11.00	11.51
model	(h_1)	($\alpha+\theta$)	(μ)	($h_2+\alpha$)	$\theta_{\alpha T}$
GVT [134–136]	4.07	5.35	8.12	12.25	
	(h_1)	($\alpha+\theta$)	(μ)	(h_2)	

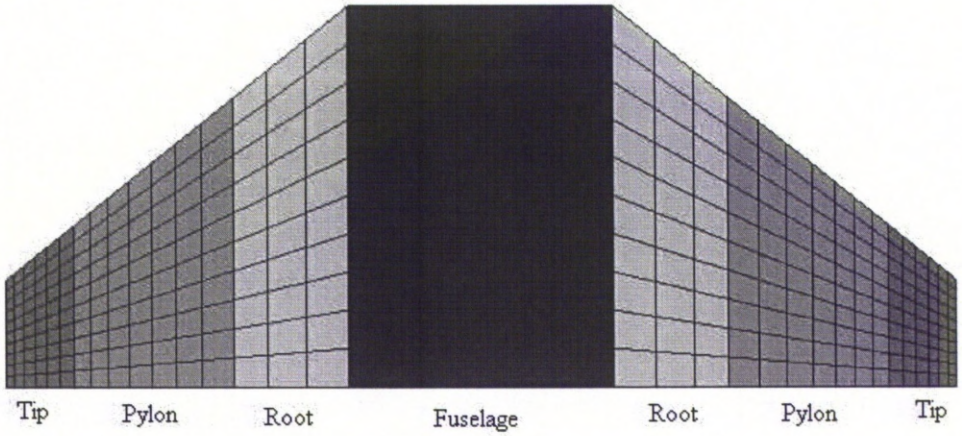

Figure 4.15: Parameterisation of the wing.

An aerodynamic model of the wing was established by dividing the left and right wing into panels with 21 span wise and 11 chord wise grid points and dividing

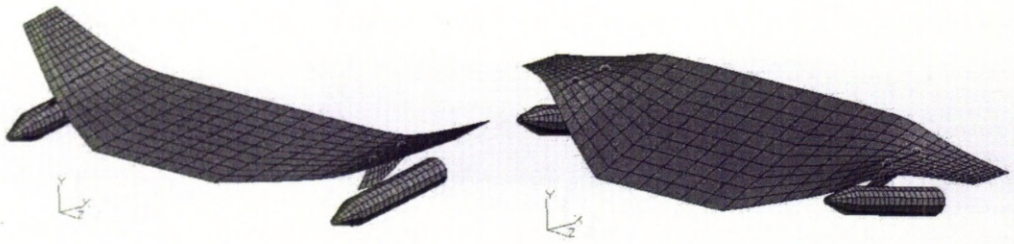

(a) (b)

Figure 4.16: Normal modes (a) mode 1, first bending (h_1), symmetric, 3.74 Hz, (b) mode 2, torsion + pitch ($\alpha + \theta$), symmetric, 5.91 Hz.

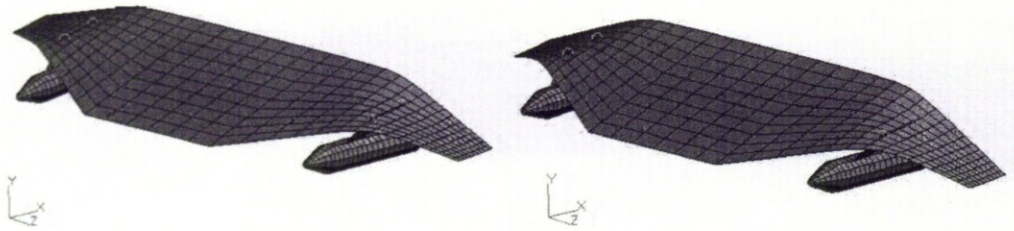

(a) (b)

Figure 4.17: Aeroelastic modes at velocity 350 m/s, (a) mode 1, 4.106 Hz, (b) mode 2, 4.136 Hz.

the fuselage with 11 span wise and 11 chord wise grid points. Figure 4.18 shows the damping and frequency of the first five symmetric modes. It can be seen that modes 1 (bending) and 2 (torsion + pitch) cross each other at a velocity of 350 m/s.

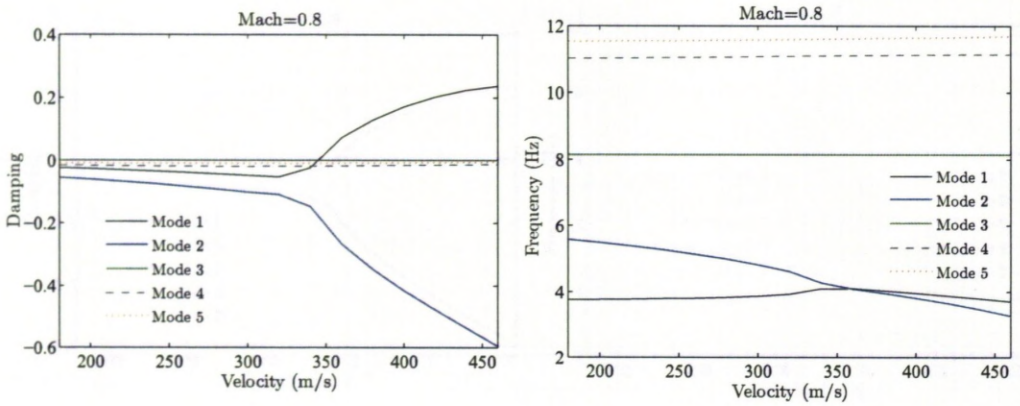

(a) (b)

Figure 4.18: The damping and frequencies of first five symmetric modes.

The sensitivities of the eigenvalues to small changes in the six spring coef-

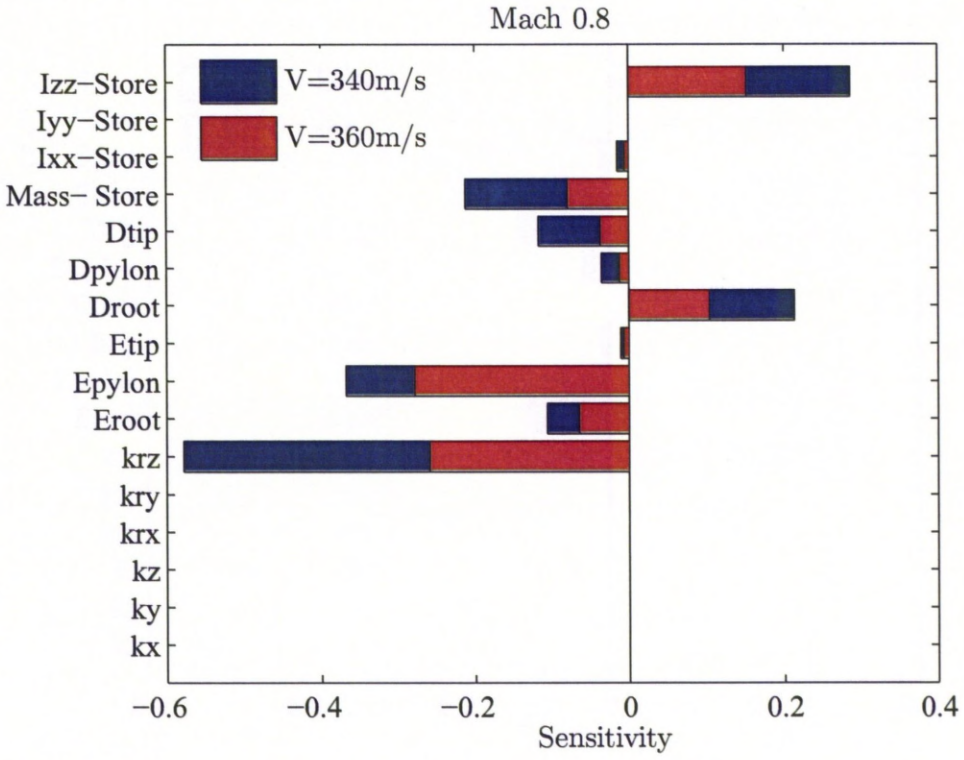

Figure 4.19: Sensitivity of the damping (first eigenvalue) to small changes in the scaled parameters (Mach 0.8).

ficients at the stores attachments, the elastic moduli and mass densities of the three regions of the wing and the mass properties of the stores (total mass and three principal moments of inertia) were determined. Figure 4.19 shows the sensitivities of the first eigenvalue to these parameters, only eight of which have a significant effect on the flutter speed. The pitching spring is the most important parameter. The mass and pitch moment of inertia (z direction) of the stores were also found to be significant but were not randomised. The reason why the mass and pitch moment of inertia were not included is that they were well defined and therefore should not be randomised. Therefore six uncertain parameters were considered in following intervals:

- Rotational spring coefficient: $[\ 0.7 \quad 1.3\ ] \times 2000$ kNm/rad.
- Young's modulus of the root: $[\ 0.9 \quad 1.1\ ] \times 1.573 \times 10^{11}$ N/m^2.
- Young's modulus of the pylon: $[\ 0.9 \quad 1.1\ ] \times 9.67 \times 10^{10}$ N/m^2.
- Mass density of the root: $[\ 0.9 \quad 1.1\ ] \times 5680$ kg/m^3.

- Mass density of the pylon: $[\ 0.6 \quad 1.1\ ] \times 3780\ \text{kg/m}^3$.

- Mass density of the tip: $[\ 0.9 \quad 1.1\ ] \times 3780\ \text{kg/m}^3$.

Figure 4.20 shows the interval analysis results for the damping of the first eigenvalue close to the flutter speed. The minimum-bound flutter speed was found to be 322 m/s, considerably lower than the deterministic flutter speed of 343 m/s. The rotational spring coefficient was found to be 1400 kNm/rad, the Young's modulus of the root was 1.416×10^{11} Pa, the Young's modulus of the pylon was 8.703×10^{10} Pa, and the mass densities of the root, pylon and tip were 6248 kg/m^3, 2268 kg/m^3 and 3402 kg/m^3, respectively at the minimum flutter speed. Increasing the wing mass at the tip and Pylon and decreasing the mass at root leads to a higher flutter speed, as does a stiffer connection between the store and pylon.

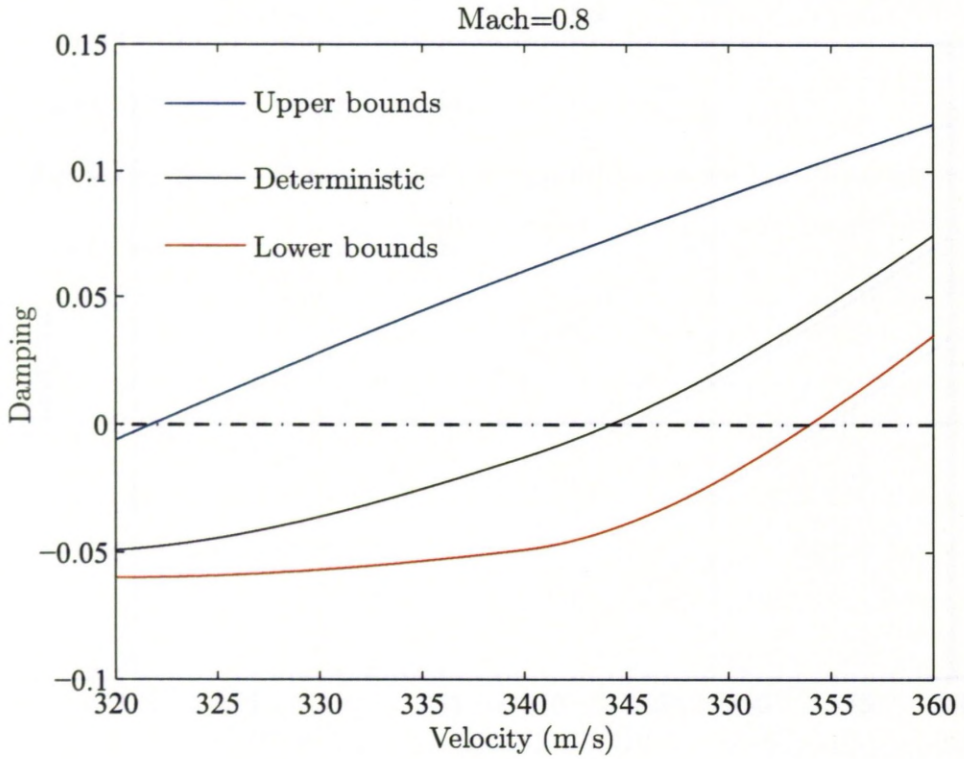

Figure 4.20: Bounds on damping for the first eigenvalue determined by interval analysis.

4.8 Numerical examples for CFD based flutter analysis

In this section, the feasibility of applying the uncertain propagation methods to CFD based Schur method, introduced in Section 4.4, is investigated in terms of computational time. Similar test cases (Goland wing and generic fighter aircraft) are considered again in this section. The linear flutter sensitivity analysis is assumed to be valid for identifying the important structural parameters in this section. Thus the uncertain structural parameters are similar to those selected in the previous section. In the first case, all propagation methods including the MCS, perturbation and interval are used again to investigate the performance of them when CFD is used for aerodynamic.

4.8.1 Goland Wing

The Goland wing, shown in Figure 4.2 is considered in this section. The structural model and uncertain model are similar to those explained in Section 4.7.1. The CFD model is constructed by the first and second authors of the paper [137] where the details of CFD model is explained in details. Four mode shapes were retained for the aeroelastic simulation. The Schur eigenvalue formulation, described in Section (4.4), was used for flutter analysis. The same 7 parameters which are key to determining the flutter speed (as explained in Section (4.7.1)), are considered as uncertain parameters.

The wing flutter response was calculated at the mean structural parameters which are shown in Table 4.1. This was done at Mach 0.5 or matched conditions. At Mach 0.5, an interaction between the wing first bending and torsion modes gives flutter between ground level and 10000 ft.

The seven identified structural parameters were randomised in similar way to Section (4.7.1) by taking a coefficient of variation of 0.05 about the mean value, and a set of 1000 normal modes was generated. The series approximation was calculated at the mean parameter values, at a cost of 64 linear solves, and this matrix was then used to drive convergence of the quasi-Newton method for the random parameter combinations. The four aeroelastic eigenvalues were then

computed for the 1000 samples. In each case the eigenvalues converged in 3-4 quasi-Newton steps, meaning that the computational cost at each altitude was 3-4 linear solves.

The mean-centred first-order perturbation method requires the calculation of the Jacobian of the aeroelastic eigenvalue with respect to each of the seven uncertain structural parameters at each altitude of interest, requiring 3-4 linear solves per parameter per altitude.

For the interval method, the first step is to calculate the mean parameter aeroelastic eigenvalues. The eigenvalues which are close to becoming undamped and the range of critical altitude for these eigenvalues are selected. The interval analysis optimisation is then run at these altitudes and for these eigenvalues. The Schur matrix is re-evaluated at the mean value for each altitude chosen to drive rapid convergence for each function evaluation during the optimisation. It was found that in the worst case around 12 optimisation steps was required to achieve convergence to the maximum or minimum eigenvalue real part, needing 96 eigenvalue calculations. In total this took around 4 hours of CPU time on a 3 GHz personal computer in the worst case to define both ends of the range.

The mode tracking, together with the influence of structural variability, is shown in Figure 4.21. In this figure the lines indicate the eigenvalues predicted using the series approximation to the residual of Eq. (4.8) whereas the points are from a full evaluation at that altitude. The two sets of results are in perfect agreement for this case. On parts (a) and (b) of this figure the mean parameter mode tracking is shown. The interaction of the first wing bending and torsion modes is clear in Figure 4.21(b) with the convergence of these frequencies below 10000 ft. The bending mode becomes undamped, as shown in Figure 4.21(a). The influence of structural variability is shown at three altitudes in Figure 4.21(c). This figure includes the Monte-Carlo simulation results (with each sample indicated by one point on the graph), the perturbation results (with the 2σ results indicated by circles) and the interval maximum and minimum indicated by the lines. As similar to the linear flutter analysis, it is observed that the scatter of the results on the real part of the eigenvalue is very small before the modes start to interact strongly. After this interaction starts the spread of results grows dramatically.

The interval results capture the Monte-Carlo samples, as they are likely to. The PDFs from the Monte-Carlo and perturbation methods are shown in Figure 4.22. There are minor differences in the tails at 2000ft where the interaction has started at this freestream Mach number.

Interval calculations at a number of altitudes allow lower and upper interval bounds to be traced as a function of altitude. These curves are shown in Figure 4.23 which shows that the altitude range for flutter onset is from 14000 ft down to 5000 ft.

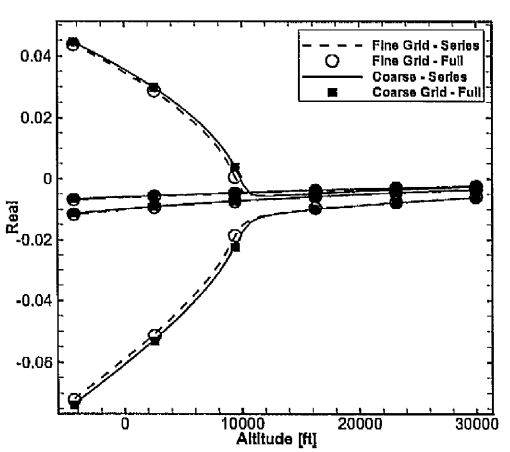

(a) Mean Eigenvalues - Real Part

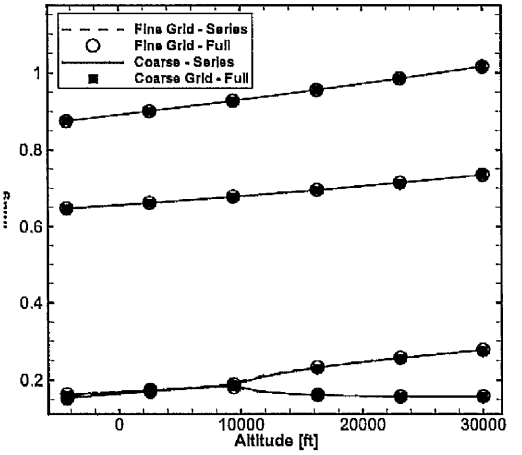

(b) Mean Eigenvalues - Imaginary Part

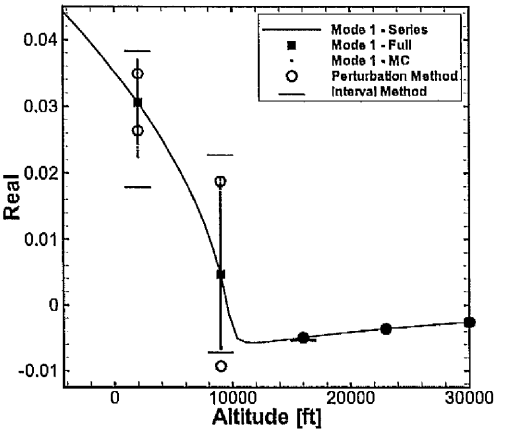

(c) Variability on Mode 1 Eigenvalue Real Part

Figure 4.21: Goland Wing mode tracking for $M = 0.5, \alpha = 0^{o}$, including the influence of structural variability. MC refers to Monte Carlo and the circles on the figure are the 2σ values from the perturbation PDF.

The costs of the different approaches are shown in Table 4.5. These costs

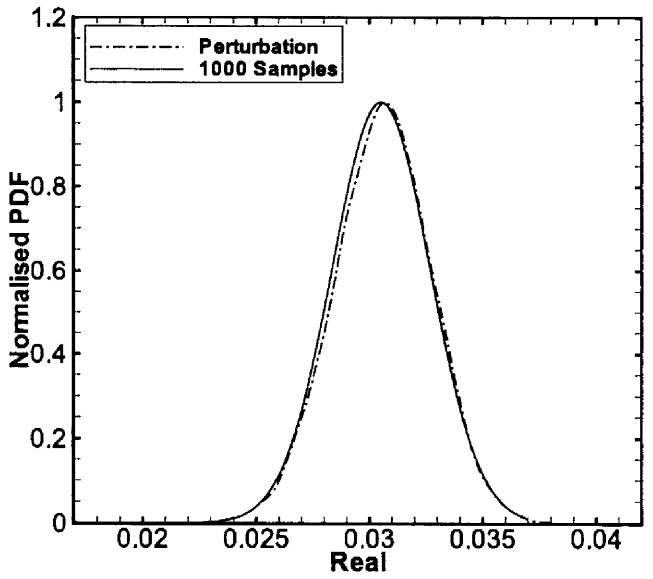

Figure 4.22: Probability Density Functions obtained from MC and Perturbation Method- Goland Wing Mode 1 at $M = 0.5$, $\alpha = 0^o$, $2000ft$.

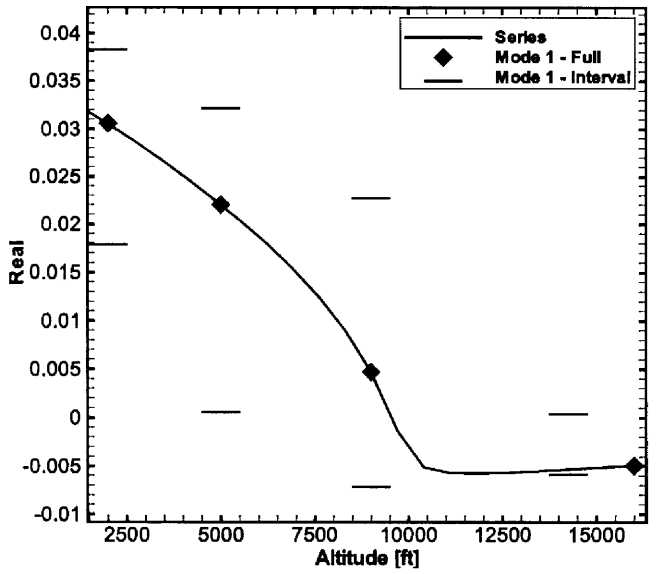

Figure 4.23: Range of flutter altitude from interval analysis for Goland wing Mode 1 at $M = 0.5$, $\alpha = 0^o$.

are shown both in terms of the number of eigenvalue calculations and also the CPU time on a Pentium 3GHz processor (i.e. a desktop computer). The linear perturbation method has a small cost, but cannot capture skewness in the PDF if this is present. The interval method requires up to 4 hours to define the worst case interval. Finally, even the Monte-Carlo simulation only requires 50 hours for

1000 samples.

Given that the choice of variability in the structural parameters is likely to be based on the intuition of an analyst rather than on hard statistical data, the essential information in the results of these analyses is in the spread of the results rather than in the PDF. If this is accepted then the interval results have a good balance between capturing the spread (including any skewness) and the computational cost, and it will be used for the next case. This is the same as the conclusion which obtained in the linear flutter analysis.

Table 4.5: Comparison of methods to calculate the eigenvalue real part variability for the critical mode at one altitude for the Goland Wing Clean case

Method	Number of eigenvalue evaluations	Wall Clock Time
Monte Carlo	1000	50h
Perturbation	7	21min
Interval	60 - 190	2.5 - 8h
Single Flutter Point	1	3min

4.8.2 Generic Fighter Model

The structural finite element model of the generic fighter wing is similar to the one that demonstrated in Section 4.7.3. As mentioned in the section, it is attempted to establish the actual behaviour of the F-16 fighter aircraft in this case. Therefore, available data for the wing geometry (dimensions and airfoil section), together with published data from wind-tunnel test was exploited. Similar to the CFD model of the Goland wing, this part of study was carried out by the first and second authors of the paper [137] which is published in the journal of aircraft. Therefore the details of the geometry, together with CFD grids can be found in this paper.

Based on linear sensitivity analysis for the flutter speed against the structural parameters which is described in Section (4.7.3), the most important structural parameters namely the rotational spring coefficient for the store attachment, the Young's modulus of the wing root section and the pylon, and the densities for the wing root and tip regions and the pylon are identified. An interval was defined

for each of these parameters as ±15% for the rotational spring coefficient and ±10% for the other parameters.

The Schur flutter analysis for the mean and varying structural parameters is shown in Figure 4.24. On parts (a) and (b) the real and imaginary parts at the mean structural parameters are shown for all modes. The asymmetric second and third modes interact, with the third mode going undamped at about 2000m. The intervals for mode 3 at 5000m, 2400m and 100m are shown in part (c) of the figure. It is seen in Figure 4.24(c) that the interval grows significantly after the modal interaction becomes strong (this behaviour was also observed in the linear results and was explained). Again the mean parameter matrices were used to drive convergence of the Schur calculations during the optimisation. This was done on 44 processors of a PC cluster and took around 7 hours. The structural variation chosen was high in this case and the mean matrices were not sufficient to drive convergence for some extreme parameter values. If Newton convergence is not observed then the iterations are stopped, the Schur matrices regenerated to provide a better Jacobian to drive convergence, and the iterations restarted.

An assessment of the variability over a range of transonic Mach numbers is shown in Figure 4.24(d). Figure 4.24(a) shows mode 3 to be lightly damped. Small changes to this mode can lead to large variations of the flutter altitude. Linear calculations using Nastran showed that mode 1 is the mode to become undamped, which for most of the envelope is not near the instability boundary and therefore can withstand structural variations for larger parts of the flight envelope. The flutter boundary shown in Figure 4.24(d) also allows the flutter onset Mach number at a fixed altitude to be estimated. The flutter altitude at M=0.8 for the mean structural parameters is 1500m, and at M=0.91 is 5000m. From the interval analysis shown in Figure 4.24(d), flutter at M=0.8 can develop at 5000m within the range of structural variation assumed.

4.9 Closure

Different forward propagation methods, interval, fuzzy and perturbation, have been applied to linear and CFD-based aeroelastic analysis for a variety of wing

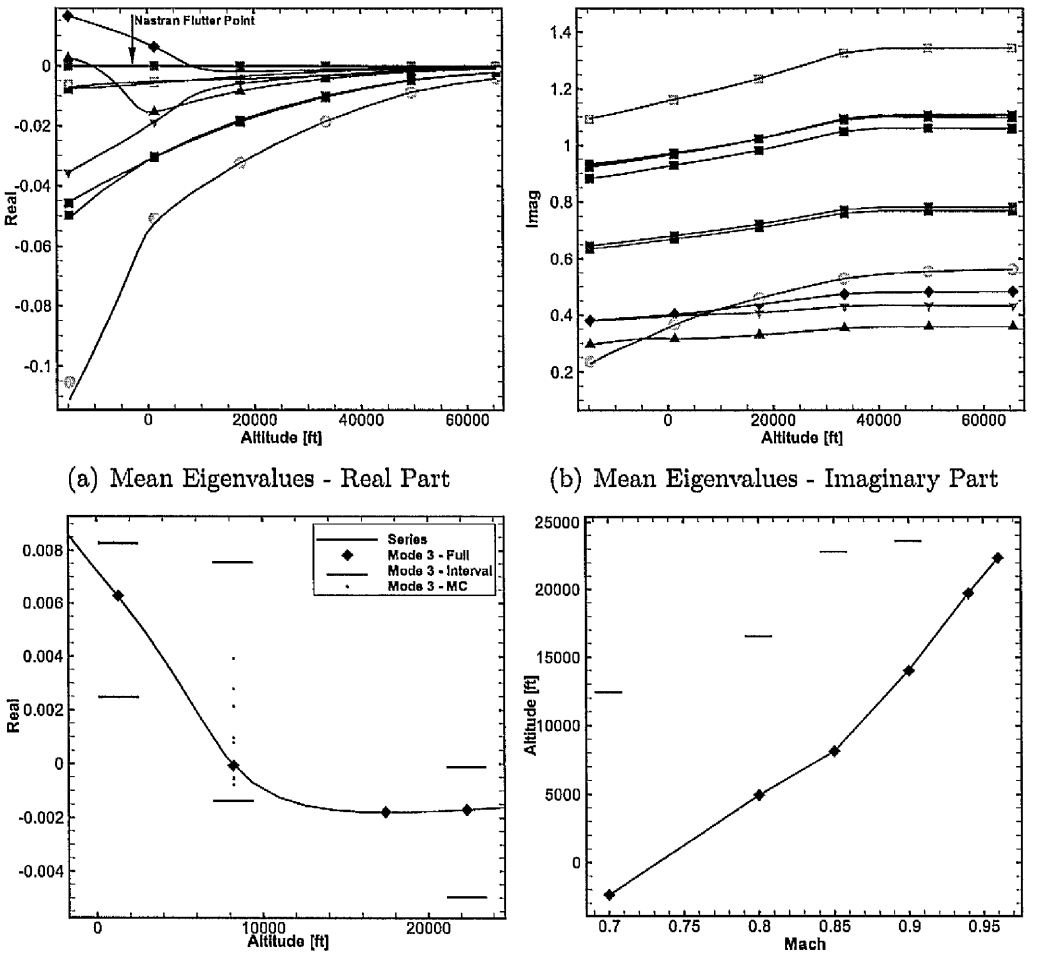

(a) Mean Eigenvalues - Real Part

(b) Mean Eigenvalues - Imaginary Part

(c) Variability on Mode 3 Eigenvalue - Real Part

(d) Flutter boundary uncertainty

Figure 4.24: Eigenvalue variation with altitude at $M = 0.85$ and $\alpha = 0^o$ for the Generic Fighter Case. The lines are generated using the series approximation and the points are from the full nonlinear solution.

models. Linear flutter sensitivity analysis was used to select parameters for randomisation that had a significant effect on flutter speed/altitude. These random parameters were then propagated through the aeroelastic analysis to obtain estimates of intervals, fuzzy membership functions or PDFs for aeroelastic damping and flutter speed/altitude. The Response Surface Method (RSM) was used to approximate the derivatives of aeroelastic response of the system with respect to uncertain structural parameters. Monte Carlo Simulation (MCS) was used for verification purposes. In both linear and CFD based uncertain flutter analysis, it was concluded that a combination of response surface method and interval

analysis is found not only to be computationally efficient but also to provide a sufficiently good approximation to flutter bounds determined by MCS.

From linear flutter analysis of the Goland wing, nonlinear behaviour was observed in tails of the damping PDFs of the flutter mode. Second-order probabilistic perturbation analysis was found to represent the behaviour at the tails with acceptable accuracy. Fuzzy analysis also correctly predicted nonlinear behaviour at the tails. Flutter analysis of the Goland wing showed the instability to be critically dependent upon certain structural mass and stiffness terms. At velocities less than the flutter speed, the intervals of uncertainty on damping were found to be small, but increase at around the flutter speed and beyond to become similar in extent to the bounds on the frequencies across the entire range of frequencies. The inclusion of structural damping was found to result in a small but significant increase in the deterministic flutter speed. Structural damping variability had virtually no effect upon the flutter intervals. At velocities close to the flutter speed particular structures were revealed, close to -45° and +45° lines, in the aeroelastic-damping and frequency scatter diagrams. Then for a chosen point where the unstable mode was rendered less damped, the stable mode became more damped to a similar degree, and vice-versa. In the linear flutter analysis of a generic fighter plane flutter instability was found to involve the coupling of wing bending with store pitching behaviour. Flutter bounds were determined by the propagation of structural stiffness parameters (including the pylon - store connection) by interval analysis.

The feasibility of the uncertain propagation methods in terms of computational cost was demonstrated, when using CFD, by exploiting an eigenvalue-based method, which can be configured for the purpose of computing stability for many similar structural models. The test cases used in linear analysis, were again considered for CFD-based analysis. For the Goland wing, 1000 structural samples were computed in two days on a desktop PC and the interval results in around 3 hours. A rapid increase in the sensitivity of the real part of the critical eigenvalue to the structural variability which was observed in linear flutter analysis was again observed after the modal interaction started by the CFD aeroelastic analysis. The interval CFD-based flutter analysis was then applied to the generic

fighter model and the bounds of flutter altitude were identified.

Chapter 5

Probabilistic perturbation methods in stochastic model updating

5.1 Introduction

In the previous chapter, it was shown how structural variability could be propagated through aeroelastic analysis. Many uncertain parameters such as thickness are measurable and the distribution or range of their variation may be measured. However, some of structural parameters such as damping and stiffness in the joints are not measurable. In this case an inverse approach may be used to identify the variability in these parameters from variability in the measured data such as natural frequencies and mode shapes. As previously mentioned, these methods are known as stochastic model updating.

In this chapter a new method, based upon the perturbation procedure, is developed in two versions for the purpose of stochastic finite element model updating. In the first version of the method, the correlation between the updated parameters and measured data is omitted. This results in a procedure that requires only the first-order matrix of sensitivities. The second procedure includes this correlation (after the first iteration) but is a more expensive computation requiring the second-order sensitivities. It is shown in numerical simulations that the first method produces results that are equally acceptable to those produced by the second method. Another method, based upon the minimisation of an objective function, is also proposed. The objective function consists of two parts: 1- the Euclidian norm of the difference between mean values of measured data and analytical outputs vectors, and 2- the Frobenius norm of the difference between

the covariance matrices of measured data and analytical outputs. This chapter also includes a discussion of different methods (including mean-centred first-order perturbation, the asymptotic integral, and Monte-Carlo simulation) used to evaluate certain covariance matrices as part of the updating procedure. Issues of sample size and regularisation of the ill-conditional stochastic model updating equations are considered. A series of simulated case studies are presented and then the first version of the perturbation method is applied to the problem of determining thickness variability in a collection of plates from measured natural frequencies. Gaussian distributions are used in the simulated and experimental examples. The method based on minimising an objective function is also verified numerically and experimentally using multiple sets of plates with randomized masses. The validity of the updated finite element model is assessed using measured higher natural frequency distributions beyond the set of distributions used for updating the first and second statistical moments of the parameters.

5.2 The perturbation method

According to the conventional, deterministic model updating method an estimate $\boldsymbol{\theta}_{j+1}$ may be updated by using a prior estimate $\boldsymbol{\theta}_j$ as

$$\boldsymbol{\theta}_{j+1} = \boldsymbol{\theta}_j + \mathbf{T}_j \left(\mathbf{z}_m - \mathbf{z}_j \right) \tag{5.1}$$

where $\mathbf{z}_j \in \Re^{n_r}$ is the vector of estimated output parameters (e.g. eigenvalues and eigenvectors), $\mathbf{z}_m \in \Re^{n_r}$ is the vector of measured data, $\boldsymbol{\theta} \in \Re^{p}$ is the vector of system parameters and $\mathbf{T}_j \in \Re^{p \times n_r}$ is a transformation matrix. In order to take into account the variability in measurements arising from multiple sources, including manufacturing tolerances in nominally identical test structures as well as measurement noise, the modal parameters are represented as

$$\mathbf{z}_m = \widehat{\mathbf{z}}_m + \Delta \mathbf{z}_m \tag{5.2}$$

$$\mathbf{z}_j = \widehat{\mathbf{z}}_j + \Delta \mathbf{z}_j \tag{5.3}$$

where the hat denotes mean values and $\Delta \mathbf{z}_m, \Delta \mathbf{z}_j \in \Re^{n_r}$ are vectors of random variables. The hyperellipses represented by $\{\widehat{\mathbf{z}}_m, \mathbf{V}_{\mathbf{z}_m}\}$ and $\{\widehat{\mathbf{z}}_j, \mathbf{V}_{\mathbf{z}_j}\}$ define the

space of measurements and predictions, respectively. Correspondingly, the variability in physical parameters at the jth iteration is defined as

$$\boldsymbol{\theta}_j = \widehat{\boldsymbol{\theta}}_j + \Delta\boldsymbol{\theta}_j \tag{5.4}$$

and now cast the stochastic model updating problem as,

$$\widehat{\boldsymbol{\theta}}_{j+1} + \Delta\boldsymbol{\theta}_{j+1} = \widehat{\boldsymbol{\theta}}_j + \Delta\boldsymbol{\theta}_j + \left(\widehat{\mathbf{T}}_j + \Delta\mathbf{T}_j\right)\left(\widehat{\mathbf{z}}_m + \Delta\mathbf{z}_m - \widehat{\mathbf{z}}_j - \Delta\mathbf{z}_j\right) \tag{5.5}$$

where the transformation matrix becomes,

$$\mathbf{T}_j = \widehat{\mathbf{T}}_j + \Delta\mathbf{T}_j \tag{5.6}$$

$$\Delta\mathbf{T}_j = \sum_{k=1}^{n_r} \frac{\partial\mathbf{T}_j}{\partial z_{mk}}\Delta z_{mk} \tag{5.7}$$

In the above equations, $\widehat{\mathbf{T}}_j$ denotes the transformation matrix at the parameter means, $\widehat{\mathbf{T}}_j = \mathbf{T}\left(\widehat{\boldsymbol{\theta}}_j\right)$, and Δz_{mk} denotes the k^{th} element of $\Delta\mathbf{z_m}$. The parameterisation, $\widehat{\boldsymbol{\theta}}_j + \Delta\boldsymbol{\theta}_j$, that converges the prediction space, $\widehat{\mathbf{z}}_{j+1} + \Delta\mathbf{z}_{j+1}$, upon the measurement space, $\widehat{\mathbf{z}}_m + \Delta\mathbf{z}_m$ is sought. Consequently, $\mathbf{T}_j$ becomes a function of measured variability $\Delta\mathbf{z}_m$ according to Eqs. (5.6) and (5.7), since the updated parameters are determined at each iteration by converging the model predictions upon the measurements. Application of the perturbation method, by separating the zeroth-order and first-order terms from Eq. (5.5), leads to,

$$\mathbf{O}\left(\Delta^0\right) : \widehat{\boldsymbol{\theta}}_{j+1} = \widehat{\boldsymbol{\theta}}_j + \widehat{\mathbf{T}}_j\left(\widehat{\mathbf{z}}_m - \widehat{\mathbf{z}}_j\right) \tag{5.8}$$

$$\mathbf{O}\left(\Delta^1\right) : \Delta\boldsymbol{\theta}_{j+1} = \Delta\boldsymbol{\theta}_j + \widehat{\mathbf{T}}_j\left(\Delta\mathbf{z}_m - \Delta\mathbf{z}_j\right) + \left(\left(\sum_{k=1}^{n_r} \frac{\partial\widehat{\mathbf{T}}_j}{\partial z_{mk}}\Delta z_{mk}\right)\left(\widehat{\mathbf{z}}_m - \widehat{\mathbf{z}}_j\right)\right) \tag{5.9}$$

Eq. (5.8) gives the estimate of the parameter means and Eq. (5.9) is used in determining the parameter covariance matrix. It will be seen that Eqs. (5.8) and (5.9) are different from the equations developed by Hua et al. [27] using an apparently similar approach. This difference arises because Hua et al. [27] expand $\mathbf{z}_m, \mathbf{z}_j$ and $\boldsymbol{\theta}_j$ in terms of Δz_{mk} (just as $\mathbf{T}_j$ in Eqs. (5.8) and (5.9) was

expanded in this work) before applying the perturbation method. Also, Hua et al. [27] worked in terms of the sensitivity matrix $\mathbf{S}_j$ rather than the matrix $\mathbf{T}_j$ used in the present analysis. Both approaches are perfectly acceptable but the method described in in Ref. [27] does not contain an equivalent to the second right-hand-side term, $\widehat{\mathbf{T}}_j\left(\Delta\mathbf{z}_m - \Delta\mathbf{z}_j\right)$. It will be seen in what follows that the presence of this term leads to significant advantages not available to users of the method by Hua et al. [27].

Changing the position of variable Δz_{mk} and the vector $(\widehat{\mathbf{z}}_m - \widehat{\mathbf{z}}_j)$ in Eq. (5.9) leads to the expression,

$$\begin{aligned}\Delta\boldsymbol{\theta}_{j+1} =& \Delta\boldsymbol{\theta}_j + \left[\begin{array}{cccc} \frac{\partial\widehat{\mathbf{T}}_j}{\partial z_{m1}}\left(\widehat{\mathbf{z}}_m - \widehat{\mathbf{z}}_j\right) & \frac{\partial\widehat{\mathbf{T}}_j}{\partial z_{m2}}\left(\widehat{\mathbf{z}}_m - \widehat{\mathbf{z}}_j\right) & \cdots & \frac{\partial\widehat{\mathbf{T}}_j}{\partial z_{mn_r}}\left(\widehat{\mathbf{z}}_m - \widehat{\mathbf{z}}_j\right) \end{array}\right]\Delta\mathbf{z}_m \\ &+ \widehat{\mathbf{T}}_j\left(\Delta\mathbf{z}_m - \Delta\mathbf{z}_j\right)\end{aligned} \tag{5.10}$$

or,

$$\Delta\boldsymbol{\theta}_{j+1} = \Delta\boldsymbol{\theta}_j + \mathbf{A}_j\Delta\mathbf{z}_m + \widehat{\mathbf{T}}_j\left(\Delta\mathbf{z}_m - \Delta\mathbf{z}_j\right) \tag{5.11}$$

where the deterministic matrix,

$$\left[\begin{array}{cccc} \frac{\partial\widehat{\mathbf{T}}_j}{\partial z_{m1}}\left(\widehat{\mathbf{z}}_m - \widehat{\mathbf{z}}_j\right) & \frac{\partial\widehat{\mathbf{T}}_j}{\partial z_{m2}}\left(\widehat{\mathbf{z}}_m - \widehat{\mathbf{z}}_j\right) & \cdots & \frac{\partial\widehat{\mathbf{T}}_j}{\partial z_{mn_r}}\left(\widehat{\mathbf{z}}_m - \widehat{\mathbf{z}}_j\right) \end{array}\right]$$

is now replaced by the matrix $\mathbf{A}_j$. The matrix $\frac{\partial\widehat{\mathbf{T}}_j}{\partial z_{mk}} = \frac{\partial\mathbf{T}_j}{\partial z_{mk}}\big|_{z_{mk}=\widehat{z}_{mk}}$ is deterministic since it is evaluated at the means of measured system responses $(z_{mk} = \widehat{z}_{mk})$.

It now becomes apparent, from Eq. (5.11) that the parameter covariance matrix can be found at $j+1^{\text{th}}$ iteration as,

$$\begin{aligned}&\mathbf{V}_{\boldsymbol{\theta}_{j+1}} = \\ &\mathrm{Cov}\left(\Delta\boldsymbol{\theta}_j + \mathbf{A}_j\Delta\mathbf{z}_m + \widehat{\mathbf{T}}_j\left(\Delta\mathbf{z}_m - \Delta\mathbf{z}_j\right), \Delta\boldsymbol{\theta}_j + \mathbf{A}_j\Delta\mathbf{z}_m + \widehat{\mathbf{T}}_j\left(\Delta\mathbf{z}_m - \Delta\mathbf{z}_j\right)\right) = \\ &\mathbf{V}_{\boldsymbol{\theta}_j} + \mathrm{Cov}\left(\Delta\boldsymbol{\theta}_j, \Delta\mathbf{z}_m\right)\mathbf{A}_j^{\mathrm{T}} + \mathrm{Cov}\left(\Delta\boldsymbol{\theta}_j, \Delta\mathbf{z}_m\right)\widehat{\mathbf{T}}_j^{\mathrm{T}} - \mathrm{Cov}\left(\Delta\boldsymbol{\theta}_j, \Delta\mathbf{z}_j\right)\widehat{\mathbf{T}}_j^{\mathrm{T}} \\ &+ \left(\mathrm{Cov}\left(\Delta\boldsymbol{\theta}_j, \Delta\mathbf{z}_m\right)\mathbf{A}_j^{\mathrm{T}}\right)^{\mathrm{T}} + \mathbf{A}_j\mathbf{V}_{\mathbf{z}_m}\mathbf{A}_j^{\mathrm{T}} + \mathbf{A}_j\mathbf{V}_{\mathbf{z}_m}\widehat{\mathbf{T}}_j^{\mathrm{T}} - \mathbf{A}_j\mathrm{Cov}\left(\Delta\mathbf{z}_m, \Delta\mathbf{z}_j\right)\widehat{\mathbf{T}}_j^{\mathrm{T}} \\ &+ \left(\mathrm{Cov}\left(\Delta\boldsymbol{\theta}_j, \Delta\mathbf{z}_m\right)\widehat{\mathbf{T}}_j^{\mathrm{T}}\right)^{\mathrm{T}} + \left(\mathbf{A}_j\mathbf{V}_{\mathbf{z}_m}\widehat{\mathbf{T}}_j^{\mathrm{T}}\right)^{\mathrm{T}} + \left(\widehat{\mathbf{T}}_j\mathbf{V}_{\mathbf{z}_m}\widehat{\mathbf{T}}_j^{\mathrm{T}}\right)^{\mathrm{T}} \\ &- \widehat{\mathbf{T}}_j\mathrm{Cov}\left(\Delta\mathbf{z}_m, \Delta\mathbf{z}_j\right)\widehat{\mathbf{T}}_j^{\mathrm{T}} - \left(\mathrm{Cov}\left(\Delta\boldsymbol{\theta}_j, \Delta\mathbf{z}_j\right)\widehat{\mathbf{T}}_j^{\mathrm{T}}\right)^{\mathrm{T}} \\ &- \left(\mathbf{A}_j\mathrm{Cov}\left(\Delta\mathbf{z}_m, \Delta\mathbf{z}_j\right)\widehat{\mathbf{T}}_j^{\mathrm{T}}\right)^{\mathrm{T}} - \left(\widehat{\mathbf{T}}_j\mathrm{Cov}\left(\Delta\mathbf{z}_m, \Delta\mathbf{z}_j\right)\widehat{\mathbf{T}}_j^{\mathrm{T}}\right)^{\mathrm{T}} + \widehat{\mathbf{T}}_j\mathbf{V}_{\mathbf{z}_j}\widehat{\mathbf{T}}_j^{\mathrm{T}}\end{aligned} \tag{5.12}$$

A common assumption, that originated with the 1974 paper of Collins et al. [26], is to omit the correlation between the measurement, $\mathbf{z}_m$, and the system parameters, $\boldsymbol{\theta}_j$. Friswell [93] corrected this omission by including the correlation after the first iteration. In this work the effect of the omitted correlation on the converged prediction space using the formulation described above is considered.

When the measurements and parameters are assumed to be uncorrelated, then $\mathrm{Cov}\left(\Delta\mathbf{z}_m, \Delta\boldsymbol{\theta}\right) = \mathbf{0}$ and also $\mathrm{Cov}\left(\Delta\mathbf{z}_m, \Delta\mathbf{z}_j\right) = \mathbf{0}$. It will be shown later that the matrix $\mathbf{A}_j$ vanishes under the same assumption. Consequently, Eq. (5.12) simplifies to give,

$$\begin{aligned}\mathbf{V}_{\theta_{j+1}} &= \mathbf{V}_{\theta_j} - \mathrm{Cov}\left(\Delta\boldsymbol{\theta}_j, \Delta\mathbf{z}_j\right)\widehat{\mathbf{T}}_j^{\mathrm{T}} \\ &+ \widehat{\mathbf{T}}_j\mathbf{V}_{\mathbf{z}_m}\widehat{\mathbf{T}}_j^{\mathrm{T}} - \widehat{\mathbf{T}}_j\mathrm{Cov}\left(\Delta\mathbf{z}_j, \Delta\boldsymbol{\theta}_j\right) + \widehat{\mathbf{T}}_j\mathbf{V}_{\mathbf{z}_j}\widehat{\mathbf{T}}_j^{\mathrm{T}}\end{aligned} \tag{5.13}$$

Eq. (5.13) does not include the second-order sensitivity matrix. This leads to very considerable reduction in computational effort, of great practical value in engineering applications if the $\mathrm{Cov}\left(\Delta\mathbf{z}_m, \Delta\boldsymbol{\theta}\right) = \mathbf{0}$ assumption is shown to be viable. Under this assumption model updating is carried out using the two recursive Eqs. (5.8) and (5.13). The transformation matrix may be expressed as the weighted pseudo inverse, which is analogous to the transformation used in deterministic model updating [3, 4]. To the zeroth order of smallness the same equation applies,

$$\widehat{\mathbf{T}}_j = \left(\widehat{\mathbf{S}}_j^{\mathrm{T}}\mathbf{W}_1\widehat{\mathbf{S}}_j + \mathbf{W}_2\right)^{-1}\widehat{\mathbf{S}}_j^{\mathrm{T}}\mathbf{W}_1 \tag{5.14}$$

In Eq. (5.14), $\widehat{\mathbf{S}}_j$ denotes the sensitivity matrix at the parameter means, $\widehat{\mathbf{S}}_j = \mathbf{S}_j\left(\widehat{\boldsymbol{\theta}}\right)$, and the choice of $\mathbf{W}_1 = \mathbf{I}$ and $\mathbf{W}_2 = \mathbf{0}$ results in the pseudo inverse. In the case of ill-conditioned model-updating equations, the minimum-norm regularised solution is obtained as described in Section 3.3 in Chapter 3.

The above procedure may be implemented in the following steps:

1. Determine the mean vector and covariance matrix of the measured data $(\widehat{\mathbf{z}}_m, \mathbf{V}_{\mathbf{z}_m})$ using Eq. (2.20) and (2.21) and set $j = 0$..

2. Initialise the means and standard deviations of the system parameters.

3. Determine the mean value of the analytical output parameters, $\widehat{\mathbf{z}}_j$, and the covariance matrices, $\mathrm{Cov}\left(\Delta\boldsymbol{\theta}_j, \Delta\mathbf{z}_j\right)$ and $\mathbf{V}_{\mathbf{z}_j}$, using a forward propagation method such as perturbation, the asymptotic integral or Monte-Carlo simulation.

4. Calculate the sensitivity matrix $\mathbf{S}_j$ at the current mean values of system parameters, choose suitable weighting matrices for regularisation and determine the transformation matrix $\widehat{\mathbf{T}}_j$ according to Eq. (5.14).

5. Update the mean values and covariance matrix of the system parameters using Eqs. (5.8) and (5.13), respectively.

6. If both the means and standard deviations of the parameters have converged go to step (7); otherwise set $j = j + 1$, go to step (3).

7. Stop.

If the correlation between the parameters and measurements is included, then $\mathrm{Cov}\left(\Delta\boldsymbol{\theta}_j, \Delta\mathbf{z}_m\right)$ and matrix $\mathbf{A}_j$ must be updated as follows,

$$\begin{aligned}\mathrm{Cov}\left(\Delta\boldsymbol{\theta}_{j+1}, \Delta\mathbf{z}_m\right) &= \mathrm{Cov}\left(\Delta\boldsymbol{\theta}_j + \mathbf{A}_j\Delta\mathbf{z}_m + \widehat{\mathbf{T}}_j\left(\Delta\mathbf{z}_m - \Delta\mathbf{z}_j\right), \Delta\mathbf{z}_m\right) \\ &= \mathrm{Cov}\left(\Delta\boldsymbol{\theta}_j, \Delta\mathbf{z}_m\right) + \left(\mathbf{A}_j + \widehat{\mathbf{T}}_j\right)\mathbf{V}_{\mathbf{z}_m} - \widehat{\mathbf{T}}_j\mathrm{Cov}\left(\Delta\mathbf{z}_j, \Delta\mathbf{z}_m\right)\end{aligned} \tag{5.15}$$

The matrix $\mathbf{A}_{j+1}$ is determined from

$$\mathbf{A}_{j+1} = \left[\begin{array}{cccc} \frac{\partial\widehat{\mathbf{T}}_{j+1}}{\partial z_{m1}}\left(\widehat{\mathbf{z}}_m - \widehat{\mathbf{z}}_{j+1}\right) & \frac{\partial\widehat{\mathbf{T}}_{j+1}}{\partial z_{m2}}\left(\widehat{\mathbf{z}}_m - \widehat{\mathbf{z}}_{j+1}\right) & \cdots & \frac{\partial\widehat{\mathbf{T}}_{j+1}}{\partial z_{mn_r}}\left(\widehat{\mathbf{z}}_m - \widehat{\mathbf{z}}_{j+1}\right) \end{array}\right] \tag{5.16}$$

where

$$\frac{\partial\widehat{\mathbf{T}}_{j+1}}{\partial z_{mk}} = \frac{\partial\mathbf{T}_{j+1}}{\partial z_{mk}}\Big|_{z_{mk}=\widehat{z}_{mk}} = \sum_{i=1}^{p}\frac{\partial\mathbf{T}_{j+1}}{\partial\widehat{\theta}_{(j+1),i}}\frac{\partial\widehat{\theta}_{(j+1),i}}{\partial z_{mk}}\Big|_{z_{mk}=\widehat{z}_{mk}} \;;\; k = 1, 2, ..., n \tag{5.17}$$

$$\frac{\partial \widehat{\mathbf{T}}_{j+1}}{\partial \widehat{\theta}_{(j+1),i}} = \left(\widehat{\mathbf{S}}_{j+1}^{\mathrm{T}}\mathbf{W}_1\widehat{\mathbf{S}}_{j+1} + \mathbf{W}_2\right)^{-1} \frac{\partial \widehat{\mathbf{S}}_{j+1}^{\mathrm{T}}}{\partial \theta_{(j+1),i}}\mathbf{W}_1$$
$$- \left(\widehat{\mathbf{S}}_{j+1}^{\mathrm{T}}\mathbf{W}_1\widehat{\mathbf{S}}_{j+1} + \mathbf{W}_2\right)^{-1} \left(\frac{\partial \widehat{\mathbf{S}}_{j+1}^{\mathrm{T}}}{\partial \theta_{(j+1),i}}\mathbf{W}_1\widehat{\mathbf{S}}_{j+1} + \widehat{\mathbf{S}}_{j+1}^{\mathrm{T}}\mathbf{W}_1\frac{\partial \widehat{\mathbf{S}}_{j+1}}{\partial \theta_{(j+1),i}}\right) \tag{5.18}$$
$$\times \left(\widehat{\mathbf{S}}_{j+1}^{\mathrm{T}}\mathbf{W}_1\widehat{\mathbf{S}}_{j+1} + \mathbf{W}_2\right)^{-1} \mathbf{S}_{j+1}^{\mathrm{T}}\mathbf{W}_1$$

and,

$$\frac{\partial \widehat{\boldsymbol{\theta}}_{j+1}}{\partial z_{mk}} = \frac{\partial \widehat{\boldsymbol{\theta}}_j}{\partial z_{mk}} + \widehat{\mathbf{T}}_j\left(\frac{\partial \widehat{\mathbf{z}}_m}{\partial z_{mk}} - \frac{\partial \widehat{\mathbf{z}}_j}{\partial z_{mk}}\right) + \frac{\partial \widehat{\mathbf{T}}_j}{\partial z_{mk}}\left(\widehat{\mathbf{z}}_m - \widehat{\mathbf{z}}_j\right) \tag{5.19}$$

The terms of $(\partial \widehat{\mathbf{z}}_m/\partial z_{mk}) = (\partial \mathbf{z}_m/\partial z_{mk})\,|_{z_{mk}=\widehat{z}_{mk}}$ are given by

$$\frac{\partial \widehat{z}_{mj}}{\partial z_{mk}} = \begin{cases} 1 & \text{if} \quad j = k \\ 0 & \text{if} \quad j \neq k \end{cases} \tag{5.20}$$

and from the chain rule,

$$\frac{\partial \widehat{\mathbf{z}}_j}{\partial z_{mk}} = \widehat{\mathbf{S}}_j \frac{\partial \widehat{\boldsymbol{\theta}}_j}{\partial z_{mk}} \tag{5.21}$$

Hence, a system of four recursive Eqs. (5.8), (5.12), (5.15) and (5.19) are required to determine the means and co-variance matrix of the parameters.

By the analysis above it is seen that the parameter covariances $\mathbf{V}_{\boldsymbol{\theta}_{j+1}}$ are expressed in terms of the measured output covariance matrix $\mathbf{V}_{\mathbf{z}_m}$ together with the covariances $\mathrm{Cov}\,(\Delta\boldsymbol{\theta}_j, \Delta\mathbf{z}_j)$, $\mathbf{V}_{\mathbf{z}_j}$ and in the case of Eq. (5.15) in terms of $\mathrm{Cov}\,(\Delta\boldsymbol{\theta}_j, \Delta\mathbf{z}_m)$ which is updated using Eq. (5.15). The derivatives $\partial \widehat{\mathbf{T}}_j/\partial z_{mk}$, $\partial \widehat{\mathbf{z}}_j/\partial z_{mk}$ and matrix $\mathbf{A}_j$ are found by using Eqs. (5.17), (5.21) and (5.16), respectively, and

$$\mathrm{Cov}\,(\Delta\mathbf{z}_j, \Delta\mathbf{z}_m) = \widehat{\mathbf{S}}_j \mathrm{Cov}\,(\Delta\boldsymbol{\theta}_j, \Delta\mathbf{z}_m) \tag{5.22}$$

This procedure may be implemented according the following steps:

1. Determine the mean vector and covariance matrix of the measured data $(\widehat{\mathbf{z}}_m, \mathbf{V}_{\mathbf{z}_m})$ using Eq. (2.20) and (2.21) and set $j = 0$.

2. Initialise the means and standard deviations of the system parameters.

3. Initialise $\mathrm{Cov}(\Delta\boldsymbol{\theta}_j, \Delta\mathbf{z}_m)$ and $\partial\widehat{\boldsymbol{\theta}}_j/\partial z_{mk}$ to zero, consequently matrix $\mathbf{A}_j$ and $\mathrm{Cov}(\Delta\mathbf{z}_j, \Delta\mathbf{z}_m)$ are zero (Eqs. (5.16), (5.17) and (5.22).

4. Determine the mean value of the analytical output parameters, $\widehat{\mathbf{z}}_j$, and the covariance matrices, $\mathrm{Cov}(\Delta\boldsymbol{\theta}_j, \Delta\mathbf{z}_j)$ and $\mathbf{V}_{\mathbf{z}_j}$, using a forward propagation method such as perturbation, the asymptotic integral or Monte-Carlo simulation.

5. Calculate the sensitivity matrix $\mathbf{S}_j$ at the current mean value of system parameters and choose suitable weighting matrices for regularisation in order to compute the transformation matrix introduced in Eq. (5.14).

6. Update the mean values and covariance matrix of the system parameters, $\mathrm{Cov}(\Delta\boldsymbol{\theta}_j, \Delta\mathbf{z}_m)$ and $\partial\widehat{\boldsymbol{\theta}}_j/\partial z_{mk}$ using Eqs. (5.8), (5.12), (5.15), and (5.19), respectively.

7. If both the mean values of the parameters and their standard deviations have converged go to step (8); otherwise set $j = j + 1$, go to step (4).

8. Stop.

5.3 Minimisation of an objective function

The second method, much simpler in concept, is based upon the minimisation of an objective function. As mentioned in the previous section, the hyperellipses represented by $(\widehat{\mathbf{z}}_m, \mathbf{V}_{\mathbf{z}_m})$ and $(\widehat{\mathbf{z}}_j, \mathbf{V}_{\mathbf{z}_j})$ define the space of measurements and predictions respectively. In order to minimise the distance and also the size difference in between these two spaces, an objective function is proposed in this work as follows,

$$(\widehat{\mathbf{z}}_m - \widehat{\mathbf{z}}_j)^{\mathrm{T}} \mathbf{W}_1 (\widehat{\mathbf{z}}_m - \widehat{\mathbf{z}}_j) + w_2 \left\| \mathbf{V}_{\mathbf{z}_m} - \mathbf{V}_{\mathbf{z}_j} \right\|_F \tag{5.23}$$

where $\|\bullet\|_F$ is Frobenius norm, $\widehat{\mathbf{z}}_m$ is estimated mean values of test results, $\mathbf{V}_{\mathbf{z}_m}$ is the covariance matrix of measured data, $\widehat{\mathbf{z}}_j$ and $\mathbf{V}_{\mathbf{z}_j}$ are the estimated mean values and the covariance matrix of predictions from mathematical model at j^{th}

iteration respectively. $\widehat{\mathbf{z}}_j$ and $\mathbf{V}_{\mathbf{z}_j}$ may be found by using different propagation method. Therefore the stochastic model updating problem can be expressed as,

$$\min_{\widehat{\theta},\mathbf{V}_\theta} \left(\left(\widehat{\mathbf{z}}_m - \widehat{\mathbf{z}}_j\right)^{\mathrm{T}} \mathbf{W}_1 \left(\widehat{\mathbf{z}}_m - \widehat{\mathbf{z}}_j\right) + w_2 \left\| \mathbf{V}_{\mathbf{z}_m} - \mathbf{V}_{\mathbf{z}_j} \right\|_F \right) \tag{5.24}$$

subject to $\theta_i \geq 0$ and $V_{\theta_{ii}} \geq 0$, $\forall i$. The weighting matrix, $\mathbf{W}_1$, and weighting coefficient, w_2, may be chosen to make two terms in objective function as the same order. This method is not concerned with any assumption of statistical independence between the updating parameters and measurements.

5.4 Case studies on the evaluation of covariance matrices

As explained in the previous section, the proposed methods require evaluation of the following vector and matrices:

$$\begin{aligned} &\widehat{\mathbf{z}} \\ &\mathbf{V}_{\mathbf{z}} \\ &\mathrm{Cov}\left(\boldsymbol{\theta}, \mathbf{z}\right) \end{aligned} \tag{5.25}$$

where the subscript j and prefix Δ on $\Delta\boldsymbol{\theta}_j$ and $\Delta\mathbf{z}_j$ is omitted for reasons of simplicity. The MCS can be used for evaluation of the above vector and matrices from the scatter of responses and the system parameters that provide the input to the simulation. Although the MCS is the most accurate method but is computationally expensive and can be extremely time consuming. Two other methods namely mean-centred perturbation and asymptotic integral which are introduced in Chapter (2) (Sections (2.3.2) and (2.3.3)) are also used for evaluation of the vector and matrices in Eq. (5.25) in this section.

Two case studies are considered, a 3 degree-of-freedom mass-spring system and a finite-element beam model with three elements having uncertain elastic moduli. In both cases the covariance matrices obtained by mean-centred first order perturbation and the asymptotic integral are compared to the covariance matrix obtained from Monte-Carlo simulation.

5.4.1 Case study 1: 3 Degree-of-freedom mass spring system

The model shown in Figure 2.13 is again considered in this section. It is assumed that the model has deterministic parameters,

$$m_i = 1.0\text{kg} \quad (i = 1,2,3)\,, \quad k_i = 1.0\text{N/m} \quad (i = 3,4)\,, \quad k_6 = 3\text{N/m} \tag{5.26}$$

and also uncertain random parameters,

$$\boldsymbol{\theta} = [k_1, k_2, k_5]^{\mathrm{T}} \in N_3\left(\widehat{\boldsymbol{\theta}}, \mathbf{V}_{\boldsymbol{\theta}}\right) \tag{5.27}$$

where

$$\widehat{\boldsymbol{\theta}} = \begin{bmatrix} 2 & 2 & 2 \end{bmatrix}^{\mathrm{T}} \quad \text{and} \quad \mathbf{V}_{\boldsymbol{\theta}} = \text{diag}\begin{bmatrix} 0.09 & 0.09 & 0.09 \end{bmatrix} \tag{5.28}$$

and N_3 denotes the multivariate normal (Gaussian) distribution in three random variables.

It is assumed that the vector of output data $\mathbf{z}$ contains three eigenvalues of the system. The covariance matrix $\mathbf{V}_{\mathbf{z}}$ being symmetric has six independent elements. The covariance matrix $\text{Cov}(\boldsymbol{\theta}, \mathbf{z})$ has nine elements. Figure 5.1 shows the errors obtained by using mean-centred first-order propagation and asymptotic approximation with respect to the results obtained by Monte-Carlo simulation. Generally, the errors are smaller when using the asymptotic integral.

5.4.2 Case study 2: Finite-element model of a cantilever beam

The beam, with a rectangular cross-section 25mm × 5.5mm and a length of 0.5 m, is modelled using 10 EulerBernoulli beam elements as shown in Figure 5.2. The elastic moduli of elements 3, 7 and 10 are considered as random variables,

$$\boldsymbol{\theta} = \begin{bmatrix} E_1 & E_7 & E_{10} \end{bmatrix}^{\mathrm{T}} \in N_3\left(\widehat{\boldsymbol{\theta}}, \mathbf{V}_{\boldsymbol{\theta}}\right) \tag{5.29}$$

where

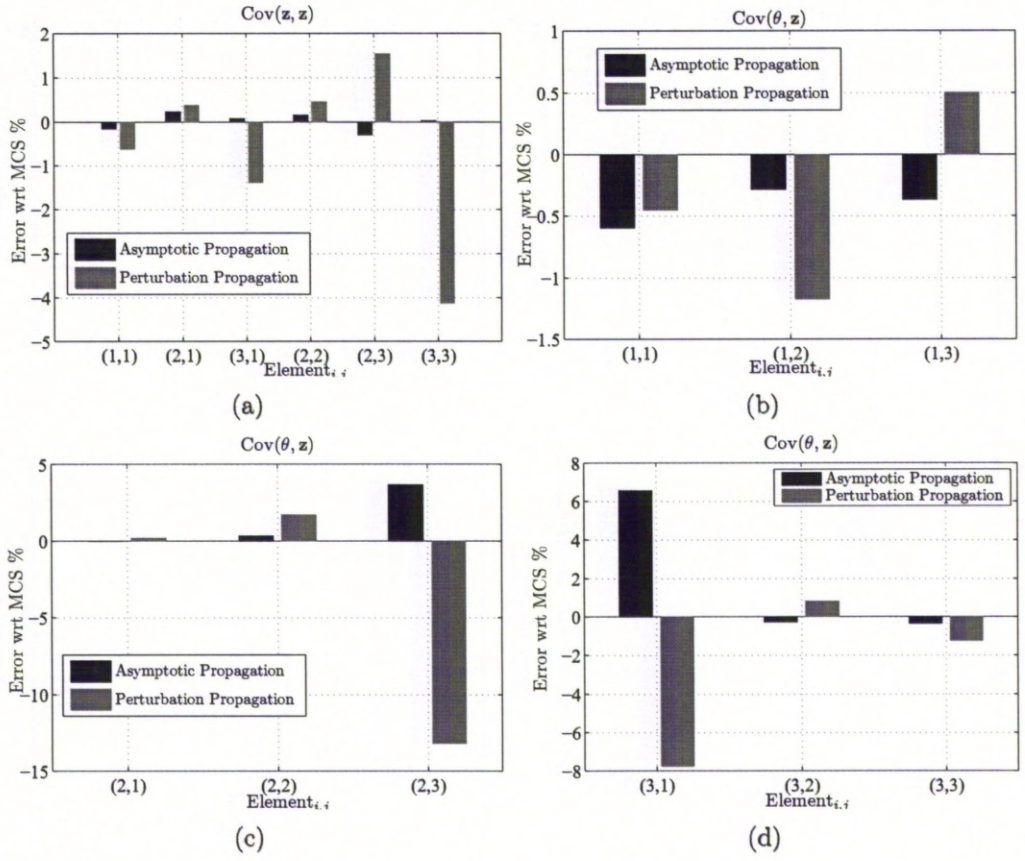

Figure 5.1: Mass spring system, estimation of $\mathbf{V_z}$ and Cov $(\boldsymbol{\theta}, \mathbf{z})$.

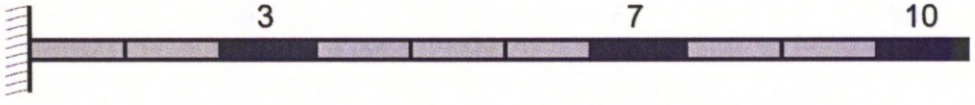

Figure 5.2: Case study 2: cantilever beam.

$$\begin{aligned} \widehat{\boldsymbol{\theta}} &= \left[\begin{array}{ccc} 2.1 \times 10^{11} & 2.1 \times 10^{11} & 2.1 \times 10^{11} \end{array} \right]^{\mathrm{T}} \\ \mathbf{V}_{\boldsymbol{\theta}} &= \mathrm{diag} \left[\begin{array}{ccc} 1.0 \times 10^{20} & 1.0 \times 10^{20} & 1.0 \times 10^{20} \end{array} \right] \end{aligned} \tag{5.30}$$

It is assumed that the vector of output data $\mathbf{z}$ contains the first three eigenvalues of the system. The errors in the estimated covariance matrices, with respect to Monte-Carlo simulation, are shown in Figure 5.3. The errors in elements (3,1) and (3,2) of Cov $(\boldsymbol{\theta}, \mathbf{z})$ appear larger than the others because the values of these terms are three orders of smallness less than the values of the other terms.

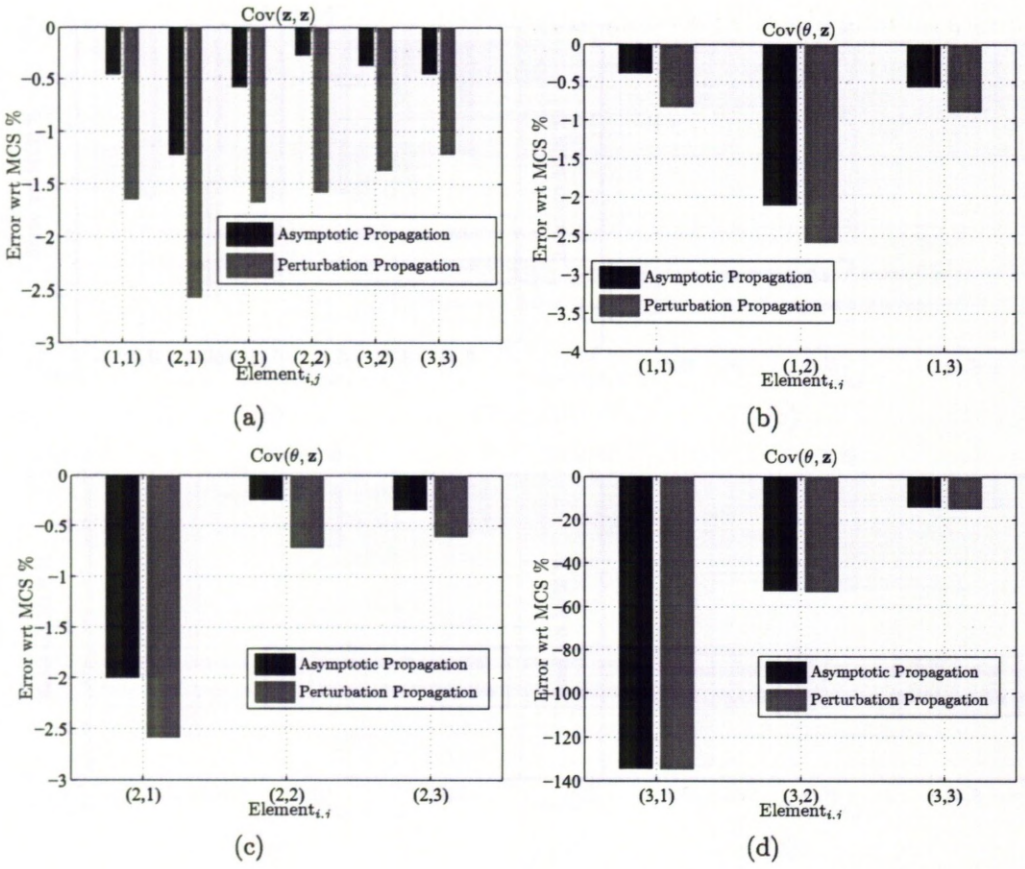

Figure 5.3: Cantilever beam, estimation of $\mathbf{V_z}$ and Cov $(\boldsymbol{\theta}, \mathbf{z})$.

5.5 Numerical case studies on the identification of uncertainty

Two numerical case studies are used to illustrate the working of the perturbation methods, namely the 3 degree-offreedom system described in Section (5.4.1) and also a finite-element pin-jointed truss structure.

5.5.1 Case study 1: 3 Degree-of-freedom mass spring system

The three methods that are developed in Sections (5.2) and (5.3) are applied to the simple 3 DOF mass-spring system that is shown in Figure 2.13. The deterministic, nominal and initial estimates of parameters are assumed to be the same as Eqs. (3.57), (3.58) and (3.59) respectively. The measured data are obtained by using Monte-Carlo simulation with 10,000 samples (similar to Section (3.5)).

Results obtained by the perturbation methods $\mathbf{W}_1 = \mathbf{I}$, $\mathbf{W}_2 = \mathbf{0}$ and the method of minimisation of an objective function are shown in Table 5.1. The numbers, (1)-(3) in the table denote the following methods:

1. The proposed method in which the correlation between measured data and system parameters is omitted (Eqs. (5.8) and (5.13)).

2. The proposed method in which the correlation between measured data and system parameters is included after the first iteration (Eqs. (5.8), (5.12), (5.15) and (5.19)).

3. Second proposed method (minimising Eq. (5.24)). The optimization problem is solved using the Matlab Optimization Toolbox.

Table 5.1: Updating results obtained by various methods (10,000 samples)

Parameters	Initial error %	Error (1)%	Error (2)%	Error (3)%
k_1	100.00	1.22	1.01	0.30
k_2	100.00	-2.57	-2.12	-4.11
k_5	100.00	0.63	0.51	1.72
σ_{k_1}	50.00	2.00	2.59	1.52
σ_{k_2}	50.00	0.97	1.81	-0.46
σ_{k_5}	50.00	-0.70	0.17	-0.17

Firstly, it is seen that the results obtained by method (1), when the correlation of system parameters with the measured data is omitted, are at least as good as when this correlation is included. Method (2) requires the evaluation of the second-order sensitivity, which is an expensive computation and not needed when using method (1). In the similar example which is used in Section (3.5), it is seen in Table (3.1) that the perturbation method developed by Hua et al. [27] is also capable of the estimation of the mean and standard deviation of uncertain parameters accurately. However, this method needs the evaluation of the second-order sensitivity as does the method (2). It is seen in Table (3.1) that the method (3) is also capable of producing accurate results. The method (3) is originally proposed in this work. Convergence of the parameter estimates by

each of the different methods is shown in Figures 5.4 to 5.6. Figure 5.7 shows the convergence of the predictions upon experimental data in the space of the first three natural frequencies using method (1). As mentioned in Section (3.5), ten thousand samples are clearly enough to obtain an accurate estimate of the parameter variability.

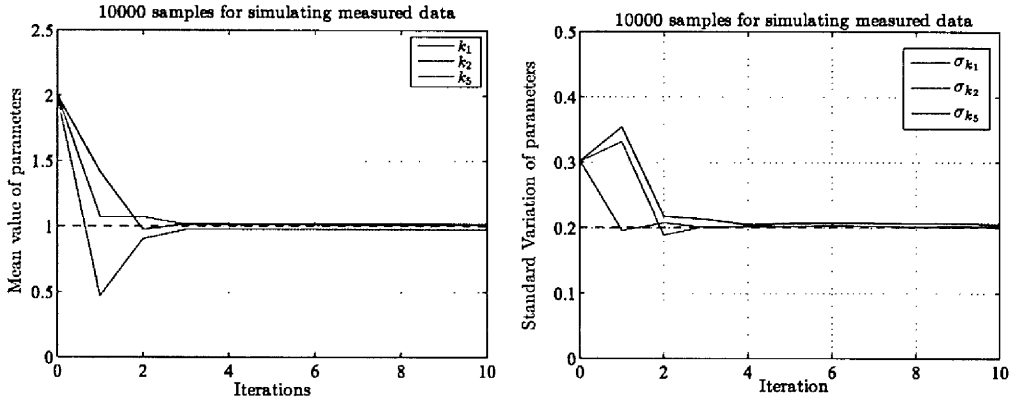

(a) (b)

Figure 5.4: Convergence of parameter estimates by method (1).

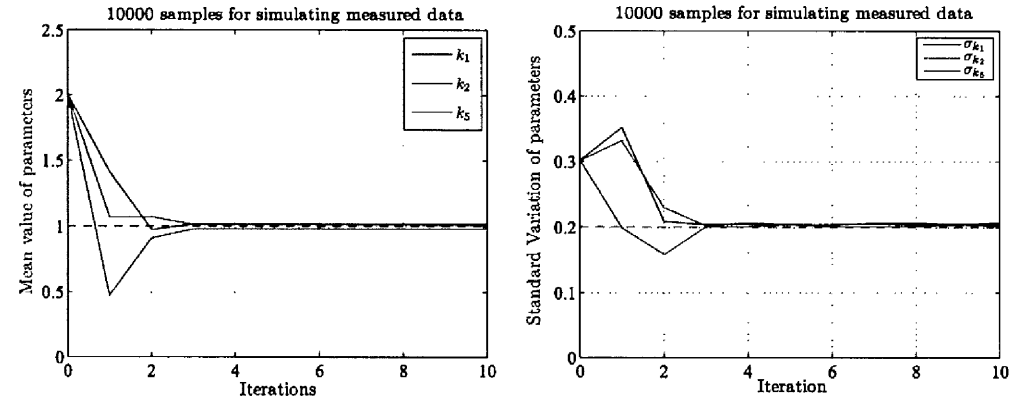

(a) (b)

Figure 5.5: Convergence of parameter estimates by method (2).

Figure 5.8 shows the convergence of the parameter standard deviations by method (1) as the number of samples is increased from 10 to 1000. In each case 10 runs of the updating algorithm were carried out to enable a range of solution errors to be determined. A different set of samples was used in each of the 10 runs. When only 10 samples were used errors were found in the range of 24-54%,

while in the case of 1000 samples the errors ranged from 3% to 7%.

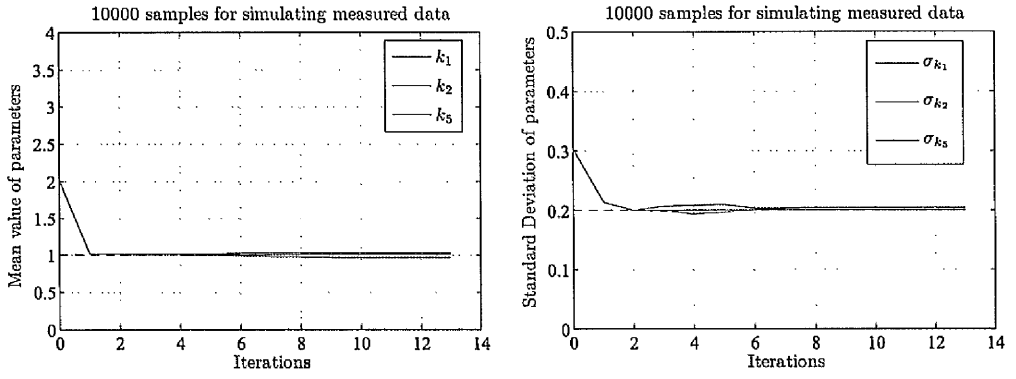

(a) (b)

Figure 5.6: Convergence of parameter estimates by method (3).

Table 5.2 shows the converged results and percentage errors of the parameter statistics using only 10 samples with methods (1), (2) and (3). The 10 samples were different in each of the three cases, which are shown to converge to similar results. Figures 5.9 and 5.10 show the convergence of scatter of predictions upon the scatter of simulated measurements in the planes of the first and second, and second and third natural frequencies, respectively. Ten measurement samples and 10,000 predictions from the estimated parameter distributions by method (1) are shown.

Table 5.2: Updating results obtained by various methods (10 samples)

Parameters	Initial error %	Error (1)%	Error (2)%	Error (3)%
k_1	100.00	4.53	5.42	-8.69
k_2	100.00	8.25	1.52	-7.78
k_5	100.00	4.21	0.69	6.75
σ_{k_1}	50.00	20.03	12.60	5.13
σ_{k_2}	50.00	14.35	19.33	31.50
σ_{k_5}	50.00	17.65	13.66	16.92

The effect of using different propagation methods (Monte-Carlo simulation, mean-centred first-order propagation, or the asymptotic integral) is considered in Table 5.3 and Figures 5.11 to 5.13. It is seen that in this case specifically there is

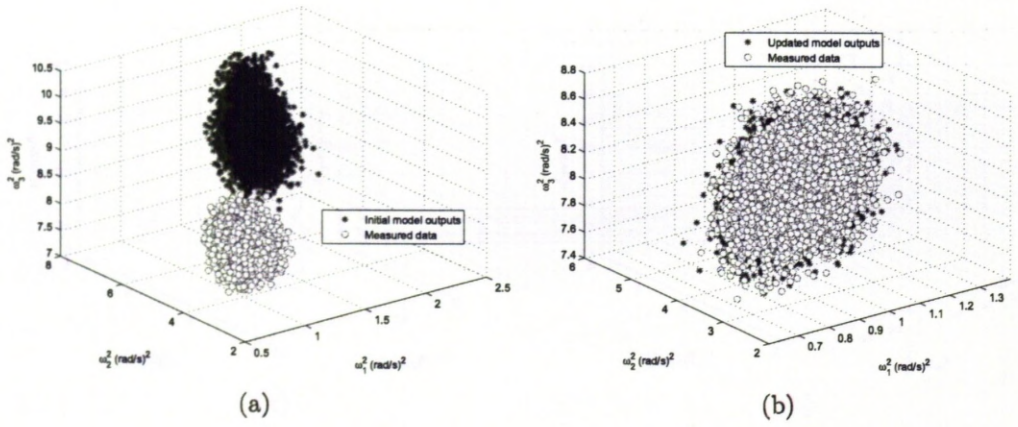

Figure 5.7: Initial and updated scatter of predicted and measured data: identification using method (1) with 10,000 samples.

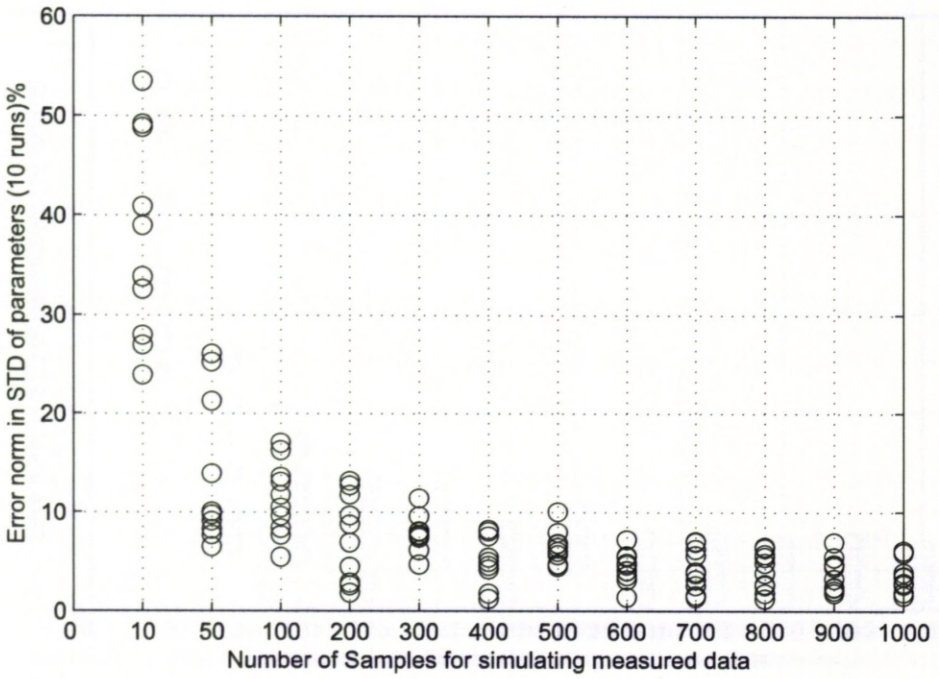

Figure 5.8: Error norm for parameter standard deviations using different sample sizes each with 10 runs of the algorithm.

little advantage gained by using the more computationally demanding approaches (Monte-Carlo simulation, and the asymptotic integral) over the mean-centred first-order perturbation technique.

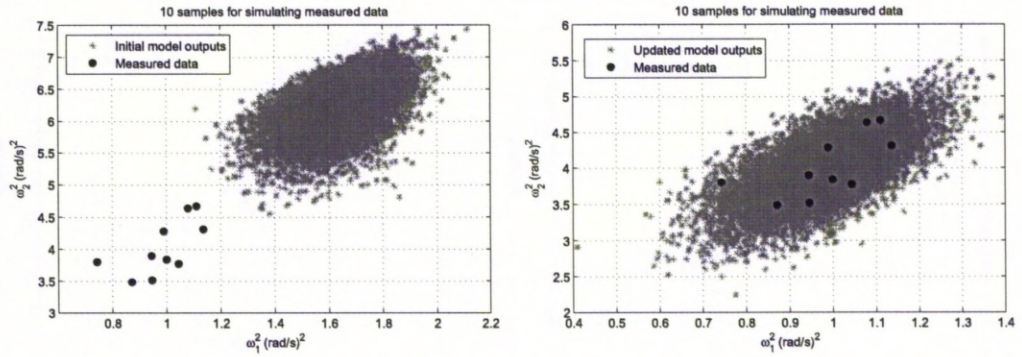

(a) (b)

Figure 5.9: Initial and updated scatter of predicted data (10,000 points) based upon 10 measurement samples: identification by method (1).

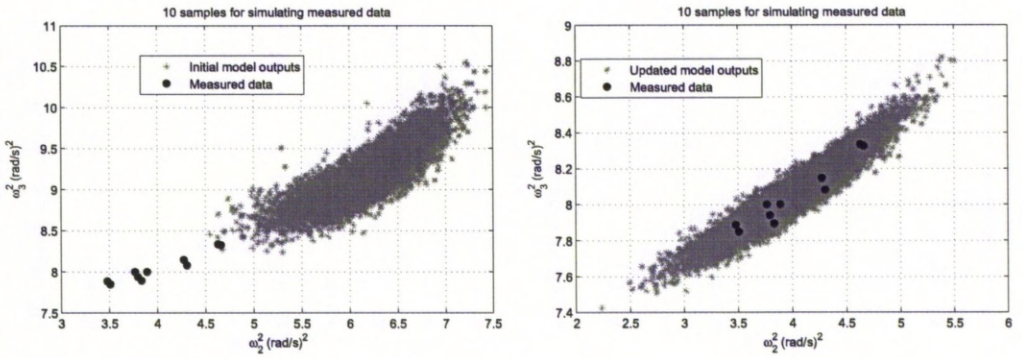

(a) (b)

Figure 5.10: Initial and updated scatter of predicted data (10,000 points) based upon 10 measurement samples: identification by method (1).

Table 5.3: Updating results obtained by various methods (10 samples)

Parameters	Initial error %	Monte Carlo %	Perturbation %	Asymptotic%
k_1	100.00	5.03	-7.51	4.79
k_2	100.00	-5.93	-13.50	-2.00
k_5	100.00	7.26	-15.63	-2.36
σ_{k_1}	50.00	5.94	10.36	-25.72
σ_{k_2}	50.00	-11.25	11.68	-1.22
σ_{k_5}	50.00	10.23	-15.42	9.11

5.5.2 Case study 2: Finite-element model of a pin-jointed truss

The finite-element model consisting of 20 planar rod elements, each having 2 degree-of-freedom at every node, is shown in Figure 5.14. The elastic modulus,

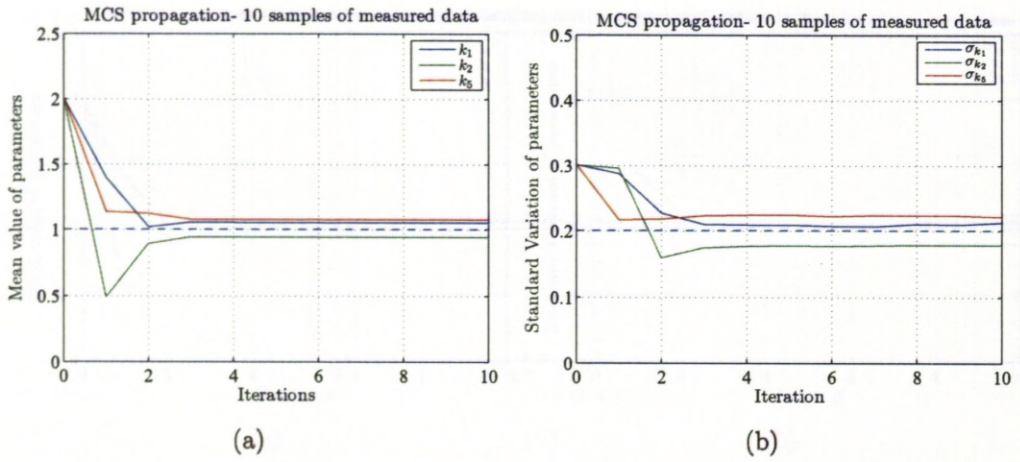

(a) (b)

Figure 5.11: Convergence of parameter estimates by method (1) using Monte-Carlo simulation.

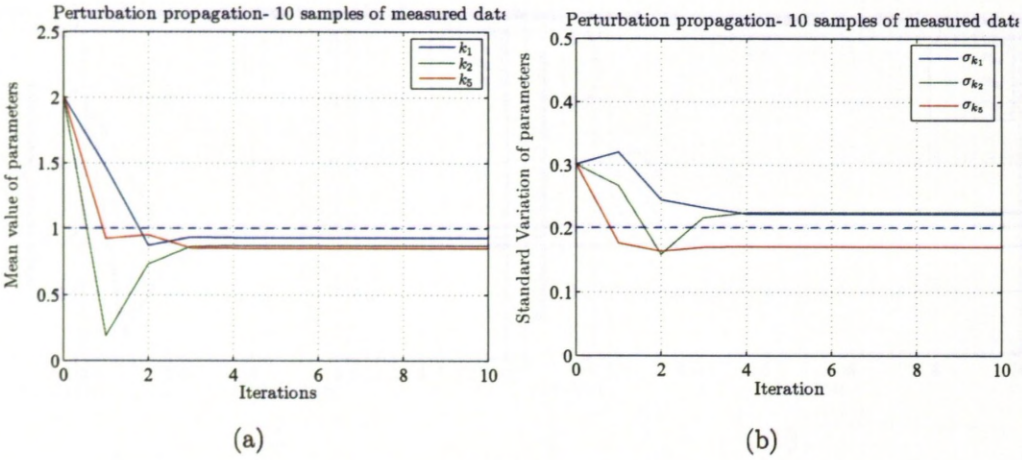

(a) (b)

Figure 5.12: Convergence of parameter estimates by method (1) using mean-centred first-order perturbation.

mass density and cross sectional area were assumed to take the values,

$$E = 70\text{Gpa}, \qquad \rho = 2700\text{kg/m}^3, \qquad A = 0.03\text{m}^2 \tag{5.31}$$

The diagonal elements in the finite-element model were represented by generic rod elements [68], having the generic stiffness matrices given by

$$\mathbf{K} = k_i \begin{bmatrix} 1 & -1 \\ -1 & 1 \end{bmatrix} \tag{5.32}$$

where k_i is generic parameter for the i^{th} diagonal element. This parameter was a Gaussian random variable defined by

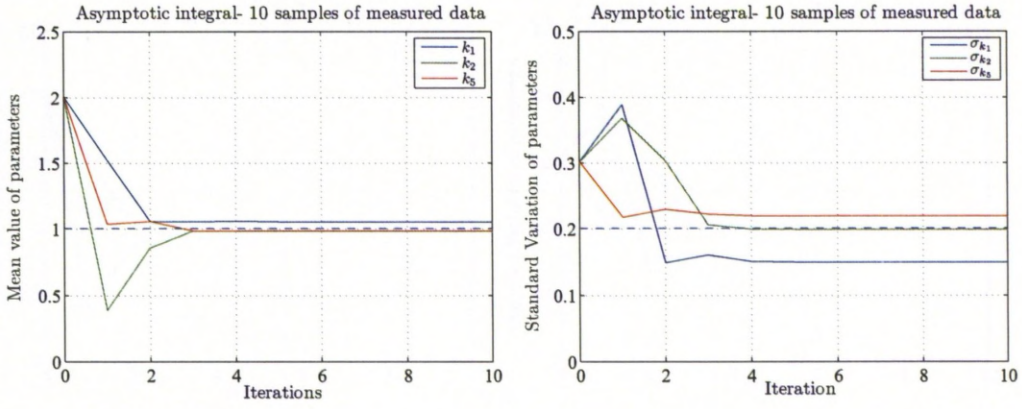

(a) (b)

Figure 5.13: Convergence of parameter estimates by method (1) using the asymptotic integral.

$$\widehat{k}_i = \frac{E_i A_i}{L_i} = 1.485 \times 10^8, \qquad \text{COV}_i = \frac{\sigma_{k_i}}{\widehat{k}_i} = 0.135, \qquad i = 1, ..., 5 \tag{5.33}$$

and the initial uncertain generic parameters were set as

$$\begin{aligned} \widehat{k}_1^{(0)} &= 0.85 \times 1.485 \times 10^8, \quad \widehat{k}_2^{(0)} = 1.05 \times 1.485 \times 10^8, \\ \widehat{k}_3^{(0)} &= 0.95 \times 1.485 \times 10^8, \quad \widehat{k}_4^{(0)} = 0.90 \times 1.485 \times 10^8, \\ \widehat{k}_5^{(0)} &= 1.10 \times 1.485 \times 10^8, \quad \text{COV}^{(0)}(k_i) = 2 \times 0.135, \ i = 1, ..., 5 \end{aligned} \tag{5.34}$$

where COV denotes the estimated coefficient of variation (ratio of the standard deviation to the mean). The measurements consisted of the first four natural frequencies and four vertical displacements at nodes 5, 6, 11 and 12 for each of the first four modes, thereby generating 20 equations for updating five randomised parameters. Firstly, it was assumed that these equations do not contain any measurement noise. As expected, method (1) is capable of regenerating the exact simulated values of mean and COV for each of the randomised parameters as shown in Figure 5.15. The weighting matrices were $\mathbf{W}_1 = \mathbf{I}$ and $\mathbf{W}_2 = \mathbf{0}$.

Method (1) was again applied, with and without regularisation, when 1% measurement noise with zero-mean Gaussian distribution was added to the measured data. Considerable errors were found in the estimated distribution when $\mathbf{W}_1 = \mathbf{I}$ and $\mathbf{W}_2 = \mathbf{0}$ as shown in Figure 5.16. Regularisation was then applied

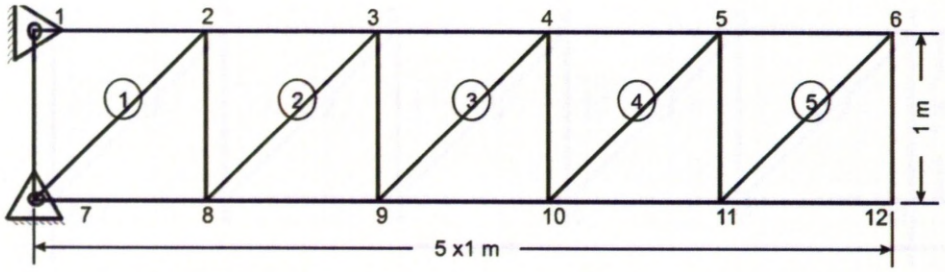

Figure 5.14: FE model of pin-jointed truss.

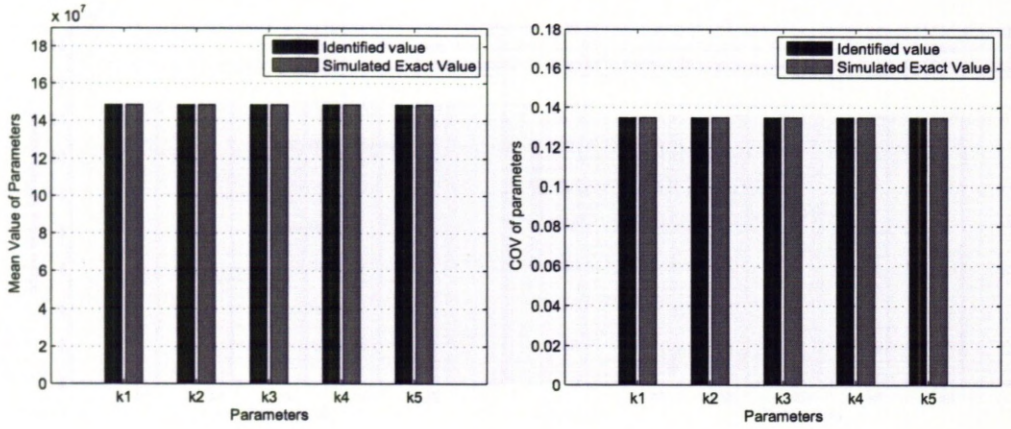

Figure 5.15: Identified parameters-zero noise.

with the regularisation parameter $r_g = 0.001$ determined from the L-curve in Figure 5.17. As can be seen from Figure 5.18, the estimated distribution was greatly improved by the regularisation. The standard deviations were affected more by the presence of the noise than were the estimated means.

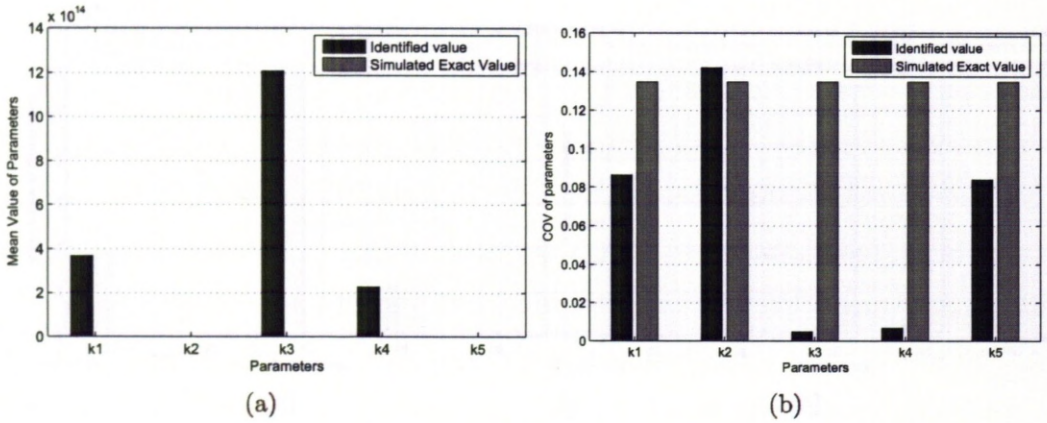

Figure 5.16: Identified parameters with 1% measurement noise and $\mathbf{W}_1 = \mathbf{I}$ and $\mathbf{W}_2 = \mathbf{0}$.

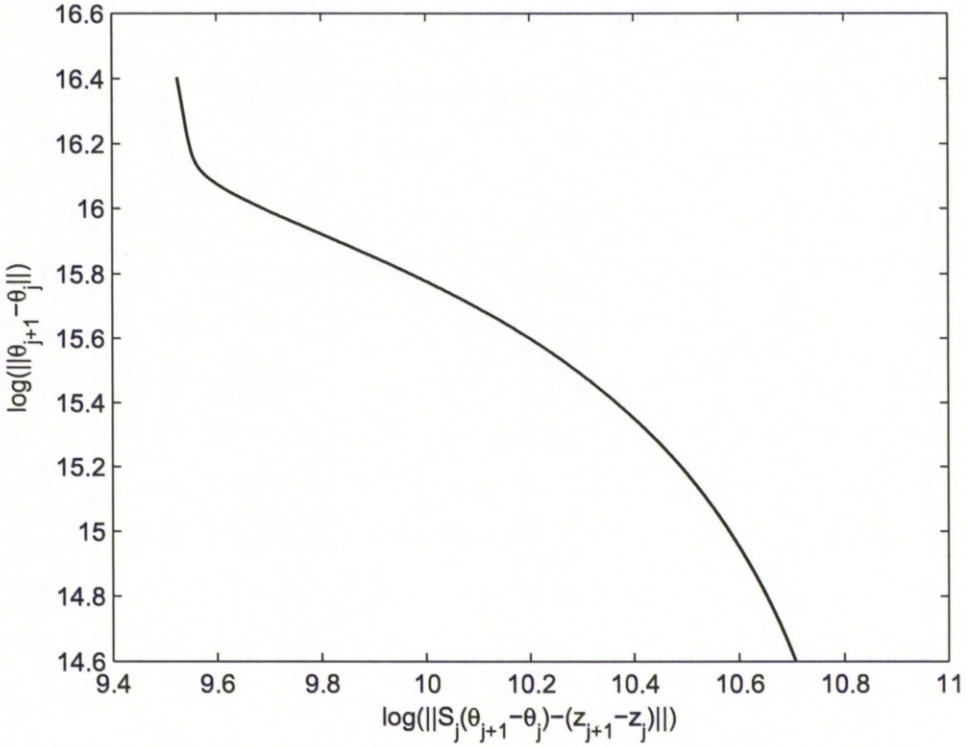

Figure 5.17: L-curve, $\|\bullet\|$ is Euclidian norm.

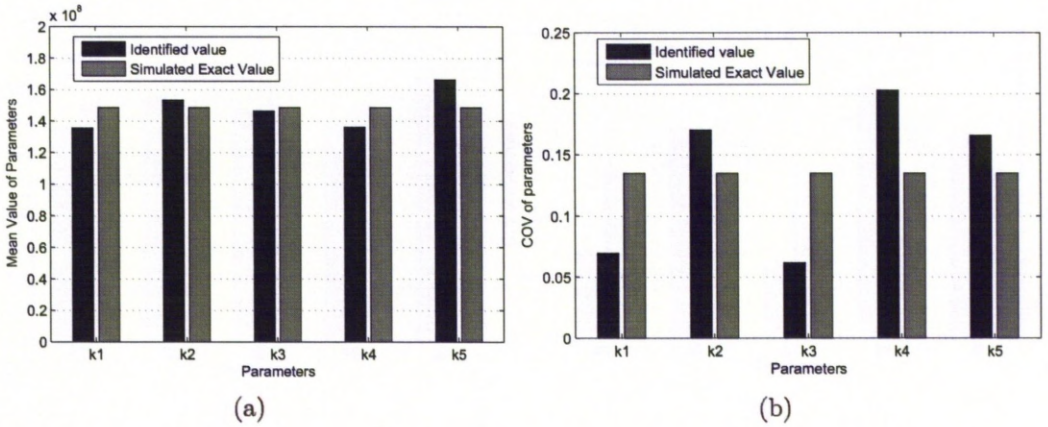

Figure 5.18: Identified parameters with 1% measurement noise and $\mathbf{W}_1 = \mathbf{I}$ and $\mathbf{W}_2 = r_g\mathbf{I}$.

5.6 Experimental case studies:

5.6.1 Case study 1: Aluminium plates with random thicknesses

Ten aluminium plates were prepared so that a contrived distribution of thicknesses, close to Gaussian, was obtained by machining. Care was taken to try to obtain a constant thickness for each plate. This was not achieved perfectly and the thickness variations were measured using a long-jaw micrometer at 4×14 points as shown in Figures 5.19 to 5.28. The distribution of nominal thicknesses is shown in Figure 5.29. The mean value of the thicknesses was 3.975mm with a standard deviation of 0.163mm. In the experimental set up (shown in Figure 5.30) free boundary conditions were used to avoid the introduction of other uncertainties due to clamping or pinning at the edges of the plates. All 10 plates had the same overall dimensions, length 0.4 m and width 0.1 m. A hammer test was carried out using four uniaxial fixed accelerometers. Figure 5.31 shows the excitation point, marked 'F', and the positions of four accelerometers, marked 'A', 'B', 'C' and 'D'. The mass of each accelerometer was 2 grams represented by lumped masses in the finite-element model. The first 10 measured natural frequencies of all 10 plates are given in Table 5.4 and Table 5.5.

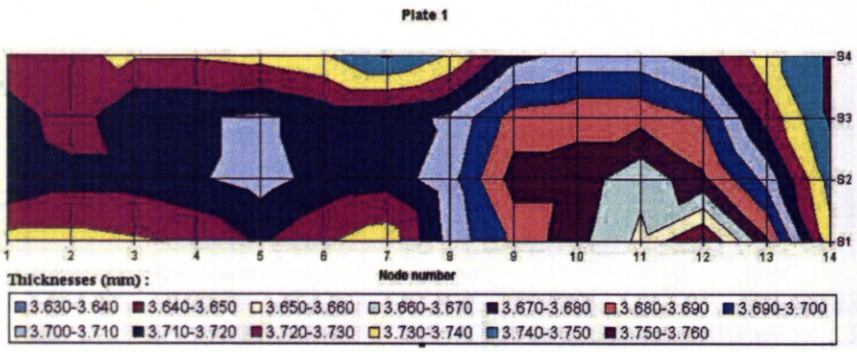

Figure 5.19: Measured thickness of plate 1.

The thickness of the plates was parameterised in four regions as shown in Figure 5.32 and a finite-element model was constructed consisting of 40×10 four-noded plate elements. The first six measured natural frequencies were used for stochastic model updating by method (1). A regularisation parameter, $r_g = 1^{10}$, was found from an L-curve. Figure 5.33 shows convergence of the mean values and

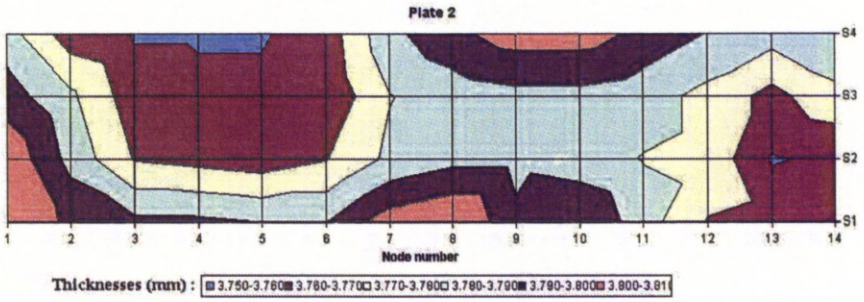

Figure 5.20: Measured thickness of plate 2.

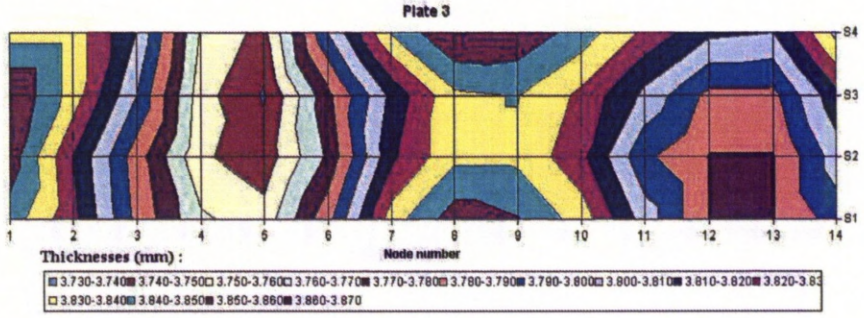

Figure 5.21: Measured thickness of plate 3.

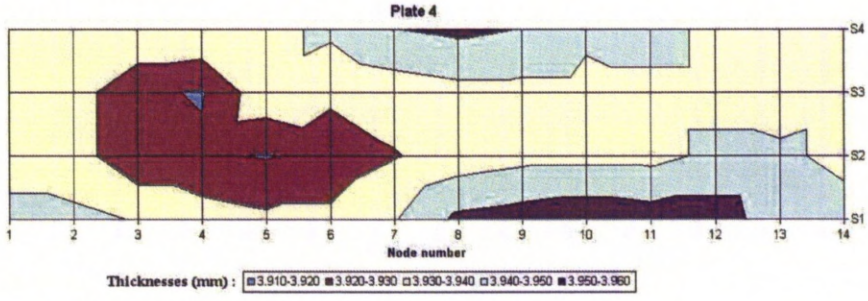

Figure 5.22: Measured thickness of plate 4.

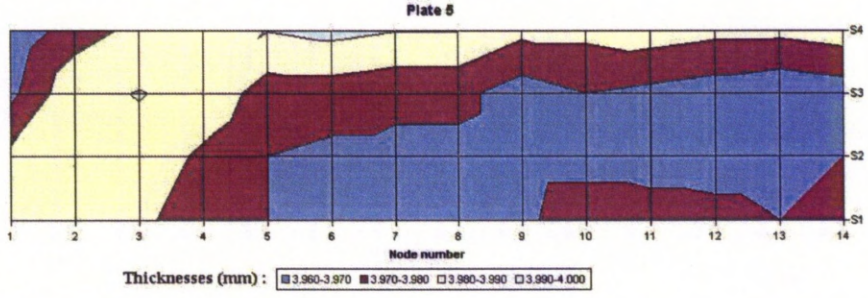

Figure 5.23: Measured thickness of plate 5.

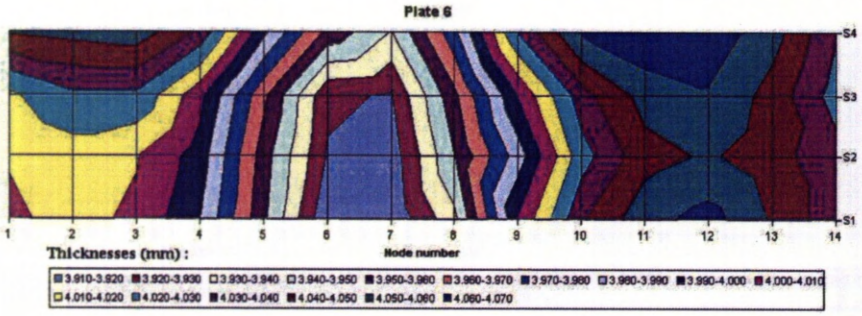

Figure 5.24: Measured thickness of plate 6.

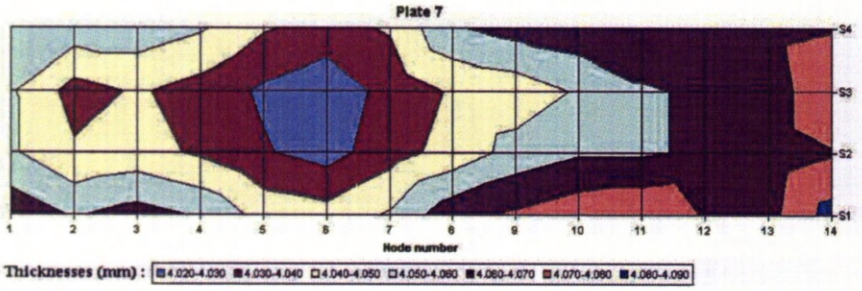

Figure 5.25: Measured thickness of plate 7.

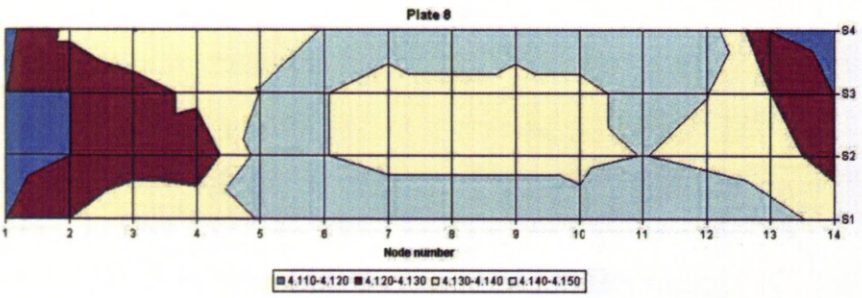

Figure 5.26: Measured thickness of plate 8.

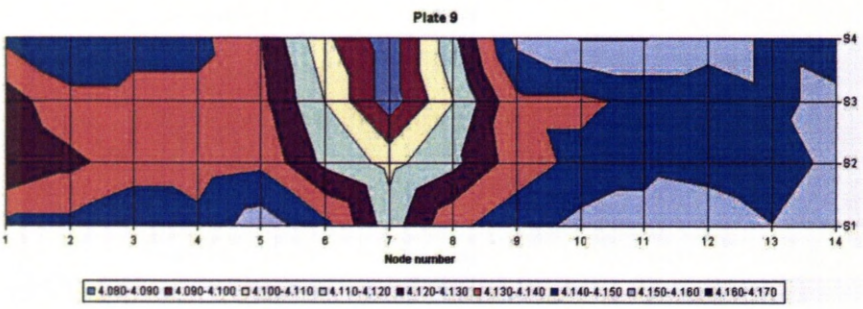

Figure 5.27: Measured thickness of plate 9.

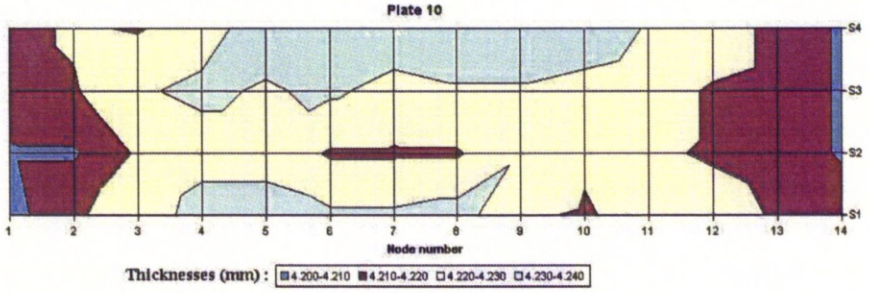

Figure 5.28: Measured thickness of plate 10.

Table 5.4: The first five measured natural frequencies (Hz) for the ten plates

	Mode Number				
Plate number	1 (Hz)	2 (Hz)	3 (Hz)	4 (Hz)	5 (Hz)
1	119.774	284.283	331.970	589.404	656.359
2	121.615	291.922	337.186	605.160	665.854
3	123.156	291.440	340.184	602.603	673.357
4	128.048	298.163	355.210	620.139	700.798
5	128.533	303.809	357.110	630.809	704.505
6	128.596	301.010	361.488	635.533	713.207
7	129.796	311.726	361.114	646.765	712.792
8	135.058	315.393	374.368	653.584	738.395
9	134.478	312.215	374.406	649.130	737.256
10	138.141	321.812	382.932	667.203	755.189
Mean	128.720	303.177	357.597	630.033	705.771
Standard deviation	6.011	12.032	17.048	25.235	32.854

COV for the four parameters. The initial mean and standard deviation of all four parameters were taken to be, $\widehat{t_i} = 4$ mm, $\sigma_{t_i} = 0.8$ mm, $i = 1, ..., 4$. The initial mean value was chosen to be close to the true mean while the initial standard deviation was deliberately overestimated to represent a realistic stochastic model updating problem where little is known other than an approximation to the mean value.

Table 5.5: The 6th to 10th measured natural frequencies (Hz) for the ten plates

	Mode Number				
Plate number	6 (Hz)	7 (Hz)	8 (Hz)	9 (Hz)	10 (Hz)
1	932.576	1091.603	1343.097	1628.879	1825.215
2	953.666	1106.861	1372.890	1650.395	1860.225
3	955.515	1119.445	1376.298	1669.899	1868.071
4	980.403	1165.177	1414.181	1736.714	1924.260
5	995.188	1169.660	1433.020	1743.750	1946.155
6	999.248	1184.455	1440.134	1765.415	1957.581
7	1019.052	1184.608	1467.366	1766.361	1987.556
8	1031.837	1225.375	1487.512	1825.602	2021.640
9	1023.229	1224.420	1479.268	1824.121	2013.354
10	1053.974	1253.610	1519.011	1866.665	2031.377
Mean	994.469	1172.521	1433.278	1747.780	1943.543
Standard deviation	38.877	53.840	56.771	79.232	72.908

The updated and measured means and standard deviations of the plate thicknesses are given in Table 5.6. These results are not in exact agreement but do show a considerable improvement in the thickness distributions when updated. It can be seen that the initial values of the means were chosen to be extremely close to the measured mean values. Small changes are observed in Table 5.6 after updating, away from the measured values obtained from averaged micrometer measurements at discrete points. The convergence of the standard deviations (shown in Table 5.6) from a considerable initial error is a much more significant result, demonstrating very clearly how well the method performs in converging the distribution of updating parameters upon the collection of measured thickness values. Of course, the measured standard deviations are likely to be less accurate

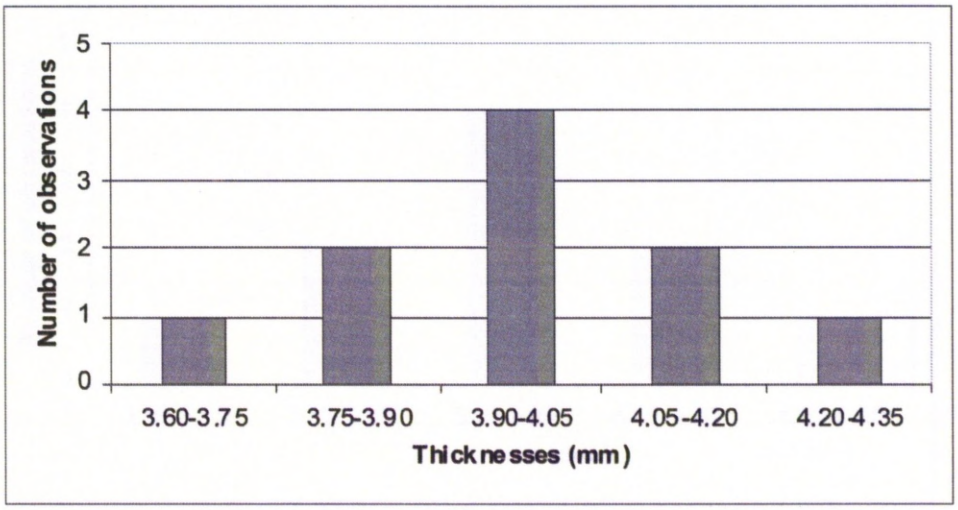

Figure 5.29: Distribution of plate thicknesses.

than the measured means.

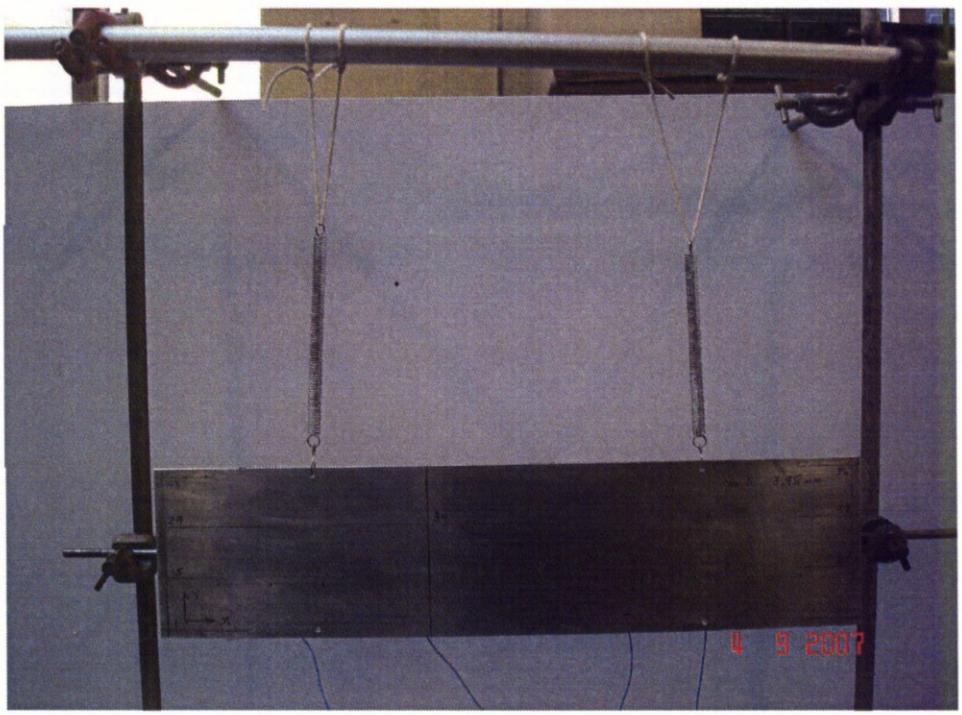

Figure 5.30: Experimental set up.

The means and standard deviations of the first six measured natural frequencies were used in updating, whereas 10 modes were measured in total. It is seen from Tables 5.7 and 5.8 that not only are the first six natural frequency distributions improved by updating but also the 7^{th} to 10^{th} natural frequency predictions

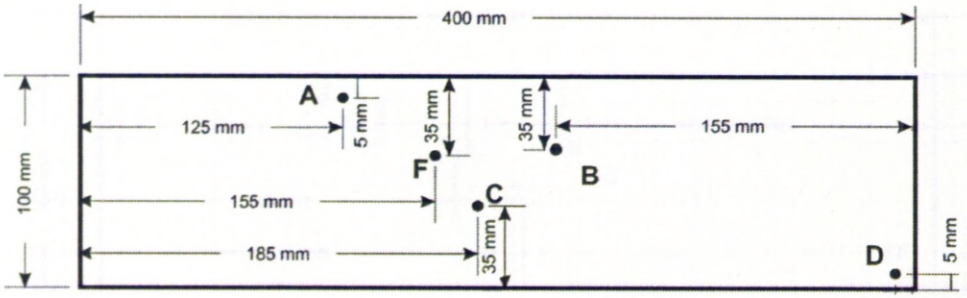

Figure 5.31: Arrangement of accelerometers (A, B, C, D) and excitation point (F).

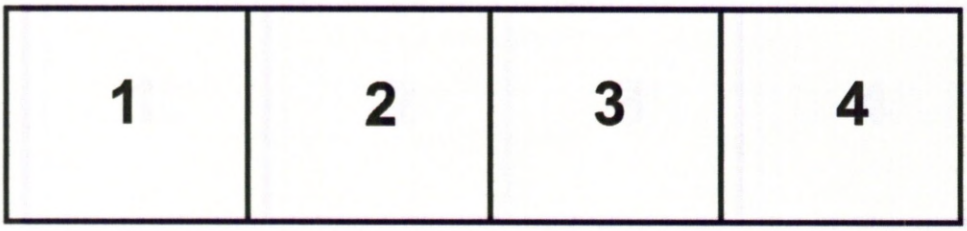

Figure 5.32: Parameterisation into four regions of plate thickness.

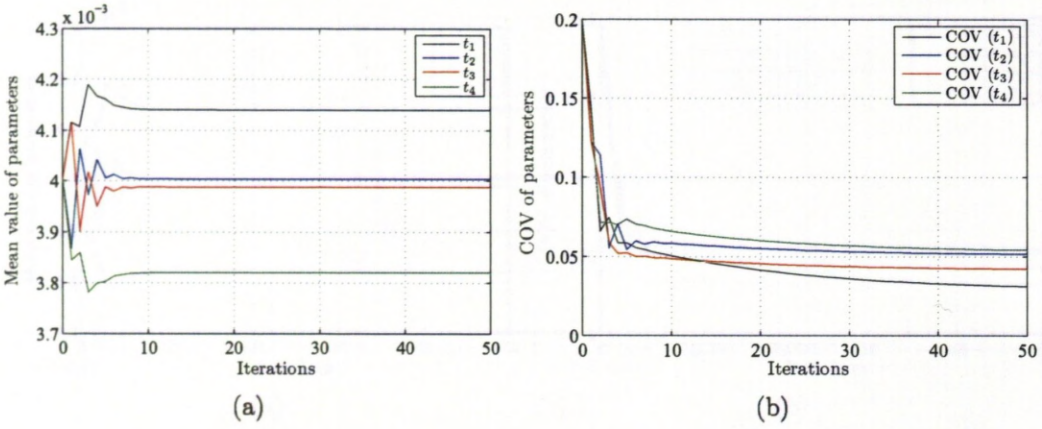

Figure 5.33: Convergence of parameter estimates.

(mean and standard deviations) are equally improved. This provides a good demonstration of the validity of the updated statistical model.

5.6.2 Case study 2: Aluminum plates with random masses

Thirteen sets of masses having a distribution close to Gaussian were prepared. The experimental set up is shown in Figure 5.34. Each set included eight equal masses. The 11.5 gram set, for example, included eight masses all of 11.5 grams. The distribution of nominal masses is shown in Figure 5.35. The mean value of

Table 5.6: Measured, initial and updated mean and standard deviation of parameters

	Mode Number				
	Measured parameters	Initial parameters	Updated parameters	Initial FE % error	Updated FE % error
$\widehat{t_1}$ (mm)	3.978	4.000	4.140	0.553	4.072
σ_{t_1} (mm)	0.159	0.800	0.129	403.145	18.868
$\widehat{t_2}$ (mm)	3.969	4.000	4.002	0.781	0.831
σ_{t_2} (mm)	0.161	0.800	0.204	396.894	26.708
$\widehat{t_3}$ (mm)	3.982	4.000	3.986	0.452	0.100
σ_{t_3} (mm)	0.164	0.800	0.166	387.805	1.219
$\widehat{t_4}$ (mm)	3.981	4.000	3.820	0.477	4.044
σ_{t_4} (mm)	0.167	0.800	0.206	379.042	23.353

Table 5.7: Measured, initial and updated mean natural frequencies

	Mode Number				
	Measured (Hz)	Initial FE (Hz)	Updated FE (Hz)	Initial FE % error	Updated FE % error
Mode (1)	128.720	128.321	128.111	0.310	0.473
Mode (2)	303.177	307.147	306.339	1.310	1.043
Mode (3)	357.597	356.645	355.185	0.266	0.675
Mode (4)	630.033	637.433	633.188	1.175	0.501
Mode (5)	705.771	705.467	701.777	0.043	0.566
Mode (6)	994.469	1002.229	996.865	0.780	0.241
Mode (7)	1172.521	1173.395	1169.087	0.075	0.293
Mode (8)	1433.278	1444.018	1435.848	0.750	0.179
Mode (9)	1747.780	1748.977	1743.491	0.069	0.245
Mode (10)	1943.543	1952.882	1935.851	0.481	0.396

the masses was 10.063 grams with a standard deviation of 2.798 grams. Each set was glued to the surface of a plate and a hammer test was carried. The experimental set up and the positions of accelerometers and excitation points were the same as previous case study. The positions of added masses on the plate are shown in Figure 5.36. Each of added mass and mass of the accelerometer were represented by lumped masses in the finite element model. The first six natural frequencies of all 13 sets are given in Table 5.9. The second proposed method (method 3 in Section 5.4.1) was used in this case. As mentioned earlier,

Table 5.8: Measured, initial and updated standard deviation natural frequencies

	Mode Number				
	Measured (Hz)	Initial FE (Hz)	Updated FE (Hz)	Initial FE % error	Updated FE % error
Mode (1)	6.011	20.943	5.750	248.411	4.342
Mode (2)	12.032	47.385	13.777	293.825	14.503
Mode (3)	17.048	39.231	15.180	130.121	10.957
Mode (4)	25.235	65.655	26.797	160.175	6.190
Mode (5)	32.854	71.379	28.644	117.261	12.814
Mode (6)	38.877	108.445	40.166	178.944	3.316
Mode (7)	53.840	118.628	46.536	120.334	13.566
Mode (8)	56.771	148.418	59.571	161.434	4.932
Mode (9)	79.232	177.244	70.452	123.702	11.081
Mode (10)	72.908	202.753	83.427	178.094	14.428

this method is an optimization problem and various optimization procedures may be used. A genetic algorithm from the MATLAB optimisation toolbox was used.

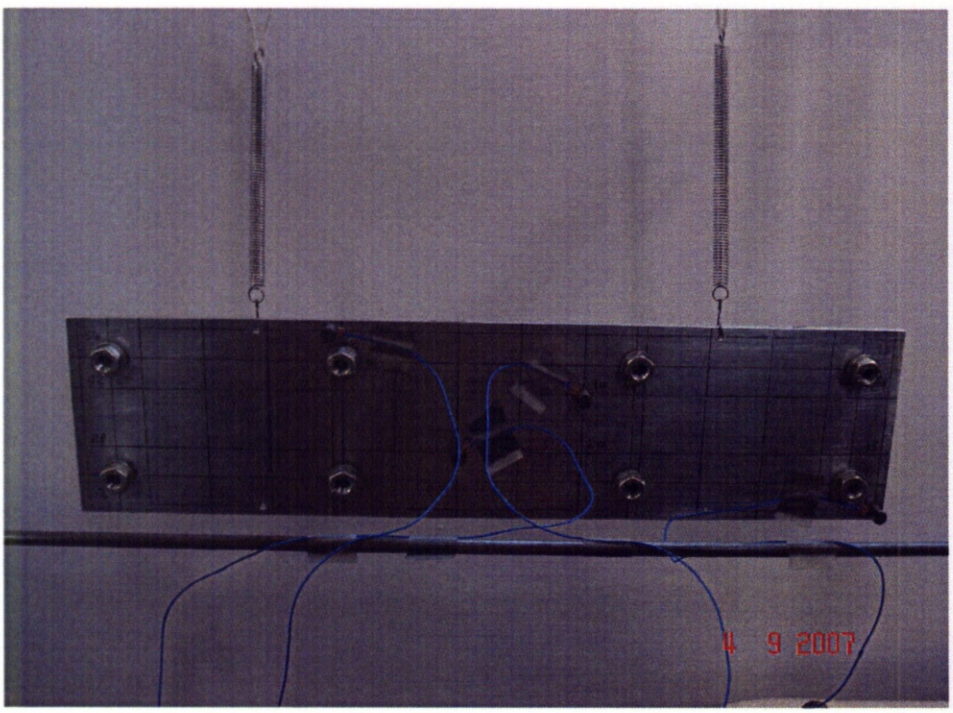

Figure 5.34: Experimental setup.

The first three measured natural frequencies were used for stochastic model updating by method 3 which is introduced in Section 5.4.1. There is no need to

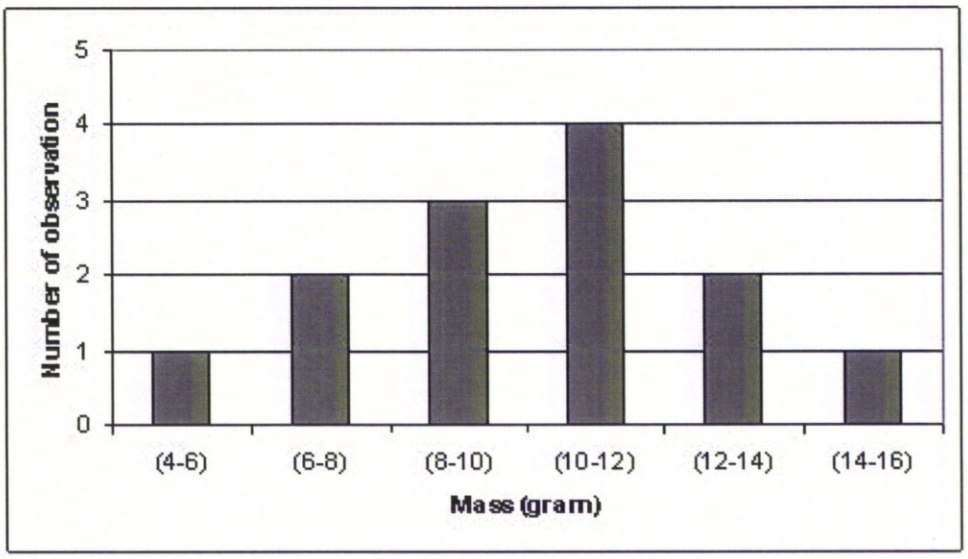

Figure 5.35: Distribution of masses.

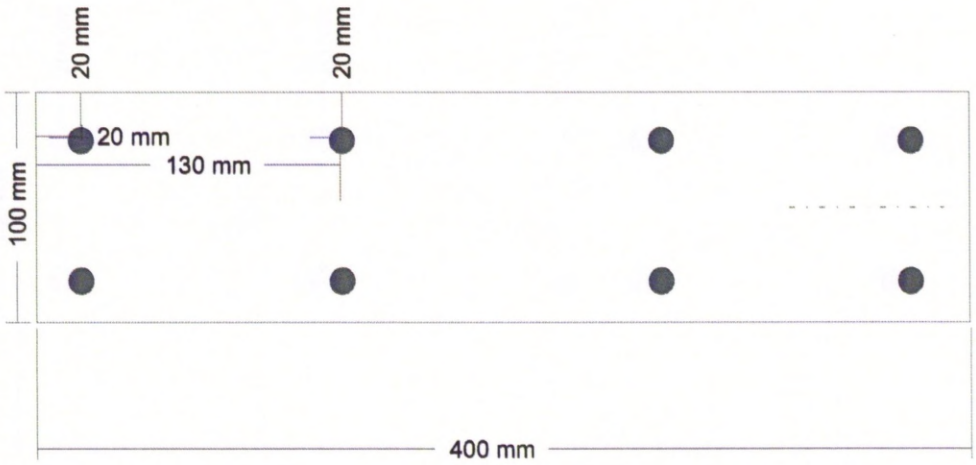

Figure 5.36: The positions of the masses on the plate.

choose initial values for mean and standard deviation of parameters in the GA algorithm but they were subjected to bounded constraints indicated in Table 5.10.

The identified and measured means and standard deviations of the masses are given in Table 5.10. As it can be seen from the table, the errors in identified mean and standard deviation of parameters with respect to measurements are reasonable. Obviously the identified standard deviations are less accurate than the identified means.

The means and standard deviations of the first three measured natural frequencies were used in the optimisation, whereas six modes were measured in

Table 5.9: The first six measured natural frequencies (Hz) for a plate with 13 different sets of 8 masses attached

Mass (grams)	Mode (1)	Mode (2)	Mode (3)	Mode (4)	Mode (5)	Mode (6)
5.025	121.080	286.799	333.896	595.693	688.093	915.365
6.588	119.002	280.460	327.573	585.042	684.618	894.911
7.538	117.817	277.315	323.931	579.240	681.073	882.836
8.55	116.385	272.994	319.427	570.238	674.886	864.382
9.088	115.659	271.367	317.253	566.972	672.319	858.409
9.563	115.071	270.059	315.601	564.025	670.297	851.946
10.075	114.413	267.771	313.152	558.999	663.869	844.604
10.613	113.766	266.462	311.447	555.173	660.905	833.890
11.113	113.021	264.995	309.576	552.080	662.606	828.573
11.5	112.802	264.543	308.426	552.121	662.895	836.105
12.575	111.514	261.684	304.884	544.291	655.675	813.238
13.575	110.809	259.442	302.668	541.900	660.888	808.048
15.013	108.870	254.557	296.379	528.127	639.655	777.946
Mean	114.632	269.111	314.170	561.069	667.522	846.943
Std	3.409	8.837	10.412	18.631	13.063	37.385

Table 5.10: Measured, identified mean and standard deviation of parameter (LB: Lower Bound, UB: Upper Bound).

	Measured parameters	[LB UB]	Identified parameters	Error %
$\widehat{m}$ (gram)	10.063	[0 20]	10.401	3.359
σ_m (gram)	2.798	[0 5]	3.278	17.155

Table 5.11: Measured and identified mean natural frequencies

	Measured (Hz)	Identified FE (Hz)	Identified FE error %
Mode (1)	114.632	113.334	-1.132
Mode (2)	269.111	270.413	0.484
Mode (3)	314.170	310.460	-1.181
Mode (4)	561.069	568.016	1.238
Mode (5)	667.522	662.697	-0.723
Mode (6)	846.943	858.850	1.406

Table 5.12: Measured and identified standard deviation of natural frequencies

	Measured (Hz)	Identified FE (Hz)	Identified FE error %
Mode (1)	3.409	3.415	0.176
Mode (2)	8.837	8.568	-3.044
Mode (3)	10.412	10.562	1.441
Mode (4)	18.631	16.182	-13.145
Mode (5)	13.063	6.949	-46.804
Mode (6)	37.385	33.486	-10.429

total. It is seen from Tables 5.11 and 5.12 that, apart from the 46.8% error in the identified standard deviation of the frequency of mode 5, identified and measured means and standard deviations of natural frequencies achieved by using method (3) are in good agreement. The results show that the updated statistical model is valid.

5.7 Closure

In this chapter, two versions of a perturbation approach to the stochastic model updating problem, with test-structure variability, are developed. Distributions of predicted modal responses (natural frequencies and mode shapes) are converged upon measured distributions, resulting in estimates of the first two statistical moments of the randomised updating parameters. Regularisation may be applied when the stochastic model updating equations are ill-conditioned. A computa-

tionally efficient solution, without any significant loss of accuracy, is obtained when the correlation between the randomised updating parameters and test data is omitted. An alternative method based on minimising an objective function to the stochastic model updating problem, is also presented. The methods are demonstrated in numerical simulations and also in experiments carried out on a collection of rectangular plates with variable thickness and also variable masses on a flat plate.

From the numerical simulation results, it is found that the perturbation method is quite sensitive to the sample size of the measured data and in some cases the estimation of the distributions of updating parameters are very poor when there are few samples of measured data. This is due to the fact that the distributions of updating parameters are represented by probabilistic model and therefore the method work well in the presence of large volumes of test data. However, having large volumes of test data available is unlikely in practice. Therefore, interval model is deemed to work better with these restrictions. This idea leads to the definition of interval model updating problem which will be discussed in the following chapter.

Chapter 6

Interval model updating

6.1 Introduction

Stochastic model updating methods, presented in the previous chapter make use of probabilistic models as do Hua's method [27] and Fonseca's approach [24]. The use of the probabilistic models usually requires large volumes of test data with consequent high costs. These methods also assume Gaussian distributions for the variability of uncertain parameters which is not always true. Probably a better approach, given that large quantities of test data will not be produced, would be to use an interval model for the uncertain parameters.

In this chapter, the problem of interval model updating in the presence of uncertain measured data is defined and solutions are made available for two cases. In the first case, the parameter vertex solution is used but is found to be valid only for particular parameterisation of the finite element model and particular output data i.e. when (i) the overall mass and stiffness matrices are linear functions of the updating parameters, (ii) the overall mass and stiffness matrices can be decomposed into non-negative-definite substructural mass and stiffness matrices and (iii) the output data are the eigenvalues of the dynamic system. Two iterative updating equations are then used in the first case to update the bounds of an initial hypercube of updating parameters. However, it is shown that the parameter vertex solution is not available generally when, for example, the output data include the eigenvectors of the structural dynamic system and the system matrices are non-linear functions of the updating parameters. In order to overcome the limitations of the parameter vertex solution, a general solution based on the use of a meta-model is considered. The meta-model acts as a surrogate for the

full finite-element /mathematical model. Thus, a region of input data is mapped to a region of output data with parameters obtained by regression analysis. The Kriging predictor is chosen as the meta-model in this work and is shown to be capable of predicting the region of input and output parameter variations with very good accuracy. The interval model updating approach is formulated based on the Kriging predictor and an iterative procedure is developed. The method is validated numerically using a three degree of freedom mass-spring system with both well-separated and close modes. Finally the method is applied to a frame structure with uncertain internal beams locations. The frame consists of two internal beams, each of which can be located at 3 different positions. Therefore nine sets of measured data corresponding to each different combination of the beams positions are available. Detailed finite element models of the frame structure with different locations of the beams and a Kriging model describing the relationship between the natural frequencies and updating parameters (beams positions) are available. The procedure of interval model updating, incorporating the Kriging model, is used to identify the locations of the beams for each case and to update the bounds of beams positions based on measured data. The interval model updating results for the frame structure are then presented.

6.2 Problem Definition

Consider the deterministic model updating equation introduced in Eq. (3.2). In the presence of irreducible uncertain measured data modelled as a vector of intervals $\widetilde{\mathbf{z}}_m$, Eq. (3.2) will be changed to the following form which describe an interval linear system of equations

$$\widetilde{\mathbf{z}}_m - \widetilde{\mathbf{z}}_j = \widetilde{\mathbf{S}}_j \left(\widetilde{\boldsymbol{\theta}}_{j+1} - \widetilde{\boldsymbol{\theta}}_j \right) \tag{6.1}$$

where $\widetilde{\bullet}$ represents uncertain vector/matrix terms which modelled as intervals. Seif et al. [138] provide a closed form solution of Eq. (6.1) when the sensitivity matrix is square and uncertainty is present either in the outputs $\mathbf{z}_m$ or sensitivity matrix $\mathbf{S}$, but not together at the same time. However, in interval model updating Eq. (6.1) is either overdetermined or underdetermined with a non-square

sensitivity matrix. The predictions $\mathbf{z}_j$, the system parameters $\boldsymbol{\theta}$ and the sensitivity matrix $\mathbf{S}_j$ are all interval vectors/matrices if the uncertain measured data $\mathbf{z}_m$ is an interval vector. In this situation, a closed-form solution generally does not exist. The solution of Eq. (6.1) is given in two cases in the following section. In the first case, the relationship between the inputs and outputs are monotonic, hence parameter vertex solution is applicable. In most cases, however, this desirable monotonic behaviour is not necessarily present and then there is a need to consider other solutions based on optimisation procedures.

6.3 Solution Methods

6.3.1 Case 1: Parameter vertex solution

In this case, the global mass and stiffness matrices may be expanded as linear functions of the updating parameters,

$$\mathbf{M} = \mathbf{M}_0 + \sum_{l=1}^{p_1} m_l \mathbf{M}_l \tag{6.2}$$

$$\mathbf{K} = \mathbf{K}_0 + \sum_{l=1}^{p_2} k_l \mathbf{K}_l \tag{6.3}$$

where $\mathbf{M}$ is the global mass matrix, $\mathbf{K}$ is the global stiffness matrix, m_l is the updating parameter for the l^{th} substructure mass matrix, $\mathbf{M}_l$, and k_l is the updating parameter for the l^{th} substructure stiffness matrix, $\mathbf{K}_l$. The Young's modulus and mass density of a substructure are examples of k_l and m_l respectively. The decompositions in Eqs. (6.2) and (6.3) are non-negative decompositions of the mass and stiffness matrices [19] because the substructure matrices are all semi-positive definite. The eigenvalue derivatives of the global system with respect to structural parameters $(\partial\omega_i^2/\partial\theta_l)$ $(\omega_i^2 = \omega_i^2)$ can be obtained from Eqs. 3.6. When the matrix of eigenvectors of the dynamic system is mass normalized, $\Phi^{\mathrm{T}}\mathbf{M}\Phi = \mathbf{I}$ where Φ is the eigenvector matrix, the eigenvalue sensitivity of the dynamic system with respect to the mass and stiffness updating parameters, described in Eq. (3.6), becomes,

$$\frac{\partial \omega_i^2}{\partial k_l} = \boldsymbol{\Phi}_i^{\mathrm{T}} \frac{\partial \mathbf{K}}{\partial k_l} \boldsymbol{\Phi}_i = \boldsymbol{\Phi}_i^{\mathrm{T}} \mathbf{K}_l \boldsymbol{\Phi}_i \tag{6.4}$$

$$\frac{\partial \omega_i^2}{\partial m_j} = -\omega_i^2 \boldsymbol{\Phi}_i^{\mathrm{T}} \frac{\partial \mathbf{M}}{\partial m_l} \boldsymbol{\Phi}_i = -\omega_i^2 \boldsymbol{\Phi}_i^{\mathrm{T}} \mathbf{M}_l \boldsymbol{\Phi}_i \tag{6.5}$$

From Eqs. (6.4) and (6.5), it can be seen that the signs of the derivatives of the eigenvalues with respect to the updating parameters do not change within the interval of variation $[\ \underline{\boldsymbol{\theta}}\ \ \overline{\boldsymbol{\theta}}\ ]$. Therefore, the eigenvalues of the dynamic system increase monotonically with the stiffness parameters and decreases monotonically with the mass parameters. Consequently, two recursive equations can be defined to update the initial hypercube of updating parameters based on the vertices of measured data as,

$$\overline{\mathbf{z}}_m = \overline{\mathbf{z}}_j + \mathbf{S}\left|_{\boldsymbol{\theta}_{j,\overline{\mathbf{z}}_m}}\right. \left(\boldsymbol{\theta}_{j+1,\overline{\mathbf{z}}_m} - \boldsymbol{\theta}_{j,\overline{\mathbf{z}}_m}\right) \tag{6.6}$$

$$\underline{\mathbf{z}}_m = \underline{\mathbf{z}}_j + \mathbf{S}\left|_{\boldsymbol{\theta}_{j,\underline{\mathbf{z}}_m}}\right. \left(\boldsymbol{\theta}_{j+1,\underline{\mathbf{z}}_m} - \boldsymbol{\theta}_{j,\underline{\mathbf{z}}_m}\right) \tag{6.7}$$

where $\boldsymbol{\theta}_{j,\overline{\mathbf{z}}_m} = \left[\overline{\mathbf{k}}_j\ \ \underline{\mathbf{m}}_j\right]^{\mathrm{T}}$ and $\boldsymbol{\theta}_{j,\underline{\mathbf{z}}_m} = \left[\underline{\mathbf{k}}_j\ \ \overline{\mathbf{m}}_j\right]^{\mathrm{T}}$ and $\mathbf{S}\left|_{\boldsymbol{\theta}_{j,\bullet}}\right.$ is the sensitivity matrix evaluated at $\boldsymbol{\theta}_{j,\bullet}$ and j is the iteration number.

The parameter vertex solution is not necessarily valid when either the output data includes the system eigenvectors or the mass and stiffness matrices are not linear functions of the updating parameters or both. Firstly, the output data are restricted to be eigenvalues of the dynamic system with mass and stiffness matrices that are nonlinear functions of the updating parameters decomposed as,

$$\mathbf{M} = \mathbf{M}_0 + \sum_{l=1}^{p} u_l\left(\theta_l\right) \mathbf{M}_l \tag{6.8}$$

$$\mathbf{K} = \mathbf{K}_0 + \sum_{l=1}^{p} v_l\left(\theta_l\right) \mathbf{K}_l \tag{6.9}$$

where u_l and v_l are nonlinear functions of the updating parameters. For example, if the updating parameter is the thickness of shell element then $u_l\left(\theta\right) = \theta$ and $v_l\left(\theta\right) = \theta^3$. In this case, the derivatives of the eigenvalues with respect to the updating parameters may be written as,

$$\frac{\partial \omega_i^2}{\partial \theta_l} = \boldsymbol{\phi}_i^{\mathrm{T}} \mathbf{K}_l \boldsymbol{\phi}_i \frac{\partial v_l}{\partial \theta_l} - \omega_i^2 \boldsymbol{\phi}_i^{\mathrm{T}} \mathbf{M}_l \boldsymbol{\phi}_i \frac{\partial u_l}{\partial \theta_l} \tag{6.10}$$

The sign of the eigenvalue derivatives with respect to the updating parameters do not necessarily remain unchanged within the region of variation of the updating parameters. Certainly, if the solution of $\boldsymbol{\phi}_i^{\mathrm{T}} \mathbf{K}_l \boldsymbol{\phi}_i \frac{\partial v_l}{\partial \theta_l} - \omega_i^2 \boldsymbol{\phi}_i^{\mathrm{T}} \mathbf{M}_l \boldsymbol{\phi}_i \frac{\partial u_l}{\partial \theta_l} = 0$ lies within the range of the updating parameters then the parameter vertex solution is no longer valid.

Now the case in which the output data includes the eigenvectors of the dynamic system is considered. The eigenvector derivatives with respect to the updating parameters may be calculated using Eq. (3.7). Therefore, the sign of the derivative of an eigenvector term generally does not remain unchanged within the variation of the updating parameters even if the mass and stiffness matrices can be decomposed as in Eqs. (6.2) and (6.3). This is because the sign of the α_{ik} terms change in the summation in Eq. (3.7) due to changes in the sign of the denominator term $\omega_i^2 - \omega_k^2$. Therefore the problem of interval model updating cannot be solved by using the parameter vertex solution when eigenvector data is included in the objective. In the following section the solution of the problem in the general case where the outputs behave non-monotonically with respect to the updating parameters is considered.

6.3.2 Case 2: General case

From the first case, the parameter vertex solution is always valid when the mass and stiffness matrices are linear functions of the updating parameters and the output data are the eigenvalues of the dynamic system. Eq. (6.1) shows that the general case may be obtained by evaluating the inverse of the interval sensitivity matrix at each iteration. However, this solution is not straightforward, may be impossible and remains as an open problem. However the use of a meta-model can lead to a solution with very good accuracy depending on the type of meta-model, the sampling used and the behaviour of the outputs within the region of variation. The relationships between the updating parameters and outputs of the meta-model are described by known functions in the region of parameter variations, which are not available when working directly with the FE models.

Therefore the use of surrogate models makes the solution of the inverse interval problem, Eq. (6.1), easier and more efficient as will be demonstrated.

The idea for the solution of the interval model updating problem using a meta-model is illustrated in Figure 6.1 which shows specifically the procedure for a dynamic system with two updating-parameter inputs and two outputs. It should be remembered that in the problem of deterministic model updating it is assumed that the measured eigenvalues and eigenvectors of one structure have been obtained from experiments in the form of Eq. (3.3) while in stochastic model updating problem, it is assumed that a set of vectors of measured data in the form of $\mathbf{Z} = \left[\mathbf{z}^{(1)}\ \mathbf{z}^{(2)} \ldots \mathbf{z}^{(n_s)}\right]^{\mathrm{T}}$ are available (e.g. from a collection of modal test data from a set of nominally identical structures, built in the same way with the same material within manufacturing tolerances). The vector of mean values of measured data can be readily obtained from n_s samples as shown in Figure 6.1. Then the problem of deterministic model updating can be applied to identify the deterministic values of updating parameters. If the solution of the updating problem is unique, then the vector of updated parameters is represented by a point in the parameter space. An initial hypercube around the updated parameters may be constructed as illustrated in Figure 6.1. The meta-model is then used to map the space of the initial hypercube of updating parameters to the space of outputs. If the mapping is good enough to represent the relationship between the input and output data then this model can be used to correct the dimensions of initial hypercube of updating parameters based on the available measured data (circles in the figure). Therefore, selection of the meta-model is a crucial step in that it influences the performance of mapping and consequently the updating procedure to a very significant degree. In the presence of multiple solutions of the deterministic FE model updating based on mean values of measured data, multiple meta-models correspond to each solution may be defined.

Amongst existing meta-model such as conventional response surface methods, neural networks and Kriging models, the later are chosen in this work due to (i) its excellent performance in dealing with non-smooth behaviour between inputs and outputs, which often occurs in dynamic systems with close modes as will be shown later in this paper, and (ii) the high level of degree of accuracy reported

in the literature [61, 139]. The application of the Kriging predictor for the solution of interval model-updating problems is explained in the following section. The Kriging predictor theory and an optimal sampling method are explained in Section 2.3.6 of Chapter 2.

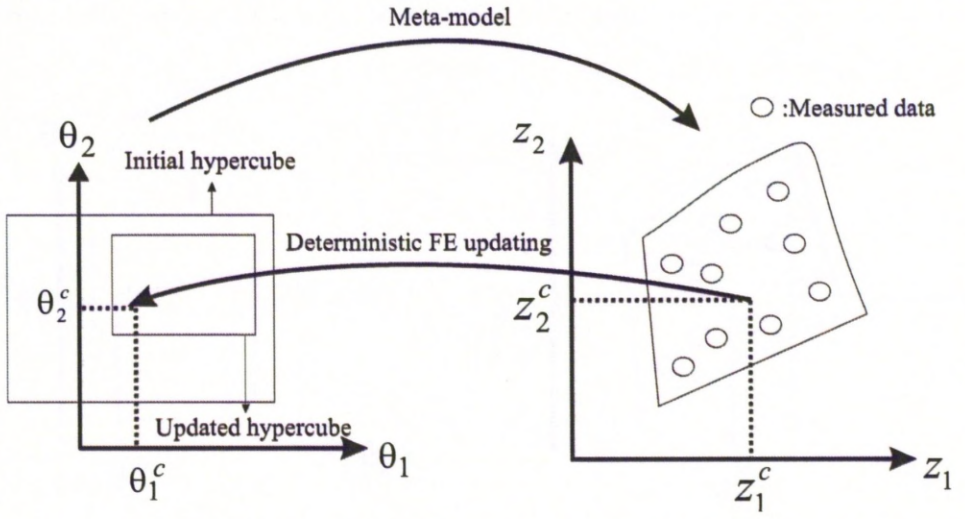

Figure 6.1: Interval model updating using Kriging model.

6.4 The Kriging Predictor in Interval Model Updating

In this section, the Kriging predictor, described in Section 2.3.6, is applied to the problem of interval model updating in structural dynamics. A generalised form of the Kriging predictor for a dynamic system with n_r output data may be written based on the equation of the Kriging predictor given in Eq. (2.78) as,

$$\hat{\mathbf{z}} = \boldsymbol{\alpha} + \breve{\mathbf{H}}(\boldsymbol{\theta})\,\boldsymbol{\theta} + \boldsymbol{\Lambda}\boldsymbol{\rho}(\boldsymbol{\theta}) \tag{6.11}$$

where $\hat{\mathbf{z}} \in \Re^{n_r}$, $\boldsymbol{\rho} \in \Re^{n_r n_s}$; $\boldsymbol{\rho} = \left[\mathbf{r}_1^{\mathrm{T}}\ \mathbf{r}_2^{\mathrm{T}}\ \ldots\ \mathbf{r}_{n_r}^{\mathrm{T}}\right]^{\mathrm{T}}$, $\boldsymbol{\alpha} = [\beta_{0,1}\ \beta_{0,2}\ \ldots\ \beta_{0,n_r}]^{\mathrm{T}}$. $\beta_{\bullet,i}$ are regression coefficients introduced in Eq. (2.78), $\mathbf{r}_i \in \Re^{n_s}$ is introduced in Eq. (2.86),

$$\breve{\mathbf{H}}(\boldsymbol{\theta}) = \left[\breve{H}_{ij}\right]_{n_r \times p} \quad ; \quad \breve{H}_{ij} = \beta_{j,i} + \theta_j \beta_{jj,i} + \frac{1}{2}\sum_{\substack{k=1 \\ k \neq j}}^{p} \beta_{kj,i}\theta_k$$

and $\Lambda = [\Lambda_{ij}]_{n_r \times n_r n_s}$

$$\Lambda_{ij} = \begin{cases} \Lambda_{j,i} & (i-1)\, n_s + 1 \leq j \leq i \times n_s \\ 0. & \text{elsewhere} \end{cases}$$

Once the initial Kriging model is constructed based on the procedure proposed in Section 6.3.2, the following error function can be defined for deterministic model updating using the Kriging predictor formed from the measured samples,

$$\boldsymbol{\epsilon} = \mathbf{z}_m - \left(\boldsymbol{\alpha} + \breve{\mathbf{H}}\boldsymbol{\theta} + \boldsymbol{\Lambda}\boldsymbol{\rho}\right) = \boldsymbol{\Upsilon} - \breve{\mathbf{H}}\boldsymbol{\theta} - \boldsymbol{\Lambda}\boldsymbol{\rho} \tag{6.12}$$

where $\boldsymbol{\Upsilon} = \mathbf{z}_m - \boldsymbol{\alpha}$ and the function of $(\boldsymbol{\theta})$, $\bullet\,(\boldsymbol{\theta})$, is omitted from $\breve{\mathbf{H}}\,(\boldsymbol{\theta})$ and $\boldsymbol{\rho}\,(\boldsymbol{\theta})$ for reasons of simplicity. Now the updating problem for each sample of measured data can be stated as an optimisation problem,

$$\min_{\boldsymbol{\theta}} \left(\boldsymbol{\epsilon}^{\mathrm{T}}\boldsymbol{\epsilon}\right) \tag{6.13}$$

It should be noted that the Kriging model has been constructed and validated for the initial hypercube of the updated parameters. Therefore if the solution of minimisation Eq. (6.13) converges to a point outside the initial hypercube then a new Kriging model should be constructed by increasing the size of initial hypercube and the procedure repeated. According to Eq. (6.12), the error function, Eq. (6.13), can be expanded as,

$$\begin{aligned} \boldsymbol{\epsilon}^{\mathrm{T}}\boldsymbol{\epsilon} = {} & \boldsymbol{\Upsilon}^{\mathrm{T}}\boldsymbol{\Upsilon} - \boldsymbol{\Upsilon}^{\mathrm{T}}\breve{\mathbf{H}}\boldsymbol{\theta} - \boldsymbol{\Upsilon}^{\mathrm{T}}\boldsymbol{\Lambda}\boldsymbol{\rho} - \boldsymbol{\theta}^{\mathrm{T}}\breve{\mathbf{H}}^{\mathrm{T}}\boldsymbol{\Upsilon} + \boldsymbol{\theta}^{\mathrm{T}}\breve{\mathbf{H}}^{\mathrm{T}}\breve{\mathbf{H}}\boldsymbol{\theta} \\ & + \boldsymbol{\theta}^{\mathrm{T}}\breve{\mathbf{H}}^{\mathrm{T}}\boldsymbol{\Lambda}\boldsymbol{\rho} - \boldsymbol{\rho}^{\mathrm{T}}\boldsymbol{\Lambda}^{\mathrm{T}}\boldsymbol{\Upsilon} + \boldsymbol{\rho}^{\mathrm{T}}\boldsymbol{\Lambda}^{\mathrm{T}}\breve{\mathbf{H}}\boldsymbol{\theta} + \boldsymbol{\rho}^{\mathrm{T}}\boldsymbol{\Lambda}^{\mathrm{T}}\boldsymbol{\Lambda}\boldsymbol{\rho} \end{aligned} \tag{6.14}$$

A necessary condition for minimising the error function Eq. (6.14) is that,

$$\boldsymbol{\nabla}\left(\boldsymbol{\epsilon}^{\mathrm{T}}\boldsymbol{\epsilon}\right) = \{0\} \quad \boldsymbol{\nabla} = \left\{\frac{\partial}{\partial\theta_l}\right\}_{p\times 1} \tag{6.15}$$

Substituting Eq. (6.14) into Eq. (6.15) leads to,

$$-\breve{\mathbf{H}}^{\mathrm{T}}\boldsymbol{\Upsilon} - \breve{\mathbf{A}}\boldsymbol{\theta} - \breve{\mathbf{u}}\,(\boldsymbol{\theta}) + \breve{\mathbf{H}}^{\mathrm{T}}\breve{\mathbf{H}}\boldsymbol{\theta} + \breve{\mathbf{D}}\boldsymbol{\theta} + \breve{\mathbf{H}}^{\mathrm{T}}\boldsymbol{\Lambda}\boldsymbol{\rho} + \breve{\mathbf{V}}\boldsymbol{\theta} + \breve{\mathbf{U}}\boldsymbol{\theta} + \breve{\mathbf{v}}\,(\boldsymbol{\theta}) = \{0\} \tag{6.16}$$

where $\bullet\,(\boldsymbol{\theta})$ is omitted from $\breve{\mathbf{H}}\,(\boldsymbol{\theta})$, $\breve{\mathbf{D}}\,(\boldsymbol{\theta})$, $\breve{\mathbf{V}}\,(\boldsymbol{\theta})$, $\breve{\mathbf{U}}\,(\boldsymbol{\theta})$, $\boldsymbol{\rho}\,(\boldsymbol{\theta})$ and

$$\breve{\mathbf{A}} = \left[\breve{A}_{ij}\right]_{p\times p}; \quad \breve{A}_{ij} = \sum_{k=1}^{n} \Upsilon_k \frac{\partial \breve{H}_{kj}}{\partial\theta_i}; \quad \frac{\partial \breve{H}_{kj}}{\partial\theta_i} = \frac{1}{2} B_{ij,k}$$

$$\breve{\mathbf{D}}(\boldsymbol{\theta}) = \left[\breve{D}_{ij}\right]_{p\times p}; \quad \breve{D}_{ij} = \frac{1}{2}\sum_{k=1}^{p}\sum_{l=1}^{n}\left(\breve{H}_{lj}\frac{\partial \breve{H}_{lk}}{\partial \theta_i} + \breve{H}_{lk}\frac{\partial \breve{H}_{lj}}{\partial \theta_i}\right)\theta_k$$

$$\breve{\mathbf{V}}(\boldsymbol{\theta}) = \left[\breve{V}_{ij}\right]_{p\times p}; \quad \breve{V}_{ij} = \sum_{k=1}^{n}\sum_{l=1}^{ns}\Lambda_{l,k}\frac{\partial \breve{H}_{kj}}{\partial \theta_i}r_{l,k}(\boldsymbol{\theta})$$

$$\breve{\mathbf{U}}(\boldsymbol{\theta}) = \left[\breve{U}_{ij}\right]_{p\times p}; \quad \breve{U}_{ij} = \sum_{k=1}^{n}\sum_{l=1}^{ns}\Lambda_{l,k}\breve{H}_{kj}\frac{\partial r_{l,k}(\boldsymbol{\theta})}{\partial \theta_i}$$

$$\breve{\mathbf{u}}(\boldsymbol{\theta}) = \{\breve{u}_i(\boldsymbol{\theta})\}_{p\times 1}; \quad \breve{u}_i(\boldsymbol{\theta}) = \sum_{j=1}^{n}\sum_{k=1}^{n_s}\Lambda_{k,j}\Upsilon_j\frac{\partial r_{k,j}(\boldsymbol{\theta})}{\partial \theta_i}$$

$$\breve{\mathbf{v}}(\boldsymbol{\theta}) = \{\breve{v}_i(\boldsymbol{\theta})\}_{p\times 1};$$

$$\breve{v}_i(\boldsymbol{\theta}) = \frac{1}{2}\sum_{l=1}^{n}\sum_{k=1}^{ns}\sum_{j=1}^{ns}\Lambda_{j,l}\Lambda_{k,l}\left(r_{k,l}(\boldsymbol{\theta})\frac{\partial r_{j,l}(\boldsymbol{\theta})}{\partial \theta_i} + r_{j,l}(\boldsymbol{\theta})\frac{\partial r_{k,l}(\boldsymbol{\theta})}{\partial \theta_i}\right)$$

where $B_{ij,k}$ is the componenet of matrix $\mathbf{B}$ introduced in Eq. (2.78). The derivative of the correlation function, given in Eq. (2.83), may be calculated as follows,

$$\frac{\partial r_{j,i}}{\partial \theta_k} = \frac{\partial C_i\left(\boldsymbol{\theta}, \boldsymbol{\theta}^{(j)}\right)}{\partial \theta_k} = -\zeta_{k,i}\left|\theta_k - \theta_k^{(j)}\right|^{\nu_i - 1}\operatorname{sign}\left(\theta_k - \theta_k^{(j)}\right)C_i\left(\boldsymbol{\theta}, \boldsymbol{\theta}^{(j)}\right) \quad (6.17)$$

In those cases when the function is not differentiable the derivative may be evaluated as,

$$\begin{aligned}\mathrm{E}\left(u_1'(\widehat{x})\right) &= \lim_{\sigma\to 0}\int_{-\infty}^{+\infty}u_1'(x)\,\varphi\left(x, \widehat{x}, \sigma^2\right)dx \\ &= -\lim_{\sigma\to 0}\int_{-\infty}^{+\infty}u_1(x)\,\varphi'\left(x, \widehat{x}, \sigma^2\right)dx\end{aligned} \quad (6.18)$$

where $'$ represents $\frac{d}{dx}$ and $\varphi\left(x, \widehat{x}, \sigma^2\right)$ is Gaussian function with parameters $\widehat{x}$ and σ^2. Eq. (6.18) is obtained using integration by parts and it should be noted that the Gaussian function $\varphi(x)$ is zero at $\pm\infty$. Eq. (6.16) can be rearranged for the solution of system parameters $\boldsymbol{\theta}$ as,

$$\left(\breve{\mathbf{H}}^{\mathrm{T}}\breve{\mathbf{H}} + \breve{\mathbf{D}} + \breve{\mathbf{U}} + \breve{\mathbf{V}} - \breve{\mathbf{A}}\right)\boldsymbol{\theta} = \breve{\mathbf{u}}(\boldsymbol{\theta}) + \breve{\mathbf{H}}^{\mathrm{T}}\boldsymbol{\Upsilon} - \breve{\mathbf{H}}^{\mathrm{T}}\boldsymbol{\Lambda}\boldsymbol{\rho} - \breve{\mathbf{g}}(\boldsymbol{\theta}) \quad (6.19)$$

Since the matrix $\left(\breve{\mathbf{H}}^{\mathrm{T}}\breve{\mathbf{H}} + \breve{\mathbf{D}} + \breve{\mathbf{U}} + \breve{\mathbf{V}} - \breve{\mathbf{A}}\right)$ is a function of $\boldsymbol{\theta}$ an iterative procedure needs to be defined. However, the solution requires the inverse of matrix $\left(\breve{\mathbf{H}}^{\mathrm{T}}\breve{\mathbf{H}} + \breve{\mathbf{D}} + \breve{\mathbf{U}} + \breve{\mathbf{V}} - \breve{\mathbf{A}}\right)$. If this matrix is not invertible an arbitrary weighting matrix can be added to the both sides of Eq. (6.19) as,

$$\left(\breve{\mathbf{H}}^{\mathrm{T}}\breve{\mathbf{H}} + \breve{\mathbf{D}} + \breve{\mathbf{U}} + \breve{\mathbf{V}} - \breve{\mathbf{A}} + \mathbf{W}\right)\boldsymbol{\theta} = \breve{\mathbf{f}}(\boldsymbol{\theta}) + \breve{\mathbf{H}}^{\mathrm{T}}\boldsymbol{\Upsilon} - \breve{\mathbf{H}}^{\mathrm{T}}\boldsymbol{\Lambda}\boldsymbol{\rho} - \breve{\mathbf{g}}(\boldsymbol{\theta}) + \mathbf{W}\boldsymbol{\theta} \quad (6.20)$$

and following recursive equation is formed for the solution of Eq. (6.16),

$$\begin{aligned}\boldsymbol{\theta}_{l+1} = &\left(\breve{\mathbf{H}}^{\mathrm{T}}\breve{\mathbf{H}} + \breve{\mathbf{D}} + \breve{\mathbf{U}} + \breve{\mathbf{V}} - \breve{\mathbf{A}} + \mathbf{W}\right)^{-1}_{|\boldsymbol{\theta}=\boldsymbol{\theta}_l} \\ &\times \left\{\breve{\mathbf{f}}(\boldsymbol{\theta}) + \breve{\mathbf{H}}^{\mathrm{T}}\boldsymbol{\Upsilon} - \breve{\mathbf{H}}^{\mathrm{T}}\boldsymbol{\Lambda}\boldsymbol{\rho} - \breve{\mathbf{g}}(\boldsymbol{\theta}) + \mathbf{W}\boldsymbol{\theta}\right\}_{|\boldsymbol{\theta}=\boldsymbol{\theta}_l}\end{aligned} \tag{6.21}$$

The iterations continue until convergence on the system parameters $\boldsymbol{\theta}$ is achieved. The matrix $\mathbf{W}$ is chosen so that the matrix $\left(\breve{\mathbf{H}}^{\mathrm{T}}\breve{\mathbf{H}} + \breve{\mathbf{D}} + \breve{\mathbf{U}} + \breve{\mathbf{V}} - \breve{\mathbf{A}} + \mathbf{W}\right)$ is invertible. The weighting matrix $\mathbf{W}$ in Eq. (6.21) has the effect of regularising the ill-conditioned Eq, (6.19), equivalent to adding the side constraint given in Eq. (3.8) [3] to the objective function Eq. (6.13).

In Eq. (6.21), the weighting matrix $\mathbf{W}$ may be chosen in the form $\mathbf{W} = r_g\mathbf{I}$. For small values of the regularisation parameter r_g the original ill-conditioned problem , Eq. (6.15), remains and when r_g takes a large value it is seen from the side constraint Eq. (3.8) that the updated parameters remain unchanged from the previous iteration. An optimal value of r_g may be obtained from the corner of the L-curve as described by Ahmadian et al. [6].

The procedure for interval model updating can be defined as follows:

1. Select and update the parameters of the mathematical FE model using the mean vector of measured data.

2. Initialize a hypercube around the updated parameters of the finite element model.

3. Construct a meta-model based on updated mathematical FE model data. This meta-model should describe the relationship between output data and input data within the initial hypercube around the updated parameters accurately.

4. Use the meta-model for updating the initial hypercube by using all sets of measured data.

5. Construct the new hypercube on the region of updated parameters. If the updated hypercube is bigger than the initial hypercube increase the size of initial hypercube and go back to step 3; otherwise go to step 6.

6. Generate output data by using the meta-model to find the region of variation of output data and compare it to the scatter of measured data.

7. End.

6.5 Numerical Case Studies

The three degree of freedom mass-spring system, shown in Figure 2.13, with well separated and close modes is used in this section to illustrate the performance of the interval model updating using the Kriging method.

6.5.1 Case study 1: 3-degree of freedom mass-spring system with well separated modes

It is assumed that the true value of the bounds of the unknown uncertain parameters of the system are given by,

$$k_1 = [0.8 \quad 1.2] \quad \text{N/m}, \quad k_2 = [0.8 \quad 1.2] \quad \text{N/m}, \quad k_5 = [0.8 \quad 1.2] \quad \text{N/m} \tag{6.22}$$

and other parameters are known and similar to those given by Eq. (3.57). The measured data are obtained by using Monte Carlo Simulation (MCS) and Latin Hypercube sampling (LHS) with 10 samples. The method is also applied with an unrealistic number of measured data (10000 samples) to demonstrate the asymptotic properties of the method. Later, different runs of the updating algorithm (with 10 different sets of 10 measured samples) are carried out and a range of solution errors are determined.

As mentioned before the interval model updating approach needs an initial estimate of the ranges of unknown parameters. The initial estimates are

$$k_1 = [0.5 \quad 1.5] \quad \text{N/m}, \quad k_2 = [0.5 \quad 1.5] \quad \text{N/m}, \quad k_5 = [0.5 \quad 1.5] \quad \text{N/m} \tag{6.23}$$

It is assumed that the mean values of the updating parameters have already been identified and the errors are in the estimation of the parameter bounds. The output data are assumed to be three eigenvalues and the absolute value of the first eigenvector at the first degree of freedom $\phi_{1,1}$,

$$\mathbf{z} = \begin{bmatrix} z_1 & z_2 & z_3 & z_4 \end{bmatrix}^{\mathrm{T}} = \begin{bmatrix} \omega_1^2 & \omega_2^2 & \omega_3^2 & |\phi_{1,1}| \end{bmatrix}^{\mathrm{T}} \tag{6.24}$$

The parameter vertex method is not applicable in this case because the mode shape term $\phi_{1,1}$ is included in the response vector. To construct the Kriging model, an initial sample was taken based on CCD with face centred points [59]. The MSE values show that these initial samples are enough for a Kriging model to map the initial hypercube of input data to the output data. The Kriging model was constructed using a second order polynomial. Results obtained by the interval model updating with 10 and 10000 measured samples are shown in Table 6.1. The weighting matrix in Eq. (6.21) was set to $\mathbf{W} = \mathbf{0}$ in this case.

Figure 6.2 shows the initial, true and updated bounding hypercube of uncertain parameters in the planes $k_1 - k_2$ and $k_2 - k_5$ in the presence of 10 measured samples. The updated hypercube of uncertain parameters are in good agreement with the true hypercube as shown in Figure 6.2 and Table 6.1. Figure 6.3 shows the convergence of the initial output data space upon the space of 10 measured samples in the planes of (a) λ_1 and λ_2, (b) λ_1 and λ_3, (c) λ_2 and λ_3, (d) λ_1 and $|\phi_{1,1}|$, (e) λ_2 and $|\phi_{1,1}|$ and (f) λ_3 and $|\phi_{1,1}|$. The results in Table 6.1 show that errors in estimating the bounds of uncertain parameters are significantly reduced even in the case of only 10 measured samples. A very slight difference is seen between the exact space of output data and the updated one, shown in Figure 6.3. It might be argued that these results are just for the one particular set of 10 samples. Therefore the interval updating procedure was repeated for 10 different sets of measured samples and it appears that the errors in estimation of bounds of updating parameters range from 0.0% to 4.9%. This shows an important advantage of using interval models rather than probabilistic models presented in Chapters 3 and 5 in stochastic model updating. The initial and updated spaces shown in Figure 6.3 are obtained by Monte Carlo Simulation (MCS) with Latin Hypercube Sampling (LHS) and the Kriging predictor. The true space achieved by MCS using eigenvalue solutions from the $\mathbf{M}$, $\mathbf{K}$ system.

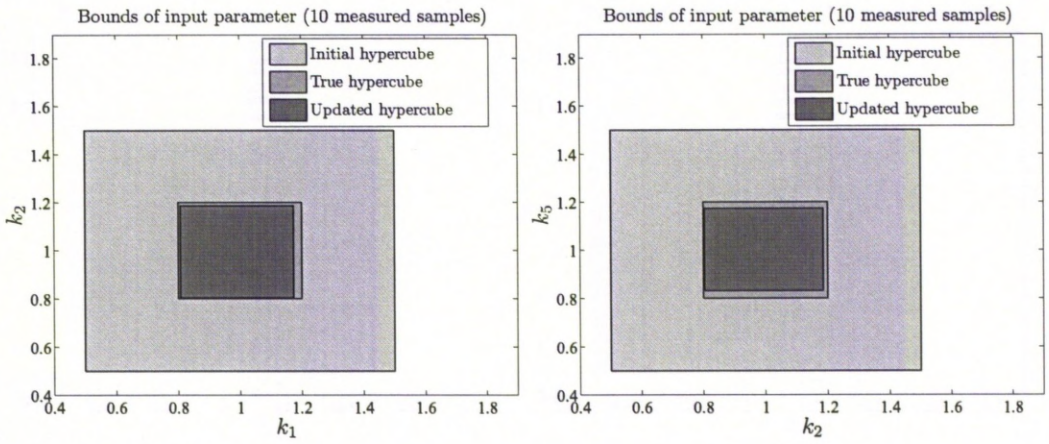

Figure 6.2: Initial, updated and true hypercube of updating parameters based upon 10 measurement samples (system with well separated modes).

Table 6.1: Updated results: 3 DOF mass-spring system with well separated modes

Parameters	Initial error %	Updated error % 10 Measured samples	Updated error % 10000 Measured samples
k_1	[−37.5 25.0]	[0.4 0.0]	[0.1 −0.2]
k_2	[−37.5 25]	[0.8 −1.7]	[0.5 0.0]
k_5	[−37.5 25]	[0.8 −0.7]	[0.3 −0.1]

6.5.2 Case study 2: 3-degree of freedom mass-spring system with close modes

The quantification of uncertainty in a system with close modes is difficult because of the non-smooth response surface. The three degree of freedom system, shown in Figure 2.13, with close modes is again considered here. It is assumed that the true value of the unknown uncertain parameters of the system are given by,

$$k_2 = [7.5 \;\; 8.5] \quad \text{N/m}, \quad k_4 = [1.8 \;\; 2.2] \quad \text{N/m}, \quad k_5 = [1.8 \;\; 2.2] \quad \text{N/m} \tag{6.25}$$

and other parameters are as given by Eq. (2.89). It is assumed that 10 samples of measured data exist. The initial estimates of the bounds of uncertain parameters are,

$$k_2 = [6.5 \;\; 9.5] \quad \text{N/m}, \quad k_4 = [1.6 \;\; 2.4] \quad \text{N/m}, \quad k_5 = [1.6 \;\; 2.4] \quad \text{N/m} \tag{6.26}$$

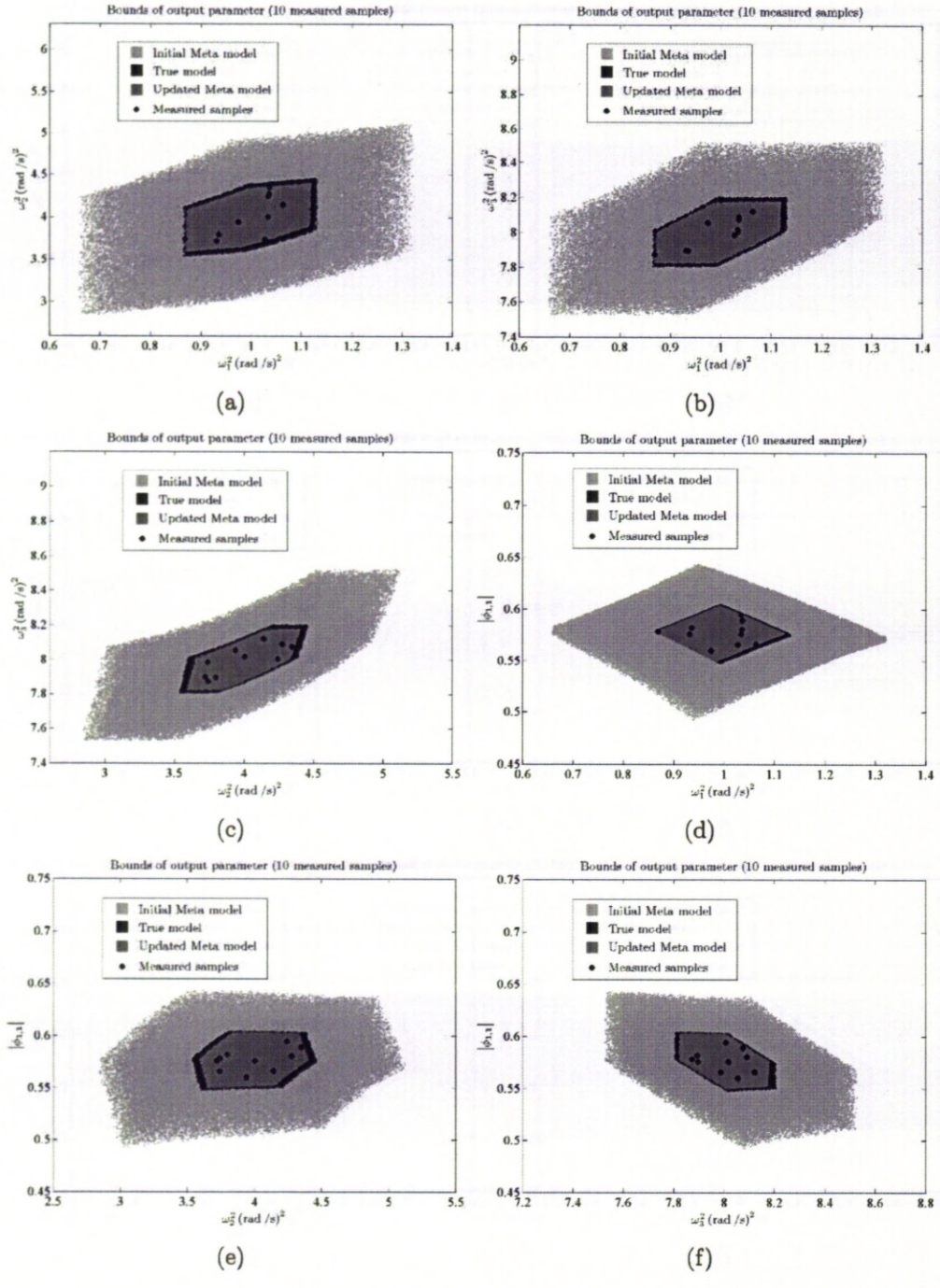

Figure 6.3: Initial, updated and true spaces of predicted data (100,000 points) based upon 10 measurement samples (system with well separated modes).

As in the previous case, the application of interval model updating is illustrated for correcting the bounds of the updating parameters. The output data are assumed to be the same as the previous case study (the first three eigenvalues and the absolute value of first component of the first eigenvector ($\phi_{1,1}$). Fifteen samples were taken from the space of the initial hypercube of updating parameters according to CCD. The MSE results showed that the initial samples based on CCD were not good enough for mapping the initial hypercube of input data to the output data. Therefore the sampling procedure described in Section 2.3.6 was used to improve the Kriging model. The procedure starts with the first output and continues until the maximum MSE value falls below a specified tolerance. Then the procedure continues for the next output and so on until all four outputs are accurately predicted by the Kriging model. Figure 6.4 shows how the maximum value of the MSE decays as the sample size is increased. The iteration numbers in Figure 6.4 represent the sample size at each step.

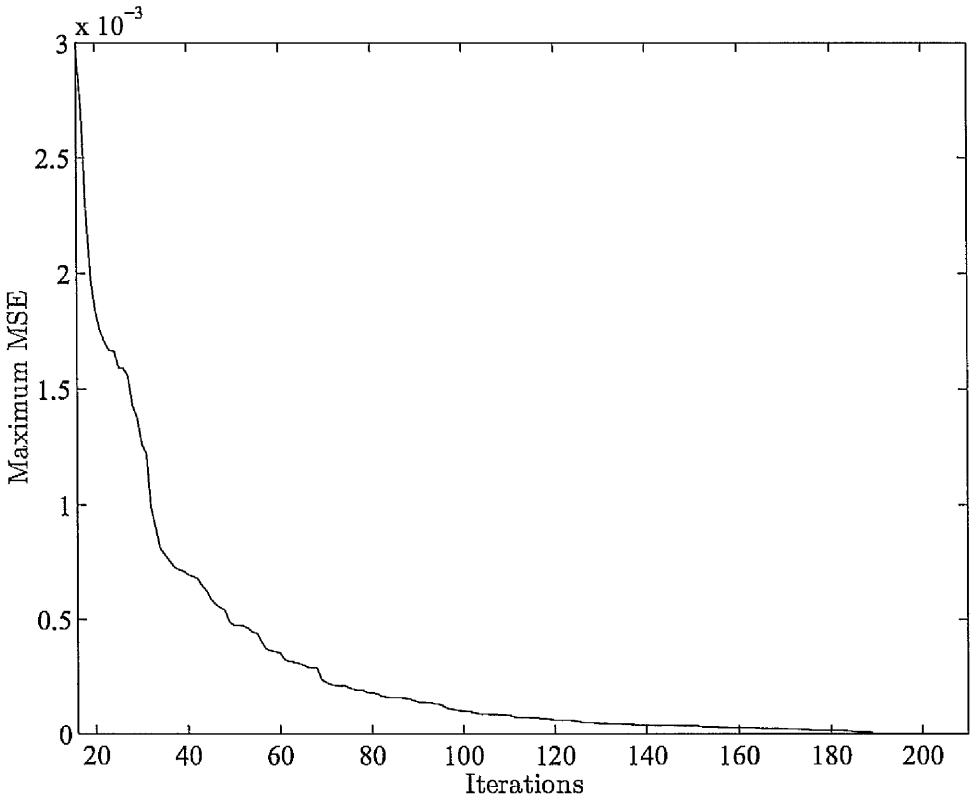

Figure 6.4: Evolution of maximum MSE values for determining the optimal sample number.

The Kriging model was constructed using a first order polynomial and results obtained using 10 measured samples are shown in Table 6.2. These results, also shown in Figure 6.5, confirm that the modified bounds of uncertain parameters have been determined with very good accuracy. Also, Figure 6.6 shows that the updated output-data spaces obtained by Kriging are in good agreement with the true output-data space. The latter were obtained by direct solution of the eigenvalue problem of the dynamic system.

Table 6.2: Updated results: 3 DOF mass-spring system with close modes

Parameters	Initial error %	Updated error %
		10 Measured samples
k_1	$[-13.3 \quad 11.8]$	$[0.6 \quad -0.7]$
k_2	$[-11.1 \quad 9.1]$	$[0.8 \quad -1.0]$
k_5	$[-11.1 \quad 9.1]$	$[0.4 \quad -0.5]$

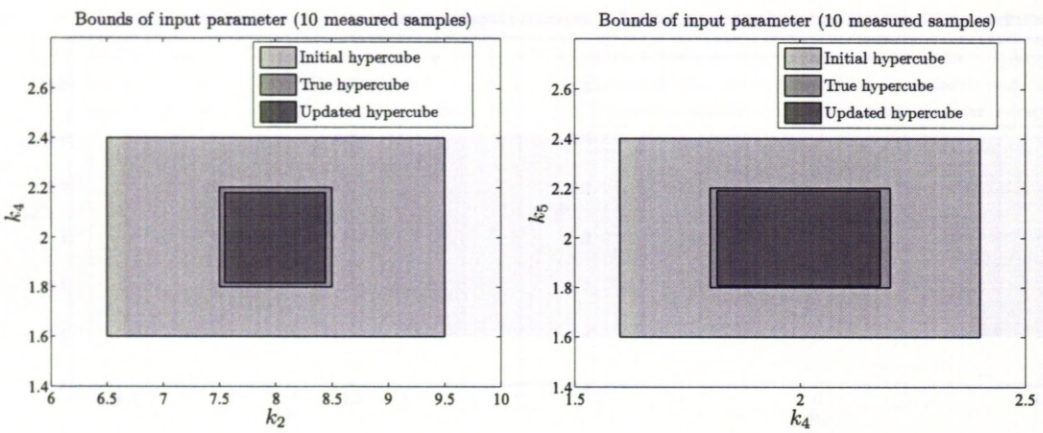

Figure 6.5: Initial, updated and true hypercube of updating parameters based upon 10 measurement samples (system with close modes).

The weighting matrix $\mathbf{W}$, introduced in Eq. (6.21), was set to $10\,\mathbf{I}$ ($\mathbf{I}$ is identity matrix) in this case. Figure 6.7 shows the evolution of error function, Eq. (6.14), in two cases: $(a)\,\mathbf{W} = \mathbf{0}$ and $(b)\,\mathbf{W} = 10\,\mathbf{I}$. It is seen in the figure that the procedure fails to converge when $(a)\,\mathbf{W} = \mathbf{0}$, due to ill-conditioning. This problem is overcome by using the technique described in Eq. (6.21).

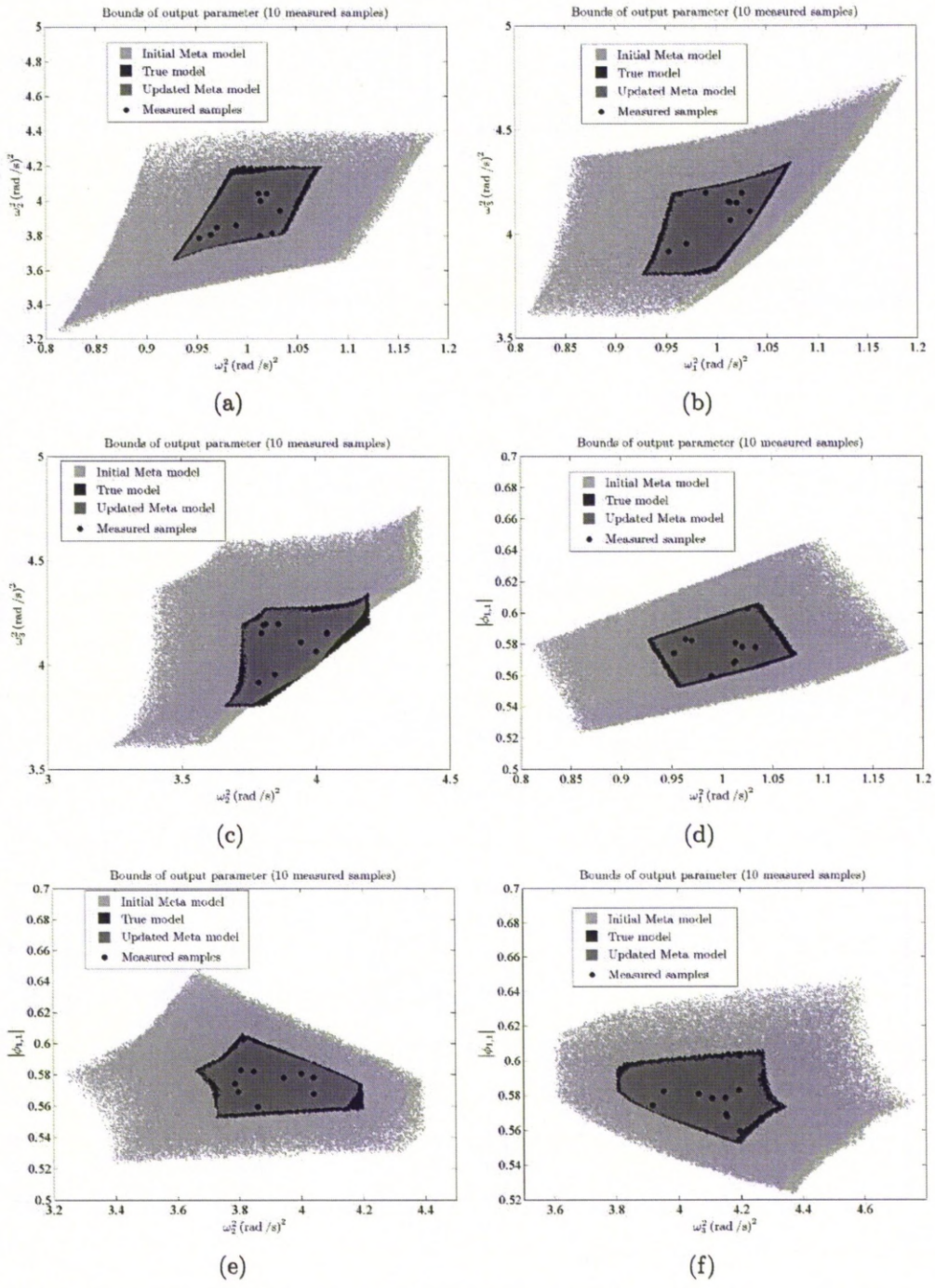

Figure 6.6: Initial, updated and true spaces of predicted data (100,000 points) based upon 10 measurement samples (system with close modes).

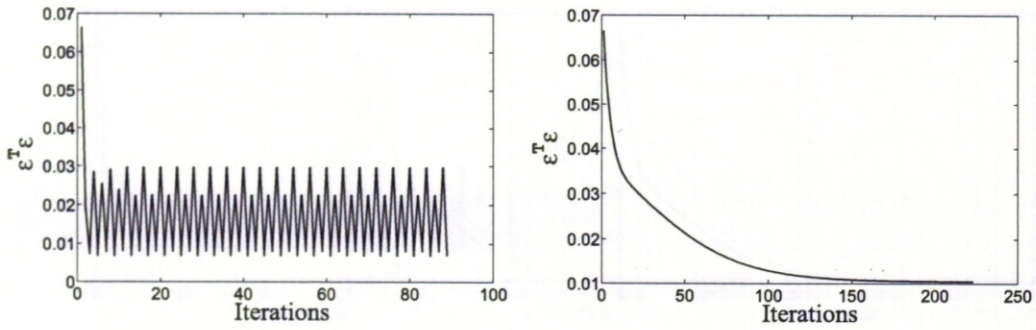

(a) $\mathbf{W} = \mathbf{0}$ (b) $\mathbf{W} = 10\,\mathbf{I}$

Figure 6.7: Evolution of error function values Eq. 6.14 during optimisation using Eq. 6.21.

6.6 Experimental case study: Frame structure with uncertain beams positions

A frame structure with two internal beams is designed in which each beam is independently located at three different positions. The design provides for 9 different combinations of beam positions as shown in Figure 6.8. Detailed finite element models of each of the nine cases were created in MSC-NASTRAN using 8-noded solid elements (CHEXA). The physical structure is shown in Figure 6.9(a) and the finite element model in one configuration of the internal beams in Figure 6.9(b). The bolted joint connections are modelled using rigid elements over an area three times greater than the cross-section of the bolts. The boundary conditions where the frame is connected to a rigid base are represented by fixing the nodal displacements in the three translational degrees of freedom over an area, the size of a washer, between the frame and the base. Modal tests using an instrumented hammer were carried out for the frame in both free-free conditions and when fixed to the rigid base. The experimental results and finite element predictions for both boundary conditions and 9 cases of internal beam locations are shown in Tables 6.3 to 6.12. The closeness of the finite element predictions to the natural frequencies found in modal test shows that the frame structure and the boundary conditions are accurately modelled. To apply the interval model updating method to this problem, the positions (θ_1 and θ_2) of the two internal beams are assumed to be the unknown updating parameters as indicated in Figure 6.10. In

conventional model updating this choice of updating parameters would require remeshing of the finite element model at each iteration, which is time consuming and inelegant. An important advantage of Kriging interpolation is that the updating of nodal coordinates is as straightforward as any other parameter.

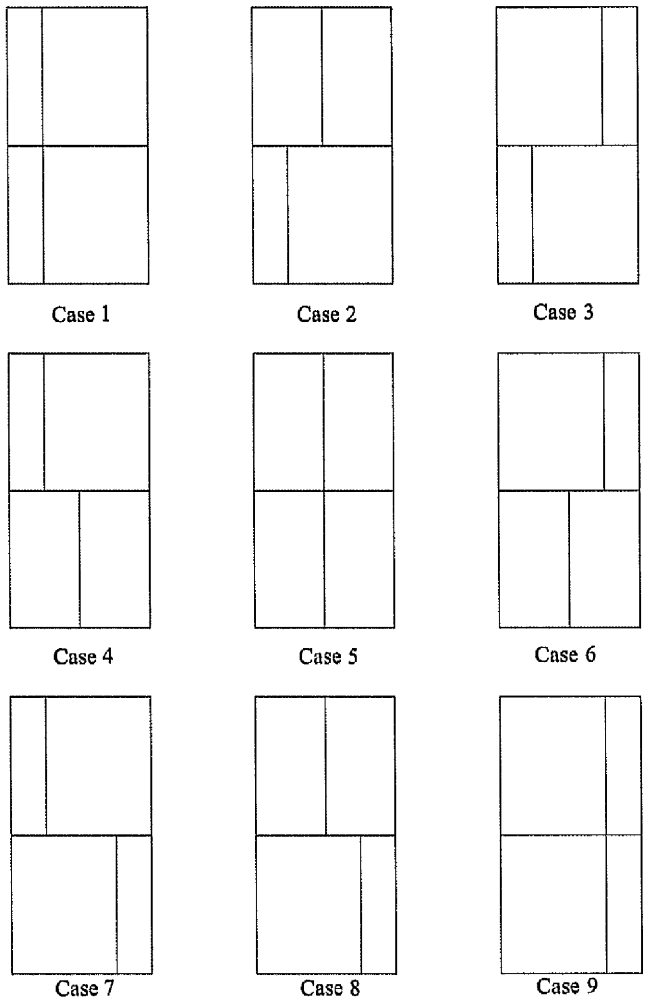

Figure 6.8: Beam locations in the frame structure.

It is supposed that the initial bounds on θ_1 and θ_2 to be $\begin{bmatrix} 0.5 & 3.5 \end{bmatrix}$ and a Kriging model is constructed over this range. The Kriging model describes the relationship between the input parameters (θ_1 and θ_2) and 6 outputs; the first and second in-plane and out-of-plane bending natural frequencies and the first and second torsion natural frequencies in Tables 6.4 to 6.12. It should be noted that the parameter vertex solution is not necessarily valid due to the type of updating

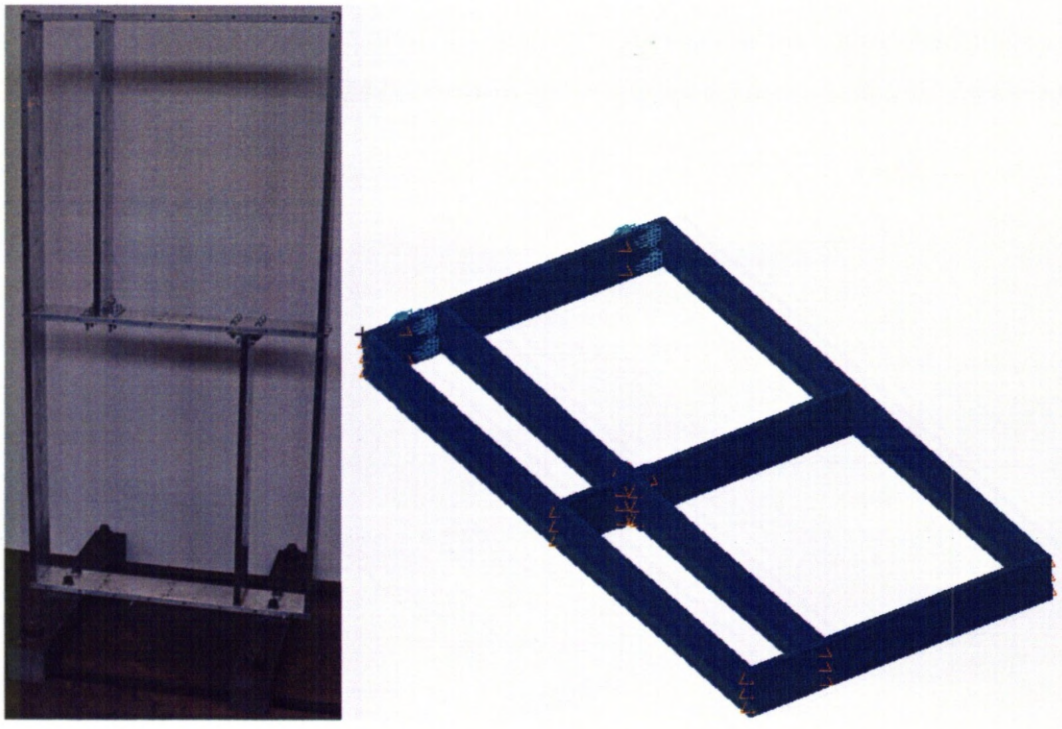

(a) (b)

Figure 6.9: (a) Frame structure (b) Finite element model.

Table 6.3: Measured and FE predictions of natural frequencies (free-free frame structure-case 1)

	Measured (Hz)	FE (Hz)	FE error %
Mode (1)	69.3	70.94	2.37
Mode (2)	79.5	80.27	0.97
Mode (3)	93.2	92.07	-1.21
Mode (4)	199.1	200.58	0.74
Mode (5)	235.6	236.17	0.24
Mode (6)	259.8	259.33	-0.18
Mode (7)	286.3	288.73	0.85
Mode (8)	297.1	296.4	-0.24
Mode (9)	299.1	303.03	1.31
Mode (10)	318.6	327.58	2.82

Table 6.4: Measured and FE predictions of natural frequencies (fixed-frame structure-case 1)

	Measured (Hz)	FE (Hz)	FE error %	Mode shape
Mode (1)	22.54	22.59	0.22	**first in-plane bending mode**
Mode (2)	27.84	27.27	-2.04	**first out-of-plane bending mode**
Mode (3)	47.63	48.14	1.08	**first torsion mode**
Mode (4)	81.19	80.89	-0.37	**second in-plane bending mode**
Mode (5)	201.35	201.55	0.10	higher order in-plane bending mode
Mode (6)	233.71	233.41	-0.13	higher order in-plane bending mode
Mode (7)	256.40	259.05	1.03	**second out-of-plane bending mode**
Mode (8)	257.68	256.54	-0.44	higher order in-plane bending mode
Mode (9)	283.09	283.35	0.09	higher order in-plane bending mode
Mode (10)	298.46	305.34	2.30	higher order in-plane bending mode
Mode (11)	312.39	316.49	1.31	**second torsion mode**

Table 6.5: Measured and FE predictions of natural frequencies (fixed-frame structure-case 2)

	Measured (Hz)	FE (Hz)	FE error %	Mode shape
Mode (1)	23.78	23.97	0.82	**first in-plane bending mode**
Mode (2)	27.43	26.97	-1.65	**first out-of-plane bending mode**
Mode (3)	49.85	50.47	1.23	**first torsion mode**
Mode (4)	79.41	79.65	0.31	**second in-plane bending mode**
Mode (5)	194.40	193.01	-0.71	higher order in-plane bending mode
Mode (6)	222.84	227.90	2.27	**second out-of-plane bending mode**
Mode (7)	226.55	227.32	0.34	higher order in-plane bending mode
Mode (8)	256.09	254.80	-0.50	higher order in-plane bending mode
Mode (9)	263.06	264.44	0.52	higher order in-plane bending mode
Mode (10)	289.42	289.28	-0.05	higher order in-plane bending mode
Mode (11)	306.56	311.63	1.65	**second torsion mode**

Table 6.6: Measured and FE predictions of natural frequencies (fixed-frame structure-case 3)

	Measured (Hz)	FE (Hz)	FE error %	Mode shape
Mode (1)	23.33	23.52	0.80	**first in-plane bending mode**
Mode (2)	26.92	26.40	-1.96	**first out-of-plane bending mode**
Mode (3)	48.94	49.43	1.00	**first torsion mode**
Mode (4)	74.60	74.73	0.17	**second in-plane bending mode**
Mode (5)	194.06	191.88	-1.12	higher order in-plane bending mode
Mode (6)	219.94	224.41	2.03	**second out-of-plane bending mode**
Mode (7)	232.23	231.90	-0.14	higher order in-plane bending mode
Mode (8)	253.54	255.83	0.90	higher order in-plane bending mode
Mode (9)	260.93	260.74	-0.07	higher order in-plane bending mode
Mode (10)	299.94	304.92	1.66	**second torsion mode**

Table 6.7: Measured and FE predictions of natural frequencies (fixed-frame structure-case 4)

	Measured (Hz)	FE (Hz)	FE error %	Mode shape
Mode (1)	24.31	24.53	0.89	**first in-plane bending mode**
Mode (2)	24.38	24.25	-0.55	**first out-of-plane bending mode**
Mode (3)	47.17	47.77	1.28	**first torsion mode**
Mode (4)	76.68	76.69	0.01	**second in-plane bending mode**
Mode (5)	198.89	199.23	0.17	higher order in-plane bending mode
Mode (6)	212.54	207.79	-2.23	higher order in-plane bending mode
Mode (7)	220.52	225.85	2.42	**second out-of-plane bending mode**
Mode (8)	248.41	247.78	-0.25	higher order in-plane bending mode
Mode (9)	257.87	258.93	0.41	higher order in-plane bending mode
Mode (10)	291.62	292.35	0.25	higher order in-plane bending mode
Mode (11)	299.65	304.99	1.78	higher order in-plane bending mode
Mode (12)	304.76	310.00	1.72	**second torsion mode**

Table 6.8: Measured and FE predictions of natural frequencies (fixed-frame structure-case 5)

	Measured (Hz)	FE (Hz)	FE error %	Mode shape
Mode (1)	24.00	24.25	1.02	**first in-plane bending mode**
Mode (2)	24.65	24.49	-0.66	**first out-of-plane bending mode**
Mode (3)	48.36	48.93	1.18	**first torsion mode**
Mode (4)	80.83	80.93	0.12	**second in-plane bending mode**
Mode (5)	201.90	195.31	-3.26	higher order in-plane bending mode
Mode (6)	206.69	207.14	0.22	higher order in-plane bending mode
Mode (7)	229.51	230.13	0.27	higher order in-plane bending mode
Mode (8)	254.23	258.02	1.49	**second out-of-plane bending mode**
Mode (9)	269.10	271.75	0.98	higher order in-plane bending mode
Mode (10)	281.61	281.08	-0.19	higher order in-plane bending mode
Mode (11)	309.67	314.89	1.69	**second torsion mode**

Table 6.9: Measured and FE predictions of natural frequencies (fixed-frame structure-case 6)

	Measured (Hz)	FE (Hz)	FE error %	Mode shape
Mode (1)	24.34	24.53	0.76	**first in-plane bending mode**
Mode (2)	24.43	24.25	-0.74	**first out-of-plane bending mode**
Mode (3)	47.13	47.77	1.37	**first torsion mode**
Mode (4)	76.63	76.69	0.07	**second in-plane bending mode**
Mode (5)	199.87	199.23	-0.32	higher order in-plane bending mode
Mode (6)	211.57	207.79	-1.79	higher order in-plane bending mode
Mode (7)	220.27	225.85	2.53	**second out-of-plane bending mode**
Mode (8)	247.48	247.78	0.12	higher order in-plane bending mode
Mode (9)	256.69	258.93	0.87	higher order in-plane bending mode
Mode (10)	289.20	292.35	1.09	higher order in-plane bending mode
Mode (11)	298.68	304.99	2.11	higher order in-plane bending mode
Mode (12)	304.66	310.00	1.75	**second torsion mode**

Table 6.10: Measured and FE predictions of natural frequencies (fixed-frame structure-case 7)

	Measured (Hz)	FE (Hz)	FE error %	Mode shape
Mode (1)	23.30	23.52	0.96	**first in-plane bending mode**
Mode (2)	26.59	26.40	-0.71	**first out-of-plane bending mode**
Mode (3)	48.83	49.43	1.22	**first torsion mode**
Mode (4)	74.38	74.73	0.46	**second in-plane bending mode**
Mode (5)	192.09	191.88	-0.11	higher order in-plane bending mode
Mode (6)	219.48	224.41	2.25	**second out-of-plane bending mode**
Mode (7)	232.17	231.90	-0.12	higher order in-plane bending mode
Mode (8)	253.90	255.83	0.76	higher order in-plane bending mode
Mode (9)	260.44	260.74	0.11	higher order in-plane bending mode
Mode (10)	299.72	304.92	1.73	**second torsion mode**

Table 6.11: Measured and FE predictions of natural frequencies (fixed-frame structure-case 8)

	Measured (Hz)	FE (Hz)	FE error %	Mode shape
Mode (1)	23.794	23.97	0.76	**first in-plane bending mode**
Mode (2)	27.088	26.97	-0.43	**first out-of-plane bending mode**
Mode (3)	49.785	50.47	1.37	**first torsion mode**
Mode (4)	79.311	79.65	0.43	**second in-plane bending mode**
Mode (5)	193.21	193.01	-0.10	higher order in-plane bending mode
Mode (6)	222.013	227.90	2.65	**second out-of-plane bending mode**
Mode (7)	226.327	227.32	0.44	higher order in-plane bending mode
Mode (8)	253.794	254.80	0.40	higher order in-plane bending mode
Mode (9)	262.621	264.44	0.69	higher order in-plane bending mode
Mode (10)	288.139	289.28	0.40	higher order in-plane bending mode
Mode (11)	305.946	311.63	1.86	**second torsion mode**

Table 6.12: Measured and FE predictions of natural frequencies (fixed-frame structure-case 9)

	Measured (Hz)	FE (Hz)	FE error %	Mode shape
Mode (1)	22.577	22.59	0.06	**first in-plane bending mode**
Mode (2)	27.497	27.27	-0.81	**first out-of-plane bending mode**
Mode (3)	47.536	48.14	1.28	**first torsion mode**
Mode (4)	81.122	80.89	-0.28	**second in-plane bending mode**
Mode (5)	200.543	201.55	0.50	higher order in-plane bending mode
Mode (6)	233.52	233.41	-0.05	higher order in-plane bending mode
Mode (7)	255.603	259.05	1.35	**second out-of-plane bending mode**
Mode (8)	256.764	256.54	-0.09	higher order in-plane bending mode
Mode (9)	280.807	283.35	0.91	higher order in-plane bending mode
Mode (10)	298.403	305.34	2.32	higher order in-plane bending mode
Mode (11)	311.538	316.49	1.59	**second torsion mode**

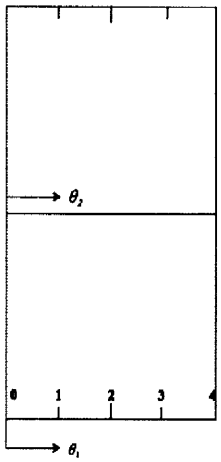

Figure 6.10: Parametrisation of internal beam locations in the frame structure.

parameters. The maximum value of the MSE shows that the CCD design together with 9 samples in Figure 6.10 provide an accurate fit. The optimisation procedure described in Section 6.4 was used to identify the locations of internal beams based on the six measured natural frequencies, thereby allowing the updating parameter bounds to be corrected. The weighting matrix was set to $\mathbf{W} = 100\mathbf{I}$ in this case. Table 6.13 shows the initial and identified beams locations in 9 cases obtained by deterministic model updating. The maximum error of 11.00 % in Table 6.13 is an indicator of good performance. The Kriging model was used to generate all possible variations of the 6 outputs due to the variation of the internal beam locations in the range of $[\ 1.00 \quad 2.99\ ]$ for θ_1 and $[\ 0.89 \quad 3.09\ ]$ for θ_2 by interval model updating.

Table 6.13: Deterministic model updating of beam locations

True parameters		Initial parameters		Updated parameters		Initial error %		Updated error %	
θ_1	θ_2	θ_1	θ_2	θ_1	θ_2	θ_1	θ_2	θ_1	θ_2
1.0	1.0	1.6	1.6	1.04	1.02	60.00	60.00	3.73	2.00
1.0	2.0	1.6	2.4	1.00	2.15	60.00	20.00	-0.21	7.56
1.0	3.0	1.6	2.4	1.00	3.08	60.00	-20.00	0.20	2.76
2.0	1.0	1.6	1.6	2.04	0.90	-20.00	60.00	1.81	-9.78
2.0	2.0	2.4	2.4	2.13	2.00	20.00	20.00	6.48	-0.12
2.0	3.0	2.4	2.4	1.95	3.09	20.00	-20.00	-2.36	3.06
3.0	1.0	2.4	1.6	2.98	0.89	-20.00	60.00	-0.58	-11.00
3.0	2.0	2.4	1.6	2.99	1.83	-20.00	-20.00	-0.31	-8.36
3.0	3.0	2.4	2.4	2.93	2.98	-20.00	-20.00	-2.18	-0.58

Figure 6.11 shows the initial and updated regions of possible natural frequency variation in (a and b) the planes of first and second natural frequencies, (c and d) the planes of third and fourth natural frequencies and (e and f) the planes of fifth and sixth natural frequencies together with 9 measured samples. It is seen from Figures 6.11(b), 6.11(d) and 6.11(f) that the updated regions encloses some measured samples but not all of them. This is due to the fact that the samples which are just outside the regions were in reality located on the points close to the boundaries. The errors from other sources of uncertainty, typically disassembly and reassembly and measurement noise, affect the results causing the samples to move over the boundaries. As can be seen in Figure 6.11, some of the areas within the updated region of output data include greater number of output samples (they look denser). These areas represent regions where the likelihood of the presence of the output data due to these inputs variations is greater than the other areas. The initial and updated bounds of natural frequencies are shown in Table 6.14 where a maximun error of 4.24% shows good agreement of the updated model output bounds with the bounds of the measaured data. The errors are calculated based on the percentage of difference between upper(lower) bounds of measured data and their numerical predictions counterparts.

Table 6.14: Measured, initial and updated bounds of natural frequencies (frame structure)

	Measured (Hz)	Initial FE (Hz)	Updated FE (Hz)	Initial FE % error	Updated FE % error
First in-plane bending mode	[22.54 24.34]	[21.62 24.61]	[22.57 24.61]	[−4.08 1.11]	[0.13 1.11]
First out-of-plane bending mode	[24.38 27.84]	[23.66 35.53]	[23.86 27.47]	[−2.95 27.62]	[−2.13 − 1.33]
First torsion mode	[47.13 49.85]	[43.72 67.57]	[45.13 50.55]	[−7.24 35.55]	[−4.24 1.40]
Second in-plane bending mode	[74.38 81.19]	[71.09 82.50]	[73.99 81.37]	[−4.42 1.61]	[−0.52 0.22]
Second out-of-plane bending mode	[219.48 256.40]	[224.08 267.34]	[224.08 259.51]	[2.10 4.27]	[2.10 1.21]
Second torsion mode	[299.72 312.39]	[300.26 339.65]	[303.58 317.20]	[0.18 8.73]	[1.29 1.54]

6.7 Closure

In this chapter, the problem of interval model updating, with test structure variability was formulated. In particular cases, when the output data are the eigenvalues of the dynamic system and updating parameters are substructure mass and stiffness coefficients, the parameter vertex solution may be used. The Kriging predictor for the solution to the inverse problem of a system with n_r outputs

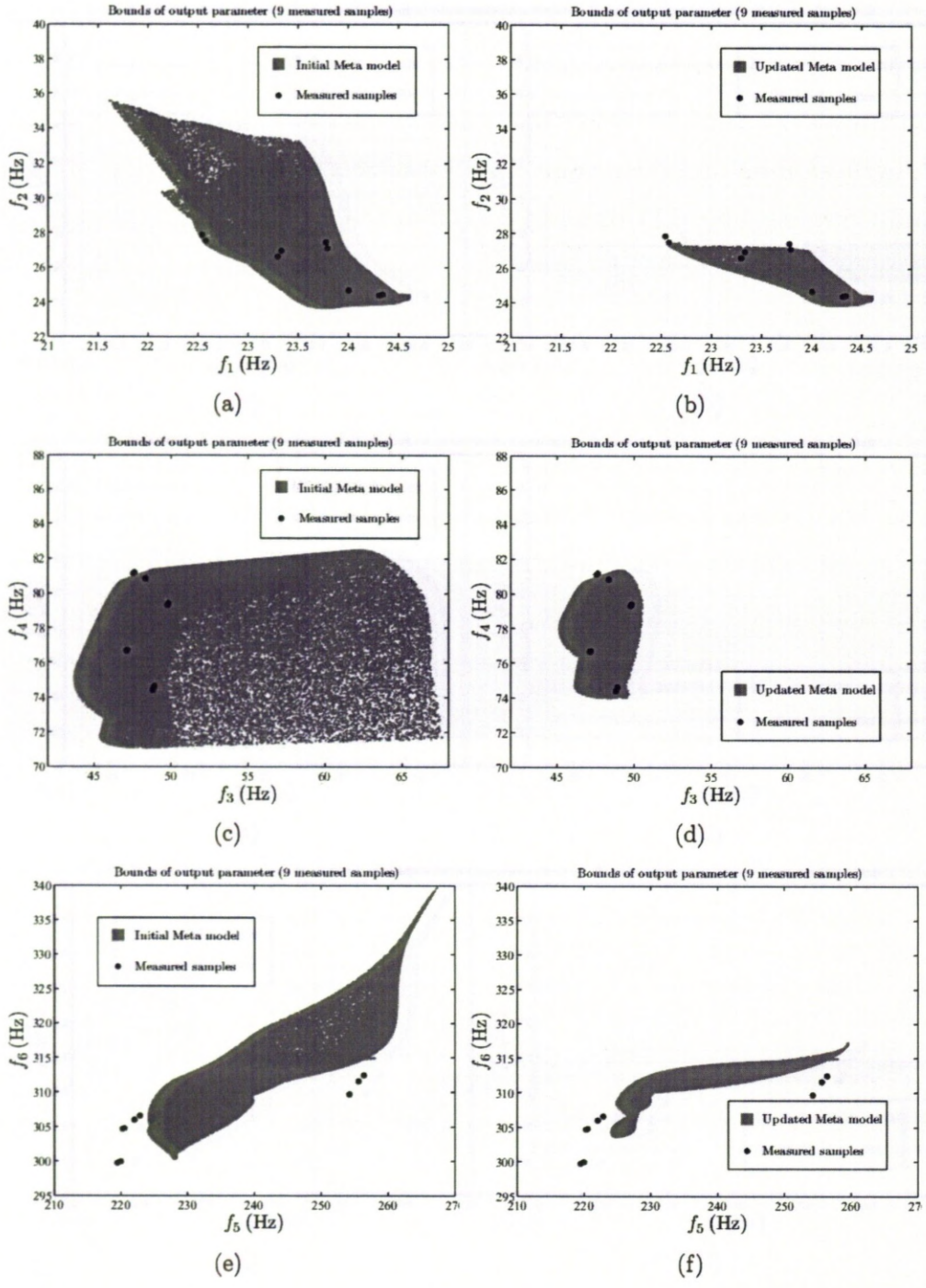

Figure 6.11: Initial and updated spaces of predicted data (100,000 points) based upon 9 measurement samples (frame structure)

was formulated and used for the solution of interval model updating in the general case. The method was verified numerically in a three degree of freedom mass-

spring system with well-separated and close modes. Results showed that interval model updating was capable of identifying uncertain input parameters with very good accuracy when only a small numbers of measured samples are available. This represents a significant advantage of interval updating over probabilistic methods, which require large volumes of test data. It was shown that by Kriging interpolation the uncertain positions of internal beams in a frame structure could be treated as updating parameters. Interval model updating with the Kriging predictor was able to correct initial erroneous bounds on the beam positions with good accuracy.

Chapter 7

Conclusions and future work

7.1 Conclusions

Uncertainty analysis in structural dynamics has recently received considerable attention since it can lead to improved confidence in the design process. Different sources of uncertainty may exist in the numerical model, that can be generally classified into two groups known as epistemic and aleatory. Epistemic uncertainty includes limitations in knowledge or lack of understanding and uncertainty due to human error. This uncertainty is reducible by further knowledge/information. The second type of uncertainty, i.e. aleatory uncertainty, is not reducible and includes randomness in parameters. For example, structural variability which arises from manufacturing tolerances, material differences, and wear are considered as aleatory uncertainty as they really exist and need to be taken into account in numerical model. This thesis considered the effect of aleatory uncertainty in structural models and its influence on aeroelastic analysis.

Firstly, an extensive review has been carried out to provide the essential mathematical tools for uncertainty modelling and propagation. Two popular classes of models known as probabilistic and nonprobabilistic are identified and used for the propagation of uncertainty through the deterministic analysis (uncertainty propagation). Various uncertainty propagation methods including Monte Carlo Simulation (MCS), first and second order perturbation methods, asymptotic integral, interval analysis, fuzzy method and meta-model are studied and explained.

Knowledge gained from the literature shows that the application of uncertainty propagation methods in the problem of flutter analysis has received less attention. However, a study conducted on the McDonnell Douglas F-4 Phantom

II [111] quantified the weight and inertia variability for this aircraft, showing changes in mass and inertia of control surfaces by up to 15% which highlighted the importance of the problem.

The propagation of structural uncertainty thorough aeroelastic analysis for determining the range/distribution of flutter speed has been carried out in two cases. In the first case, the linear aerodynamic theory based on the Doublet-Lattice Method (DLM) is considered. Random parameters which have significant effect on flutter speed have been identified through flutter sensitivity analysis, which is then propagated through the aeroelastic analysis to obtain estimates of intervals, fuzzy membership functions or PDFs for aeroelastic damping and flutter speed. The derivatives of aeroelastic response of the system within the region of variation of the uncertain structural parameters are approximated using the Response Surface Method (RSM). Three test cases: (1) Goland wing without structural damping, (2) Goland wing with structural damping, and (3) a generic fighter aircraft are considered in this study. In the analysis of the Goland wing, nonlinear behaviour has been observed in tails of the aeroelastic damping PDFs (obtained from MCS). This nonlinear behaviour has been predicted well when second-order probabilistic perturbation analysis is used. Fuzzy analysis including a number of interval analysis at different levels of membership function, also correctly predicts the nonlinear behaviour at the tails. A rapid increase in the sensitivity of the real part of the critical eigenvalue to the structural variability has been observed after the modal interaction starts. At velocities close to the flutter speed, particular structures are revealed, close to a -45° line, in the aeroelastic-damping scatter diagrams and to a +45° line, in the aeroelastic-frequency scatter diagrams. These behaviours demonstrate if a chosen point on the unstable mode decreases the damping and frequency then it will increase the damping and decrease the frequency on the stable mode to a similar degree, and vice-versa. In the analysis of the Goland wing, a velocity where two crossing modes have no correlations has been determined. This velocity is called a zero-correlation velocity. The inclusion of structural damping in the Goland wing is found to result in a small but significant increase in the deterministic flutter speed. Structural damping has virtually no effect upon the flutter intervals. The MCS is used for assessing the

accuracy of the results obtained by the interval analysis, fuzzy and perturbation methods which are computationally more efficient. From the results achieved by the linear flutter analysis of the Goland wing, a combination of response surface method and interval analysis is found not only computationally efficient but also provide a sufficiently good approximation of flutter bounds determined by the MCS. The interval flutter analysis is then carried out in the analysis of a generic fighter plane for flutter instability involving the coupling of wing bending with store pitching behaviour. Flutter bounds are determined by the propagation of structural stiffness parameters (including the pylon - store connection) by interval analysis.

In the second case, the feasibility of using uncertain propagation methods to aeroelastic stability prediction when CFD is used for the aerodynamic has been investigated. The feasibility in terms of computational cost is demonstrated by exploiting an eigenvalue-based method, which can be configured for the purpose of computing stability for many similar structural models. The same test cases used in linear flutter analysis including the Goland wing and generic fighter aircraft are considered. At altitudes higher than the flutter altitude, the intervals of uncertainty on aeroelastic damping are found to be small, but increase at around the flutter altitude and beyond to become similar in extent to the bounds on the frequencies across the entire range of frequencies. This behaviour has also been observed in the problem of uncertain linear flutter analysis. Similar uncertain structural parameters which have been determined through a linear sensitivity analysis are again used for the purpose of the uncertainty propagation. The uncertain propagation methods including the MCS (with 1000 samples), perturbation method and interval analysis are then applied to the CFD based aeroelastic analysis. For the Goland wing, the application of the MCS method takes two days on a desktop PC while the interval analysis is accomplished in around 3 hours. As previously mentioned, the important information obtained from the uncertain flutter analysis are in the spread of the eigenvalue real parts and also the skewness about the mean, which have been well captured by the interval method in a reasonable computational cost. Therefore it may be concluded that this method is favoured based on this consideration. The results of these studies

are published in [137, 140–142].

Whichever propagation method is used for uncertainty propagation, an interesting question is how to use these methods for applications. For those uncertain parameters which are measurable (such as thickness), the direct measurements may be used to identify their ranges or distributions. However, the immeasurable uncertain parameters need to be identified in an inverse approach known as stochastic model updating method. In the stochastic model updating approach, it is assumed that modal parameters of a number of identical structures, taken from a production line, are obtained by a series of experimental modal analysis. Then the ranges/distributions of the uncertain input parameters are identified based on the ranges/distributions of the modal data. Statistics have been incorporated in the development of the model updating methods known as the minimum variance methods [26, 93] or the Bayesian method [94, 95, 108] to overcome the issues related to noisy measured data. However, it is shown in this work that these methods are not applicable to the problem of model updating in the presence of irreducible uncertainty in the measured data. Among existing model updating approaches which deal with the irreducible uncertain measured data, two methods namely the maximum likelihood estimator [24] and the perturbation method [27] are found to be capable of predicting the ranges/distributions of the updating parameters. The performance of these methods are assessed in a simple numerical example and it is found that the maximum likelihood method has a poor estimation of standard deviations of the updating parameters due to the fact that it does not consider the correlation between the elements of the output modal parameters.

In the present work a new method, based upon the perturbation procedure, is developed in two versions. In the first version of the method, the correlation between the updated parameters and measured data is omitted. This results in a procedure that requires only the first-order matrix of sensitivities. The second procedure includes this correlation (after the first iteration) but is a more expensive computation requiring the second-order sensitivities as does the method proposed by Hua et al. [27]. It is shown in numerical simulations that the first method produces results that are equally acceptable as those produced by the

second method or by Hua's approach [27]. These methods are demonstrated in numerical simulations and also in an experiment carried out on a collection of rectangular plates with variable thickness. Another stochastic model updating approach based on minimising an objective function has also been proposed in this study. The proposed objective function is the weighted sum of the Euclidian norm of the difference between mean values of measured data and analytical outputs vectors, and the Frobenius norm of the difference between the covariance matrices of the measured data and analytical outputs. This method does not involve any assumption of statistical independence between the parameters and measurements. This method is also verified in numerical simulation and also in experiments carried out on a collection of rectangular plates with variable masses on it. In both methods, it is observed that the quality of identified parameters is very sensitive to sample size of the measured data and also to the measurement noise. Regularisation may be applied when the stochastic model updating equations are ill-conditioned due to measurement noise. However, the issue of sample size may not be overcome with probabilistic approach and therefore it is decided to use the interval model which probably requires fewer of measured data. Above studies are published in [143, 144].

In order to overcome the issue of sample size in the probabilistic perturbation method, the problem of interval model updating with test structure variability is defined and formulated. It is shown that when the output data are the eigenvalues of the dynamic system and updating parameters are substructure mass and stiffness coefficients, the parameter vertex method can be used for the solution. However, in general cases, another solution needs to be considered. In this thesis, the meta-model is used to solve the interval model updating problem in general cases. The Kriging predictor is chosen for the meta-model and the inverse problem of a system with n_r outputs is formulated and used for the solution of the interval model updating in the general case. The method is validated numerically using a three degree of freedom mass-spring system with both well-separated and close modes. Results show that the interval model updating is capable of identifying input parameters with very good accuracy even when only a small number of measured samples exist. This represents a significant advantage of the interval

updating over the probabilistic methods, which require large amounts of data. Another advantage of Kriging interpolation is that it enables the use of updating parameters that are difficult to use by conventional correction of the finite element model at each iteration. An example of this is demonstrated in an experimental exercise where the positions of two beams in a frame structure are selected as the updating parameters. Finally it is shown that the interval model updating with the Kriging predictor is capable of correcting initial erroneous bounds on the beam positions with good accuracy. This study is published in [145, 146]

7.2 Suggestions for future work

The development of the probabilistic and nonprobablistic uncertainty propagation and identification methods has led to several questions and idea which can be considered in future work. A very important question is that how these methods can be applied to the aeroelastic applications. By using stochastic model updating it would, in principle, be necessary to carry out ground vibration tests on a sufficient number of samples of nominally identical aircraft. A database of information obtained from such an exercise might be deemed applicable to a range of aircraft and not just the particular type of aircraft tested, depending upon design similarities and engineering judgement etc.

The choice of parameters in the stochastic model updating is as important as in the conventional model updating and requires considerable physical insight. The effect of different parameterisations on the performance of the stochastic updating procedure can be investigated in a set of identical realistic structures.

All uncertainty propagation methods, proposed in this thesis, can be used for robust design of structures and may be worth investigating. At design stage the uncertainty in design parameters may affect the performance of the product. It is important to ensure that the design is robust enough with respect to the uncertainties. This investigation can be done by implementing the propagation methods in the design process of structure.

The analysis of uncertainty in the subject of nonlinear structural dynamics is a challenging problem. This is due to the fact that discrimination between uncer-

tainty and nonlinearity from measured data does not seem to be straightforward. However, the effects of nonlinearity together with uncertainty in structural parameters can be investigated in numerical models and analysis.

In the stability analysis of aircraft structures, Limit Cycle Oscillation (LCO) phenomenon is considered as a fatigue problem and must not be reached in the flight envelope of aircraft [147]. The LCO can be triggered by either nonlinearity in the structural model or the aerodynamic model. The uncertainty propagation methods which are used in this thesis may be used for the LCO analysis in the presence of nonlinear uncertain structural parameters in future work.

Finally, as mentioned in Chapter 6, a general solution of interval model updating problem based on evaluation of inverse of interval matrix is an open problem and can be considered in future work.

7.3 Outcomes of the research

Four journal papers [137, 140, 143, 145] and four conference papers [141, 142, 144, 146] have been submitted and published from this thesis.

Bibliography

[1] O.C. Zienkiewicz and R.L. Taylor. *The finite element method, Volume 1, the basis.* Butterworth Heinemann, 2000.

[2] R.A. Ibrahim and C.L. Pettit. Uncertainties and dynamic problems of bolted joints and other fasteners. *Journal of Sound and Vibration*, 279(3-5):857–936, 2005.

[3] M.I. Friswell and J.E. Mottershead. *Finite element model updating in structural dynamics.* Kluwer Academic Press, 1995.

[4] J. E. Mottershead and M. I. Friswell. Model updating in structural dynamics: a survey. *Journal of Sound and Vibration*, 167(2):347–375, 1993.

[5] H. Ahmadian, M.I. Friswell, and J.E. Mottershead. Minimisation of the discretization error in mass and stiffness formulation by an inverse method. *International journal for numerical methods in engineering*, 41:371–387, 1998.

[6] H. Ahmadian, J.E. Mottershead, and M.I. Friswell. Regularisation methods for finite element model updating. *Mechanical Systems and Signal Processing*, 12:47–64, 1998.

[7] J.A. Rice. *Mathematical statistics and data analysis.* Wadsworth and Brooks, 1988.

[8] J.M.R Fonseca. *Uncertainty in structural dynamic models.* PhD thesis, University of Wales Swansea, 2005.

[9] A. Haldar and S. Mahadevan. *Reliability assessment using stochastic finite element analysis.* Wiley: New York, 2000.

[10] K. Binder. *Application of the Monte Carlo Method in statistical physics.* Springer: Berlin, 1984.

[11] R.Y. Rubenstein. *Simulation and the Monte Carlo method.* Wiley: New York, 1981.

[12] A.W. Bowman and A. Azzalini. *Applied smoothing techniques for data analysis.* Oxford University Press, 1997.

[13] J.D. Collins and W.T. Thomson. The eigenvalue problem for structural systems with statistical properties. *AIAA Journal*, 7(4):642–648, 1969.

[14] T.K. Hasselman and G.C. Hart. Modal analysis of random structural system. *Journal of Engineering Mechanics (ASCE)*, 98(EM3):561–579, 1972.

[15] D. Song, S. Chen, and Z. Qiu. Stochastic sensitivity analysis of eigenvalues and eigenvectors. *Computers and Structures*, 54(5):891–896, 1995.

[16] S. Adhikari and M.I. Friswell. Random matrix eigenvalue problems in structural dynamics. *International Journal for Numerical Methods in Engineering*, 69(3):562–591, 2007.

[17] R. Moore. *Interval analysis.* Prentice Hall, Englewood Cliffs, 1966.

[18] D. Moens and D. Vandepitte. An interval finite element approach for the calculation of envelope frequency response functions. *International Journal for Numerical Methods in Engineering*, 61:2480–2507, 2004.

[19] Z. Qui, X. Wang, and M.I. Friswell. Eigenvalue bounds of structures with uncertain-but-bounded parameters. *Journal of Sound and Vibration*, 282(1-2):297–312, 2005.

[20] L.A. Zadeh. Fuzzy sets. *Information and Control*, 8(3):338–353, 1965.

[21] D. Moens and D. Vandepitte. Recent advances in non-probabilistic approaches for non-deterministic dynamic finite element analysis. *Archives of Computational Methods in Engineering*, 13(3):389–464, 2006.

[22] L. Chen and SS. Rao. Fuzzy finite-element approach for the vibration analysis of imprecisely-defined systems. *Finite element in analysis and design*, 27(1):69–83, 1997.

[23] D. Moens and D. Vandepitte. A fuzzy finite element procedure for the calculation of uncertain frequency response functions of damped structures: part 1 procedure. *Journal of sound and vibration*, 288(3):431–462, 2005.

[24] J.R. Fonseca, M.I. Friswell, J.E. Mottershead, and A.W. Lees. Uncertainty identification by the maximum likelihood method. *Journal of Sound and Vibration*, 288(3):587–599, 2005.

[25] C. Mares, J.E. Mottershead, and M.I. Friswell. Stochastic model updating: Part 1: Theory and simulated example. *Mechanical Systems and Signal Processing*, 20(7):1674–1695, 2006.

[26] J.D. Collins, G.C. Hart, T.K. Hasselman, and B. Kennedy. Statistical identification of structures. *AIAA Journal*, 12(2):185–190, 1974.

[27] X.G. Hua, Y.Q. Ni, Z.Q. Chen, and J.M. Ko. An improved perturbation method for stochastic finite element model updating. *International Journal for Numerical Methods in Engineering*, 73(13):1845–1864, 2008.

[28] R.E. Melchers. *Structural reliability analysis and prediction.* John Wiley & Sons, New-York, 1999.

[29] R. Walters and L. Huyse. Uncertainty analysis for fluid mechanics with applications. Technical report, NASA CR 2002-211449, 2002.

[30] M. Abramowitz and I.A. Stegun. *Handbook of Mathematical Functions, with Formulas, Graphs, and Mathematical Tables.* Dover Publications, New York, U.S.A., 1965.

[31] E. Vanmarcke. *Random fields: analysis and synthesis.* The MIT press, 1983.

[32] S. Adhikari and M.I. Friswell. Distributed parameter model updating using the Karhunen-Loeve expansion. *Mechanical Systems and Signal Processing*, 24(2):326–339, 2010.

[33] C. Manohar and R. Ibrahim. Progress in structural dynamics with stochastic parameter variations: 1987-1998. *ASME Applied Mechanics Reviews*, 52(5):177–197, 1999.

[34] R. Ghanem and P. Spanos. *Stochastic finite elements: a spectral approach.* Springer-Verlag, New-York, 1991.

[35] T.G. Chondros. *Distinguished Figures in Mechanism and Machine Science.* Springer Netherlands, 2007.

[36] L.A. Zadeh. Fuzzy sets as a basis for a theory of possibility. *Fuzzy Sets and Systems*, 100(1):9–34, 1999.

[37] M. Hanss and K. Willner. A fuzzy arithmetical approach to the solution of finite element problems with uncertain parameters. *Mechanics Research Communications*, 27(3):257–272, 2000.

[38] C. Bucher. *Computational analysis of randomness in structural mechanics.* Taylor & Francis group: Netherlands, 2009.

[39] M.D. McKay, R.J. Beckman, and W.J. Conover. A comparison of three methods for selecting values of input variables in the analysis of output from a computer code. *Technometrics*, 42(1):55–61, 2000.

[40] J.R. Koehler and A.B. Owen. Computer experiments. *In: S Ghosh and CR Rao, Editors, Handbook of Statistics, Elsevier Science B V, Amsterdam*, 13:261–308, 2000.

[41] R.A. Horn and C.R. Johnson. *Matrix analysis.* Cambridge University Press, 1985.

[42] A.A. Giunta, M.S. Eldred, and J.P. Castro. Uncertainty quantification using response surface approximation. In *9th ASCE Specially conference on probabilistic mechanics and structural reliability*, Albuquerque, New Mexico, July 26-28, 2004. American Society of Civil Engineers Sandia National Laboratories.

[43] A.W. Bowman and A. Azzalini. *Applied smoothing techniques for data analysis.* Oxford University Press, 1997.

[44] W. Hardle, M. Muller, and S. Sperlich. *Non-parametric and Semiparametric Models.* Springer Verlag, 2003.

[45] R.E. Melchers. *Structural Reliability Analysis and Prediction.* John Wiley and Sons Ltd, 1999.

[46] NL. Johnson and S. Kotz. *Distributions in Statistics: Continuous Univariate Distributions Vol.2.* The Houghton Mifflin Series in Statistics, Houghton Mifflin Company: Boston, U.S.A., 1970.

[47] A.M. Mathai and S.B. Provost. *Quadratic Forms in Random Variables: Theory and Applications.* Marcel Dekker: New York, NY,, 1992.

[48] G.A. Suzuki. Consistent estimator for the mean deviation of the pearson type distribution. *Annals of the Institute of Statistical Mathematics*, 17(1):271–285, 1965.

[49] K. Pearson. Contributions to the mathematical theory of evolution, ii: skew variation in homogeneous material. *Philosophical transaction of royal society London ARRAY*, 186:343–414, 1895.

[50] M. Hanss. The transformation method for the simulation and analysis of systems with uncertain parameters. *Fuzzy Sets and Systems*, 130(3):277–289, 2002.

[51] W. Dong and H. Shah. Vertex method for computing functions of fuzzy variables. *Fuzzy Sets and Systems*, 24:65–78, 1987.

[52] S. Rao and P. Sawyer. Fuzzy finite element approach for the analysis of imprecisely defined systems. *AIAA Journal*, 33(12):2364–2370, 1995.

[53] U. Koyluoglu, A. Cakmak, and S. Nielsen. Interval algebra to deal with pattern loading and structural uncertainties. *Journal of Engineering Mehanics*, 121(11):1149–1157, 1995.

[54] B. Moller, W. Graf, and M. Beer. Fuzzy structural analysis using α-level optimization. *Computational Mechanics*, 26:547–565, 2000.

[55] D.R. Jones, M. Schonlau, and W.J. Welch. Efficient global optimization of expensive black-box functions. *Journal of Global Optimization*, 13(4):455–492, 1998.

[56] J. Sacks, W.J. Welch, T.J. Mitchell, and H.P. Wynn. Design and analysis of computer experiments. *Statistical Science*, 4(4):409–435, 1989.

[57] E.H. Isaaks and R.M. Srivastava. *An Introduction to Applied Geostatistics.* Oxford University Press, 1989.

[58] S.N. Lophaven, H.B. Nielsen, and J. Søndergaard. Dace, a matlab kriging toolbox. Technical Report I MM-TR-2002-12, Technical University of Denmark, DK-2800 Kgs. Lyngby Denmark, 2002.

[59] R.H. Myers and D.C. Montgomery. *Response surface methodology; process and product optimisation using designed experiments.* John Wiley and Sons, 2002.

[60] G.E.P. Box and K.B. Wilson. On the experimental attainment of optimum conditions (with discussion). *Journal of the Royal Statistical Society Series B*, 13(1):1–45, 1951.

[61] M. Ghoreyshi, K.J. Badcock, and M.A. Woodgate. Accelerating the numerical generation of aerodynamic models for flight simulation. *Journal of Aircraft*, 46(3):972–980, 2009.

[62] M.I. Friswell, Z.P. Qiu, and F. Zhang. The determination of convex sets of uncertainty in structural dynamics. In *Proceedings of 1st International Conference on Uncertainty in Structural Dynamics, USD2007*, The University of Sheffield, UK, 2007.

[63] D.J. Ewins. *Modal testing: theory and practice.* Research Studies Press LTD, Letchworth, Hertfordshire, England, 1984.

[64] N.M.M. Maia, J.M.M. Silva, J. He, N.A.J. Lieven, R.M. Lin, G.W. Skingle, W.M. To, and A.P.V. Urgueira. *Theoretical and experimental modal analysis.* Research Studies Press, Taunton, 1997.

[65] W. Heylen, S. Lammens, and P. Sas. *Modal analysis theory and testing.* KUL Press, Leuven, 1997.

[66] G. Lallement and J. Piranda. Localisation methods for parameter updating of finite element models in elastodynamics. In *Proceedings of the 8th International Modal Analysis Conference (IMAC VIII)*, Orlando, Florida, U.S.A, 1990.

[67] M. Link and O.F. Santiago. Updating and localising structural errors based on minimisation of equation errors. In *International Conference on Spacecraft Structures and Mechanical Testing (ESA/ESTEC)*, Noordwijk, Holland, 1991.

[68] G.M. Gladwell and H. Ahmadian. Generic element matrices suitable for finite element updating. *Mechanical Systems and Signal Processing*, 9(6):601–614, 1996.

[69] J.E. Mottershead, M.I. Friswell, G.H.T. Ng, and J.A. Brandon. Geometric parameters for finite element model updating of joints and constraints. *Mechanical Systems and Signal Processing*, 10(2):171–182, 1996.

[70] M.I. Friswell, J.E. Mottershead, and H. Ahmadian. Combining subset selection and parameter constraints in model updating. *Transactions of the ASME, Journal of Vibration and Acoustics*, 120(4):854–859, 1998.

[71] H. Ahmadian, J.E. Mottershead, S. James, M.I. Friswell, and C.A. Reece. Modelling and updating of large surface-to-surface joints in the awe-mace structure. *Mechanical Systems and Signal Processing*, 20(4):868–880, 2006.

[72] R.J. Guyan. Reduction of stiffness and mass matrices. *AIAA Journal*, 3(2):380–380, 1965.

[73] M. Paz. Dynamic condensation. *AIAA Journal*, 22(5):724–727, 1984.

[74] J. O'Callahan, P. Avitabile, and R. Riemer. System equivalent reduction expansion process. In *7th International modal analysis conference, IMAC*, Las Vegas, 1989.

[75] R.J. Allemang and D.L. Brown. A correlation coefficient for modal vector analysis. In *Proceedings of the 1st International Modal Analysis Conference (IMAC I)*, Orlando, Florida, U.S.A, 1982.

[76] N.A. Lieven and D.J. Ewins. Spatial correlation of mode shapes: the coordinate modal assurance criterion (comac). In *Proceedings of the 6th International Modal Analysis Conference (IMAC VI)*, Kissimmee, Florida, U.S.A, 1988.

[77] W. Wang, J.E. Mottershead, and C. Mares. Vibration mode shape recognition using image processing. *Journal of Sound and Vibration*, 326(3-5):909–938, 2009.

[78] M. Baruch and I.Y. Bar-Itzhak. Optimal weighted orthogonalization of measured modes. *AIAA Journal*, 16:346–351, 1978.

[79] A. Berman. Mass matrix correction using an incomplete set of measured modes. *AIAA Journal*, 17:1147–1148, 1979.

[80] A.M. Kabe. Stiffness matrix adjustment using mode data. *AIAA Journal*, 23:1431–1436, 1985.

[81] B. Caeser and J. Pete. Direct update of dynamic mathematical models from modal test data. *AIAA Journal*, 25:1494–1499, 1987.

[82] F.S. Wei. Mass and stiffness interaction effects in analytical model modification. *AIAA Journal*, 28:1686–1688, 1990.

[83] E.T. Lee and H.C. Eun. Update of corrected stiffness and mass matrices based on measured dynamic modal data. *Applied Mathematical Modelling*, 33(5):2274–2281, 2009.

[84] R. Fox and M. Kapoor. Rates of change of eigenvalues and eigenvectors. *AIAA Journal*, 6(12):2426–2429, 1968.

[85] R.J. Allemang and D.L. Brown. A correlation coefficient for modal vector analysis. In *1st International Modal Analysis Conference, IMAC*, Las Vegas, 1982.

[86] A.N. Tikhonov and V.Y. Arsenin. *Solutions of ill-posed problems.* John Wiley, New York, 1977.

[87] M. Link. Updating of analytical models-procedures and experience. In *Conference on Modern Practice in Stress and Vibration Analysis*, Sheffield,England, 1993.

[88] D. Goge. Automatic updating of large aircraft models using experimental data from ground vibration testing. *Aerospace Science and Technology*, 7(1):33–45, 2003.

[89] H. Shahverdi, C. Mares, and J.E. Mottershead. Model-structure correction and updating of aero engine casings using fictitious mass modifications. *Proceedings of the Institution of Mechanical Engineers, Part C, Journal of Mechanical Engineering Science*, 219(1):19–30, 2005.

[90] H. Shahverdi, C. Mares, W. Wang, and J.E. Mottershead. Clustering of parameter sensitivities: examples from a helicopter airframe model updating exercise. *Shock and Vibration*, 16(1):75–87, 2009.

[91] C.P. Fritzen and S. Zhu. Updating of finite element models by means of measured information. *Computers and Structures*, 40(2):457–486, 1991.

[92] R.I. Levin and N.A.J. Lieven. Dynamic finite element model updating using simulated annealing and genetic algorithms. *Mechanical Systems and Signal Processing*, 12(1):91–120, 1998.

[93] M.I. Friswell. The adjustment of structural parameters using a minimum variance estimator. *Mechanical Systems and Signal Processing*, 3(2):143–155, 1989.

[94] J.L. Beck and L.S. Katafygiotis. Updating models and their uncertainties. i: Bayesian statistical framework. *Journal of Engineering Mechanics*, 124(4):455–461, 1998.

[95] J.L. Beck and S.K. Au. Bayesian updating of structural models and reliability using markov chain monte carlo simulation. *Journal of Engineering Mechanics*, 128(4):380–391, 2002.

[96] G. Kerschen, J.C. Golinval, and F.M. Hemez. Bayesian model screening for the identification of nonlinear mechanical structures. *Journal of Vibration and Acoustics*, 125(3):389–397, 2003.

[97] L.S. Katafygiotis and J.L. Beck. Updating models and their uncertainties. ii: Model identifiability. *Journal of Engineering Mechanics*, 124(4):463–467, 1998.

[98] C. Mares, B. Dratz, J.E. Mottershead, and M.I. Friswell. Model updating using bayesian estimation. In *Proceedings of International Conference on Noise and Vibration, ISMA2006*, Katholieke Universiteit Leuven, Leuven ,Belgium, 2006. Katholieke Universiteit Leuven.

[99] C. Soize, E. Capiez-Lernout, and R. Ohayon. Robust updating of uncertain computational models using experimental modal analysis. *AIAA Journal*, 46(11):2955–2965, 2008.

[100] T. Haag, J. Herrmann, and M. Hanss. Identification procedure for epistemic uncertainties using inverse fuzzy arithmetic. *Mechanical Systems and Signal Processing*, 24(7):2021–2034, 2010.

[101] J.E. Mottershead, C. Mares, S. James, and M.I. Friswell. Stochastic model updating: Part 2: Application to a set of physical structures. *Mechanical Systems and Signal Processing*, 20(8):2171–2185, 2006.

[102] Y. Xia, H. Hao, J.M.W. Brownjohn, and P.Q. Xia. Damage identification of structures with uncertain frequency and mode shape data. *Earthquake Engineering and Structural Dynamics*, 31(5):1053–1066, 2002.

[103] Y. Xia and H. Hao. Statistical damage identification of structures with frequency changes. *Journal of Sound and Vibration*, 263(4):853–870, 2003.

[104] Y. Govers, M. Boswald, U. Fullekrug, D. Goge, and M. Link. Analysis of sources and quantification of uncertainty in experimental modal data. In *Proceedings of International Conference on Noise and Vibration, ISMA2006*, Katholieke Universiteit Leuven, Leuven ,Belgium, 2006. Katholieke Universiteit Leuven.

[105] Y. Govers and M. Link. Stochastic model updating: Covariance matrix adjustment from uncertain experimental modal data. *Mechanical Systems and Signal Processing*, 24(3):696–706, 2010.

[106] W.R. Gilks, S. Richardson, and D.J. Spiegelhalter. *Markov Chain Monte Carlo in Practice*. Chapman & Hall, London, 1996.

[107] N. Metropolis, A. Rosenbluth, M. Rosenbluth, H. Teller, and E. Teller. Equation of state calculations by fast computing machines. *Journal of Chemical Physics*, 21(6):1087–1092, 1953.

[108] M.W. Vanik, J.L. Beck, and S.K. Au. Bayesian probabilistic approach to structural health monitoring. *Journal of Engineering Mechanics*, 126(7):738–745, 2000.

[109] J.R. Wright and J.E.Cooper. *Introduction to aircraft aeroelasticity and loads*. John Wiley & Sons, 2007.

[110] C. Pettit. Uncertainty quantification in aeroelasticity: Recent results and research challenges. *Journal of Aircraft*, 41(5):1217–1229, 2004.

[111] D. Pitt, P. Haudrich, and M. Thomas. Probabilistic aeroelastic analysis and its implications on flutter margin requirements. In *AIAA-2008-2198 in the proceedings of 49th AIAA/ASME/ASCE/AHS/ASC Structures, Structural Dynamics and Materials Conference*, Schaumburg, Illinois, 2008. AIAA.

[112] F. Poirion. Impact of random uncertainties on aircraft aeroelastic stability. In *In Proceedings of the third international conference on stochastic structural dynamics*, 1995.

[113] J. Kuttenkeuler and U. Ringertz. Aeroelastic tailoring considering uncertainties in material properties. *Structural Optimization*, 15(3-4):157–162, 1998.

[114] M. Kurdi, N. Lindsley, and P. Beran. Uncertainty quantification of the goland wing's flutter boundary. In *AIAA-2007-6309 in the proceedings of the AIAA Atmospheric Flight Mechanics Conference and Exhibit*, Hilton Head, South Carolina, 2007. AIAA.

[115] P.S. Beran, C.L. Pettit, and M.R. Daniel. Uncertainty quantification of limit-cycle oscillations. *Journal of Computational Physics*, 217(1):217–247, 2006.

[116] S.C. Catravete and R.A. Ibrahim. Effect of stiffness uncertainties on the flutter of cantilever wing. *AIAA Journal*, 46(4):925–935, 2008.

[117] P.J. Attar and E.H. Dowell. Stochastic analysis of a nonlinear aeroelastic model using the response surface method. *Journal of Aircraft*, 43(4):1044–1052, 2006.

[118] Z. Wang, Z. Zhang, D.H. Lee, P.C. Chen, and D.D. Liu. Flutter analysis with structural uncertainty by using CFD based aerodynamic rom. In *49th AIAA/ASME/ASCE/AHS/ASC Structures, Structural Dynamics, and Materials Conference*, Schaumburg, IL, 2008. AIAA.

[119] A. Manan and J. Cooper. Design of composite wings including uncertainties: A probabilistic approach. *Journal of Aircraft*, 46(2):601–607, 2009.

[120] K. Willcox and J. Peraire. Application of reduced-order aerodynamic modeling to the analysis of structural uncertainty in bladed disks. In *Proceedings of ASME TURBO EXPO 2002 International Gas Turbine & Aeroengine Congress & Exhibition*, Amsterdam, The Netherlands, 2002. ASME.

[121] C. Verhoosel, T. Scholcz, S. Hulshoff, and M. Gutiérrez. Uncertainty and reliability analysis of fluid-structure stability boundaries. *AIAA Journal*, 47(1):91–102, 2009.

[122] S. Rao and L. Majumder. Optimization of aircraft wings for gust loads: Interval analysis-based approach. *AIAA Journal*, 46(3):723–732, 2008.

[123] E. Albano and W.P. Rodden. A doublet-lattice method for calculating lift distributions on oscillating surfaces in subsonic flows. *AIAA Journal*, 7(2):279–285, 1969.

[124] J. Katz and A. Plotkin. *Low-speed aerodynamics*. Cambridge university press, 2001.

[125] W.P. Rodden and E.H. Johnson. Msc/nastran user manual, aeroelastic analysis users guide. Technical report, MSC Nastran, 1994.

[126] K.J. Badcock, M.A. Woodgate, and B.E. Richards. The application of sparse matrix techniques for the CFD based aeroelastic bifurcation analysis of a symmetric aerofoil. *AIAA Journal*, 42(5):883–892, 2004.

[127] K.J. Badcock, M.A. Woodgate, and B.E. Richards. Direct aeroelastic bifurcation analysis of a symmetric wing based on the euler equations. *Journal of Aircraft*, 42(3):731–737, 2005.

[128] K.J. Badcock and M.A. Woodgate. Prediction of bifurcation onset of large order aeroelastic models. In *49th Structural Dynamics and Materials Conference, AIAA-2008-1820*, Illinois, Schaumberg, 2008. AIAA.

[129] K. Bekas and Y. Saad. Computation of smallest eigenvalues using spectral Schur complements. *SIAM Journal of Scientific Computing*, 27(2):458–481, 2005.

[130] S. Adhikari. Complex modes in stochastic systems. *Advances in Vibration Engineering*, 3(1):1–11, 2004.

[131] S. Rao. *Optimisation theory and applications.* India: Wiley Eastern Limited, 1979.

[132] T.F. Coleman and Y. Li. A reflective newton method for minimising a quadratic function subject to bounds on some of the variables. *SIAM Journal on Optimization*, 6(4):1040–1058, 1996.

[133] P.S. Beran, N.S. Knot, F.E. Eastep, R.D. Synder, and J.V. Zweber. Numerical analysis of store-induced limit cycle oscillarion. *Journal of Aircraft*, 41(6):1315–1326, 2004.

[134] J. Cattarius. *Numerical wing/store interaction analysis of a parametric F-16 Wing.* PhD thesis, Virginia Polytechnic Institute and State University, 1999.

[135] FW.Jr. Cazier and MW. Kehoe. Flight test of a decoupler pylon for wing/store flutter suppression. In *AIAA flight testing conference, AIAA paper 19869730*, 1986.

[136] FW.Jr. Cazier and MW. Kehoe. Ground vibration test on an f-16 airplane with modified decoupler pylons. Technical report, Technical memorandum NASA-TM-87634, NASA, 1986.

[137] S. Marques, K.J. Badcock, H. Haddad Khodaparast, and J.E. Mottershead. Transonic aeroelastic stability predictions under the influence of structural variability. *Journal of Aircraft*, 47(4):1229–1239, 2010.

[138] N.P. Seif, M.A. Hassanein, and A.S. Deif. Inverse problem of the interval linear system of equations. *Computing*, 63(2):185–200, 1999.

[139] M. De Munck, D. Moens, W. Desmet, and D. Vandepitte. An efficient response surface based optimisation method for non-deterministic harmonic and transient dynamic analysis. *Computer Modeling in Engineering and Sciences*, 1(1):1–48, 2009.

[140] H. Haddad Khodaparast, J.E. Mottershead, and K.J. Badcock. Propagation of structural uncertainty to linear aeroelastic stability. *Computers and Structures*, 88(3-4):223–236, 2010.

[141] S. Marques, K.J. Badcock, H. Haddad Khodaparast, and J.E. Mottershead. CFD based aeroelastic stability predictions under the influence of structural variability. In *50th AIAA/ASME/ASCE/AHS/ASC Structures, Structural Dynamics, and Materials Conference, AIAA 2009-2324*, Palm Springs, California, 2009. AIAA.

[142] H. Haddad Khodaparast, S. Marques, K.J. Badcock, and J.E. Mottershead. Estimation of flutter boundaries in the presence of structural uncertyainty by probabilistic and fuzzy methods. In *International Conference on Structural Engineering Dynamics.ICEDyn 2009, Paper number 40*, PORTUGAL.Ericeira, 2009. IST Lisbon.

[143] H. Haddad Khodaparast, J.E. Mottershead, and M.I. Friswell. Perturbation methods for the estimation of parameter variability in stochastic model updating. *Mechanical Systems and Signal Processing*, 22(8):1751–1773, 2008.

[144] H. Haddad Khodaparast and J.E. Mottershead. Efficient methods in stochastic model updating. In *Proceedings of International Conference on Noise and Vibration, ISMA2008*, Leuven ,Belgium, 2008.

[145] H. Haddad Khodaparast, J.E. Mottershead, and K.J. Badcock. Interval model updating in structural dynamics. *Mechanical Systems and Signal Processing*, 2010.

[146] H. Haddad Khodaparast, J.E. Mottershead, and K.J. Badcock. Interval model updating: Method and application. In *Proceedings of International Conference on Uncertainty in Structural Dynamics, USD2010*, Leuven ,Belgium, 2010.

[147] G.A. Vio and J.E. Cooper. Limit cycle oscillation prediction for aeroelastic systems with discrete bilinear stiffness. *International Journal of Applied Mathematics and Mechanics*, 3:100–119, 2005.